

Geophysical Field Trip Guide
Carlin Trend, Nevada

Supplementary Reading

November 17, 1996
Post Convention Field Trip
Society of Exploration Geophysicists
Sixty-sixth Annual Meeting

Concealed Mineral Deposits Insights from Three-Dimensional Gravity and Magnetic Analysis

Richard J. Blakely and Robert C. Jachens

U. S. Geological Survey, Menlo Park, CA 94025

Introduction

Pre-Tertiary basement is exposed over only about 20 percent of the area of Nevada, yet this 20 percent is host to two-thirds of the base and precious metal deposits and prospects in the state (Maureen Sherlock, oral commun., 1988). Basement rocks buried beneath Cenozoic volcanic and sedimentary deposits presumably are similarly endowed and could be targets for mineral exploration in areas where the Cenozoic cover is thin. Quantitative interpretations of gravity data can provide information on the depth to basement beneath Cenozoic rocks and thereby help identify accessible target areas.

Magnetic interpretations complement gravity interpretations by providing information on igneous rocks. Magnetic anomalies commonly occur over areas where volcanic and plutonic rocks crop out, and the pattern of magnetic anomalies is often diagnostic of rock type. Consequently, it is possible to predict from the pattern of magnetic anomalies where volcanic and plutonic rocks are located at shallow depth beneath less magnetic rocks, an important constraint for regional mineral appraisals insofar as igneous rocks are associated with mineral commodities.

Analysis of Gravity Data

Analysis of regional gravity data from Nevada was undertaken with two main objectives: to define the location and shape of the surface of pre-Tertiary basement and to produce a gravity map that reflects variations of density within the pre-Tertiary basement. Both objectives contribute directly to the analysis of mineral resources of Nevada, the first by specifying the three-dimensional distribution of potential host rocks, and the second by placing constraints on the density and, therefore, the permissible lithology of concealed basement.

The most striking characteristic of the isostatic residual gravity map of Nevada (Fig. 1) is the pervasive regional pattern of long, narrow gravity highs and lows. This anomaly pattern is closely correlated with both the local topography and near-surface geology and reflects the strong difference in density between the rocks that make up the basement and the materials that overlie

them. A longer wavelength pattern of gravity variations also is apparent on the residual gravity map, most readily seen as broad regions of high gravity in the northern and southern parts of the state compared to generally lower values present throughout the center. This broader pattern is an expression of density variations within the pre-Tertiary basement.

We have developed a method which, for the most part, succeeds in separating the observed isostatic residual gravity field of Nevada into its component parts: the field caused by density variations within the basement, and the field caused by variations in thickness of young cover. The process is an iterative one. The estimate of basement gravity starts by using only gravity stations located on exposed basement. The estimate then is refined by successive attempts to remove the effects of Cenozoic cover using an empirical density-depth function.

The primary products of this separation procedure are shown in Figures 2 and 3. Figure 2 shows the gravity field produced by pre-Tertiary basement. The pervasive short-wavelength grain of the original residual anomaly (Fig. 1) has been eliminated, yet the major long-wavelength features persist. The dominant, first-order feature of the basement gravity of Nevada (Fig. 2) is the enormous area of low gravity that spans the entire state between lat 37deg and 40.5deg N. The regional gravity low reflects sources within the pre-Tertiary basement, but its strongest geologic correlation is with the distribution of middle Tertiary silicic ash-flow tuffs. The broad gravity low may reflect silicic intrusions within the middle and upper crust that are the counterparts of the volcanic rocks at the surface.

The map showing the thickness of Cenozoic cover (Fig. 3) suggests that a vast area of Nevada may have basement at relatively shallow depth. Although about 80 percent of the state is covered by Cenozoic deposits, Figure 3 shows that these deposits are thicker than 1 km only over about 20 percent of the state. Consequently, 60 percent of the state is covered by Cenozoic deposits sufficiently thin that pre-Tertiary basement rocks are within reach of current exploration techniques.

The cover-thickness map also reflects late Tertiary deformation in Nevada. Linear basins, volcanic depressions, and large areas of thick volcanic deposits are all evident on Figure 3. The distribution of these features

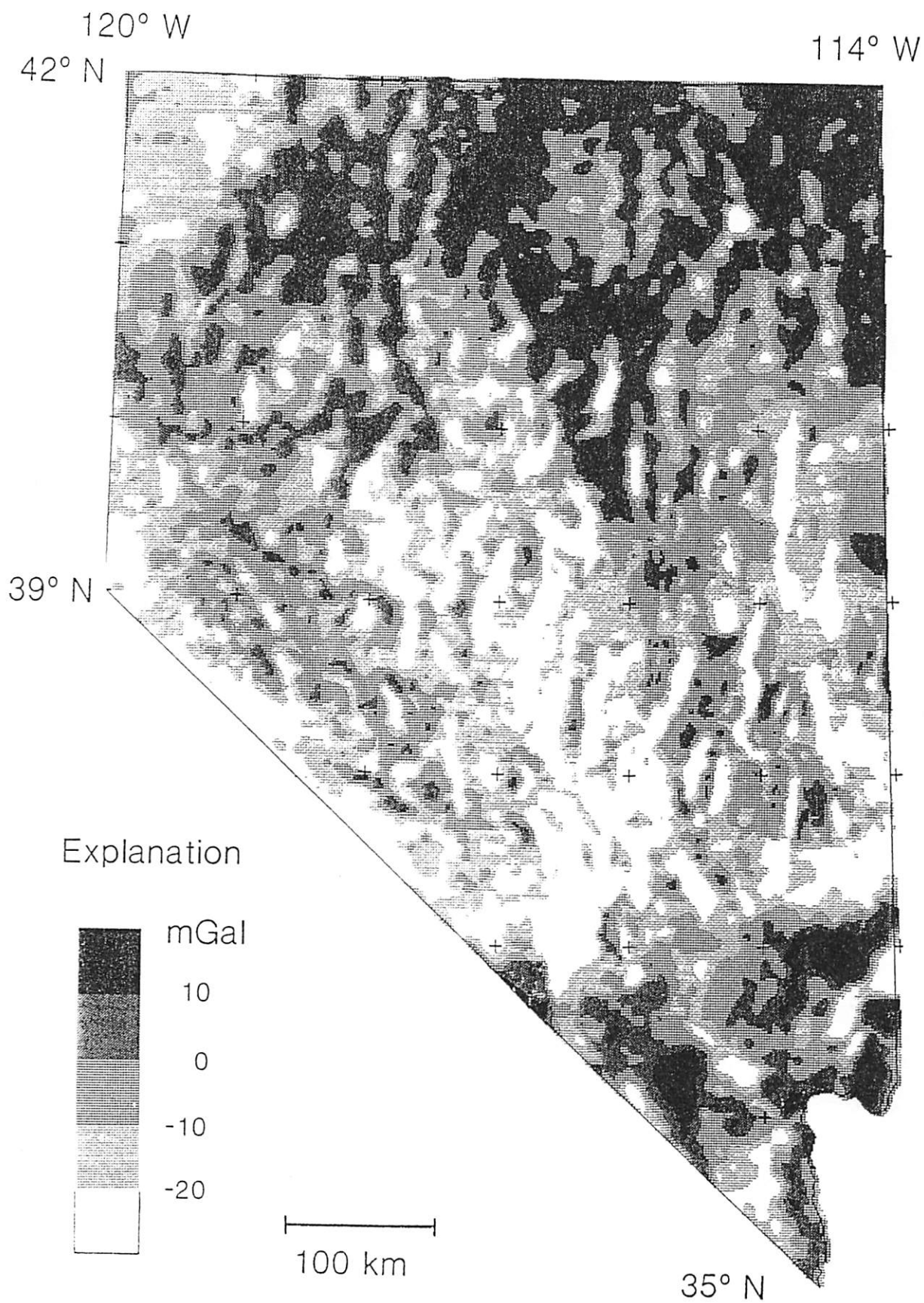


Fig. 1. Isostatic residual gravity map of Nevada. Contour interval 10 mGal. Data from Saltus (1988).

indicates that late Tertiary deformation has not been uniform over the state; distinct areas with consistent deformation patterns can be recognized. The west-central part of the state, for example, is characterized by northwest-trending, generally shallow basins. This area includes much of the Walker Lane belt of Stewart (1988). In contrast, the amagmatic zone in southern Nevada has fewer and more scattered basins than surrounding areas.

Thick sequences of Tertiary volcanic rock occur in numerous places in Nevada. Calderas of the southwestern Nevada volcanic field that contain 16-6.5 Ma volcanic deposits (Byers and others, 1989) many kilometers thick (Snyder and Carr, 1984) show prominently on Figure 3, while deposits of similar age located due east appear to be much thinner. Two large areas of northern Nevada, one in the extreme northwestern corner and the other along the northern border at long 117deg W., are blanketed by volcanic rocks having ages in the range 6-17 Ma (Stewart, 1980). Although the two areas appear quite similar on geologic maps, Figure 3 indicates that the northwestern corner contains a thick volcanic sequence whereas the deposits in the north-central area are either substantially thinner or have densities nearly equal to underlying basement. The crust in the northwestern corner of Nevada must be dramatically different from anywhere else in the state.

Analysis of Magnetic Data

Two compilations of aeromagnetic data were used in the interpretations described herein. Aeromagnetic data from Nevada (Fig. 4) compiled by Hildenbrand and Kucks (1988) from 38 separate surveys were used for insights into the regional tectonic framework of the area. A second regional survey, acquired under contract to the U.S. Department of Energy as part of the National Uranium Resource Evaluation (NURE) program, was used in our interpretations. The NURE survey includes the entire conterminous United States plus Alaska and varies widely in flight specifications. In Nevada, flightlines were spaced roughly 5 km apart, except in the Death Valley and part of the Kingman 1deg by 2deg quadrangles where flightlines were spaced approximately 1.6 km apart. NURE profiles were measured approximately 120 m above terrain, and this low altitude provides a significant advantage in the detection of shallow magnetic sources.

NURE magnetic profiles were plotted along flightlines at 1:250,000 scale. Boundaries between areas with and areas without shallow (< 1 km) magnetic sources were sketched on each map based on patterns of anomalies along individual profiles. Specific anomalies were selected in areas where source depth was ambiguous; these anomalies were analyzed with the method of Peters (1949) to provide estimates of depth to magnetic source at these discrete locations. We also applied a computer-based method to estimate depth to source, modified

from Blakely and Hassanzadeh (1981), to all NURE data from Nevada in order to aid and modify the above qualitative interpretation. Boundaries were subsequently digitized and merged into the statewide compilation discussed below.

Areas of Nevada with magnetic sources interpreted to be within 1 km of the surface are shown in Figure 5. This analysis shows that 46 percent of the state of Nevada is underlain by magnetic sources within 1 km of the surface, a testimony to the widespread magmatic events that accompanied the Mesozoic and Cenozoic tectonic development of this region. Figure 5 shows the location of shallow magnetic sources only. Some anomalies in aeromagnetic compilations are caused by deep magnetic sources with no shallow counterparts and are not expected to appear in Figure 5. The so-called Charleston Peak anomaly (Fig. 4, lat 36deg00' N., long 115deg00' W.) in the amagmatic zone of southern Nevada, for example, is a significant feature of most aeromagnetic compilations. The source of this anomaly is buried several kilometers below the topographic surface (Blank, 1988) and, therefore, does not appear in our map of shallow magnetic sources.

Aeromagnetic compilations (Fig. 4) show a narrow anomaly with north-northwest trend extending 280 km through north-central Nevada. The association of this anomaly in some locations with basaltic and andesitic extrusive and intrusive rocks suggests that similar rocks exist along the entire length of the anomaly, and the feature has been interpreted as a rift zone active during the middle Miocene (for example, Zoback and Thompson, 1978). Two hot-spring gold deposits are associated with basaltic rocks of the northern Nevada rift, and other hot-spring gold deposits and several hot-spring mercury deposits are associated with similar anomalies to the west (Cox and others, this volume). Contoured aeromagnetic maps show that the northern Nevada rift continues south to about lat 39deg N., but interpretation of NURE profiles suggests that it extends considerably farther to the south-southeast. A narrow band of shallow magnetic sources (Fig. 5), approximately on strike with the northern Nevada rift, extends to at least lat 38deg N. and perhaps to the amagmatic zone (lat 37deg N.). Magnetic sources in this southern part of the rift are obscured by nonmagnetic cover less than 1 km thick in most locations. By analogy with the northern part of the rift, they may be targets for hot-spring gold and mercury deposits.

Magnetic anomalies in the Walker Lane belt of southwestern Nevada (Stewart, 1988) have arcuate, northwesterly trends generally parallel to the Walker Lane (Fig. 4). Blakely (1988) noted that the width of the northwest-trending pattern of magnetic anomalies is considerably wider than the belt described by Albers (1967) and Stewart and others (1968), extending in some places over 150 km north-northeast of the Walker Lane and into topography with north to northeast trends more typical of the Basin and Range province. The magnetic anomalies may indicate an underlying tectonic

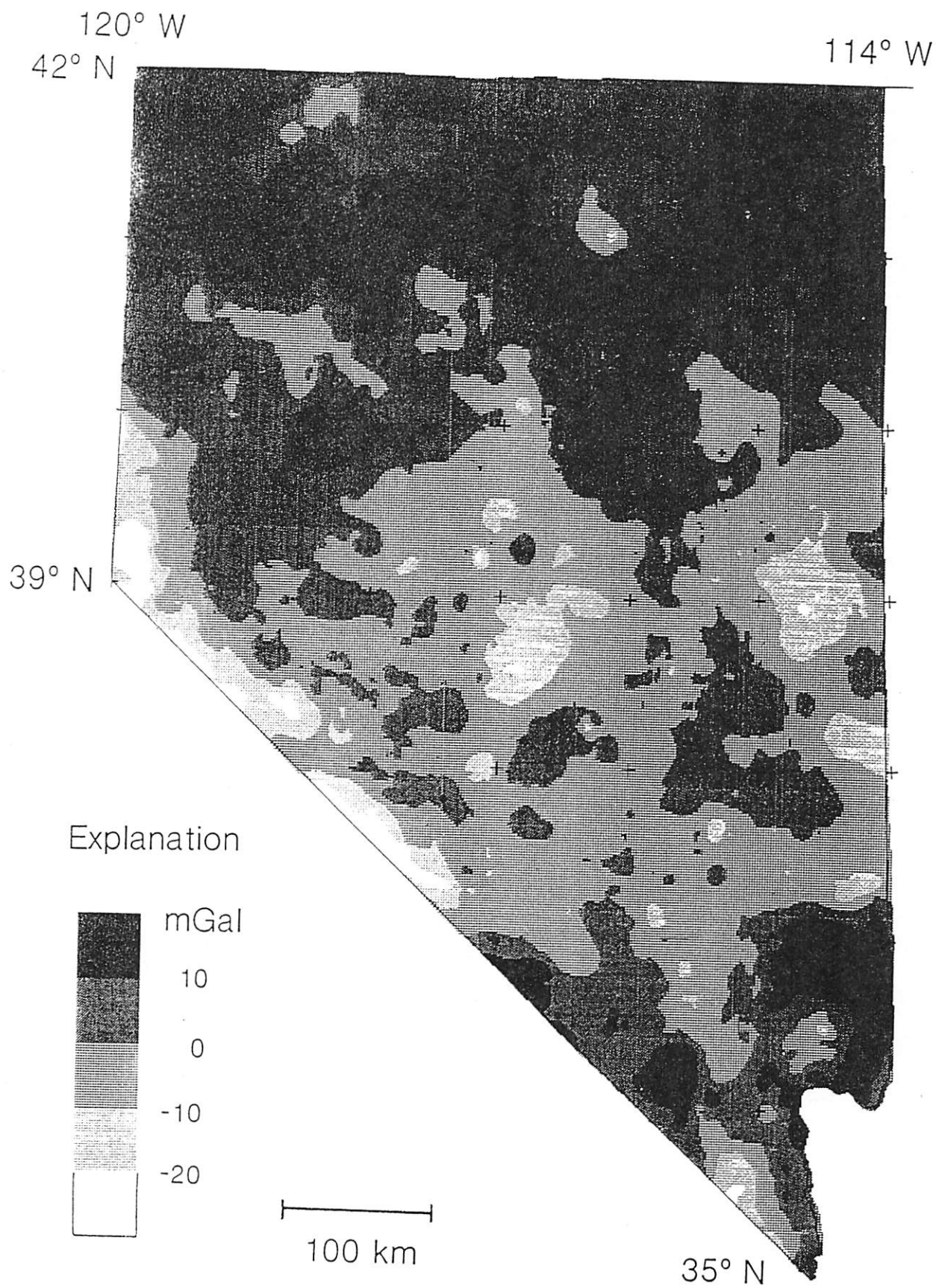


Fig. 2. Basement gravity map of Nevada. Contour interval 10 mGal.

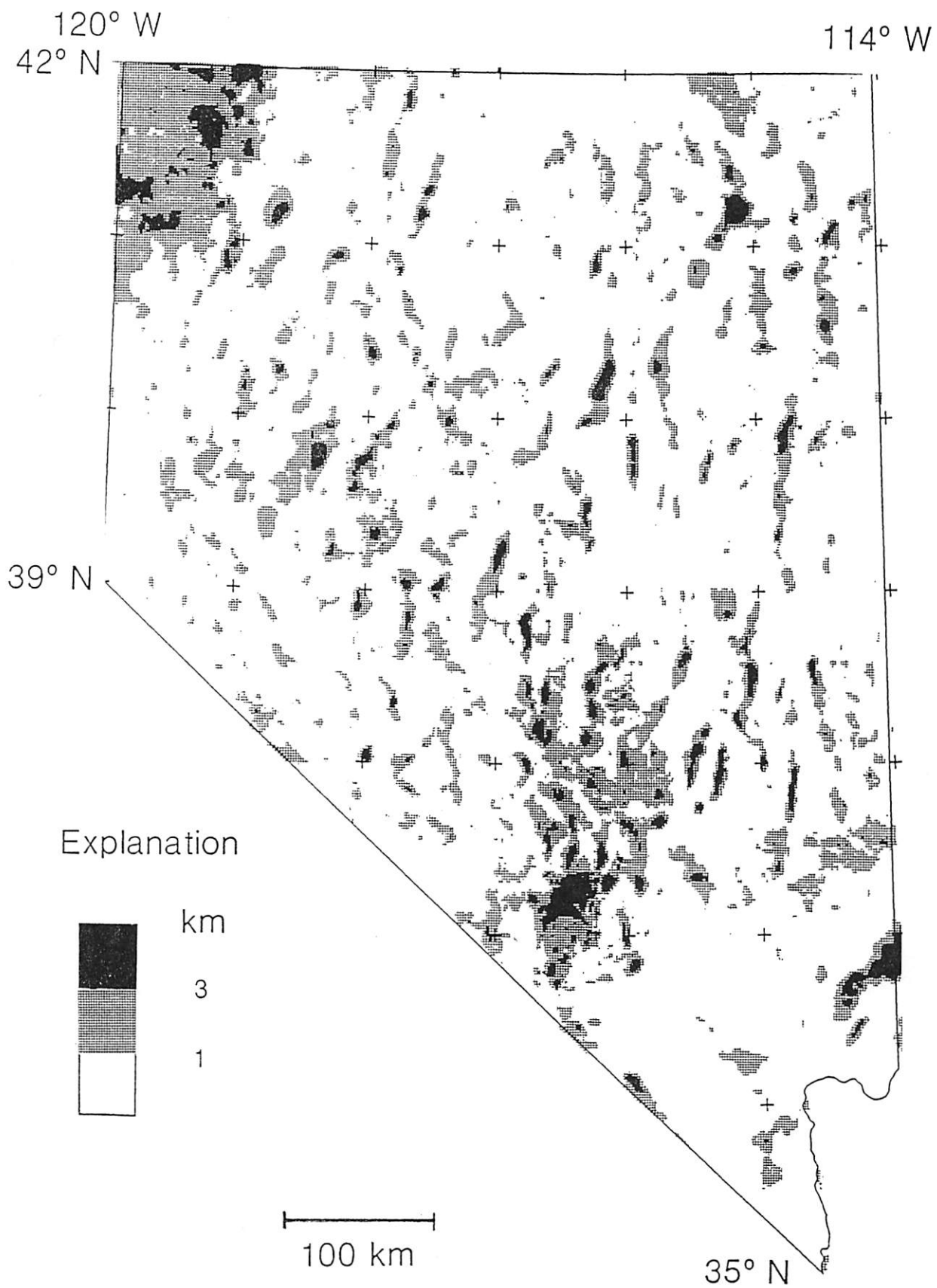


Fig. 3. Thickness of Cenozoic cover in Nevada. A constant density contrast of 0.25 g/cm³ between pre-Tertiary basement rocks and Cenozoic cover material was assumed for all regions below a depth of 1.2 km but above the basement surface.

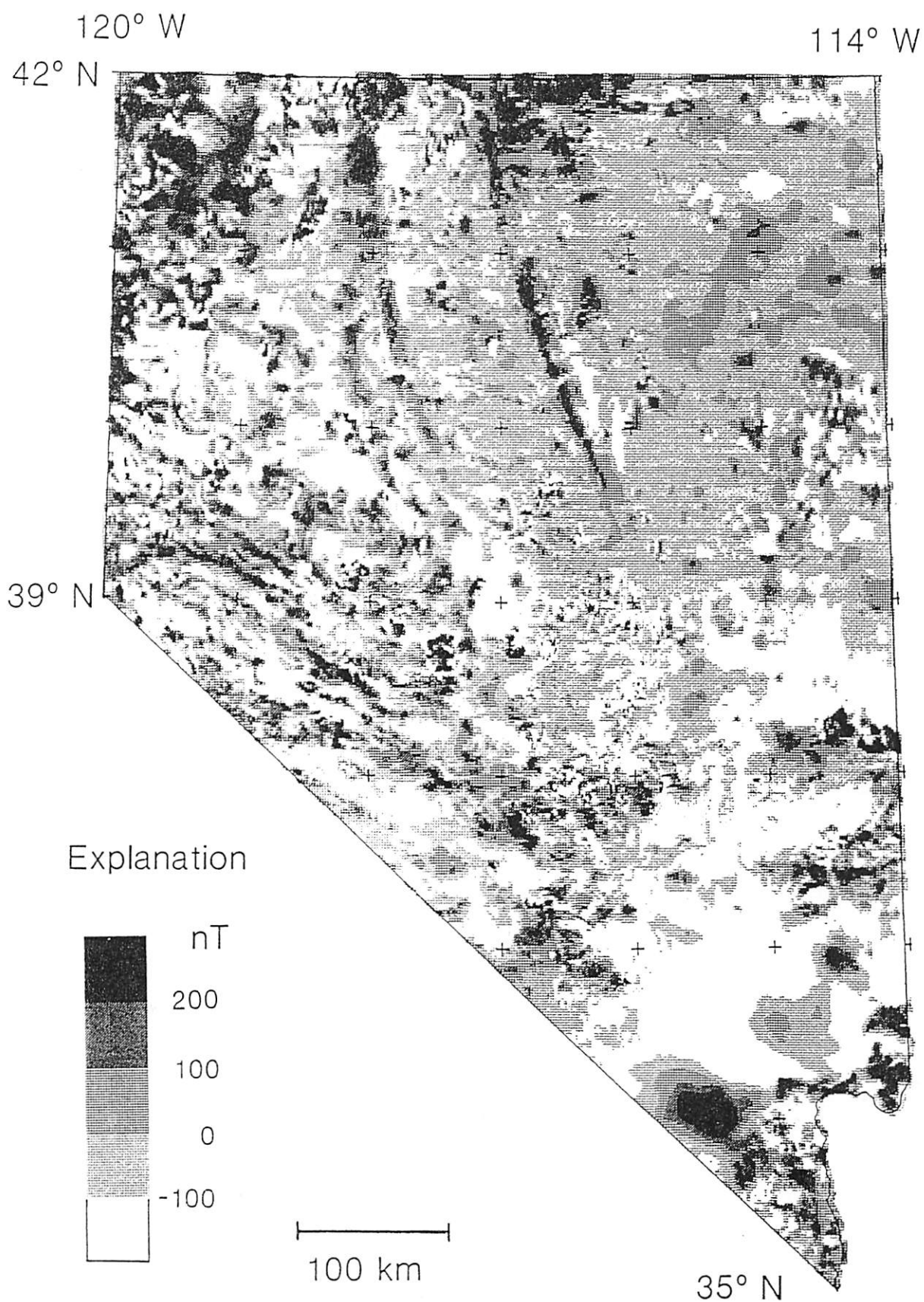


Fig. 4. Aeromagnetic anomaly map of Nevada. Total field anomalies from Nevada analytically continued to 305 m above terrain. Contour interval 100 nT. Modified from the compilation by Hildenbrand and Kucks (1988).

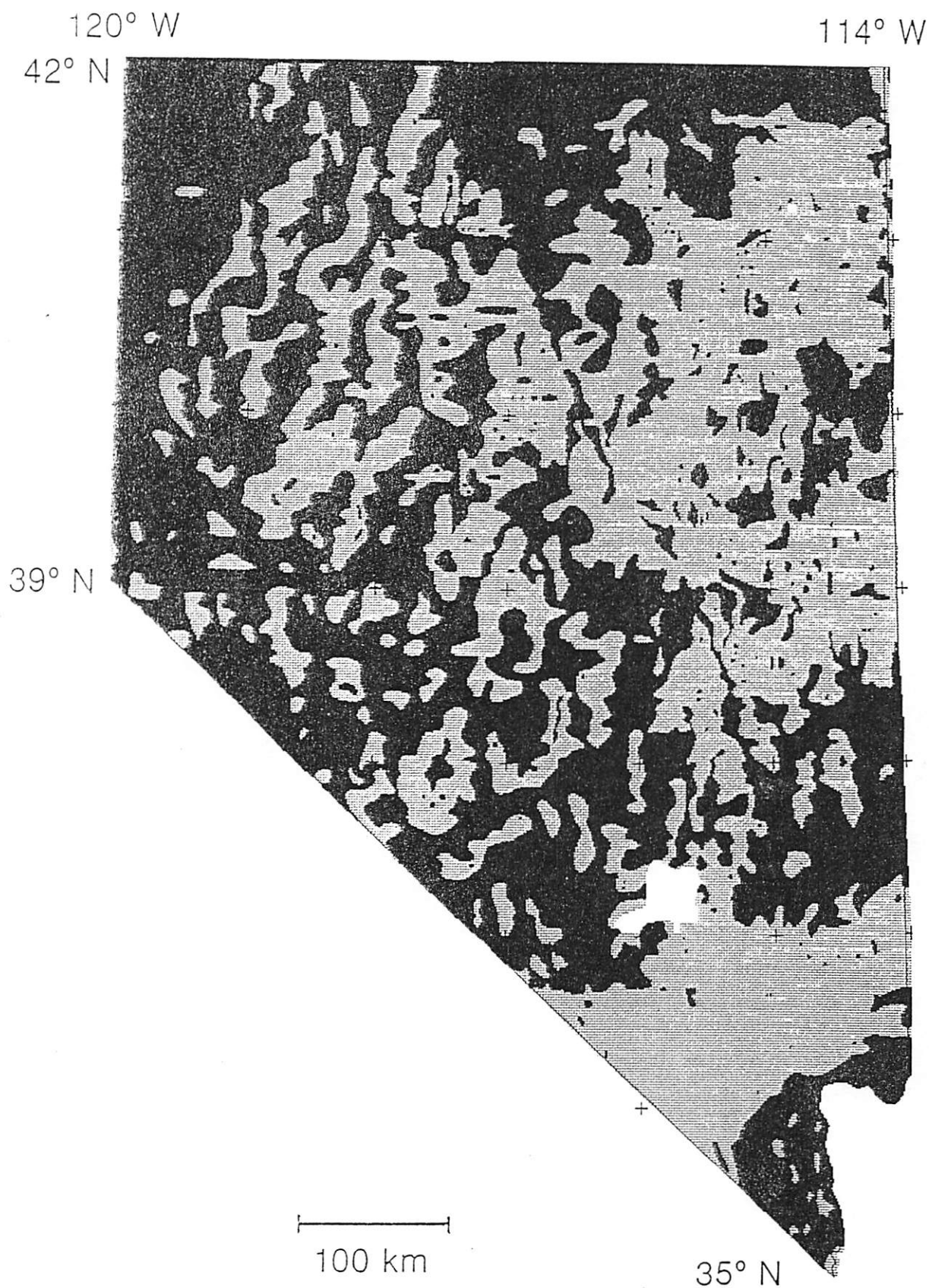


Fig. 5. Location of shallow magnetic sources in Nevada as interpreted from NURE magnetic profiles. Areas with magnetic sources within 1 km of the topographic surface are shown in black; areas without magnetic sources within 1 km of the surface are shown in stipple pattern. Blank area indicates insufficient data to make a reliable interpretation.

fabric older than modern topography and exposed geology. A surprising correlation between this regional magnetic anomaly pattern and the distribution of mineral deposits was noted by Cox and others (this volume). All of the volcanic-hosted epithermal deposits in southwestern Nevada are located within the Walker Lane magnetic zone. Cox and others (this volume) proposed that late-Tertiary faulting influenced the present-day magnetic anomaly patterns and was partially responsible for the distribution of volcanic-hosted deposits. Moreover, pluton-related deposits and most of the sediment-hosted gold deposits are absent from this magnetic zone, suggesting that these classes of deposits require an environment of tectonic quiescence (Cox and others, this volume).

References

- Albers, J. P., 1967, Belt of sigmoidal bending and right-lateral faulting in the western Great Basin: *Geological Society of America Bulletin*, v. 78, p. 143-156.
- Blakely, R. J., 1988, Curie temperature isotherm analysis and tectonic implications of aeromagnetic data from Nevada: *Journal of Geophysical Research*, v. 93, p. 11,817-11,832.
- Blakely, R. J., and Hassanzadeh, Siamak, 1981, Estimation of depth to magnetic source using maximum entropy power spectra, in *Crustal formation and Andean convergence: Geological Society of America Memoir 154*, p. 667-682.
- Blank, H. R., 1988, Basement structure in the Las Vegas region from potential-field data [abstract]: *Abstracts with Programs*, 84th Annual Meeting, Cordilleran Section, Geological Society of America, v. 20, p. 144.
- Byers, F. M., Carr, W. J., and Orkild, Paul P., 1989, Volcanic centers of southwestern Nevada: evolution of understanding, 1960-1988: *Journal of Geophysical Research*, v. 94, p. 5908-5924.
- Cox, D. P., Ludington, Steve, Sherlock, M. G., Singer, D. A., Berger, B. R., and Tingley, J. V., 1990, Mineralization patterns in time and space in the Great Basin of Nevada: this volume.
- Hildenbrand, T. G., and Kucks, R. P., 1988, Filtered magnetic anomaly maps of Nevada: Nevada Bureau of Mines and Geology Map 93B, scale 1:1,000,000 (4 sheets) and 1:2,000,000 (1 sheet).
- Peters, L. J., 1949, The direct approach to magnetic interpretation and its practical applications: *Geophysics*, v. 14, p. 290-320.
- Saltus, R. W., 1988a, Gravity data for the state of Nevada on magnetic tape: EROS Data Center, Sioux Falls, S. Dak.
- Snyder, D. B., and Carr, W. J., 1984, Interpretation of gravity data in a complex volcano-tectonic setting, southwestern Nevada: *Journal of Geophysical Research*, v. 89, p. 10,193-10,206.
- Stewart, J. H., 1980, *Geology of Nevada*, a discussion to accompany the geology map of Nevada: Nevada Bureau of Mines and Geology Special Publication 4, 136 p.
- Stewart, J. H., 1988, Tectonics of the Walker Lane belt, western Great Basin—Mesozoic and Cenozoic deformation in a zone of shear, in *Metamorphism and crustal evolution of the western United States*, Rubey volume VII, p. 683-713, Prentice Hall, Englewood Cliffs, New Jersey.
- Stewart, J. H., Albers, J. P., and Poole, F. G., 1968, Summary of regional evidence for right-lateral displacement in the western Great Basin: *Geological Society of America Bulletin*, v. 79, p. 1407-1413.
- Zoback, M. L., and Thompson, G. A., 1978, Basin and Range rifting in northern Nevada: Clues from a mid-Miocene rift and its subsequent offsets: *Geology*, v. 6, p. 111-116.

A relation among geology, tectonics, and velocity structure, western to central Nevada Basin and Range

R. D. CATCHINGS *U.S. Geological Survey, 345 Middlefield Road, M.S. 977, Menlo Park, California 94587*

ABSTRACT

In the northwestern to central Nevada Basin and Range, there are correlations between velocity and specific geologic structures of the crust. Mapped range-bounding faults at the surface can be traced to appreciable (10 km) depths based on velocity variations and are consistent with subsurface projections of the faults based on seismic reflection images. The limiting depth of the faults, as indicated by the velocity variations, corresponds to the maximum depth of earthquakes along the seismic profile. Correlations between velocity and the surface geology show that in the upper crust the pre-Cenozoic rocks are underlain by high-velocity (6.0 km/s) rocks, whereas the Tertiary ranges are underlain by lower-velocity (4.0–5.7 km/s) rocks to depths as great as 10 km. Although the Tertiary rocks differ in composition from the Mesozoic rocks, the lower-velocity Tertiary rocks may also be attributed to rock masses which are broken (4.0–5.7 km/s), and the higher-velocity Mesozoic rocks (6.0 km/s) may be attributed to largely unbroken rock masses. The regional seismicity pattern is consistent with this interpretation, as earthquakes are largely confined within or near the base of the low-velocity rocks. These low-velocity, highly fractured rocks are laterally distributed in discrete zones, suggesting that extension is not uniformly distributed but occurs in discrete, highly extended zones. Beneath these highly extended zones, the lower-crustal layers show structural evidence of extension, and velocity measurements suggest that the lowermost crust has been magmatically underplated. The superposition of Tertiary volcanic rocks, highly fractured upper crust, and lower-crustal magmatic underplating suggests that the Tertiary volcanic rocks originated from lower-crustal magmas that migrated to the surface via the highly extended zones. The velocity structure of one of the highly extended zones and the Lahonton Basin resembles that of many continental rifts. The velocity structure beneath central Nevada, however, is much more like normal continental crust. On the basis of isotopic studies, it is concluded that the transition between highly extended crust and more normal crust occurs in the area inferred to be the edge of the North American craton.

INTRODUCTION

Structural variations, in conjunction with velocity data and other geophysical data, provide a basis for interpreting some of the processes associated with Basin and Range tectonism. Structure is derived from surface geologic mapping, near-vertical reflection data, and wide-angle reflection and refraction data. Velocity models are derived from refraction data and are compared directly with each of the structural models. Next,

an estimate of composition and physical parameters based on structure, velocity, and additional geologic and geophysical data is presented.

In order to investigate processes associated with Basin and Range tectonism, the Program for Array Seismic Studies of the Continental Lithosphere (PASSCAL) acquired a variety of seismic data (Whitman and Catchings, 1988; Catchings and others, 1988) in the northwestern Basin and Range (Fig. 1). The PASSCAL seismic survey was largely coincident with a series of seismic reflection profiles acquired by the Consortium for Continental Reflection Profiling (COCORP) near the 40°N parallel (Allmendinger and others, 1987). The availability of COCORP data and other geophysical data within the study area affords a rare opportunity to investigate characteristics of the extended crust.

Interpretations of the PASSCAL data have been made by several investigators using different interpretative techniques. Jarchow (1991) used near-vertical and wide-angle reflection data. Benz and others (1990) used one-dimensional (1-D), forward, reflectivity modeling of wide-angle reflection and refraction data, and Hawman and others (1990) used 1-D inversions of near-vertical and wide-angle reflections and refractions; both 1-D methods provided a profile of average velocity as a function of depth using a subset of the available seismic data. Holbrook (1990) and Catchings and Mooney (1991) used two-dimensional (2-D), forward raytracing and Bouguer gravity modeling techniques on the entire data set. Models developed by Catchings and Mooney (1991) were also checked against near-vertical and wide-angle reflection data and existing seismic reflections and refraction data. Although there are some differences in the models, these investigations broadly suggest much the same general velocities and gross structure of the crust.


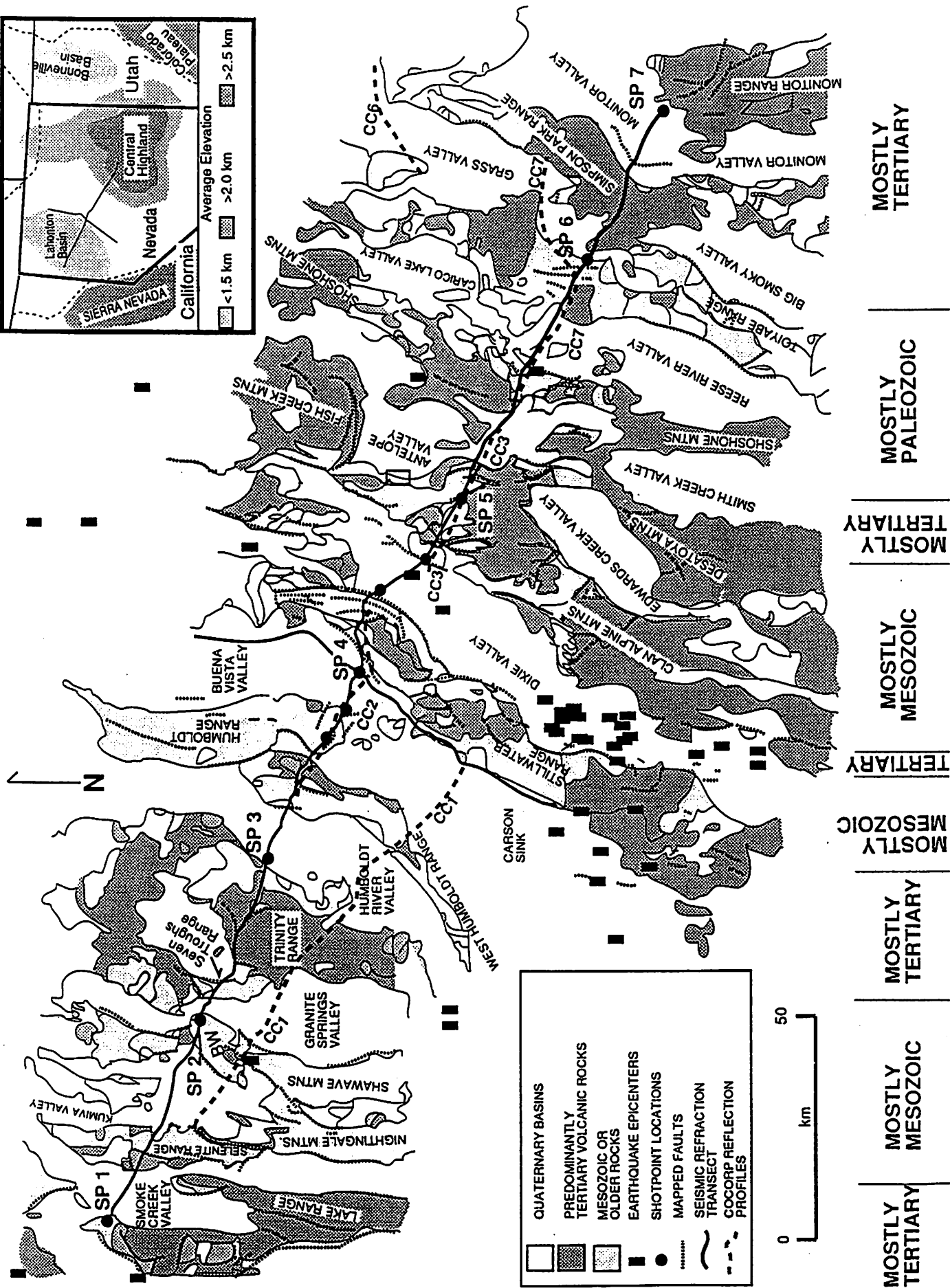
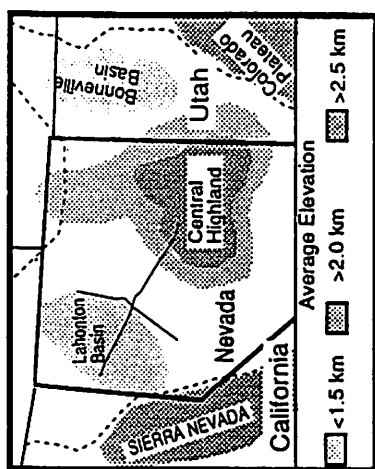


Figure 1. Location of PASSCAL seismic refraction profiles (solid bold lines) and COCORP seismic reflection profiles (CC#, bold dashed lines) are shown with respect to the basins and ranges traversed and the simplified geology along northwest-southeast transect (after Stewart and Carlson, 1977, 1978). The predominant ages of ranges where the seismic transect crosses them are shown at the bottom. Note the alternation between Mesozoic and Tertiary ranges, especially in the western half of the transect, which corresponds to velocity variations in the upper crust (see Fig. 2). BW refers to the Bluewing Mountains. The black rectangles are epicenters for the better located earthquakes from the 1970s and early 1980s near the seismic line (Ryall and Vetter, 1982). The inset also shows major regional topographic variations and the approximate outline of the Basin and Range province (dashed line).



GEOLOGICAL AND GEOPHYSICAL CHARACTERIZATIONS OF THE BASIN AND RANGE AT 40°N

The Basin and Range province (BRP) has undergone a complex geologic history, and the resulting tectonic activity has greatly influenced the present lithospheric structure. Any seismic image of the lithospheric structure is but a snapshot in time and must be interpreted in the context of the past. A number of authors have presented elegant recountings and supplied documentary evidence for the tectonic development of the Basin and Range province (Burchfiel and Davis, 1972; Kistler, 1974; Zoback and others, 1981; Speed, 1982; Farmer and DePaolo, 1983); tectonic events of greatest importance to the development of the present crustal and upper-mantle structure at 40°N can be summarized from their work as follows. (1) A Proterozoic episode of rifting of the North American craton resulted in the formation of a passive continental margin in the area that is now central Nevada. (2) Multiple episodes of Paleozoic and Mesozoic shortening resulted in accretion of various terranes to the rifted edge of cratonic North America, the suture zones of which are inferred to lie beneath the eastern half of the PASSCAL transect. (3) Initial stages of back-arc rifting and calc-alkaline volcanism developed between 40 and 50 Ma, whereas basaltic volcanism began in the southern BRP ca. 20 Ma and migrated into the northern BRP (including the 40°N area) by ca. 17 Ma.

(4) Two separate episodes of Cenozoic extension involved west-southwest-east-northeast extension from ca. 20 to 10 Ma and west-northwest-east-southeast extension from 10 Ma to the present.

At 40°N latitude, the average latitude of PASSCAL seismic investigation, the latter extensional episodes have given rise to a topographically lower-lying region between the Sierra Nevada Range and the Colorado Plateau, commonly referred to as the "Great Basin." The valleys within the Great Basin at 40°N are >1 km in elevation, as is typical of areas of continental extension worldwide (Thompson and Burke, 1974). The topography is dominated by at least two different wavelengths (Eaton and others, 1978; Fletcher and Hallet, 1983), the shorter wavelength (~30 km) of individual basins and ranges and a longer wavelength (~500 km) expressed by two topographic depressions (Fig. 1). The long-wavelength topographic depressions, the Lahonton and Bonneville Basins (Russell, 1885), have a minimum elevation of ~1.2 km and are separated by a topographic high with an average range elevation of ~2.5 km in central Nevada (see inset, Fig. 1).

Other reported geophysical characteristics of the Great Basin include thin (20–30 km) crust and low (7.3–7.9 km/s) upper-mantle velocity (Eaton, 1963; Pakiser, 1963; Prodehl, 1979; Priestley and others, 1982), active faulting and seismicity (Thompson and Burke, 1974; Ryall and Vetter, 1982), high (as much as 90 mW/m²) heat flow (Lachenbruch and Sass, 1978), variable Bouguer gravity anomalies (Eaton and others, 1978),

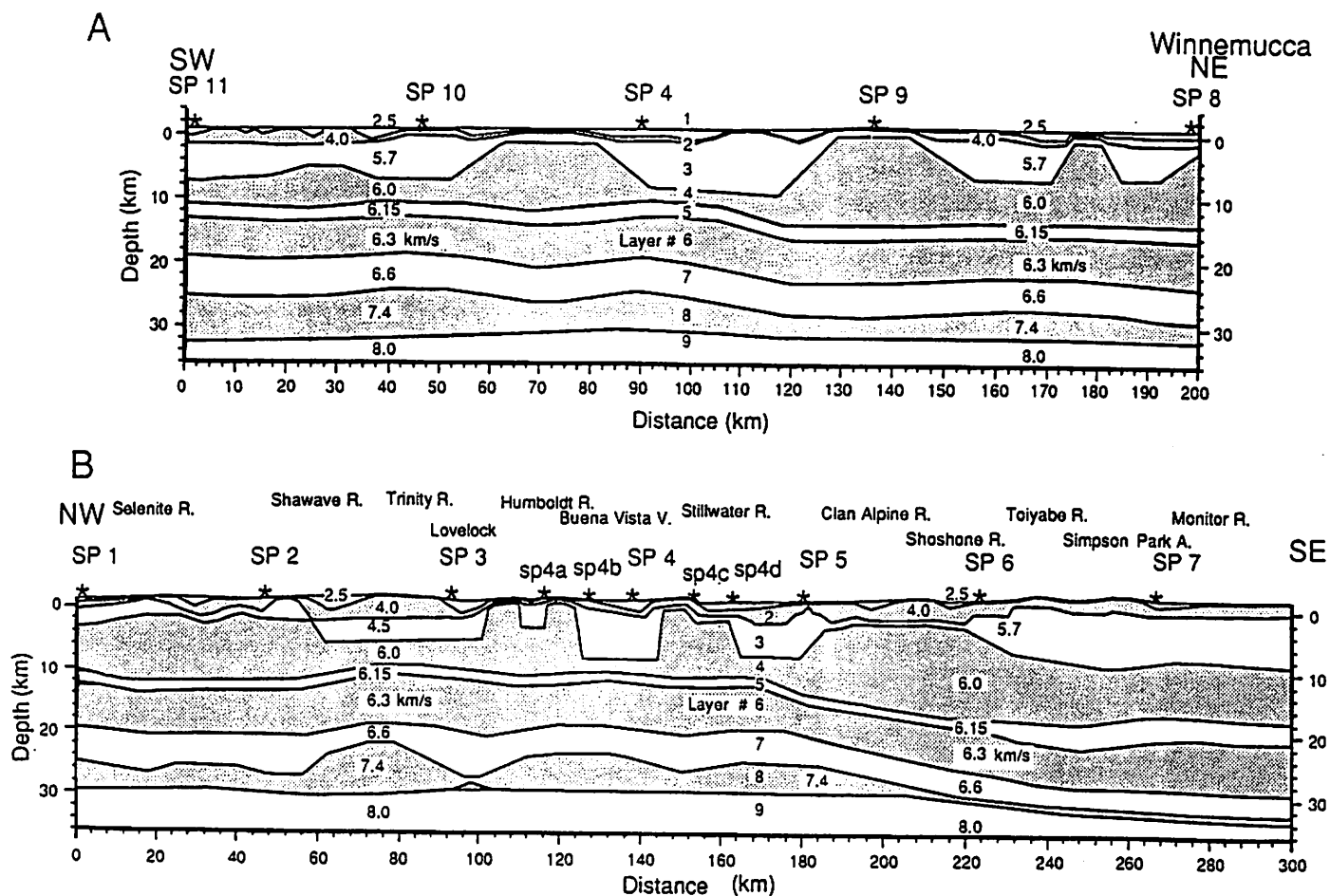


Figure 2. Seismic velocity models of Catchings and Mooney (1991) for the seismic refraction lines shown in Figure 1. Depth is relative to sea level, and velocities are in km/s.

and Quaternary volcanism (Stewart and Carlson, 1978). Although these anomalies may be considered characteristic of the Great Basin, they are confined primarily to the area near the Lahonton and Bonneville Basins. Central Nevada is characterized by geophysical observations more typical of normal continental crust, including thicker (35–40 km) crust, lower (<60 mW/m²) heat flow, a lack of Quaternary faulting, and normal upper-mantle velocities (7.9+ km/s).

STRUCTURAL/VELOCITY RELATIONS

Velocity models discussed in this paper (Fig. 2) were determined from a large volume of seismic refraction data by employing a two-dimensional raytrace modeling technique; the velocity models then were compared with a variety of geophysical data (see Catchings and Mooney, 1991). Each of the features discussed was traversed by multiple ray paths ($\sim 1,200$ for a 30-km-wide feature). Details on statistical resolving ability are beyond the scope of this paper, but all features discussed here are large enough in scale to be resolved by the refraction data; a limited discussion of resolution is provided by Catchings and Mooney (1991). Velocity models are shown for each of the two profiles of the PASSCAL survey (Fig. 1), but discussions in this paper focus on the northwest-southeast-oriented

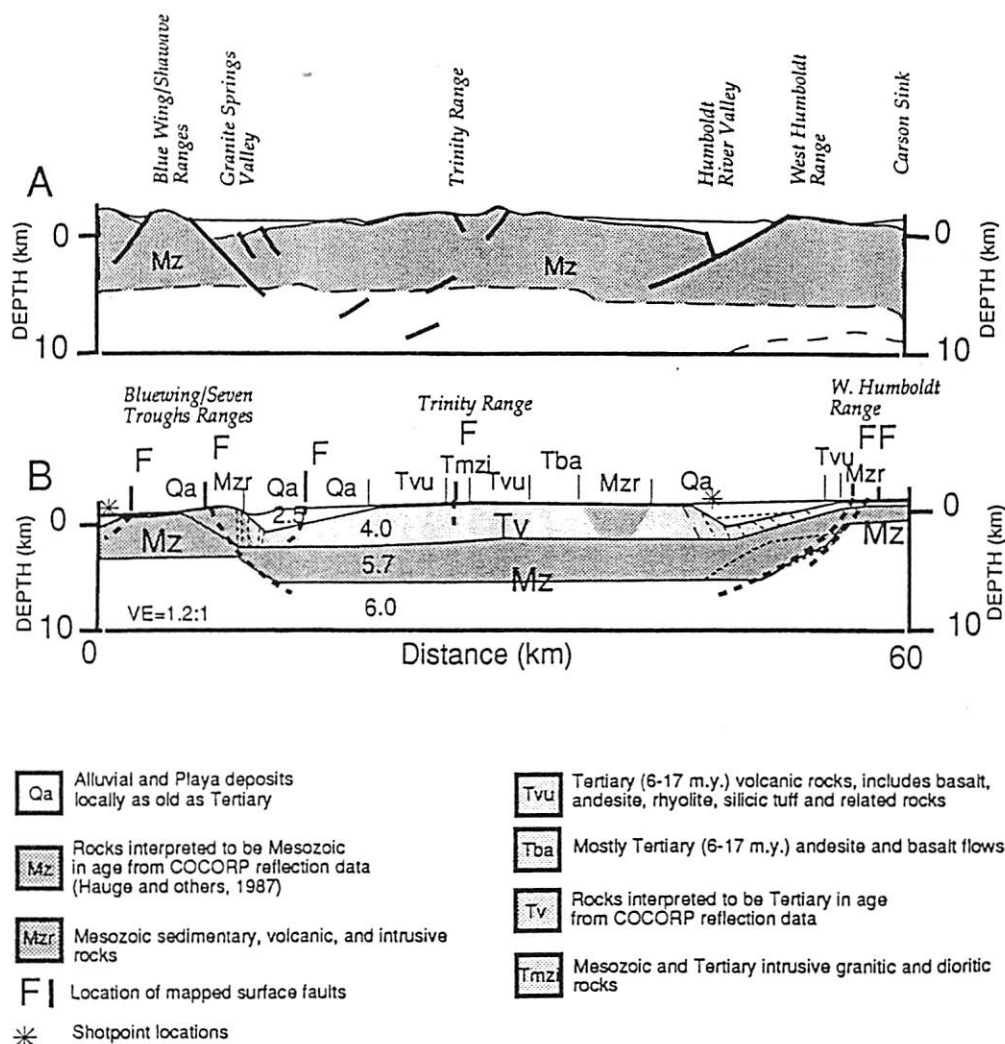
model because that profile crosses many ranges and depicts the regional variation in structure associated with many of the geophysical anomalies of the Basin and Range.

Variations in velocity can be correlated with apparent structural variations at all levels of the crust. At the surface and within the near surface, where comparison of mapped contacts (Stewart and Carlson, 1978) with the velocity data shows that a large velocity contrast exists between the basins (~ 2.5 km/s) and the ranges (~ 4.0 – 6.0 km/s), the correlation between velocity and structure is unambiguous.

There is, furthermore, a difference in velocity between individual ranges according to their age. Within the first few kilometers of the crust, the ranges which are composed of pre-Cenozoic rocks have upper-crustal velocities of ~ 6.0 km/s, whereas the ranges which are composed of Tertiary rocks have upper-crustal velocities of ~ 4.0 – 5.7 km/s (compare Figs. 1 and 2); thus, the older ranges are cored by higher velocity rocks. This correlation between velocity and age is observed for all ranges on each profile and is examined below in conjunction with other geophysical data.

The surface or near-surface correlation between structure and velocity can be made by comparing surface observations with the velocity data, but for the deeper structure, velocity/structural correlations require geophysical methods.

Figure 3. Comparison of independent interpretations of the upper 10 km of the crust along ~ 60 km of COCORP lines 1 and 2 (CC1 and CC2). Bases for interpretations are (A) COCORP seismic reflection images (Hauge and others, 1987) and (B) PASSCAL seismic refraction data (Catchings and Mooney, 1991). The velocity model of part B is a computerized contour model derived from the seismic model of Figure 2B. Although the PASSCAL and COCORP profiles are separated by 5 to 30 km (see Fig. 1), many of the same large-scale features are observed. Subsurface fault dips of the major range-bounding faults are inferred by the projection of dipping velocity contours (Catchings and Mooney, 1991) to the surface. Mapped surface faults (Stewart and Carlson, 1977, 1978) at those surface projections and consistency with COCORP reflection images (Hauge and others, 1987) add support to the interpretation. Note that the ranges cored by Mesozoic rocks are appreciably higher in velocity than those cored by Tertiary rocks, especially the Trinity Range.



Upper Crust

Beneath the surface, structural variations can be characterized by near-vertical reflection images of the crust. Because the PASSCAL transect was near or coincident with several of the COCORP reflection profiles (Allmendinger, 1987), the interpretations of the COCORP data provide a good basis for comparing structural images with velocity variations. Direct comparisons have been made between velocity and apparent structure (Catchings and Mooney, 1991), which was determined from COCORP reflection data (Hauge and others, 1987; Potter and others, 1987) for coincident or nearly coincident reflection and refraction profiles (Figs. 3–6). These correlations in velocity and structure are likely representations of true structures, because the COCORP reflection and the PASSCAL refraction data were independently interpreted with different techniques.

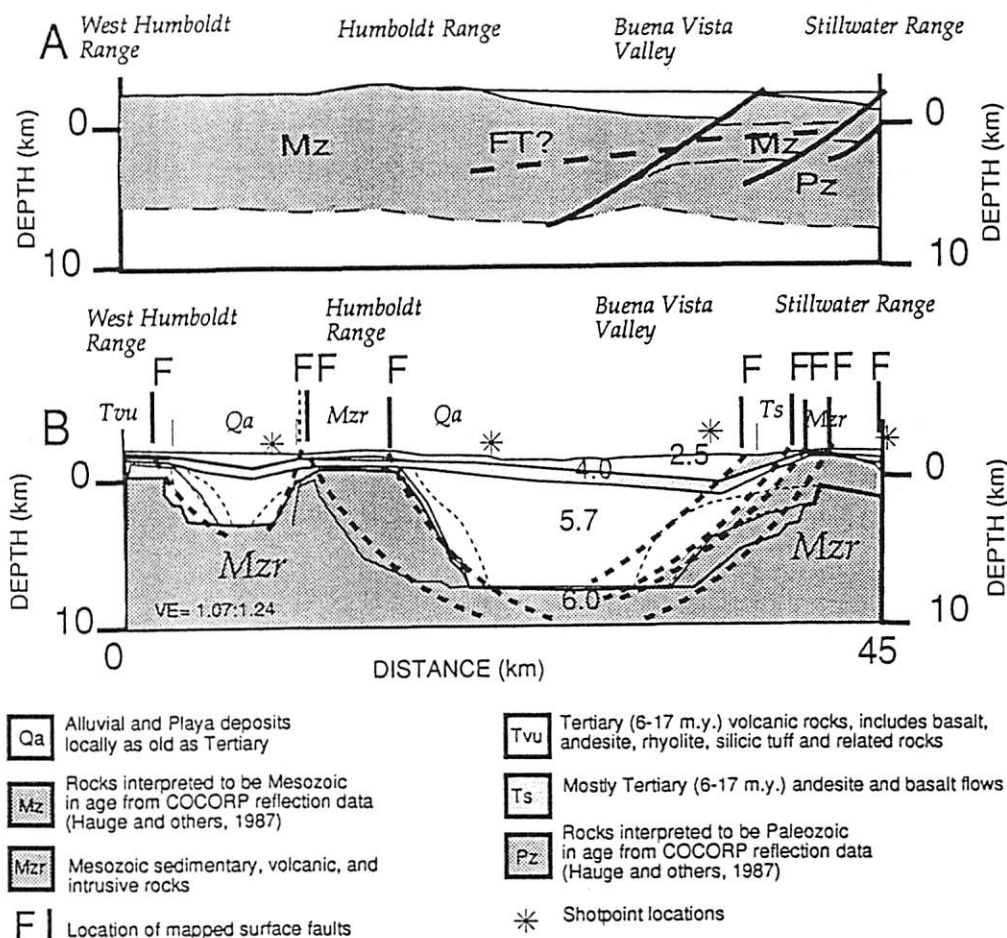
One correlation between structure and velocity discontinuities involves the major range-bounding faults. Large, lateral changes in velocity data coincide with mapped range-bounding faults at the surface (Stewart and Carlson, 1978). The subsurface continuation of the range-bounding faults, as interpreted from COCORP reflection data (Hauge and others, 1987; Potter and others, 1987), coincides with the similarly dipping velocity discontinuities. The faults apparently occur along a velocity discontinuity, and first arrival and second arrival traveltimes are highly sensitive to the dips of velocity discontinuities; thus, both the reflection and refraction data apparently map the major faults with depth (Figs. 3–6). Along COCORP line 1 (Figs. 3A and 3B), such major range-bounding faults are inferred to bound the Bluewing/Shawave/Seven Troughs Ranges and the

West Humboldt Range based on interpretations of COCORP reflection data (Hauge and others, 1987) and PASSCAL refraction data (Catchings and Mooney, 1991). The upper 3 km of the crust between the range-bounding faults contain low-velocity (4.0 km/s) rocks, with a higher velocity (5.7 km/s) between 3-km and 7-km depth (Fig. 3). Both of these velocities are low relative to the velocity beneath the adjacent ranges (6.0 km/s).

In our model, along COCORP line 2, the variation in the depth of the 5.7/6.0 km/s discontinuity closely follows the trend of the faults interpreted by Hauge and others (1987) to bound the Stillwater Range (Fig. 4A). The PASSCAL refraction model, however, implies that a similar east-dipping fault bounds the West Humboldt Range, based on the variation in the 5.7/6.0 km/s velocity discontinuity (Fig. 4B). Where this velocity discontinuity projects to the surface, a major east-dipping fault is mapped (Stewart and Carlson, 1978).

Along the segment of our model that coincides with COCORP line 3 (Fig. 5A), a complex array of faults was inferred from reflection data (Hauge and others, 1987), and the PASSCAL refraction data show that the velocity beneath the valleys is much lower (5.7 km/s) than that beneath the ranges (6.0 km/s) at similar depths (Fig. 5B). A major bounding velocity discontinuity, coinciding with what Hauge and others (1987) referred to as the "Golconda Thrust," is approximately consistent in geometry with the velocity discontinuities of our seismic model, and the base of their interpreted Mesozoic section correlates with a velocity discontinuity between the 4.0 km/s layer and the 5.7 km/s layer. Fewer velocity discontinuities, however, are in the refraction model than major faults

Figure 4. Comparison of independent interpretations of the upper-crustal structure along ~50 km of COCORP line 2 (CC2). The two profiles largely coincide (see Fig. 1). Bases for the interpretations of the upper 10 km of the crust are (A) COCORP seismic reflection images (Hauge and others, 1987) and (B) PASSCAL seismic refraction data (Catchings and Mooney, 1991) as described in Figure 3. Velocity contours in the PASSCAL model correlate geographically with mapped (Stewart and Carlson, 1977, 1978) surface faults (see Fig. 1), and interpreted faulting of the COCORP model.



inferred by Hauge and others (1987), perhaps owing to differences in resolution of the two methods.

Another apparent difference between structures determined from reflection and refraction data along COCORP line 3 involves a high-velocity body in the shallow crust. The refraction data reveal a high-velocity body (the top of the 5.7 km/s layer) in the shallow subsurface beneath the Clan Alpine Range. In the 2-D view, this feature is conical in shape and coincides with a magnetic high (Blakely, 1988) and a gravity high (Saltus, 1988), suggesting that it may be a mafic intrusive body. This feature, however, lacks a corresponding reflection image. The absence of a reflection image of the high-velocity body may indicate that the velocity discontinuity associated with this body is gradational.

COCORP line 7 coincides with the PASSCAL transect west of the Toiyabe Range, and close correlations are evident between structures interpreted by Potter and others (1987) from the COCORP reflection data (Fig. 6A) and those determined from PASSCAL refraction data (Fig. 6B). A major east-dipping fault, bounding the eastern Shoshone Mountains and extending beneath the Reese River Valley (Potter and others, 1987), coincides with the 5.7/6.0 km/s velocity boundary of the refraction model. The feature that Potter and others (1987) tentatively identified as the

Roberts Mountain Thrust coincides with the 4.0/5.7 km/s discontinuity of the seismic refraction model. The fault bounding the Toiyabe Range is also similarly determined by the two data sets, but east of the Toiyabe Range, different structures are imaged because the two profiles are not coincident (see Fig. 1).

Middle Crust

Less structural complexity exists in the middle crust than in the upper crust (6.15 and 6.3 km/s layers). The middle crust is marked on reflection sections by a sudden onset of highly reflective crust (Fig. 7A) at about 4 sec two-way traveltime (TWTT) (~11–12 km depth). This reflectivity continues to the Moho but varies in strength with depth. The onset of reflectivity corresponds to a small positive change in the average velocity from ~6.0 to 6.15 km/s (compare Figs. 7A and 8B) and is reflective at wide angles in the refraction profiles. A similar change in average velocity and sudden increase in reflectivity has been observed in a deep borehole elsewhere in the Basin and Range (Goodwin and Thompson, 1988). At 40°N, both the COCORP data and the PASSCAL model show lateral variations in the depth to the highly reflective zone. As a result of uncor-

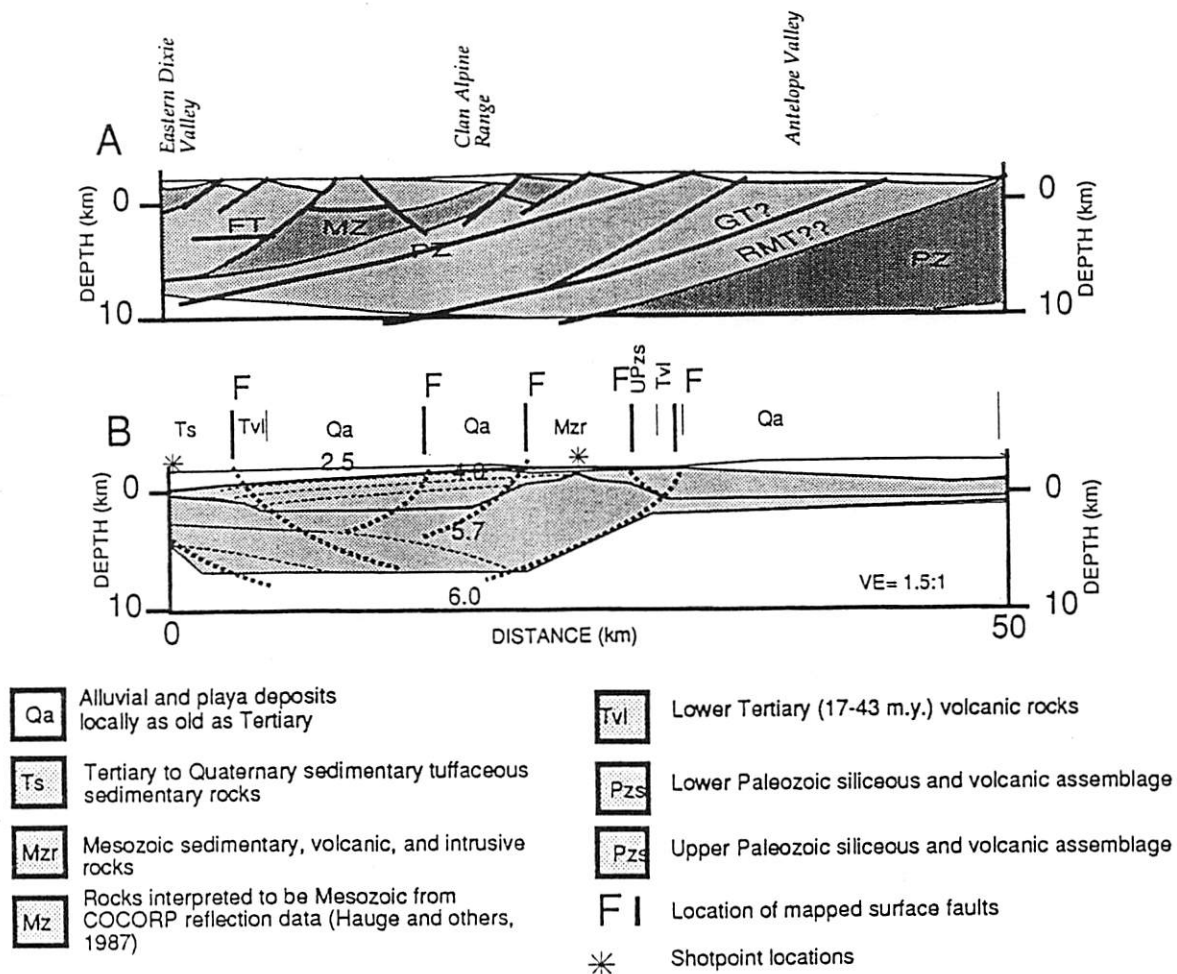


Figure 5. Comparison of independent interpretations of the upper-crustal structure along ~40 km of COCORP line 3 (CC3). The two profiles largely coincide (see Fig. 1). Bases for interpretations of the upper 10 km of the crust are (A) COCORP seismic reflection images (Hauge and others, 1987) and (B) PASSCAL seismic refraction data (Catchings and Mooney, 1991) as described in Figure 3. Detail structures are not consistent between the two models, but the overall variation in structure is similar with respect to (1) the dip of interpreted contacts between major faulted units and (2) the lower velocity of highly faulted units.

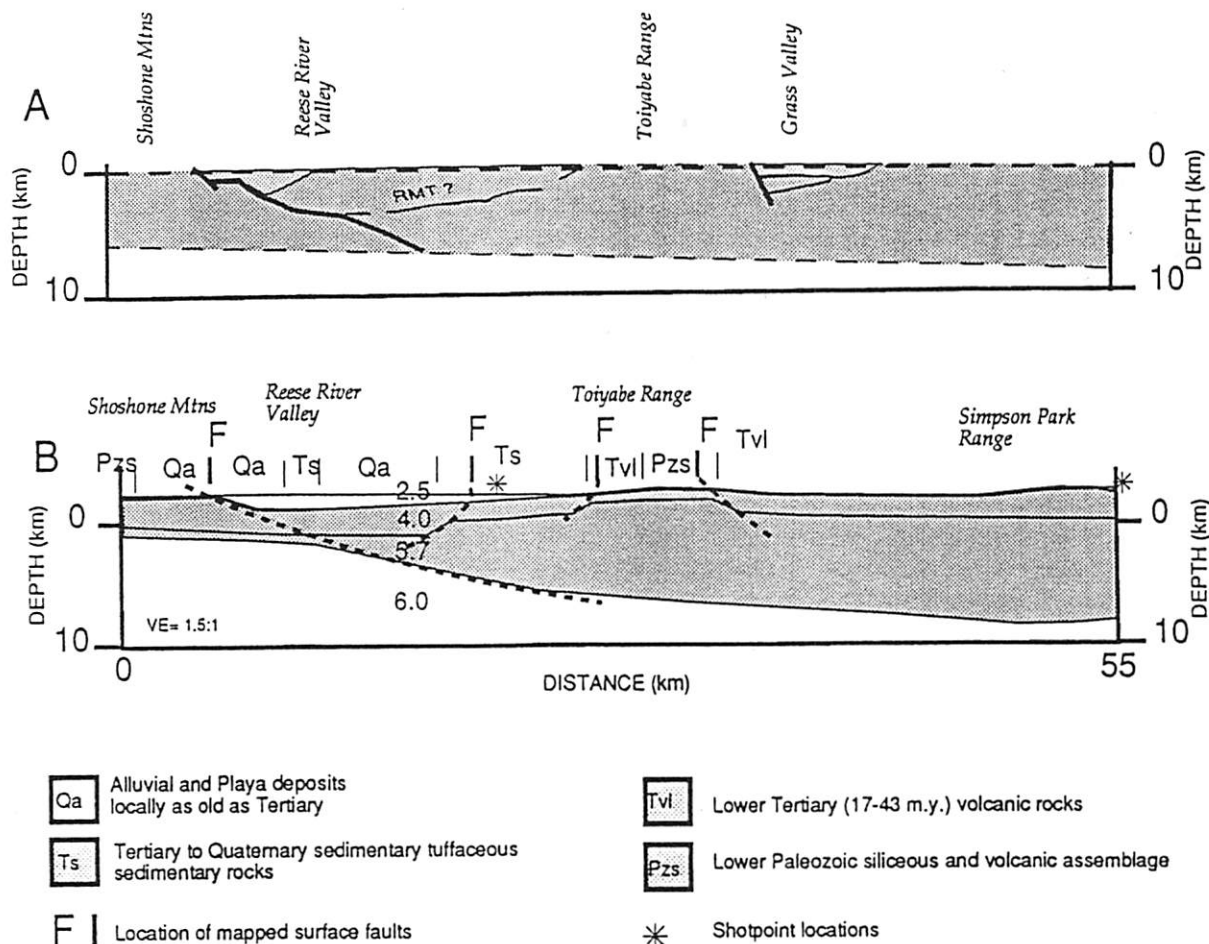


Figure 6. Comparison of independent interpretations of the upper-crustal structure along ~50 km of COCORP line 7 (CC7). The two profiles largely coincide except east of the Toiyabe Range (see Fig. 1). Bases for interpretations of the upper 10 km of the crust are (A) COCORP seismic reflection images (Potter and others, 1987) and (B) PASSCAL seismic refraction data (Catching and Mooney, 1991) as described in Figure 3. The COCORP model does not include the structure above sea level, whereas elevation above sea level is included in the PASSCAL model. Mapped surface faults (Stewart and Carlson, 1977, 1978) coincide with subsurface velocity discontinuities and reflection images described in the text.

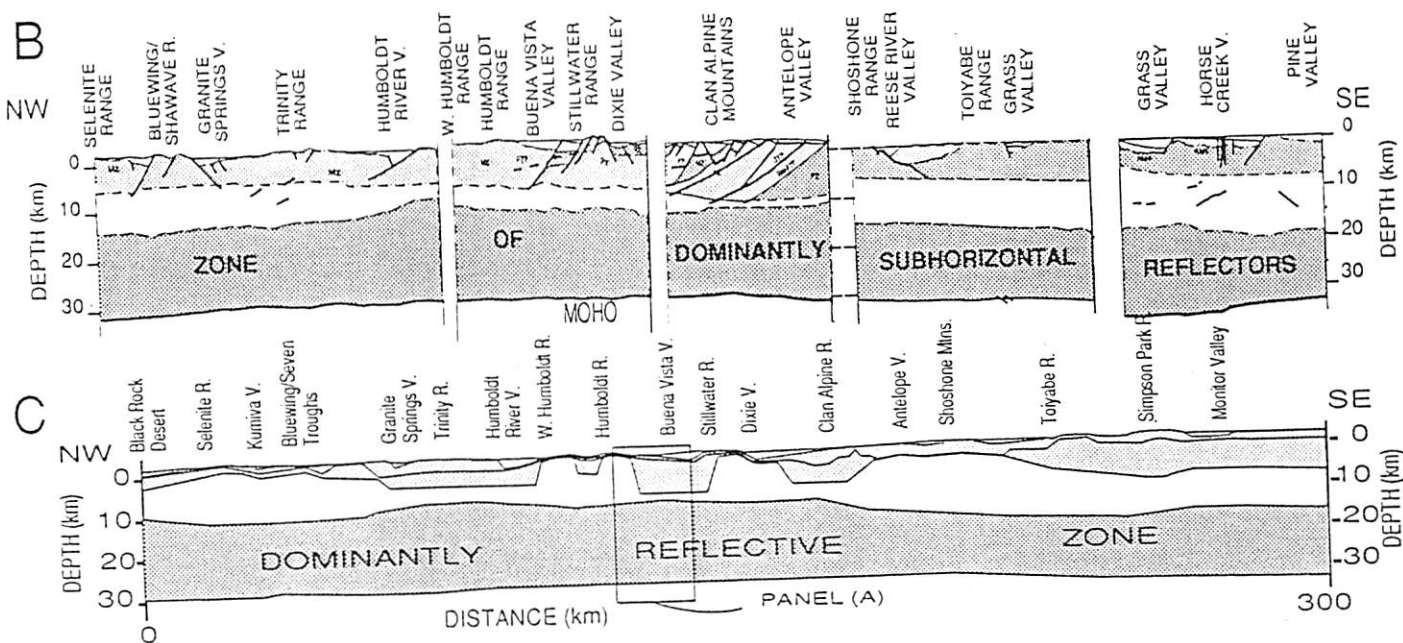
rected velocity variations in the upper few kilometers beneath the Trinity Range, however, the reflection images appear slightly shallower than the refraction model indicates. Nevertheless, the long-wavelength pattern of the highly reflective crust that is shallow (~12 km) near the center of the PASSCAL transect and deeper (~20 km) near the ends of the transect (Fig. 7C) is consistent in the two independently developed models.

By examining the thickness of individual layers (Figs. 7 and 8), a pattern of crustal thinning is apparent. Near the center of the transect, the maximum depth to the base of the middle crust (6.3 km/s layer) is about 20 km (~6 s), but to the east and west, the base of this layer increases in depth to about 32 km (~10 s). Although the entire middle crust thickens slightly to the east and west, the 6.3 km/s layer (base of the middle crust) maintains approximately the same thickness over the entire transect. This observation suggests that crustal thinning over the central part of the transect appears to be largely accomplished by a reduction in the thickness of the upper crust (layers with velocities less than 6.15 km/s), assuming that the crust was at a constant thickness across the transect prior to extension.

Lower Crust

Independent observations of the lower crust (6.6 and 7.4 km/s layers) can also be compared with the reflectivity pattern and the velocity structure. Line drawings from the COCORP reflection data (Klemperer and others, 1986) show considerable complexity in the lower crust (Fig. 8A), but the origin of these reflectors and their relation to differing rock types are unclear. By superimposing the TWTT representation of the refraction model on the reflectivity pattern (Fig. 8B), however, several observations are apparent. (1) The highly reflective lower crust varies laterally in thickness, and the changes in thickness correlate with thickening and thinning of the lower-crustal layers derived from the refraction data. The velocity/reflectivity correlation is particularly noticeable beneath the Trinity Range, where a thick zone of reflective crust correlates with the thickened 7.4 km/s layer. (2) The lateral variation in thickness of the lower crust is mirrored in the uppermost crust, where velocity depressions (5.7 km/s) overlie the thickened lower (7.4 km/s) crust (Fig. 2). (3) Each lower-crustal layer has a different average velocity as well as a

Figure 7. Comparison of the middle crust based on velocity variations and reflectivity. (A) Shot gather from a PASSCAL seismic reflection profile coincident with the PASSCAL seismic refraction transect. Above ~4 sec (11–12 km), the crust is largely reflection free, with a sudden onset of reflectivity beneath that depth. (B) Composite drawing of COCORP lines CC1, CC2, CC3, CC6, and CC7. A zone of increased reflectivity is suggested for the middle and lower crust as shown in part A. (C) Northwest-southeast seismic model of Figure 2 determined from PASSCAL refraction data modeling. The box shows the approximate location of the coincident PASSCAL reflection spread; part of the data from that spread is shown in the shot gather of part A. The top of the dominantly reflective zone corresponds to the 4-s onset of reflectivity. Lateral variation in this onset of reflectivity correlates with the 6.15 km/s layer (compare parts B and C with Fig. 8).



different degree of reflectivity, suggesting that individual layers are both physically and compositionally different. One of the most striking observations is that the 6.6 km/s layer is relatively nonreflective, whereas the overlying 6.3 km/s mid-crustal layer and the underlying 7.4 km/s lower-crustal layer are highly reflective (Fig. 8B). The upper mantle (8.0 km/s) is largely reflection free, and the cessation in reflectivity coincides with the refraction-determined Moho.

Lateral Variation

In addition to vertical correlations between velocity and structure, there are lateral variations. In the lower crust, the lateral variations can be seen by comparing structure observed from wide-angle reflection images with independently derived velocity boundaries determined from in-line refraction data (Fig. 9). The wide-angle reflections provide a direct reflec-

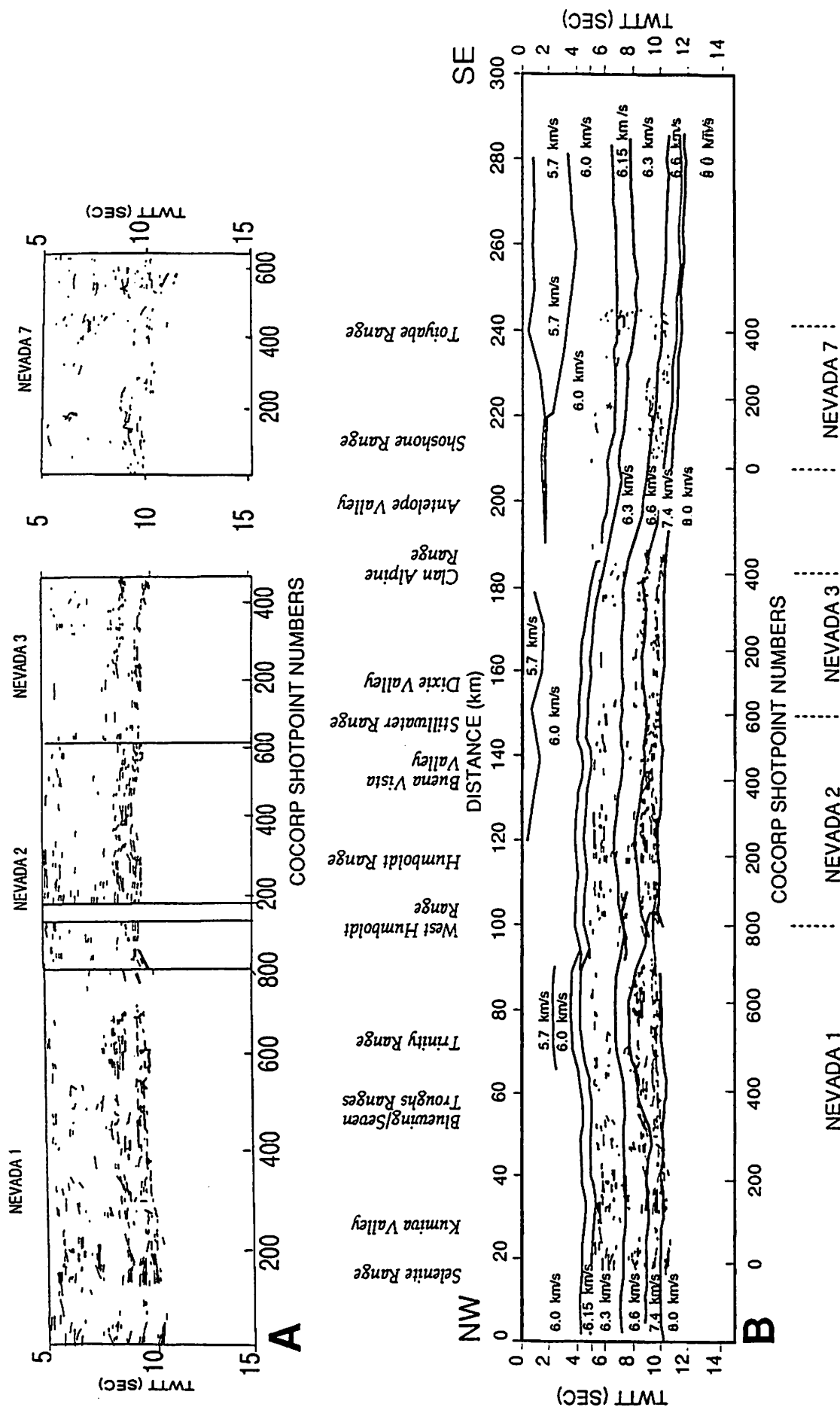


Figure 8. Comparison between lower-crustal reflectivity and velocity discontinuities. (A) Composite of line drawings of middle- and lower-crustal reflections for COCORP lines CC1, CC2, CC3, and CC7 (Klemperer and others, 1986). Where CC1 and CC2 overlap (see Fig. 1), CC2 is closer to the northwest-southeast seismic refraction transect and is used in this figure. (B) Velocity boundaries determined from seismic refraction data for the northwest-southeast transect superposed on the line drawings of part A. Velocity boundaries were converted to a time section by near-vertical raytracing of the refraction model using the datum reported by Allmendinger and others (1986). The variation in reflectivity correlates with the shapes of the velocity boundaries. Variations in the degree of reflectivity correlate with differing velocities.

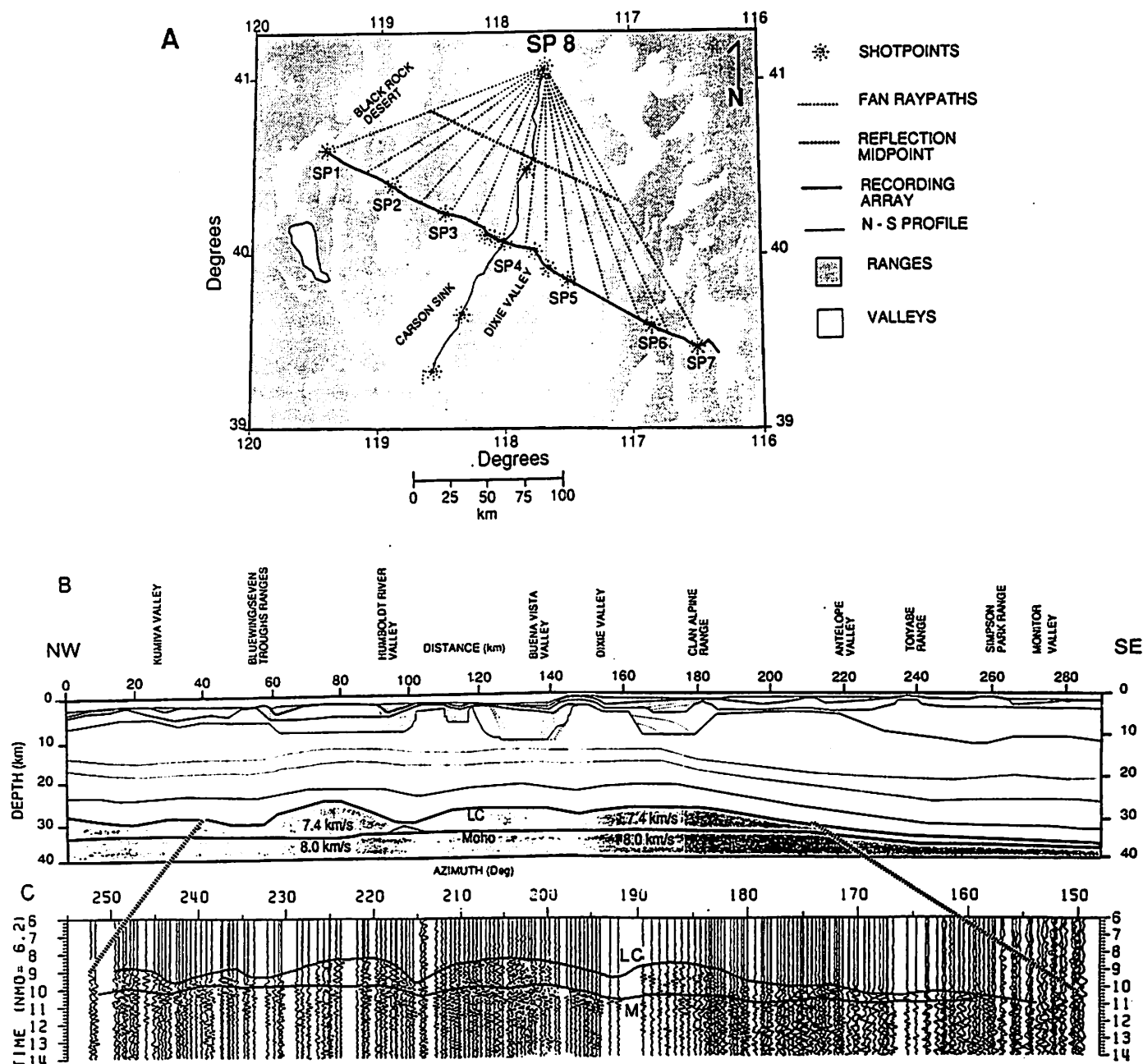


Figure 9. Location map of the PASSCAL experiment showing the configuration of a fan shot. Shots at shotpoint 8 were recorded by the northwest-southeast recording array. The heavy dotted line marks the approximate midpoint from which reflections are presumed to be generated. (B) Contoured seismic profile for the northwest-southeast transect, with the lower crust and upper mantle emphasized (shaded) for comparison with the reflection section of part C. (C) Wide-angle seismic reflection section generated along the midpoint line of part A. The vertical axis is time and the horizontal axis is azimuth. A normal move out (NMO) correction of 6.2 km/s has been applied, but static corrections have not been applied. The dashed lines between parts B and C show the approximate width of the midpoint reflecting line in comparison to the seismic model. The large offset between the shot and receivers permits only deep-crustal and upper-mantle reflectors to be imaged. NMO calculations show that the two reflections correspond to the 7.4 km/s lower crust and the Moho.

tion image of the lower-crustal layers that is similar to the reflectivity shown by line drawings from COCORP data. Each seismic representation of the lower crust and Moho suggests much the same structural variation, where there is appreciable (~5 km) topography on the Moho beneath the central transect and marked thickening of the lower crust beneath central Nevada as the high-velocity lower crust pinches out.

The change in crustal structure from western to central Nevada is not confined to the lower crust. Whereas the velocity and reflectivity data suggest that the crust thickens by only about 5 km from western to central Nevada, the upper crust (<6.15 km/s) thickens by about twice that amount. The combined changes in upper- and lower-crustal structure effectively lower the average velocity of the crust of central Nevada rela-

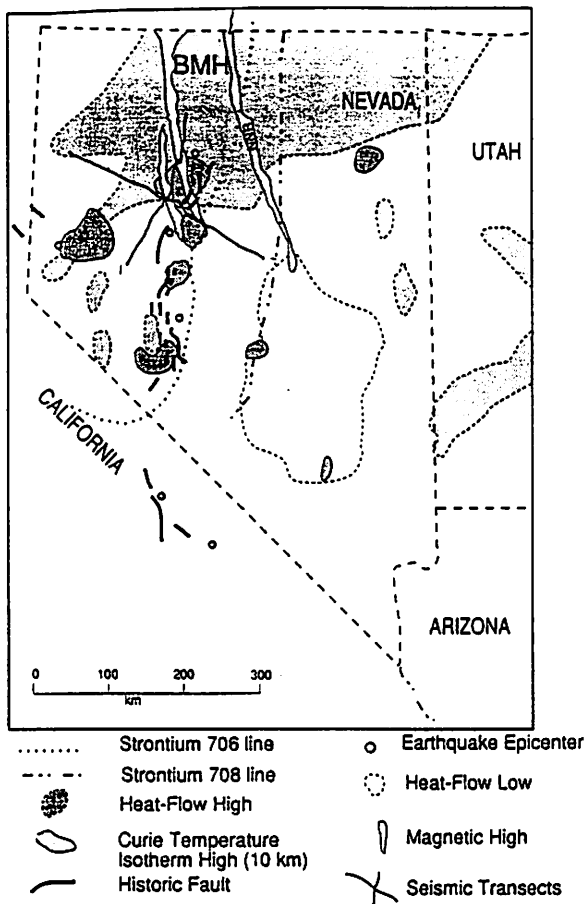


Figure 10. Location of various geological and geophysical anomalies within the state of Nevada. The Battle Mountain heat-flow high (BMH) and Eureka heat-flow low (EL) of Lachenbruch and Sass (1978) are shown in relation to the PASSCAL seismic transects. Curie temperature isotherm high and linear magnetic highs described by Blakely (1988) are also shown. A linear zone of historic fault breaks, recent earthquake epicenters, shallow Curie temperature isotherms, and heat-flow highs trend approximately north-northeast-south-southwest. The strontium 706 line (dotted line; Farmer and DePaolo, 1983) approximately follows the trend of the geophysical anomalies, suggesting that the western extent of the rifted edge of the North American continental margin may be related to present tectonism.

tive to that of western Nevada. The change in velocity structure occurs approximately between 180 km and 240 km along the transect (Fig. 2). The westernmost extent of the North American craton has been identified in this region (Figs. 8 and 10) on the basis of strontium-isotope studies (Farmer and DePaolo, 1983) and geologic studies (Speed, 1982). This change in structure also correlates with a large (~90 mgals) eastward decrease in the Bouguer gravity field in the same general area (Catchings and Mooney, 1991).

EXTENSIONAL FEATURES

Throughout the crustal column, strong correlations exist between velocity and structure. Important questions to be answered are (1) what exactly are these major structures, and (2) how have they formed? An

interpretation of some of the major structures may be made by correlating these observations with other geological and geophysical observations.

Zones of Concentrated Extension

At the surface, an alternation between older (Mesozoic) and younger (Tertiary volcanic) rocks exists from range to range along the western half of the seismic profile (Fig. 1), and this age difference coincides with the 5.7/6.0 km/s interface with depth. For example, where the seismic transect crosses the Selenite Range, the Bluewing Mountains, the Seven Troughs Range, and the West Humboldt Range, the ranges are composed largely of Mesozoic rocks, and the depth to the top of the 6.0 km/s layer is relatively shallow. The Trinity Range and a small area between the West Humboldt and Humboldt Ranges, however, are composed largely of Tertiary rocks, and the depth to the top of the 6.0 km/s layer is relatively great (Figs. 1 and 2B). This same pattern holds for the entire transect; where the transect crosses pre-Cenozoic rocks, the top of the 6.0 km/s interface is relatively shallow, and where the transect crosses Tertiary or younger rocks, the top of the 6.0 km/s layer is relatively deep (Figs. 1 and 2B).

The difference in upper-crustal velocity (0.3 km/s) between ranges cored by Mesozoic and Tertiary rocks may be caused by (1) a difference in composition between the Mesozoic and Tertiary rocks, (2) a difference in the intensity of faulting and fracturing of the silicic upper crust, or (3) a combination of the two. I suggest that faulting and fracturing may be the predominant cause, because these are the velocities that correspond to fractured (5.7 km/s) and nonfractured (6.0 km/s) granitic rocks at those depths (Nur and Simmons, 1969; Stierman, 1977). Such laterally varying fracture zones (5.7 km/s) may define local zones where extension is concentrated, and the unbroken rock masses (6.0 km/s) may correspond to zones of the crust where much less extension takes place.

Along the central and western part of the transect, a lateral variation in the intensity of faulting and fracturing of the upper crust is also implied by the present-day seismicity pattern, where most of the earthquakes are confined to the basins rather than the ranges (Fig. 1). Such a geographic distribution of seismicity suggests that deformation is more concentrated beneath the basins to depths of 12 km. Correspondingly, these basins are underlain by a thick 5.7 km/s layer (Fig. 11). Although the velocity-age correlation may result entirely from compositional differences, it is equally possible that the Tertiary volcanic rocks overlie a thick 5.7 km/s layer only because such faulted and fractured zones have provided a more accessible path for magma and volcanics to migrate through the crust.

Concentrated zones of extension may also be indicated by the lowermost crustal layer. Although there are other possibilities, the velocity of this layer is consistent with the velocity of magmatic rocks of basaltic composition that have been underplated to the base of the crust (Furlong and Fountain, 1986). In addition, the observation that this layer is thickest directly beneath the thick 5.7 km/s (highly fractured?) zones suggests that such concentrated extension affects the entire crustal column. Because the surface Tertiary volcanic deposits are concentrated above the 5.7 km/s (highly fractured?) and 7.4 km/s (magmatically underplated?) zones, the present crustal structure is consistent with a model where the volcanic rocks originated from the lower-crustal magma and migrated to the surface via the highly fractured zones of the crust.

The upper-crustal (5.7 km/s) velocity depressions are similar to those in a model presented by Okaya (1985). He concluded that Buena Vista Valley and Dixie Valley are underlain by highly broken rock masses to appreciable (20-km) depths, and the Stillwater Range is largely a solid rock mass (Fig. 12). Such a model, developed from geologic reasoning, accounts nicely for the large difference in velocity between the upper crust

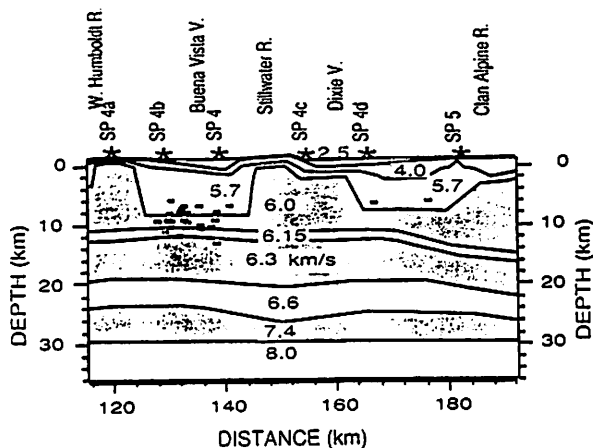


Figure 11. Plot of the best located earthquakes (Ryall and Vetter, 1982) within 50 km of the center of the northwest-southeast seismic transect projected onto the seismic model. The seismicity that projects onto the seismic model beneath Buena Vista Valley actually occurs within the southern part of Dixie Valley; however, because of the northeast trend of Dixie Valley, northward projection places it beneath Buena Vista Valley (see Fig. 1). Nevertheless, the earthquakes are largely confined to, or immediately beneath, the 5.7 km/s velocity depression and are largely confined to the valleys.

beneath Stillwater Range (6.0 km/s) and that beneath the adjacent valleys (5.7 km/s).

Okaya's model and our velocity model, however, differ in the depth of apparent brittle faulting. Whereas his model suggests that faulting may exist to depths of ~20 km, the interpreted sections from reflection (COCORP) data (Hauge and others, 1987) and the velocity variations from the PASSCAL refraction data suggest that range-bounding faults do not extend to depths below ~10–12 km near the center of the profiles

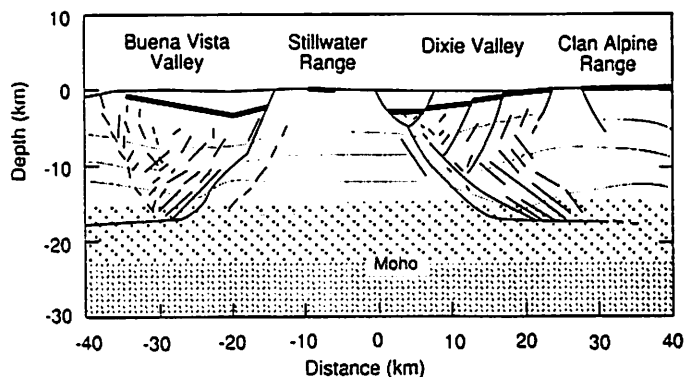


Figure 12. Okaya's (1985) model of deformation, which is approximately coincident with the segment of the northwest-southeast profile shown in Figure 11. Okaya's model is derived from independent seismic reflection and gravity and geological data; the model shows the Stillwater Range to be composed of a fairly solid block, whereas the adjacent valleys are highly faulted and fractured down to depths of about 15–20 km. These structures are consistent with the PASSCAL velocity model and seismicity data.

(Figs. 3–6). According to the COCORP data, these faults flatten with depth and the refraction data do not reveal lateral velocity variations indicative of faulting below ~10-km depth. Furthermore, earthquakes in areas near the seismic profile (Fig. 12) do not extend deeper than ~12 km (Ryall and Vetter, 1982).

If the 5.7 km/s velocity depressions are zones of concentrated faulting and fracturing and the 7.4 km/s lower crust has been magmatically added to the crust, then the crustal velocity structure implies that the crust as a whole is extending laterally in a boudinage fashion, with lateral pinches and swells (Fig. 13).

A DISCRETE WESTERN NEVADA RIFT ZONE

Geophysical anomalies associated with active rift zones include high heat flow; active seismicity; velocity anomalies within the lower crust; historic fault breaks; and high-amplitude, short-wavelength Bouguer gravity anomalies (such anomalies are concentrated along a north-northeast-trending, linear zone along the eastern edge of the Lahonton depression; see Figs. 1 and 10). Individually, these geophysical anomalies are not necessarily indicative of rifting, but combined with other geological and geophysical observations, they suggest that northern Basin and Range extension is presently concentrated along this narrow zone.

Of particular importance to the rift interpretation presented here are new aeromagnetic data that address the temperature characteristics of the crust. Blakely (1988) determined that shallow, high-temperature anomalies are concentrated in the upper crust along the north-northeast-trending zone (Fig. 10), and recent seismic investigations (Catchings and Mooney, 1991; Jarchow, 1991; K. F. Priestley, 1988, personal commun.) show strong seismic attenuation and reflection bright spots, indicative of lower-crustal and upper-mantle partial melts along this north-northeast-trending zone.

Strain rates and the direction of extension (Eddington and others, 1987), combined with the geophysical anomalies, suggest that the Basin and Range is presently extending at a higher rate within the north-northeast-trending zone than within any other area of the Basin and Range. By contrast, central Nevada is characterized by more normal geophysical anomalies.

Recent geophysical investigations (Catchings, 1987; Blakely, 1988; Thompson and others, 1989; Catchings and Mooney, 1991) show anomalies that may extend as far south as the 39°N parallel, suggesting a minimum length of about 300 km for the inferred rift zone. The 300-km length compares favorably with active segments of some other rift zones, including the Rhinegraben and the Rio Grande Rift.

GEOLOGIC MODEL

Composition of the Crust

Although rock type–velocity associations are not unique, gross compositions of crustal layers can be estimated on the basis of velocity, depth (that is, pressure), temperature data, and laboratory measurements (Christensen, 1979, 1982). Alternative interpretations have been published by Benz and others (1990), Hawman and others (1990), and Holbrook (1990).

Rock types for the surface ranges are observable from geologic mapping (Fig. 1), where metasedimentary and volcanic rocks are abundant at the surface and undoubtedly present within the first few kilometers of the surface. The Tertiary volcanic rocks have a velocity of ~4.0 km/s. Upper-crustal crystalline rocks (5.7–6.15 km/s) are likely in the felsic range of

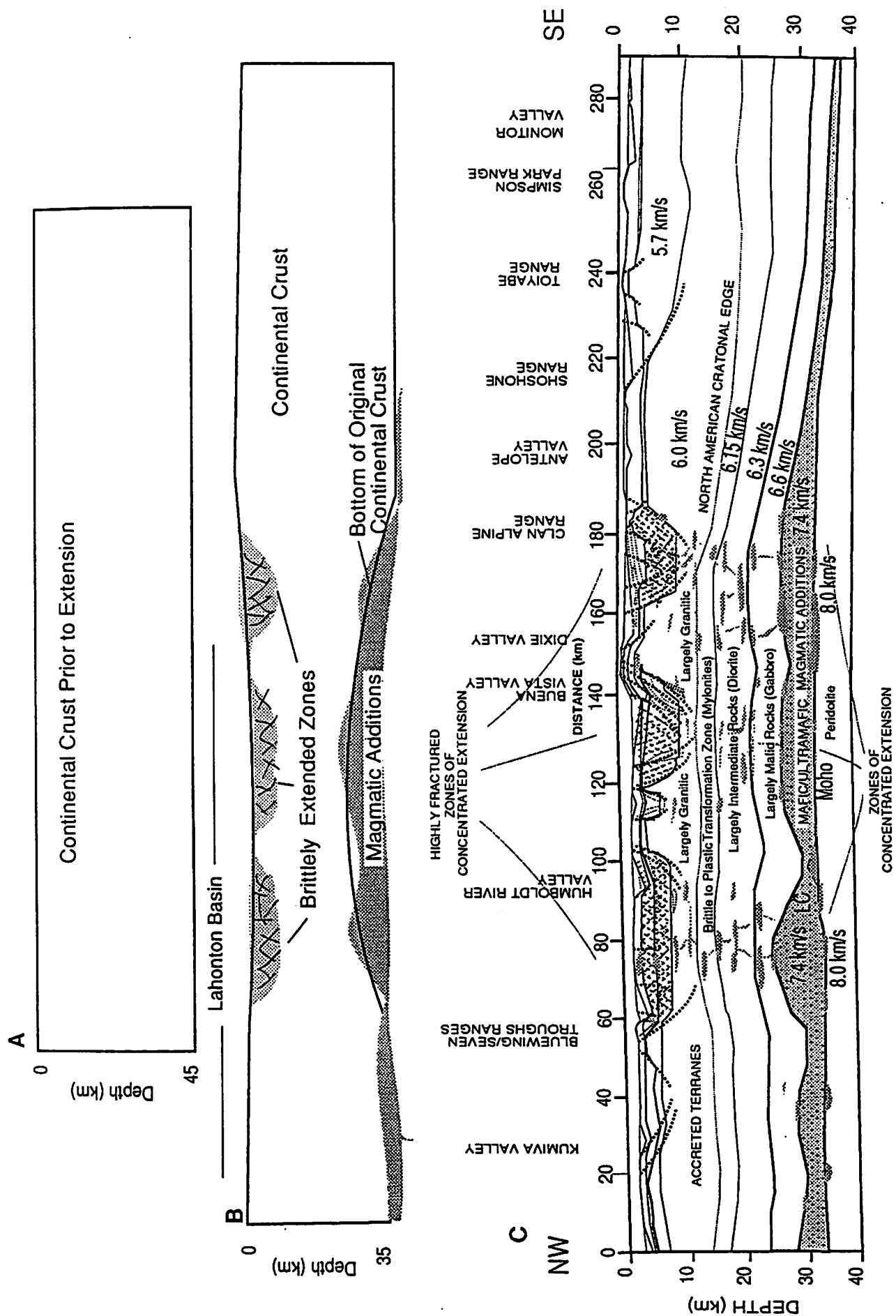


Figure 13. Model of crustal extension for the Nevada region. (A) Hypothetical model of uniform crustal thickness prior to extension. (B) The hypothetical model of part A after extension, with magmatic additions at the base of the crust and brittlely deformed upper crust. The extended crust deforms in a boudinage fashion at a minimum of two wavelengths, an overall long wavelength (solid line) and a shorter wavelength (shaded pattern). The original continental crust is in white. (C) A geological interpretation of the seismic model of Catchings and Mooney (1991). The original crust deforms in a boudinage fashion with brittle deformation zones in the upper crust, underlain by thinned and underplated zones in the lower crust. The original crust (in white) has the appearance of a series of pinches and swells as in part B.



compositions, as inferred from petrologic and isotopic data from central Nevada (Barton and Trim, 1990). The 5.7 km/s velocity is that expected of granitic rocks which are highly fractured and faulted, and the 6.15 km/s velocity is common for unbroken granitic rocks at depths (10 km) with equivalent pressures of 3 kbar (Nur and Simmons, 1969; Christensen, 1979, 1982).

Given the high (90 mW/m³) heat flow (Lachenbruch and Sass, 1978) and velocities as high as 6.3 km/s in the middle crust, it is likely that rocks of the middle crust are more basic in composition than those of the upper crust, because at similar depths, basic rocks are typically higher in velocity than are felsic rocks (Christensen, 1979, 1982). I suggest that the gross composition of the middle crust is in the diorite range and that the metamorphic grade is in the amphibolite facies (500–700 °C and 6–8 kbar). Lower-crustal rocks (6.6 km/s to 7.4 km/s) are likely in the mafic to ultramafic range of compositions because their velocities are relatively high given the likely thermal (estimated to be ~700–1200 °C), and pressure (granulite to pyroxene-hornfels facies at 8–10 kbar) conditions. Such high-temperature conditions in the lower crust/upper mantle are consistent with evidence of partial melts (Jarchow, 1991; Catchings and Mooney, 1991) beneath the central part of the seismic profile.

Upper-mantle rocks (8.0 km/s) are likely composed of peridotite and other ultramafic rocks, and the measured velocity is that expected for upper-mantle, high-temperature (1000–1200 °C) Basin and Range rocks (Furlong and Fountain, 1986).

Nature of Crustal Boundaries

The velocity and structural data indicate that the crust is layered with differing rock types. At the surface, the contacts between the differing rock types are typically sharp and sometimes fault bounded; little is known about the nature of contacts in the middle and lower crust. The seismic data, however, do provide information about the nature of the contacts based on boundary conditions necessary to yield reflections.

Seismic energy is reflected or transmitted depending on the impedance contrast between layers and the wavelength of the seismic energy. For example, seismic energy with sonic frequencies (short wavelengths) would not detect a velocity boundary that is 100 m thick, because the energy would pass through the thick boundary without detecting it; if the boundary were 0.01 m thick, however, the sonic energy would be reflected. This same principle can be used to place limits on the thickness of the velocity boundaries in the lower crust and at the Moho.

Because the recorded signals from wide-angle and near-vertical reflections differ in frequency and both types of data are available for the study area, the reflected signals can be compared. For example, the boundary between the 6.3 and the 6.6 km/s layers and Moho is highly reflective in the low-frequency (~5 Hz), wide-angle reflection/refraction data (Fig. 9C; see Catchings and Mooney, 1991) but is largely nonreflective in the higher-frequency (~20 Hz), near-vertical, PASSCAL and COCORP reflection data (Figs. 7A and 8B). The variation in the reflectivity of these discontinuities suggests that they are gradational at the wavelengths (0.25 km) of the near-vertical reflection data but are rather abrupt discontinuities at the wavelengths (~1 km) of wide-angle data. Assuming a one-fourth wavelength criteria in order to produce a reflection, these discontinuities are probably between 60 m and 250 m thick. Individual reflecting boundaries which give rise to the near-vertical reflectivity are clearly much thinner, but the overall change from one dominant velocity to another apparently occurs over many tens of meters. Jarchow (1991) concluded that some of the lower-crustal reflections are prominent in data with frequencies as high as 70 Hz, suggesting that some of the reflecting boundaries within velocity layers are as thin as 20–25 m.

DISCUSSION AND CONCLUSIONS

The crustal structure of the Basin and Range has been shaped by a number of tectonic events, including pre-Cenozoic extension, shortening, and volcanism. Each event has influenced the present crustal composition and structure.

Evidence of a Proterozoic rifting may include the apparent change in the crustal thickness and velocity from western to central Nevada (Fig. 13). The thickness of the crust (37 km) along the rifted cratonal edge of central Nevada is consistent with that of many continental areas and continental margins (Prodehl, 1984), and the uppermost-mantle velocity (8.0 km/s) is approximately that of the worldwide average (Prodehl, 1984). By contrast, the crustal thickness (32 km) of the accreted terrains in western Nevada (within the Lahonton Basin) is less than that of typical continental crust, and the velocity of the lowermost crust (7.4 km/s) is higher than normal (6.8–7.0 km/s) continental crust (Prodehl, 1984). Beneath the Lahonton Basin, ~4–7 km of the lower crust may have been added by magmatic underplating, and the original crust may now be only ~25–28 km thick.

It is difficult to ascertain whether the difference in crustal structure results from extension of the crust or a difference between accreted crust and the cratonal edge. At the surface, however, extension has clearly been the predominant feature shaping the crust, as indicated by mapped extensional faulting. In the subsurface, a coincidence of seismicity, surface volcanic rocks, and velocity anomalies in laterally discrete zones is consistent with extension as the predominant post-Tertiary tectonic force shaping the crustal structure.

The Lahonton Basin area continues to experience more extension than does the rest of the Basin and Range, as shown by historic faulting, high strain rates, and thin crust. The velocity structure of the Lahonton Basin area is much like that observed beneath many other continental rift zones, suggesting that a north-northeast-trending zone along the Lahonton Basin forms a discrete spreading zone. High heat flow, partial melting in the lower crust, and mafic/ultramafic lower crust are consistent with rifting along the north-northeast-trending zone.

Extension, accretion, and volcanism have produced a crust which is largely felsic in composition in the upper 10–12 km, intermediate in composition from 12–25 km, and mafic to ultramafic from 25–32 km in western Nevada. In central Nevada, however, the crust appears largely felsic in the upper 20 km, intermediate from 20–32 km, and mafic from

32–37 km. Extension may have been accommodated in western Nevada by a reduction in the thickness of the upper crust and magmatic underplating in the lower crust. The differences in crustal structure between western Nevada and central Nevada occur in an area determined by isotopic measurements to be the rifted edge of the North American craton.

ACKNOWLEDGMENTS

Reviews from and discussions with Rick Blakely, Walter Mooney, Gary Fuis, Marian McGee, G. Randy Keller, Robert Hawman, A. G. Sylvester, Bob Smith, and Jill McCarthy are greatly appreciated. Thanks to Martha Savage for providing the seismicity data.

REFERENCES CITED

- Allmendinger, R. W., Hauge, T. A., Hauser, E. C., Potter, C. J., Klempner, S. L., Nelson, K. D., Kneuper, P., and Oliver, J., 1987, Overview of the COCORP 40°N transect, western United States: The fabric of an orogenic belt: *Geological Society of America Bulletin*, v. 98, p. 308–319.
- Barton, M. D., and Tripp, H. E., 1991, Late Cretaceous two-mica granites and lithophile-element mineralization in the Great Basin, in Raines, G. L., Lisle, R. E., Schafer, R. W., and Wilkinson, W. H., eds., *Geology and Ore Deposits of the Great Basin Symposium*, Proceedings: Reno, Nevada, Geological Society of Nevada, p. 529–538.
- Benz, H. M., Smith, R. B., and Mooney, W. D., 1990, Crustal structure of northwestern Basin and Range province from the 1986 Program for Array Seismic Studies of the Continental Lithosphere seismic experiment: *Journal of Geophysical Research*, v. 95, p. 21823–21842.
- Blakely, R. J., 1988, Curie temperature isotherm analysis and tectonic implications of aeromagnetic data from Nevada: *Journal of Geophysical Research*, v. 93, p. 11817–11832.
- Burchfiel, B. C., and Davis, G. A., 1972, Structural framework and evolution of the southern part of the Cordilleran orogen, western United States: *American Journal of Science*, v. 272, p. 97–118.
- Catchings, R. D., 1987, Crustal structure of the northwestern United States [Ph.D. thesis]: Stanford, California, Stanford University, 186 p.
- Catchings, R. D., and Mooney, W. D., 1991, Basin and Range crustal and upper mantle structure, northwest to central Nevada: *Journal of Geophysical Research*, v. 96, p. 6247–6267.
- Catchings, R. D., and 14 others, 1988, The 1986 PASSCAL Basin and Range lithospheric seismic experiment: *Eos (American Geophysical Union Transactions)*, v. 69, p. 593–598.
- Christensen, N. I., 1979, Compressional wave velocities in rocks at high temperatures and pressures, critical thermal gradients, and crustal low-velocity zones: *Journal of Geophysical Research*, v. 84, p. 6849–6857.
- , 1982, Seismic velocities, in Carmichael, R. S., ed., *Handbook of physical properties of rocks*, Volume 2: Boca Raton, Florida, CRC Press, p. 1–228.
- Eaton, J. P., 1963, Crustal structure from San Francisco, California, to Eureka, Nevada, from seismic-refraction measurements: *Journal of Geophysical Research*, v. 68, p. 5789–5806.
- Eaton, G. P., Wahl, R. R., Prostka, H. J., Mabey, D. R., and Kleinkopf, M. D., 1978, Regional gravity and tectonic patterns: Their relation to late Cenozoic epeirogeny and lateral spreading in the western Cordillera, in Smith, R. B., and Eaton, G. P., eds., *Cenozoic tectonics and regional geophysics of the western Cordillera*: Boulder, Colorado, Geological Society of America Memoir 152, p. 51–92.
- Eddington, P. J., Smith, R. B., and Renggli, C., 1987, Kinematics of Basin-Range intraplate extension, in Coward, M. P., Dewey, J. F., and Hancock, P. L., eds., *Continental extensional tectonics*: Geological Society of London Special Publication 28, p. 371–392.
- Farmer, G. L., and DePaolo, D. J., 1983, Origin of Mesozoic and Tertiary granite in the western United States and implications for pre-Mesozoic crustal structure: Nd and Sr isotopic studies in the geoclinal of the northern Great Basin: *Journal of Geophysical Research*, v. 88, p. 3379–3401.
- Fletcher, R. C., and Hallet, B., 1983, Unstable extension of the lithosphere: A mechanical model for Basin and Range structure: *Journal of Geophysical Research*, v. 88, p. 7457–7466.
- Furlong, K. P., and Fountain, D. M., 1986, Continental crustal underplating: Thermal considerations and seismic-petrologic consequences: *Journal of Geophysical Research*, v. 91, p. 8285–8294.
- Goodwin, E. B., and Thompson, G. A., 1988, The seismically reflective crust beneath highly extended terranes: Evidence for its origin in extension: *Geological Society of America Bulletin*, v. 100, p. 1616–1626.
- Hauge, T. A., Allmendinger, R. W., Caruso, C., Hauser, E. C., Klempner, S. L., Opdyke, S., Potter, C. J., Sanford, W., Brown, L., Kaufman, S., and Oliver, J., 1987, Crustal structure of western Nevada from COCORP deep seismic-reflection data: *Geological Society of America Bulletin*, v. 98, p. 320–329.
- Hawman, R. B., Colburn, R. H., Walker, D. A., and Smithson, S. B., 1990, Processing and inversion of refraction and wide-angle reflection data from the 1986 Nevada PASSCAL experiment: *Journal of Geophysical Research*, v. 95, p. 4657–4691.
- Holbrook, W. S., 1990, The crustal structure of the northwestern Basin and Range province, Nevada, from wide-angle seismic data: *Journal of Geophysical Research*, v. 95, p. 21843–21869.
- Jarchow, C. M., 1991, Investigations of magmatic underplating beneath the northwestern Basin and Range province, Nevada: seismic data acquisition and tectonic problems of the Columbia Plateau, Washington; and the nature of the Mohorovicic discontinuity worldwide [Ph.D. thesis]: Stanford, California, Stanford University, 258 p.
- Kistler, R. W., 1974, Phanerozoic batholiths in western North America: A summary of some recent work on variations in time, space, chemistry, and isotopic composition: *Earth and Planetary Science Annual Review*, v. 2, p. 403–418.
- Klempner, S. L., Hauge, T. A., Hauser, E. C., Oliver, J. E., and Potter, C. J., 1986, The Moberly in the northern Basin and Range province, Nevada, along the COCORP 40° seismic-reflection transect: *Geological Society of America Bulletin*, v. 97, p. 603–618.
- Lachenbruch, A. H., and Sass, J. H., 1978, Models of an extending lithosphere and heat flow in the Basin and Range province, in Smith, R. B., and Eaton, G. P., eds., *Cenozoic tectonics and regional geophysics of the western Cordillera*: Boulder, Colorado, Geological Society of America Memoir 152, p. 209–250.
- Nur, A., and Simmons, G., 1969, The effect of saturation on velocity in low porosity rocks: *Earth and Planetary Science Letters*, v. 7, p. 183–193.
- Okaya, D. A., 1985, Seismic reflection studies in the Basin and Range province and Panama [Ph.D. thesis]: Stanford, California, Stanford University, 133 p.
- Pakiser, L. C., 1963, Structure of the crust and upper mantle in the western United States: *Journal of Geophysical Research*, v. 68, p. 5747–5756.
- Potter, C. J., Liu, C., Huang, J., Zheng, L., Hauge, T. A., Hauser, E. C., Allmendinger, R. W., Oliver, J. E., Kaufman, S., and Brown, L., 1987, Crustal structure of north-central Nevada: Results from COCORP seismic profiling: *Geological Society of America Bulletin*, v. 98, p. 330–337.
- Priestley, K. F., Ryall, A. S., and Fesie, G. S., 1982, Crust and upper mantle structure in the northwest Basin and Range province: *Seismological Society of America Bulletin*, v. 72, p. 911–923.
- Prodehl, C., 1979, Crustal structures of the western United States: U.S. Geological Survey Professional Paper 1034, p. 74.
- , 1984, Structure of the Earth's crust and upper mantle, in Fuchs, K., and Soffel, H., eds., *Geophysics of the solid Earth, the Moon and the planets*: New York, Springer-Verlag, v. 2, p. 97–206.
- Russell, I. C., 1885, Geological history of Lake Lahontan. A Quaternary lake of northwestern Nevada: U.S. Geological Survey Monograph 11, 288 p.
- Ryall, A. S., and Yetter, U. R., 1982, Seismicity related to geothermal development in Dixie Valley, Nevada: Reno, Nevada, U.S. Department of Energy Contract DE-AC08-79NV 10054 Final Report, University of Nevada.
- Saltus, R. W., 1988, Gravity data for the state of Nevada on magnetic tape, report: Sioux Falls, South Dakota, EROS Data Center.
- Speed, R. C., 1982, Evolution of the sialic margin in the central western United States, in Watkins, J., and Drake, C., eds., *Geology of continental margins*: American Association of Petroleum Geologists Memoir 34, p. 457–486.
- Stewart, J. H., and Carlson, J. E., 1977, Geologic map of Nevada: Reno, Nevada, Nevada Bureau of Mines and Geology Map 57, scale 1:1,000,000.
- , 1978, Geologic map of Nevada: U.S. Geological Survey Miscellaneous Field Studies Map MF-900, scale 1:500,000.
- Stierman, D. J., 1977, A study of stress-dependent velocity variations in situ [Ph.D. thesis]: Stanford, California, Stanford University, 85 p.
- Thompson, G. A., and Burke, D. B., 1974, Regional geophysics of the Basin and Range province: *Earth and Planetary Science Annual Review*, v. 2, p. 213–238.
- Thompson, G. A., Catchings, R., Goodwin, E., Holbrook, S., Jarchow, C., Mann, C., McCarthy, J., and Okaya, D., 1989, Geophysics of the western Basin and Range province, in Pakiser, L. C., and Mooney, W. D., eds., *Geophysical framework of the continental United States*: Boulder, Colorado, Geological Society of America Memoir 172, p. 177–203.
- Whitman, Dean, and Catchings, R. D., 1988, Data report for the vertical-component seismic refraction data obtained during the 1986 PASSCAL Basin and Range lithospheric seismic experiment, northern Nevada: U.S. Geological Survey Open-File Report 87-415, 72 p.
- Zoback, M. L., Anderson, R., and Thompson, G. A., 1981, Cenozoic evolution of the Basin and Range province of the western United States: *Royal Society of London Philosophical Transactions*, v. 300, p. 407–434.

MANUSCRIPT RECEIVED BY THE SOCIETY JUNE 25, 1991

REVISED MANUSCRIPT RECEIVED JANUARY 15, 1992

MANUSCRIPT ACCEPTED FEBRUARY 6, 1992

Overview of Geophysical Methods Applied to Precious Metal Exploration in Nevada

Jack D. Corbett

Consulting Geophysicist

Many of the geophysical methods are applicable to mineral exploration. Several are direct detectors of sulfide mineralization, but most are indirect, that is they respond to a geological environment, rather than a particular mineral suite. In precious metal exploration, the application of geophysics is indirect and use should be considered more as a mapping tool than just an anomaly finder.

The following is a review of where and how the various geophysical methods might be applied. All geophysical methods have some application to gold exploration in the Great Basin of Nevada, but not in a casual or routine sense. No geophysical method detects gold mineralization *per se*, with the possible exception of nuclear activation which has only limited application and is not specifically listed. Several methods can detect and map gold-bearing lithology or an associated alteration envelope; others can locate structures or lithologies that may be permissible for mineralization. No one method will work satisfactorily all of the time, and all methods will provide useful information under certain geologic conditions, and therefore will work some of the time.

In Nevada, gold deposits may occur in a wide variety of geologic units, including volcanic tuffs and flows, sandy sediments and carbonates, and along intrusive margins. Hydrothermal alteration is characteristic but complex; variations range from advanced argillic to pervasive silicification. On a broader scale, key indicators that simply characterize gold deposits are favorable lithology and alteration, structure which permits circulation of hydrothermal fluids, and intrusive activity which provides a source of metals, hot waters, and heat to drive the system.

The list of geophysical methods with potential application to gold exploration, Figure 1, includes the five main classifications, each responding to a different physical property of the earth (susceptibility, density, resistivity, velocity, and radioactivity). Two secondary properties, magnetic remanence and chargeability, have been added. Applied to an exploration project, the critical factor is the change or contrast in physical properties - lateral for some, vertical for others - in the shallow, near-surface crust that is detected and measured.

Many gold deposits are small targets, which in a bulk sample concept, have low physical property contrasts. Locally, however, the mineralization or alteration assemblages may vary widely in intrinsic properties, e.g.

from silicic (high resistivity, low chargeability) to advanced argillic (low resistivity, high chargeability). Significant sulfide mineralization is only sometimes a significant component of an anomaly.

Geophysical surveys are not just aimed at producing anomalies over mineralized zones, but also may be designed to determine pediment depths, basement highs, location of buried faults, lithologic contacts under cover, or areas of significant alteration.

Range of Physical Properties

The range of physical properties, and their respective units, is shown in Figure 2. The range or variation of resistivity and susceptibility is tremendous, as much as 7-9 orders of magnitude for the former, and is usually plotted on a logarithmic scale. Susceptibility can range from >50,000 micro cgs for magnetite deposits to almost zero for alteration assemblages where the destruction of magnetite is complete. Density, on the other hand, has probably the least variability and least range for many of the common rock types. Certain minerals, gold (>19 g/cc) or metallic sulfides, for instance, have a high specific gravity but rarely do they occur in nature in the quantity or extent necessary to effect or cause a significant and measurable response at the surface. Massive sulfides, usually of relatively limited overall size, are probably the most dense of the common geologic features.

Susceptibility (k) is a function of the volume percent magnetite in a rock, and to a certain extent the size of the magnetite grains. While magnetite generally increases toward the mafic end of the petrologic sequence, susceptibility cannot be tied directly to rock composition. For instance granite may produce a relative high anomaly due to accessory magnetite or a relative low (with no accessory magnetite) if intruded into an intermediate or mafic host environment. Remanence, if present, causes unusual magnetic anomalies and, if recognized, limits the interpretation potential of the magnetic data.

Resistivity ρ , or its reciprocal conductivity σ , has the greatest range of any physical property. Massive sulfides and graphitic shales are on one end of the scale, metamorphics on the other. Most rocks, volcanics as well as sediments, can have widely variable resistivity, due primarily to porosity and permeability, and water content and salinity. No value is particularly diagnostic

List of Methods

Magnetics

- * Aeromagnetics

Gravity

Electrical

- * Resistivity
- * Induced Polarization – IP
- * Electromagnetic – EM
 - VLF – Very Low Frequency
 - Frequency Domain (Horizontal Loop)
 - Time Domain
 - MT – Magnetotelluric
 - CSAMT – Controlled Source
Audio Magnetotelluric
 - Airborne EM
 - Self-Potential – SP

Seismic

- * Reflection
- * Refraction

Radiometric

- * Natural
- * Artificial

***Well-Logging* (all methods)**

Remote Sensing Imagery

Figure 1. List of Methods.

until correlated with a particular unit in a particular environment. Significant changes within a project area are not unusual.

Massive sulfides are a low resistivity (high conductivity) target; porphyry systems with disseminated sulfides are high chargeability, generally low resistivity, targets. Precious metal targets cannot be so classified or defined and interpretation must consider both the highs and lows of anomalous response.

Density has the least variability over the types of rock composition. Silica and feldspars are similar in density. The mafic minerals are usually more dense, but the range of rock density is usually not more than 2.6 to 2.85 g/cc. Porosity and permeability of both carbonate and clastic rocks usually will have more effect on bulk density than mineral composition. Dry alluvium is usually the least dense unit of concern; ultra mafics and/or metamorphics

the greatest. Sulfide minerals are dense, but commonly are disseminated and usually are so small a percentage that the effect on the bulk rock density is insignificant.

Seismic velocity is related to the "strength" (elastic moduli and density) of the rock unit. Sediments and large intrusives may be reasonably consistent within a mining district; volcanics flows, tuffs, and intrusives, on the other hand, may be limited in areal extent, show large changes in thickness over short distances, and vary widely in hardness and density. Alteration and mineralization show velocity anomalies both higher and lower than the host rock environment. Dry alluvium is the low end of the velocity scale, dense crystalline basement rocks are the high end in Nevada geology.

The effect of alteration on physical properties, Figure 3, is the modification of the normal or background value of the intrinsic physical property, which either increases or

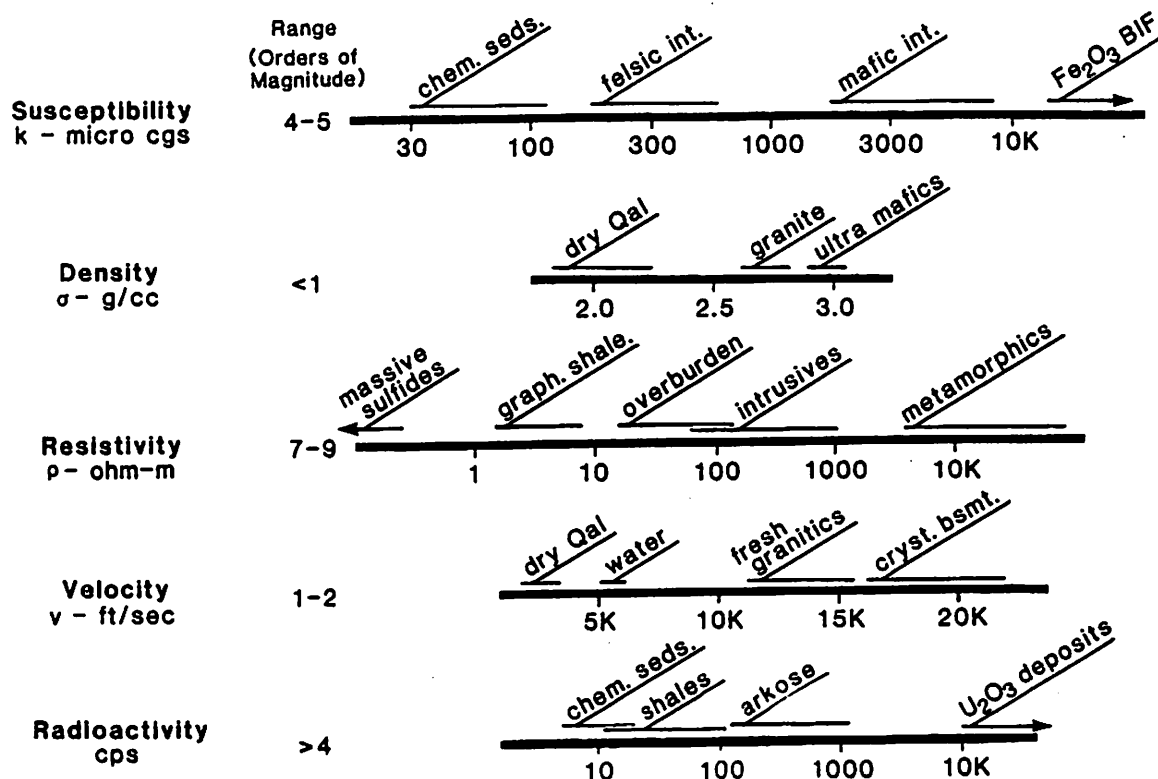


Figure 2. Range of Physical Properties

decreases it, producing anomalous highs or lows respectively. Magnetite is generally destroyed in many alteration processes, but can be formed with certain types of skarns. Resistivity can be increased by the addition of silica, or decreased by the formation of clays and related alteration products. For these reasons, particularly in gold exploration programs, an anomaly of interest cannot be assumed to be either a high or a low — both are feasible, and both may have exploration potential.

Applications

In this section, one or two typical applications of each method are shown in a simple schematic fashion. The word "schematic" is used because rarely are the applications this simple and straightforward. While simple, the examples are not trivial. The first (Geology, Figure 4) is a section of a "typical" basin-and-range environment at a "regional" scale. Volcanics, faulted sediments, buried intrusive rocks and a thick section of colluvium in the down-dropped basin-and-range valleys are characteristic.

Magnetics

A regional airborne magnetic survey will map the

extent of volcanics under cover and, within limits, the location, depth and susceptibility contrast of intrusive bodies. Figure 5 shows a computer calculated profile of a 2½-D model of the magnetic response of the geologic section equivalent to that of a low level draped survey. The volcanics typically produce a strong anomaly; however, due to either topographic effects or magnetic remanence (or a combination of both), the resulting anomaly may be a dominant low. Because the intrusive may be small and at depth, as in the example, its anomaly has a low amplitude, broad profile. Therefore, such small indistinct anomalies should not be omitted from consideration.

The final product of an airborne survey is usually a contour map. Figure 6 is an example of a low level, fixed wing draped survey flown nominally 400 feet above the ground surface at one-quarter mile line spacing in a north-south direction. The resulting anomalies are, in part, small and tight, often intense, closures — some may say noisy — indicating surface volcanics. Helicopter surveys, often in conjunction with electromagnetics, are often flown at 0.1 mile spacing at 200 feet flight elevation.

Alternatively, magnetic surveys may be flown at a constant barometric elevation several thousand feet above the surface, either on a grid (typically 1.5 miles) or single line direction (at .5 to 1.0 mile spacing). Anomalies are relatively broad and smooth which reflects the increased distance between source and sensor. Line spacing necessary

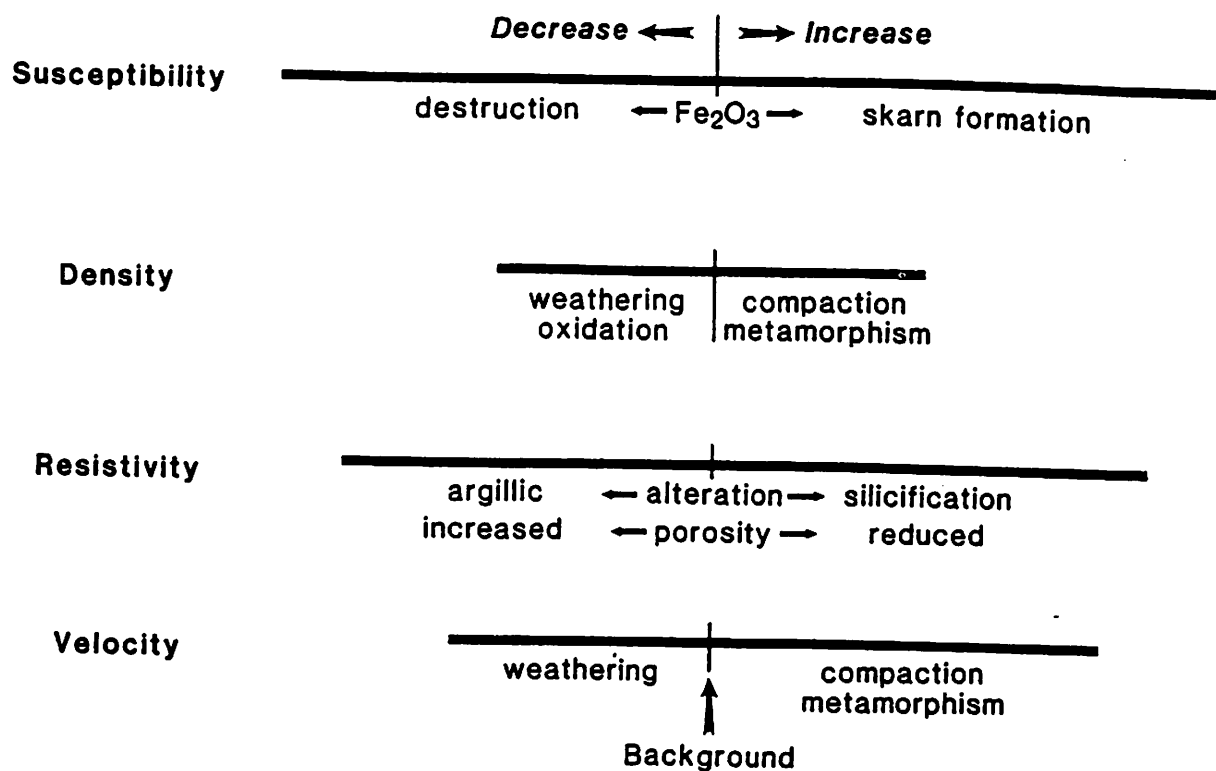


Figure 3. Effect of Alteration on Physical Properties.

to define small features may be opened up providing more areal coverage for the same dollar amount. Small, strong amplitude, features, such as in the example shown, would be smoothed or smeared simply because of the size-distance function implicit in potential field methods. Figure 7 shows the magnetic data of Figure 6 continued upward 1000 feet, which is approximately equivalent to a high level, constant barometric survey.

Similar broad patterns, linears and other equivalent features can be discerned in both contour maps. The differences, however, are in what can be interpreted from each contour map and the relative unit cost of the survey. The tight patterns in the west half of Figure 6 are a typical pattern indicative of surface volcanics, probably with some terrain effect. Closures on the "high level" (Figure 7) reflect the same sources, but are reduced in amplitude and broader when measured at the greater height. Linear features indicate faults or lithologic contacts. The sharp north-south demarkation in contour pattern in the center is a mapped fault throwing Paleozoic sediments on the east against volcanics on the west. North-northeast and west-northwest linears, in the west and north respectively, show well on both maps. With study other equivalent features can be discerned. One primary difference is that the signature of any small anomaly is attenuated and smoothed when measured at a greater height. Other differences might be in the width

and depth estimates of small anomalies with dimensions less than that of the flight elevation. On the other hand regional features are enhanced and near-surface effects (volcanics, or "noise" in some interpretations) are suppressed with high level surveys. Selection of type survey and flight specifications to be flown are based upon the area of interest, concepts of target size and depth, and budget. Either approach has advantages and limitations.

Filters, derivatives, and/or reduction-to-the-pole can be used to aid interpretation in either data set. Frequency filters, either low or high cut, to eliminate regional features or surface (or noise) effects respectively, or upward continuation can be useful to isolate certain types of anomalies and to otherwise enhance interpretation.

On either regional or detail scales, in addition to the contour map a number of other map products can be generated to aid in magnetic interpretation. Color maps, in particular, are very useful, and in effect when properly done, become an optical filter. Shaded relief or shadowgraphs with different illumination angles and azimuths are used to emphasize linear features such as structures. Individual and stacked profiles show the data without the smoothing effect of the contour algorithm.

Airborne magnetics is a sound basic geophysical mapping tool that can be effectively applied to most exploration prospects. Relatively inexpensive, it can provide data on the extent of certain lithologies, on

GEOLOGY

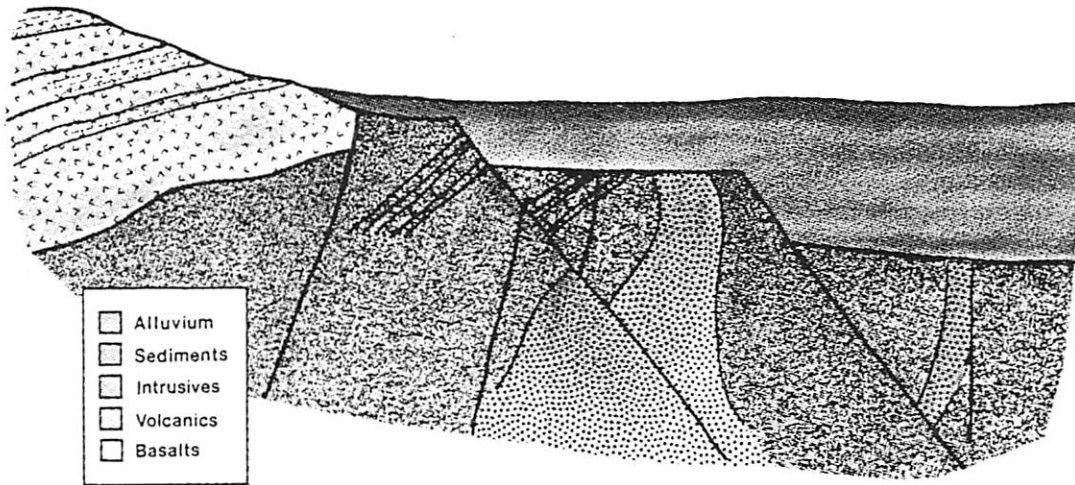


Figure 4. Geology.

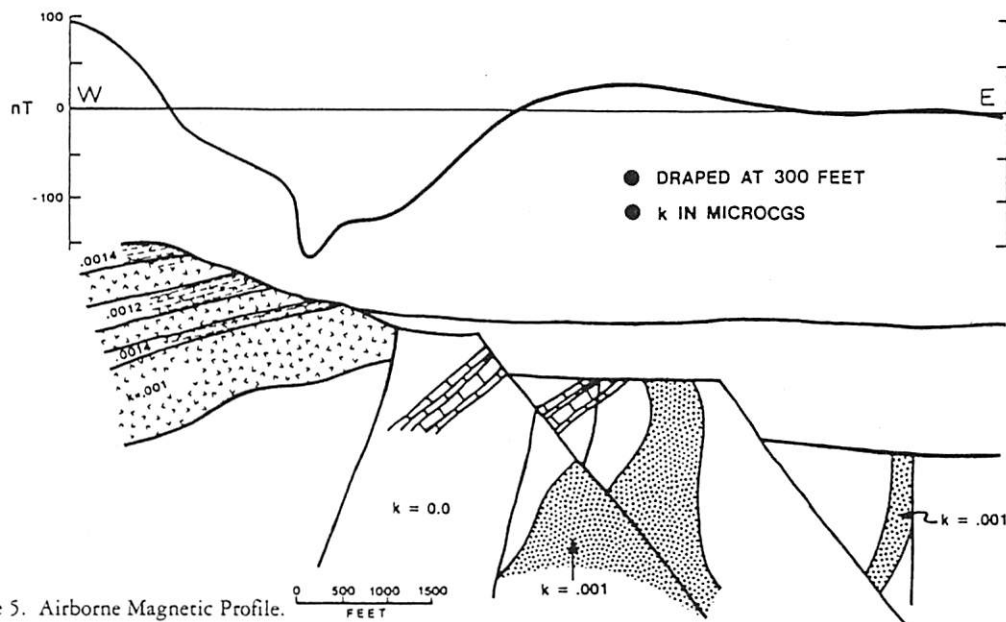


Figure 5. Airborne Magnetic Profile.

structure, and on the location, depth and susceptibility contrast (or composition to the extent that susceptibility is diagnostic) of the intrusive.

Ground mag in either a total field or vertical gradient configuration is a common follow-up technique. Use of the gradient enhances or sharpens broad features but can be a handicap if near-surface effects (volcanic noise) are high. The use of a 8-foot staff and a single sensor reduces the noisy effects of detrital magnetite on the surface or the magnetic noise produced by many surface volcanics, e.g. basalt flows.

Survey design - line separation and station spacing - can be crucial to an effective survey and satisfactory interpretation. Twenty-five foot stations on 200 foot lines are a typical detail specification. Too often lines are

spaced on a budget basis and not on a realistic attempt to define the anticipated target.

Gravity

A gravity profile over the same geology section, with typical densities assigned to the rock units, shows the gravity low due to the "block" of low density alluvium, Figure 8. The locations of the faults, downdropping basement to the east, are indicated by a change in gradient of the profile. In this case the subtle changes are the significant characteristic of fault location. Under ideal circumstances depth to pediment surfaces can be calculated, but in most cases the variability of the

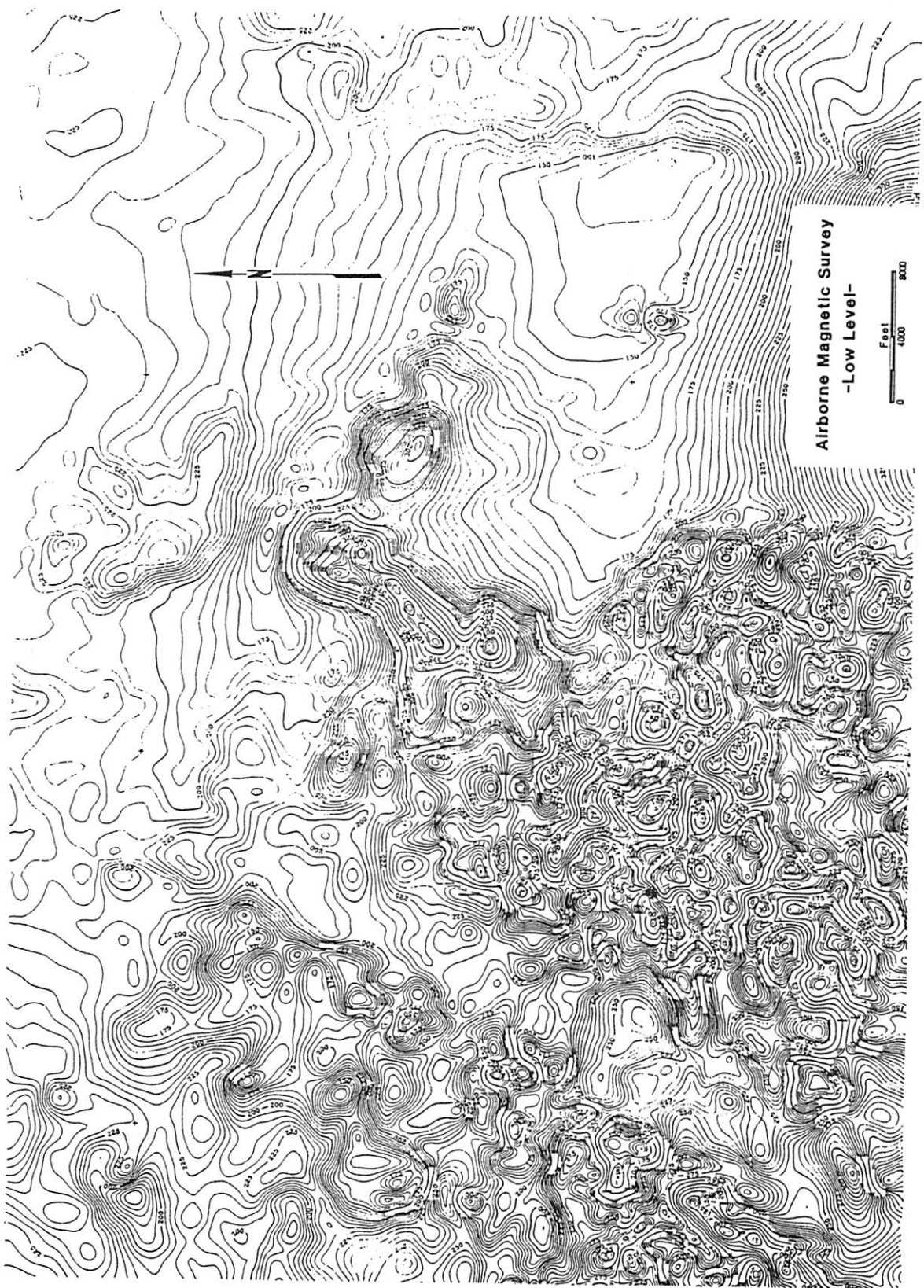


Figure 6. Airborne Magnetic Survey - Low Level.

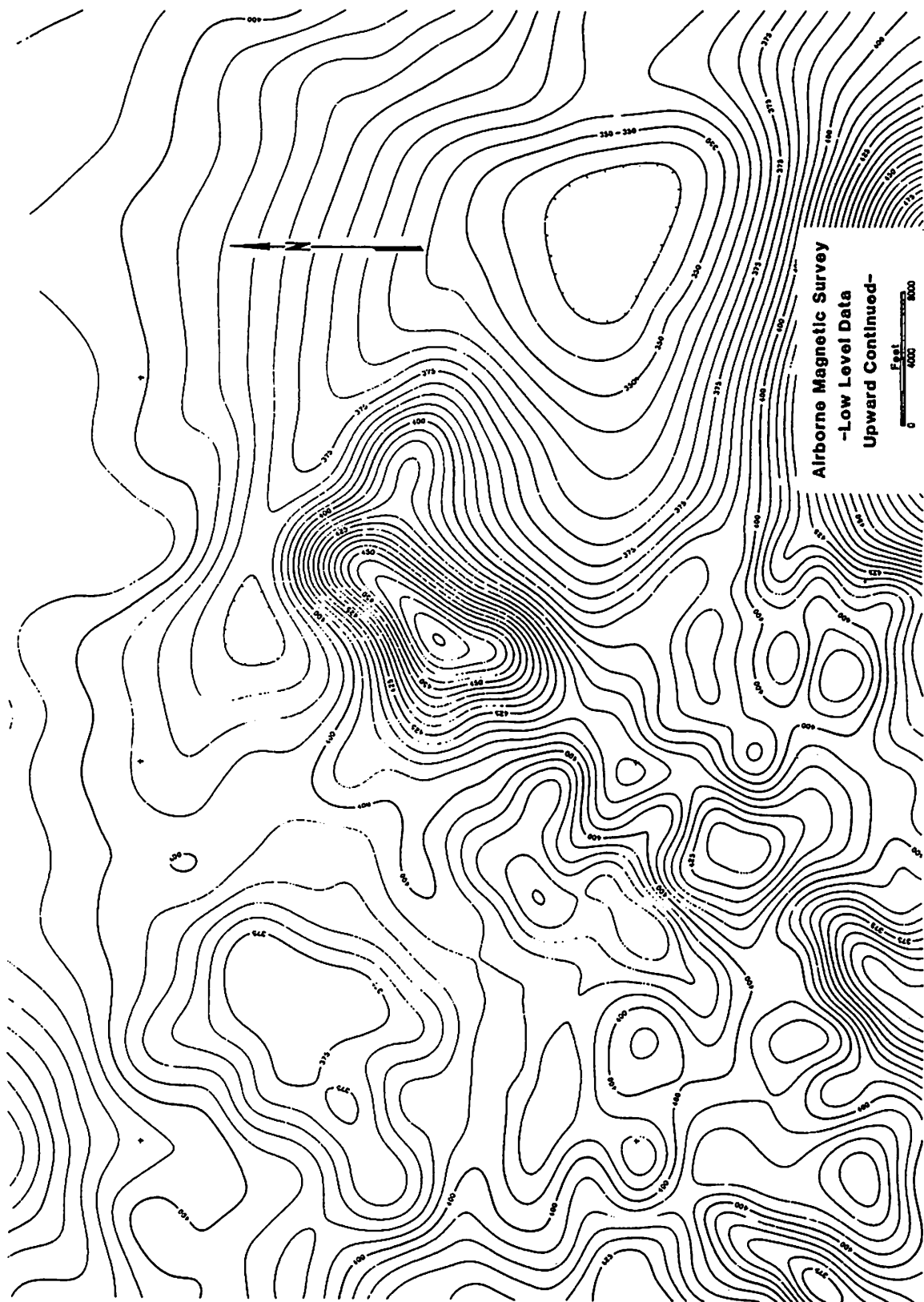


Figure 7. Airborne Magnetic Survey - Low Level Data Upward Continued

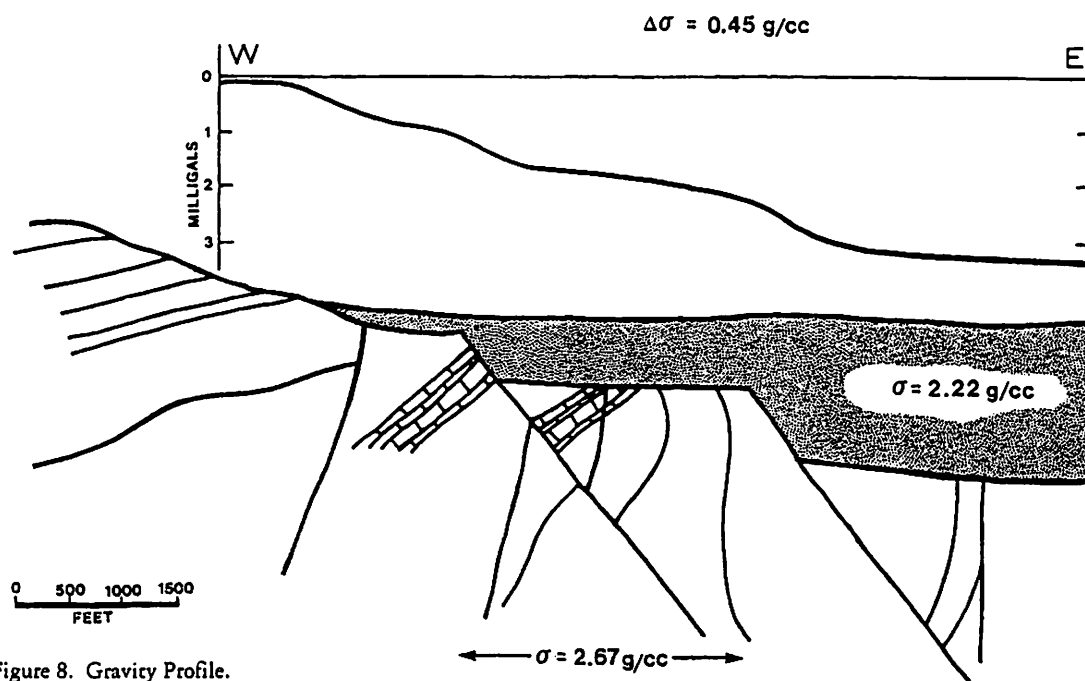


Figure 8. Gravity Profile.

alluvium density, due to compaction and grain size, water saturation, and intercalated volcanic flows, are such that a depth may be estimated, but accuracy is limited unless other constraints are available. On a regional basis, gravity can map the major offset structures within the basin-range valleys, outline many buried intrusive bodies, provide crude estimates of the depth of valley fill, and in correlation with magnetics provide constraints to the regional mapping of structure and lithology.

Electromagnetics

Using the same geologic model, possible applications of several of the inductive source electrical methods, Time Domain EM (TEM) and Controlled Source Audiomagnetotelluric (CSAMT), are shown, Figure 9. Measurement of intrinsic electrical properties is feasible, but usually the lateral and/or vertical changes in resistivity (conductivity), are the more important anomalous effect in an exploration context. In-loop TEM can map the geoelectric section to depths of perhaps +1500 feet but is dependent, as with all electrical methods, upon the resistivity of the overlying material and contrast with bedrock units. An estimate of the resistivity of the bedrock unit is determinable, so that interpretation of small changes in the bedrock are feasible. Large loop methods provide more signal and a greater depth of investigation.

The TEM soundings identified on the section are calculated and shown in Figure 10. Simple two layer cases are modelled. Water table, or interbedded volcanics could make any a multiple layer case. In this example the TEM curves appear quite similar, but are in fact related to different bedrock resistivities. In practice, careful field work by competent operators and use of inverse

computations, relatively small contrasts in bedrock resistivities and/or changes in depths can be identified. Although there are a number of reasonable solutions that will fit the curve, such differences in depths and bedrock resistivity can be demonstrated. For instance, three layers can be forced to fit the two layer case shown without significant differences in the resulting curve match. Typically, however, a complex multiple layer section is replaced by a simplified three or four layer model - the principle of equivalence - with practically indistinguishable response. Often, however, the more significant interfaces (or resistivity values) are within reasonable limits. Interpretation implies knowledge of the principles, experience, and some understanding and appreciation of the local geology and geologic model.

CSAMT is another alternative to map the electrical character of the subsurface, and has the potential to outline both conductive and resistive features (structures and/or lithologies) at greater depth with reasonable resolution. A grounded electric dipole is used for the transmitter. Located several miles away - the distance is dependent upon the resistivity of the area - the measurement of both the electric and magnetic fields is made. From the ratio of these two fields, an apparent resistivity is calculated. The next two figures show the calculated model of a deep conductive feature, Figure 11, the apparent resistivity, and Figure 12, the impedance phase shift between the electric and magnetic fields.

VLF

The next geological schematic, Figure 13, is that of a more detailed geological section with shallow bedrock and several buried alteration zones. The zones of the more productive application of several common geophysical methods are shown, Figure 14.

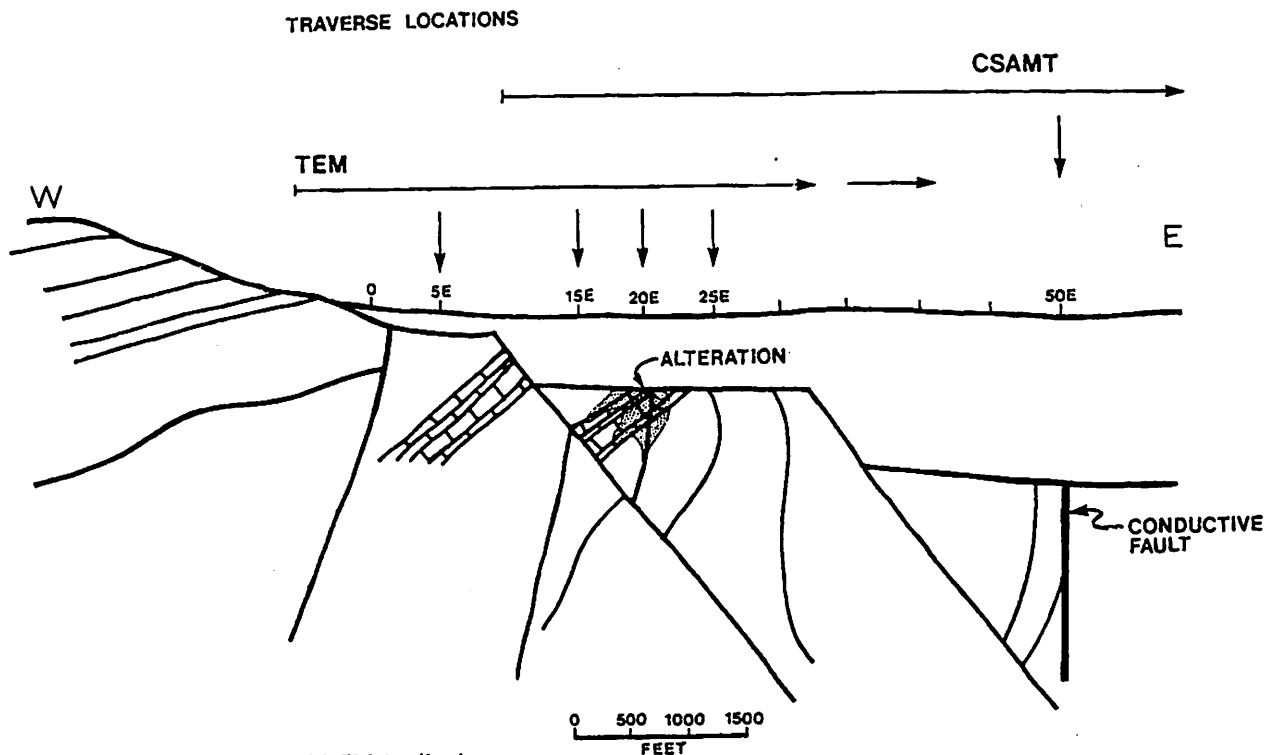


Figure 9. Geology Section with EM Applications.

Figure 15 shows a typical VLF (Very Low Frequency EM) profile derived from a ground survey and plotted in a tilt-angle format. Similar results would be obtained from an airborne survey. The number of conductors, which can arise from conductive faults, edges of water channels or bedrock edges in the alluvium are often a severe handicap to interpretation. In this plot the con-

ductor location is at the inflection point between high and low tilt angle readings (or change in slope on the profile, sometimes called a "crossover"). Airborne and some ground systems will plot the percent intensity of the in-phase and quadrature rather than tilt angle.

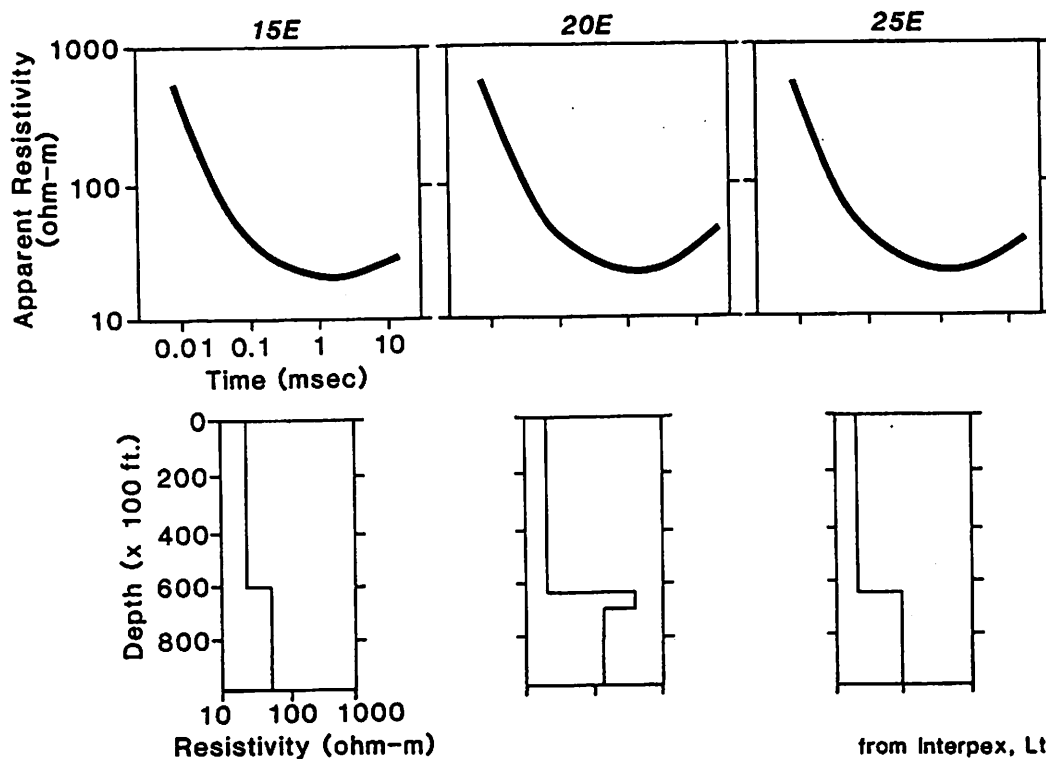


Figure 10. TEM Model A.

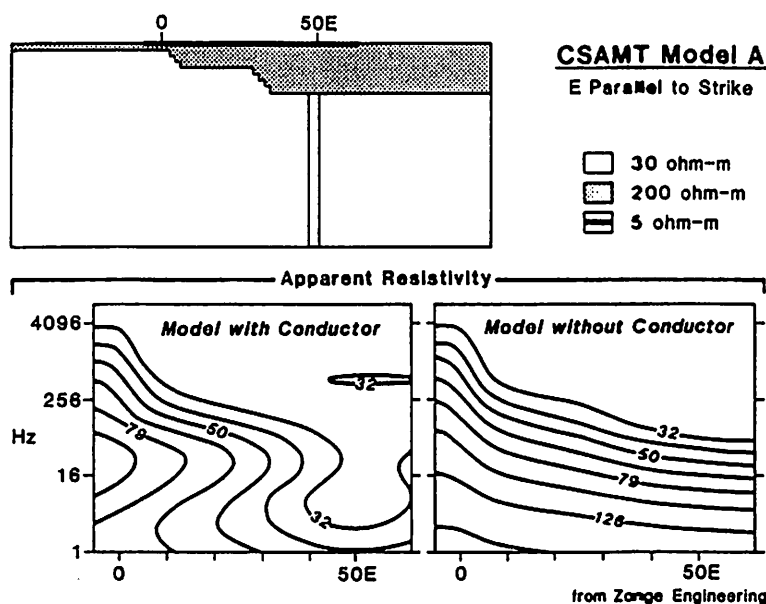


Figure 11. CSAMT Model A - Apparent Resistivity.

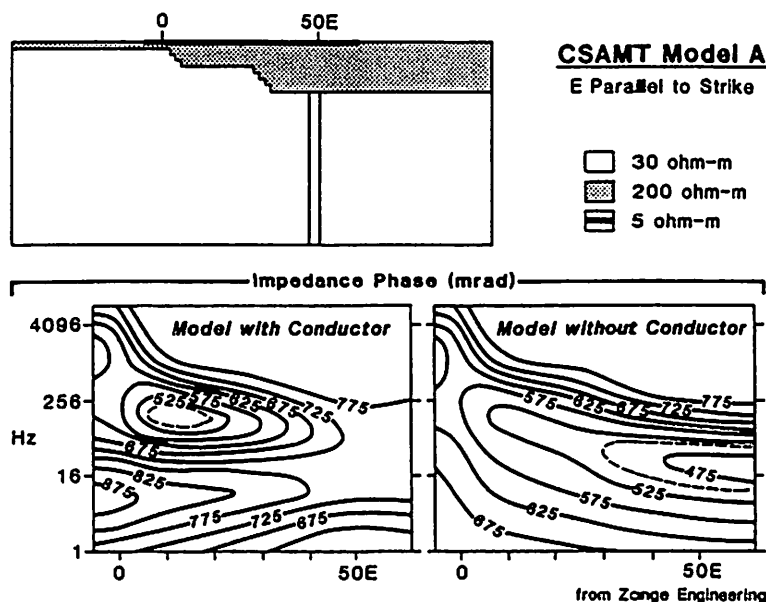


Figure 12. CSAMT Model A - Impedance Phase.

Air EM

This shallow covered environment also may be suitable for air EM methods as well as both airborne and ground magnetics and VLF.

In the airborne mode, helicopter EM systems incorporating magnetometer, VLF and EM systems, are currently in use in Nevada. The EM systems comprise four frequencies (in the ranges of 500-900, 3500-5000 (2), and 30,000-55,000 Hz), usually in two co-axial and two co-planar coil orientations, mounted in a rigid 7-8 meter bird. Application to gold exploration in Nevada is relatively new, and little data have been released and made available for study and open discussion (see suggested readings).

Calculated resistivities are another product of interest derived from airborne EM surveys, particularly in geologic environments, such as the Great Basin, where massive sulfides are the exception. Interpretation focuses on changes in resistivity indicating different lithologies, contacts, alteration and/or structure. EM profiles and color contour maps of one or more of the calculated apparent resistivities are used in the interpretation process.

As with any EM system the penetration or effective depth of investigation is limited by the frequency used and the resistivity of the near-surface, which is usually described by the skin-depth relationship. The depth of investigation is probably several hundred feet in a typical situation. The usual targets of EM surveys are "good conductors" which produce sharp discrete anomalies,

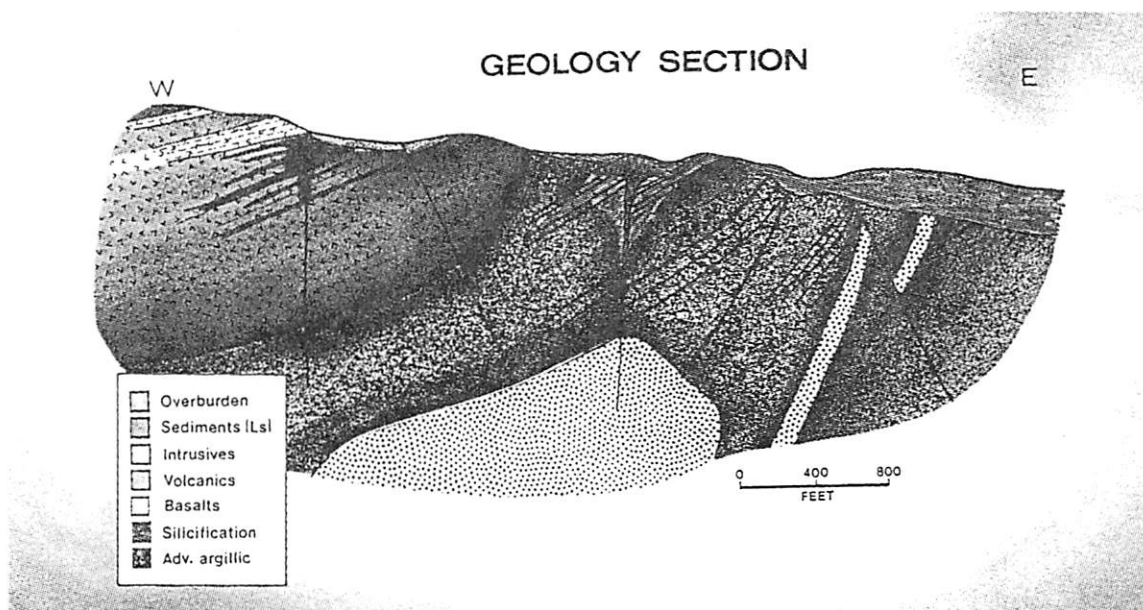


Figure 13. Geology Section

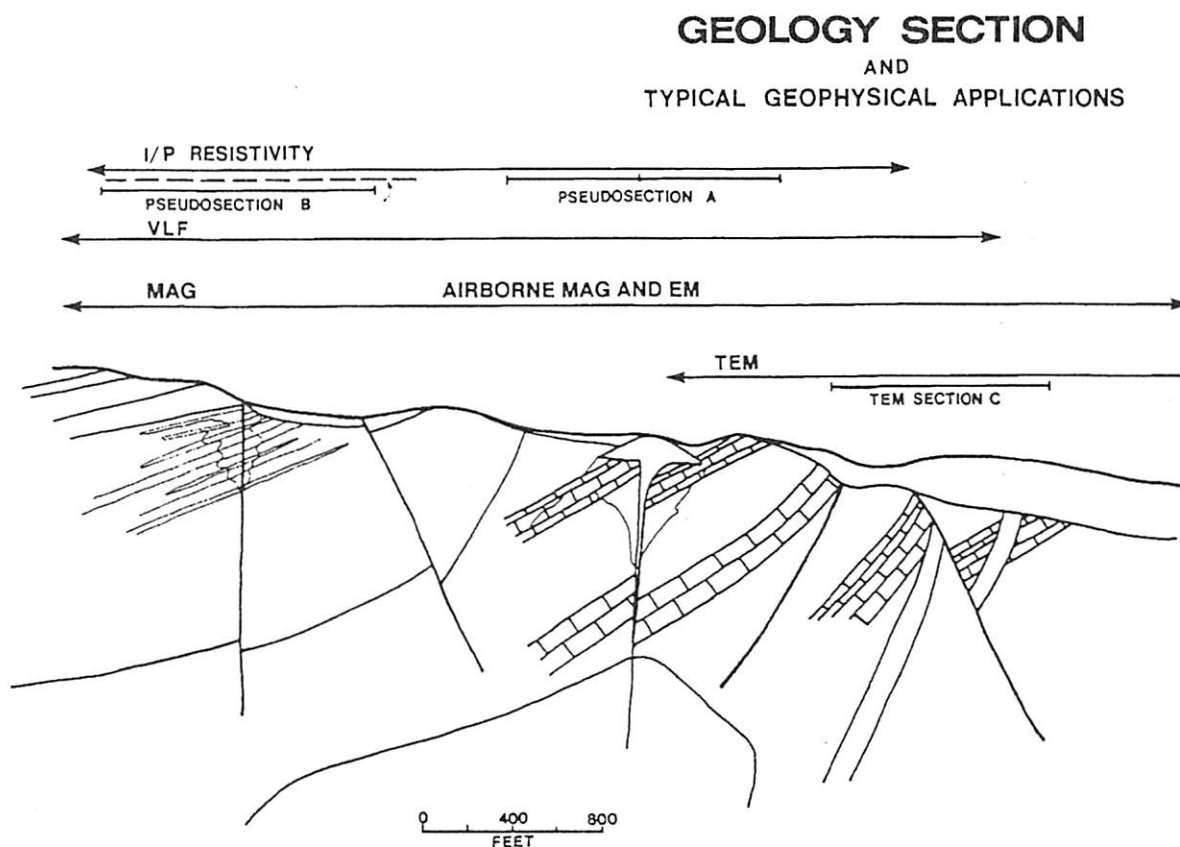


Figure 14. Geology Section and Typical Geophysical Applications

typically massive sulfides or many fault structures.

Induced Polarization and Resistivity

Resistivity techniques differ from EM in that current is

introduced into the earth through electrodes in direct contact with the ground. A variety of electrode arrays, current waveforms, and frequencies are used for measurement - the dipole-dipole array using either a time or frequency domain waveform probably being the most common.

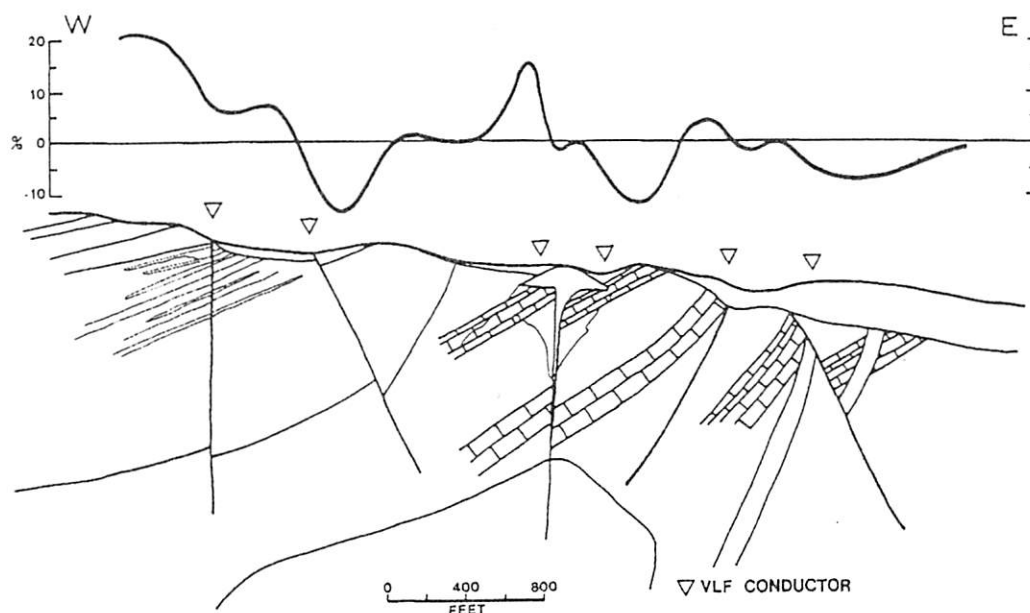


Figure 15. VLF Profile.

Resistivity is primarily a function of rock porosity and water salinity. In an exploration context complex patterns of resistive highs due to silica alteration and lows due to clay alteration and conductive structure are superimposed on alluvial or bedrock resistivities. Interpretation is complicated by the fact that variations in host rock itself due to water porosity and permeability may approach that of many anomalies of exploration interest. Induced polarization or chargeability effects result from the electrical polarization of sulfide minerals, clay minerals in alteration suites, and graphite or graphitic shales.

The next several figures show, in larger scale, two types of alteration, with significantly different physical properties in different host rock environments. A 2-D IP/resistivity model was calculated for each. The first, Figure 16, is a silicified, resistive alteration in sedi-

ments; Figure 17 is the IP/resistivity pseudosection. The second, Figures 18 and 19, show a conductive advanced argillic alteration envelope in a host rock of volcanics or tuff sequence, and the calculated IP model.

Seismic

Although not commonly applied, seismic methods have application in mineral exploration, particularly for sedimentary and fault structures at depths where most other methods are severely limited. Refraction seismic has obvious and historic use in depth determinations of placer deposits or alluvium. Shallow high resolution reflection techniques have been applied in certain geologic environments in Nevada to map low angle thrust faults with mixed results. An impedance contrast in

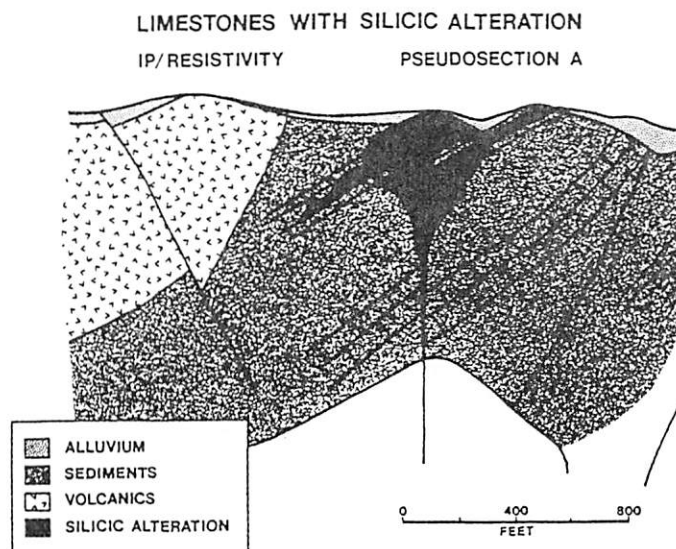


Figure 16. Ip/resistivity model of silicified limestone.

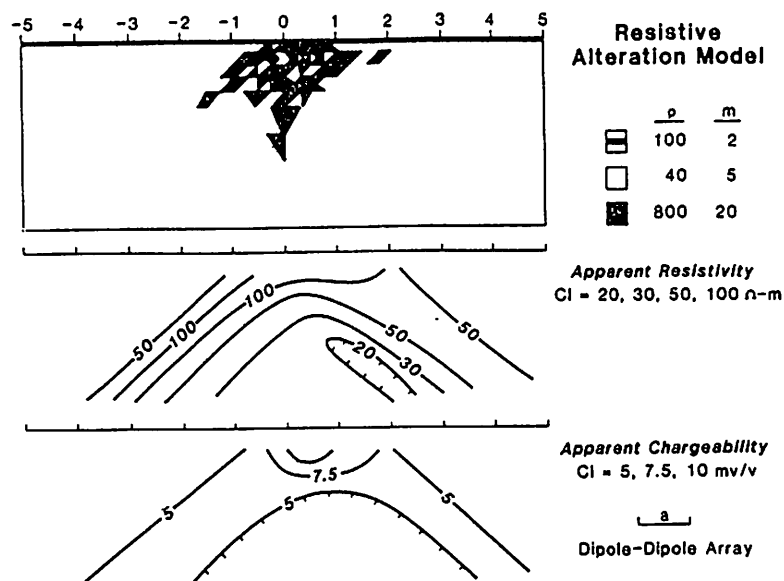


Figure 17. IP/Resistivity Pseudosection A.

zones of hydrothermal alteration and/or mineralization is expected in ore zones, but complex shape, relatively small sizes, steeply dipping contacts, gives reflections and dispersions which are difficult to understand. In areas where application is feasible, interpretation can provide information on structure, bedding angles, and displacement of beds but becomes increasingly difficult with steep dips, multiple faulting (often of small scale relative to depth) and irregular intrusions typical of many mining districts.

Other Methods and Techniques

Other variants of electrical method techniques (e.g. frequency domain EM, large loop TEM systems, resistivity arrays, etc) are feasible and have useful application,

but description and comparative advantages and limitations are beyond the scope of this paper. Use of any, or all, requires expertise and knowledge for proper application and interpretation.

Radioactivity has occasionally been used in precious metal prospecting. Using a spectrometer, concentrations of three radionuclides can be inferred from measurement of the radiation directly from potassium and indirectly from the daughter products of thorium and uranium. The geologic application maps the quantity and changes in relative ratios of the "background" response of the three elements (K, Th and U) with lithology and alteration. Potassic metasomatism is of particular interest as it is associated with the alteration assemblages of many different types of gold deposits. Airborne application, in particular, shows interesting mapping potential.

IP/RESISTIVITY

PSEUDOSECTION B

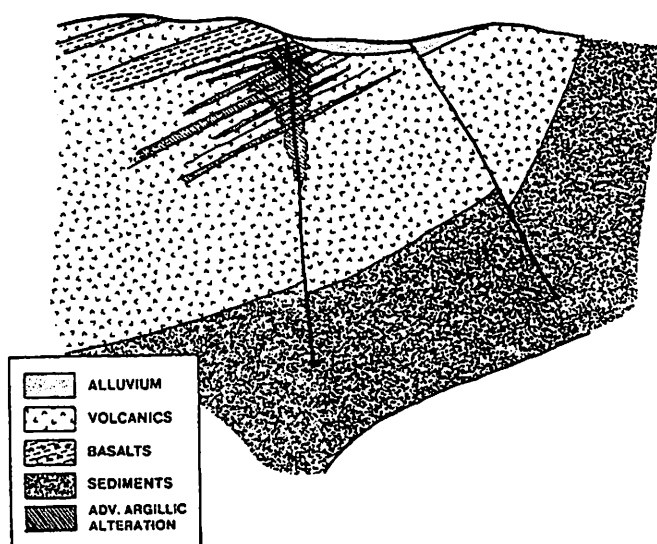


Figure 18. Volcanics with Advanced Argillic Alteration.

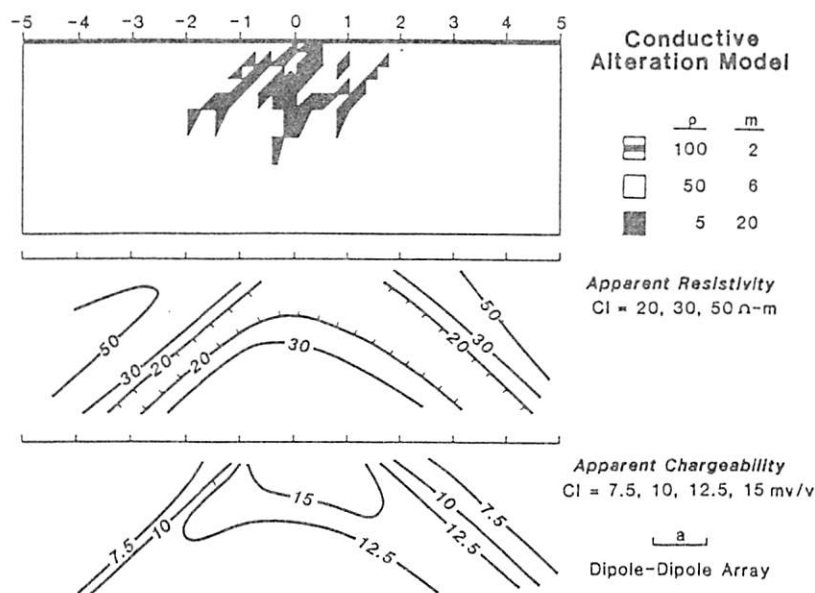


Figure 19. IP/Resistivity Pseudosection B.

Borehole logging techniques utilize the same physical properties, some of which are measured in different ways, e.g. density, porosity and sonic tools. Logging is important for several reasons, including in-situ physical property measurements, exploration at depth adjacent to the hole, and/or engineering studies. Applied to interpretation of surface data or correlation of geologic units where core is not available, in-situ measurement downhole is the best determination of physical properties. Interpretation is a complex process. Costs are relatively high because of the numerous short holes (2-400 feet) typical of mineral prospects and high relative call-out charges.

Survey Design

Some geophysical methods, particularly those of a regional nature (magnetics and gravity), are designed to map the environment and locate those key "district" scale features related to many deposits, namely, favorable lithology, structure and intrusive bodies.

The more detailed methods, particularly the electrical methods, are designed for more specific targets on a smaller "prospect" scale. Selection of method is based in part upon estimates of the size, depth, physical property contrast expected from the alteration and host rock, and the topographic and surface conditions (dry and non-conductive or wet and highly conductive alluvium). Three criteria must be addressed before selection of an optimum and cost effective electrical method; 1) lateral resolution, 2) vertical resolution, and 3) sensitivity of the method to anticipated geologic noise of the area. The depth and size of the target determine the electrode spacing of IP/resistivity or loop size of EM methods. Forward modelling of the assumed parameters is a very useful exercise in planning a survey, but too often is

ignored for the more traditional "it's worked before, let's try it again in the same way" approach.

In addition, other factors concerning cost, logistics, timing, and interpretation potential must be considered in survey design.

None of the geophysical methods produce unique solutions, all have inherent limitations in both field application and interpretation.

Relative Costs

Costs and production rates have many variables. In airborne work, survey size (areal extent and line mile totals) is a dominant factor. A detail survey of four square miles can generate up to 65 line miles per square mile (at 100 meter line spacing), so that survey areas are selected with particular care and may not be extensive. Although brief, incomplete, and approximate, some examples of relative cost are listed below for interest and comparison.

	Line Miles	Line Spacing	Cost/mile
regional mag (fixed wing)	1000's	.5 - 2 miles	\$12-25
mag (helicopter)	100's	.1 - .5 mile	\$ >60
air EM w/ mag	100's	200-500 m (meter)	\$ >100

Ground surveys may consist of several lines to extensive grids; surveys are typically in the range of 2 to 10 line miles. Because of limited size, often uncertain ground conditions (steep terrain and ground cover), and contact resistance (IP/resistivity), resulting in unknown production rates, survey costs typically are based upon a daily rate rather than a per mile basis. As target anomalies are shallow, relatively small, and often of low amplitude, close station spacing (25-50 feet) and line

Preliminary Results of Aeromagnetic Studies of the Getchell Disseminated Gold Deposit Trend, Osgood Mountains, North-Central Nevada

V. J. S. Grauch and Viki Bankey

U. S. Geological Survey, Box 25046, Federal Center, MS 964, Denver, Colorado 80225

Introduction

Purpose of this Report

In 1988, the U. S. Geological Survey (USGS) initiated an integrated airborne geophysical demonstration program in the area of the Getchell trend, a northeasterly alignment of six sediment-hosted disseminated gold deposits along the eastern side of the Osgood Mountains in Humboldt County, Nevada (Fig. 1). The purpose of the program is to test the usefulness of various airborne geophysical methods in mineral deposit studies. To that end, aeromagnetic, gamma-ray, electromagnetic, and

64-channel visible and near-infrared remote sensing data were acquired in the summer and fall of 1988 in cooperation with several mining companies that have land holdings in the area.

This paper reports the progress of studies of the aeromagnetic data. Progress reports on the other geophysical methods and related geochemical and geological studies are presented elsewhere in this volume. The aeromagnetic features discussed in this paper are most apparent in color displays, but because both use of color and length are restricted for this paper, the scope and detail of our discussion is limited. More detailed descriptions of the aeromagnetic data, color maps at 1:100,000 scale, and

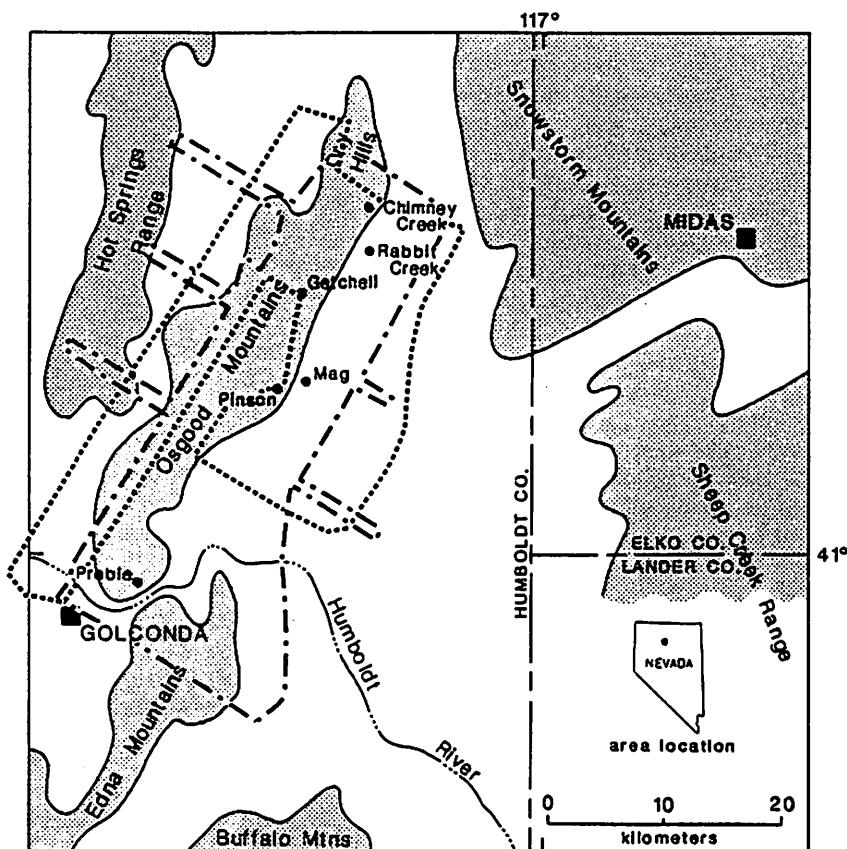


Fig. 1. Location map of the Osgood Mountains and Getchell trend area. Sediment-hosted, disseminated gold deposits of the Getchell trend are indicated by the solid circles; stippling indicates mountain ranges. The aeromagnetic survey area flown by the U. S. Geological Survey (USGS survey) is outlined by the short-dashed line; the survey area contracted to DIGHEM, Inc. (contract survey) by the dash-dot line.

discussions of the observations and interpretations presented in this paper are in preparation as a USGS publication. Meanwhile, interested readers can view color maps of the geophysical data at the Nevada Bureau of Mines and Geology library in Reno, Nev., or at USGS Earth Science Information Centers located in Menlo Park, Calif., Tucson, Ariz., Spokane, Wash., Denver, Colo., Salt Lake City, Utah, and Reston, Va.

Suitability of Aeromagnetic Studies

Aeromagnetic data are sensitive to variations in magnetic properties of rocks, which are dependent on the quantity of magnetic minerals and the thermal and alteration history of the rock. Aeromagnetic anomalies generally express structural, topographic, and lithologic variations. Anomalies due to igneous and metamorphic rocks commonly dominate aeromagnetic maps because these rocks generally are more magnetic than other rock types (Dobrin, 1976). Thus, detailed aeromagnetic data over the Getchell trend area should be useful for mapping the character and subsurface extents of plutonic and volcanic rocks. This information is crucial to an understanding of the three-dimensional geologic setting of gold deposits.

Geologic Background

The Getchell trend lies along the eastern side of the Osgood Mountains (Fig. 1), a structurally complicated range composed of Paleozoic sedimentary rocks, Cretaceous granodiorite, and Tertiary extrusive rocks (Fig. 2). The following geologic history is summarized from Hotz and Willden (1964), Berger and Taylor (1980), and Erickson and Marsh (1974a, b). A more detailed summary is presented in Hoover and others (this volume).

At least two episodes of thrusting and folding during Paleozoic time juxtaposed lower and middle Paleozoic eugeosynclinal chert, and clastic and volcanic rocks with lower, middle, and upper Paleozoic continental-shelf chert and clastic and carbonate rocks. This sedimentary package was intruded in Cretaceous time by granodiorite of the Osgood Mountains pluton and related stocks. North- to northeast-striking normal faults, such as the Getchell fault (Fig. 2), were first activated at this time. Ensuing widespread deposition of Tertiary andesitic and rhyolitic tuffs overlain by basalt and basaltic andesite flows is preserved only in scattered areas. Late Tertiary extension, which produced the horst and graben features of modern Basin and Range physiography, effected the uplift of the Osgood Mountains along new and existing faults. During late Tertiary to Quaternary time, alluvium and gravels filled the intervening basins, and relatively minor amounts of basalt were erupted.

The Osgood Mountains host gold, silver, tungsten, barite, and manganese deposits (Fig. 2). The gold deposits, presently of mining interest, are hosted in sedimentary rocks and disseminated, similar to the well-known

Carlin deposit. Mineralization is controlled by the Getchell fault system at the Getchell, Pinson, and possibly Preble deposits (Bagby and Berger, 1986). The ore-forming processes may be similar to those active in hot-spring environments (Berger, 1985).

The age of gold mineralization and its relation to the Osgood Mountains pluton has not been resolved. Silberman and others (1974) asserted that gold mineralization coincided with emplacement of the pluton, which probably heated and drove the ore-bearing fluids. Joralemon (1975) argued for a post-Miocene to Pleistocene age and shallow depth of formation. Recent fluid-inclusion data that suggest mineralization occurred at deep levels restricts the age to pre-uplift (A. R. Wallace, USGS, written commun., 1989).

Data Acquisition

This report concentrates on data merged from two aeromagnetic surveys flown in 1988 for the Getchell trend airborne demonstration program: one flown by the USGS using fixed-wing aircraft (USGS survey) and one flown by DIGHEM, Inc., using a helicopter (contract survey). Data digitized from contour maps of two other surveys are also available: a regional survey flown by the USGS in 1967 and an exploration survey on the western side of the Osgood Mountains flown by the Minerals Department of Continental Oil in 1973. The regional survey was flown at constant 2,743 m (9,000 ft) above sea level with a 1.6-km (1 mi) flight-line spacing. The contour maps are presented in USGS (1968), and the digital data are incorporated in a statewide aeromagnetic compilation by Hildenbrand and Kucks (1988). The Continental Oil survey was flown at 805-m (0.5 mi) spacing at 152 m (500 ft) constant height above ground. Magnetic tapes of the gridded data from the USGS, contract, and Continental Oil surveys are available from the tape librarian, Mountain Administrative Support Center, U. S. Department of Commerce, Boulder, Colo.

The USGS survey data were acquired in October 1988 by the USGS Branch of Geophysics over the eastern and western sides of the Osgood Mountains (Fig. 1). The survey was designed in two pieces. The western half was designed for magnetic interpretation and flown parallel with topography to reconcile good resolution with the limitations of fixed-wing aircraft. The flight lines were directed northeast-southwest and spaced about 200 m (0.125 mi) apart. The eastern half, flown perpendicular to topography, primarily tested an experimental electrical system; acquisition of aeromagnetic data was secondary. The lines for the eastern half were directed northwest-southeast and spaced 400 m (0.25 mi) apart. Both parts of the survey were flown at a roughly constant height of 137 m (450 ft) above the ground but along considerably smoother lines than is usual for draped surveys. The smoothing minimizes the height disparities between adjacent lines and thus reduces later gridding problems.

The contract aeromagnetic data were acquired over the eastern side of the Osgood Mountains (Fig. 1) by DIGHEM, Inc., in October 1988 as an add-on to an electromagnetic survey (Pierce and Hoover, this volume). The flight lines were spaced 400 m (0.25 mi) apart except over the vicinity of the Rabbit Creek, Getchell, Preble, and Pinson deposits, where they were spaced 200 m (0.125 mi) apart. The magnetometer was generally 40 m (130 ft) above the ground. Three extended flights across the area (the armlike extensions shown on Fig. 1) are for future magnetic modeling purposes.

In order to simplify discussion and interpretation, data from the USGS and contract surveys were digitally merged together. First, the contract survey data were analytically continued to the altitude of the USGS survey by the method of Cordell (1985). Then the data sets were splined together using the principal of minimum curvature (computer program GMERGE from USGS (1989)). In areas of overlap, the USGS data set took priority because it is unfiltered.

Aeromagnetic Signatures of Geologic Features

The map of merged aeromagnetic data is displayed in shades of gray on Figure 3. The small dots overlain on this map align over boundaries between rocks of contrasting magnetic properties (magnetization boundaries), which commonly occur at faults and other geologic contacts. Maps of magnetization boundaries help delineate buried faults and lithologic contacts. The dots were derived from the aeromagnetic data using a method described by Cordell and Grauch (1985) and Blakely and Simpson (1986). The method utilizes properties of the horizontal gradient of the pseudogravity transformation of the data. The pseudogravity transformation eliminates the magnetic polarity effects that produce offsets between anomalies and magnetic sources (Baranov, 1957).

The discussion of the aeromagnetic data will proceed by lithology, then to faults and alteration. The locations of aeromagnetic features discussed are sketched and labeled on Figure 4.

Sedimentary Rocks

Neither the Paleozoic geologic units nor Quaternary sedimentary deposits produce anomalies in the aeromagnetic data. Rather, where these units are isolated from outcrops of igneous rocks, they are generally characterized by low-amplitude, relatively constant magnetic values, a signature typical of effectively nonmagnetic rocks. This signature, which is expected for clastic and carbonate rocks (Nettleton, 1971), encompasses exposures of Paleozoic volcanic and metavolcanic rocks and greenstones as well. The low susceptibilities of these rocks are confirmed by field measurements.

On the other hand, secondary pyrrhotite, including the magnetic variety, is common in certain parts of the Osgood

Mountains area in sedimentary rocks and dikes (B. R. Berger, USGS, oral commun., 1988). Whether or not pyrrhotite occurs in sufficient quantity in the Osgood Mountains area to produce aeromagnetic anomalies is not known.

Intrusive Rocks

The most prominent anomaly near the center of the study area (I1, Fig. 4) is a magnetic high attributed to Cretaceous granodiorite (unit Kg of Fig. 2). Magnetization boundaries follow the mapped contact well, and field susceptibility measurements corroborate the high magnetization indicated for the granodiorite. Narrow magnetic highs on the western side of the mapped granodiorite (I2) identify shallow, dike-like apophyses of the pluton and are substantiated by extensive contact metamorphism mapped in this area (Hotz and Willden, 1964). Magnetization boundaries both along the west sides of the I2 anomalies and paralleling the intrusive contact 1-1.5 km east of the pluton (F1) may locate places where the pluton wall is steeply dipping or fault bounded in the subsurface. The southernmost boundary marked F1 is near the Mag deposit; a new discovery near the Getchell pits (not shown) occurs in the space between the two northernmost lines marked F1.

Magnetic highs north of the mapped granodiorite body (I3) and exposed dike-like apophyses of the granodiorite in this area (Hotz and Willden, 1964) suggest that the granodiorite, or intrusive rocks related to it, are present just below the surface. However, the much lower magnitudes of these anomalies, as compared to the anomaly over the exposed pluton, imply lower magnetization values or very little depth extent.

Broad and somewhat circular magnetic highs are typical signatures of intrusions. Anomalies of this type are I4 and I5 in the north, I6, I7, and I8 south of center, I9 in the south, and IV east of center (Fig. 4). Cretaceous dacite dikes are exposed in the Chimney Creek pit near I4 (Osterberg, 1988) and skarns were encountered during drilling at I5 (B. R. Berger, USGS, oral commun., 1989). Anomalies I6, I7, and I8 are near a granodiorite exposure at Lone Butte (E. Kretschmer, Pinson Mining Co., oral commun., 1988) and granodiorite crops out at I9 (Fig. 2). On the other hand, the granodiorite exposure at Lone Butte does not correspond to a magnetic high (Fig. 3), as would be expected if I6, I7, and I8 were produced by granodiorite.

The broad, somewhat low-amplitude magnetic highs in the east-central part of the survey area (IV) probably indicate either intrusions or basalt at depth. Depth estimates using the profile data indicate that the tops of the bodies are about 350-850 m (1,150-2,800 ft) below the surface. The east-northeast alignment of the anomalies and orientation of some of the magnetization boundaries are mimicked east of the study area by the orientation of an alluvial scarp and by discontinuous linear features in LANDSAT and thermal-infrared images. These east-northeast trends may reflect an east-northeast trending structural pattern related to the

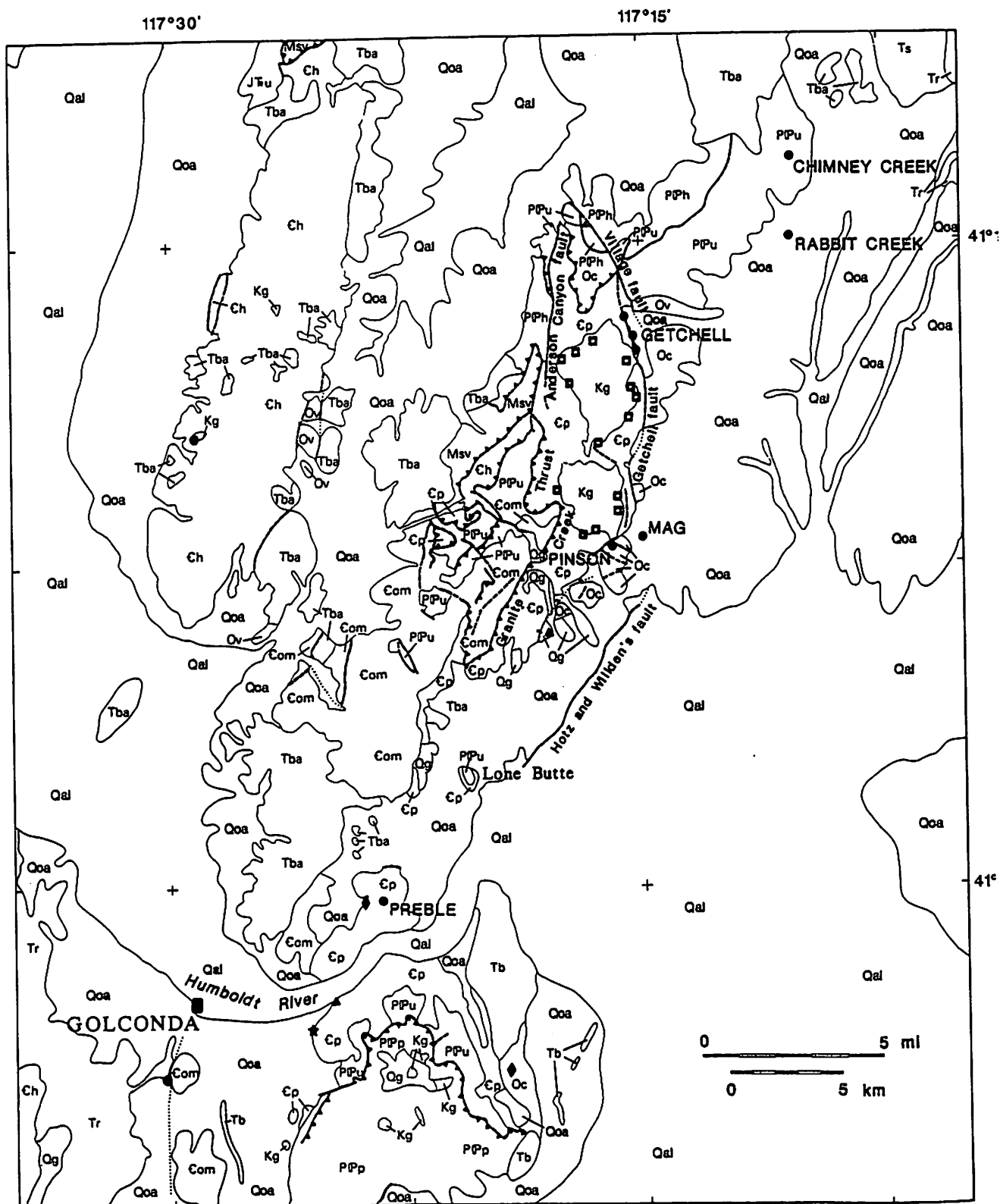


Fig. 2. Generalized geologic map for the Osgood Mountains and vicinity. Rock units primarily follow Willden (1964). Additional geologic names from Hotz and Willden (1964); ages from Erickson and Marsh (1974b) and Silberman and others (1974).

DESCRIPTION OF MAP UNITS
(Listed in approximate stratigraphic order)

- Qal - Quaternary alluvium
- Qoa - Older Quaternary alluvium
- Qg - Quaternary gravel
- Tb - Pliocene basalt
- Tr - Miocene rhyolite flows and tuffs
- Ts - Miocene clastic rocks and tuffs
- Tba - Miocene basalt and basaltic andesite
- Kg - Cretaceous granodiorite (about 90 Ma)
- JTu - Jurassic and Triassic metaclastic rocks, undivided
- PPu - Permian and Pennsylvanian clastic and carbonate rocks, undivided. Includes Edna Mountain Formation (Permian), Antler Peak Limestone (Pennsylvanian and Permian), Highway Limestone (Pennsylvanian), and Battle Formation (Pennsylvanian). In the Osgood Mountains, includes the Etchart Limestone (Pennsylvanian and Permian) and the Adam Peak Formation (Pennsylvanian and Permian).
- PPp - Pumpnickel Formation (Pennsylvanian and Permian)--siliceous sedimentary and volcanic rocks
- PPh - Pennsylvanian and Permian siliceous sedimentary and volcanic rocks, undivided. Includes the Havallah Formation (Pennsylvanian and Permian), rocks similar to the Havallah and Pumpnickel Formations in the Hot Springs range, and the Farrel Canyon Formation (Pennsylvanian and Permian) in the Osgood Mountains.
- Msv - Mississippian siliceous sedimentary and volcanic rocks. In the Osgood Mountains includes the Goughs Canyon Formation.
- Ov - Valmy Formation (Ordovician)--Chert and greenstone
- Oc - Comus Formation (Ordovician)--Carbonate rocks and sandstone
- Ch - Harmony Formation (Cambrian)--Sandstone and shale. Includes small exposures of Paradise Valley Chert (Cambrian) on the west side of the Hot Springs Range.
- Ep - Preble Formation (Cambrian)--Shale and limestone
- Com - Osgood Mountain Quartzite (Cambrian)
- Contact
- - - Fault, dashed where approximately located, dotted where concealed
- ▶ Thrust fault, sawteeth on upper plate
- ^{MAG} Gold deposit; names indicate operational or developing mines
- Tungsten deposit
- ◆ Silver deposit
- ▲ Barite deposit
- ★ Manganese deposit

Midas structural trough to the east (M. D. Krohn, USGS, written commun., 1989).

Volcanic Rocks

Narrow, high-amplitude anomalies that correlate well with topography indicate shallow, highly magnetic rocks and are typically produced by volcanic rocks. In addition, positive and negative correlations between the magnetic and topographic highs indicate magnetizations that are dominated by a normal-polarity or reverse-polarity component, respectively. Differences in polarity can indicate differences in age (a reversed polarity suggests the rock formed at a time when the Earth's magnetic field was reversed). Areas exhibiting this anomaly pattern with positive correlations between anomalies and topography are N1, N2, and N3 along the western edge of the study area, and N5 in the southeastern part (Fig. 4). Anomaly patterns that show negative correlations are R1 in the northern part of the study area, and R2 and R3 on the west-central edge. All these patterns correspond in large part to areas of exposed basalt and basaltic andesite (units Tba and Tb, Fig. 2), but also extend over mapped alluvium (units Qal and Qoa, Fig. 2). The extensions identify where the volcanic rocks continue under shallow cover. The strong northeasterly and northwesterly trends of anomalies in area N3 correlate with topographic features and suggest a structural control.

Anomaly patterns at N4 and N6 in the southwestern and southeastern corners of the area, respectively, occur in areas mapped as alluvium; they consist of subdued, narrow-anomaly patterns similar to those of neighboring areas where volcanic rocks are exposed, but are separated from the neighboring areas by magnetization boundaries F2 and F3, respectively. The similar anomaly patterns imply similar magnetic sources; the subdued amplitudes imply the sources are at greater depth. Thus, basalts exposed in areas N3 and N5 probably extend under cover in areas N4 and N6, respectively, and the abrupt change in elevation at the magnetization boundaries suggests normal faulting. The anomalies caused by unknown igneous rocks at IV, discussed previously, may express further extensions of the Pliocene basalt under cover northeast of N6.

Faults

As mentioned above, normal faults are probably represented by magnetization boundaries F2 and F3 in the southern part of the study area (Fig. 4). Evidence for faulting along F3 is convincing: all or parts of F3 correlate with a topographic cliff, a steep gradient in the electrical data (Pierce and Hoover, this volume), and a normal fault down to the east (Erickson and Marsh, 1974b). Northeasterly and northwesterly "dog legs" mimic structural trends elsewhere. A magnetization boundary (F4) parallel with F3 and 1-3 km to the east can be traced from the southern edge of the survey area

northward for about 15 km. The parallelism of the magnetization boundaries suggest that F4 also represents a normal fault. The lower amplitude of anomalies in area N6 and possibly even lower amplitudes east of F4 suggest that basalt-capped blocks may have been dropped down two times successively to the east. Exposures of Pliocene basalt along the southern part of F4 (unit Tb, Fig. 2) support either scissoring of the normal faults, having a greater dip component to the north, or an opposing basalt-floored graben hypothesis.

A magnetization boundary near the center of the study area (F5, Fig. 4), is associated with the southern part of a fault mapped by Hotz and Willden (1964; Fig. 2) but is consistently offset about 200 m westward. The fault is evident in the electromagnetic data along most of its length without offset (Pierce and Hoover, this volume). The offset of the magnetization boundary can be explained by subsurface, faulted basalt flows having large, reversely polarized remanent magnetizations. If the magnetization directions differ considerably from the Earth's present-day field direction, which is the direction assumed when deriving the plotted magnetization boundaries, erroneous boundary locations would result.

A fairly straight, continuous magnetization boundary (F6, Fig. 4) follows the western bank of the Rabbit Creek drainage in the northeastern part of the survey area. The boundary separates a magnetically low, featureless area on the west from an area of slightly higher values on the east. The abrupt change in magnetic values continues further south and swings to the west in the magnetic data (Fig. 3), but is not mapped by a magnetization boundary. Linear features analogous to the magnetization boundary are evident in the thermal-infrared (M. D. Krohn, USGS, written commun., 1989) and 900-Hz electromagnetic data (Pierce and Hoover, this volume), and a map of potassium radioelement values mimics the magnetic expression (Pitkin and Hoover, this volume). The sharpness of the magnetic contrast, which indicates a shallow source, and the correlation with the shallow-looking potassium data imply that the change in magnetic values is produced by a lithologic difference in the alluvium. Moreover, the linearity of the magnetization boundary and electrical and remote-sensing features suggests that the lithologic change is fault controlled. This deduction is corroborated by field checking, which indicates considerable offset down to the east (A. R. Wallace, USGS, oral commun., 1989) and an increase in susceptibility of the soil east of the drainage. Perhaps detritus shed from rhyolitic and dacitic rocks to the northeast preferentially accumulated on the downdropped block.

Altered Rocks

Hydrothermally altered granodiorite in which magnetite has been destroyed (Neuerberg, 1966) corresponds to magnetically low areas A1, A2, and A3 (Fig. 4). Magnetic values are the lowest in the vicinities of A1 and A2 and indicate that altered rocks are extensive at

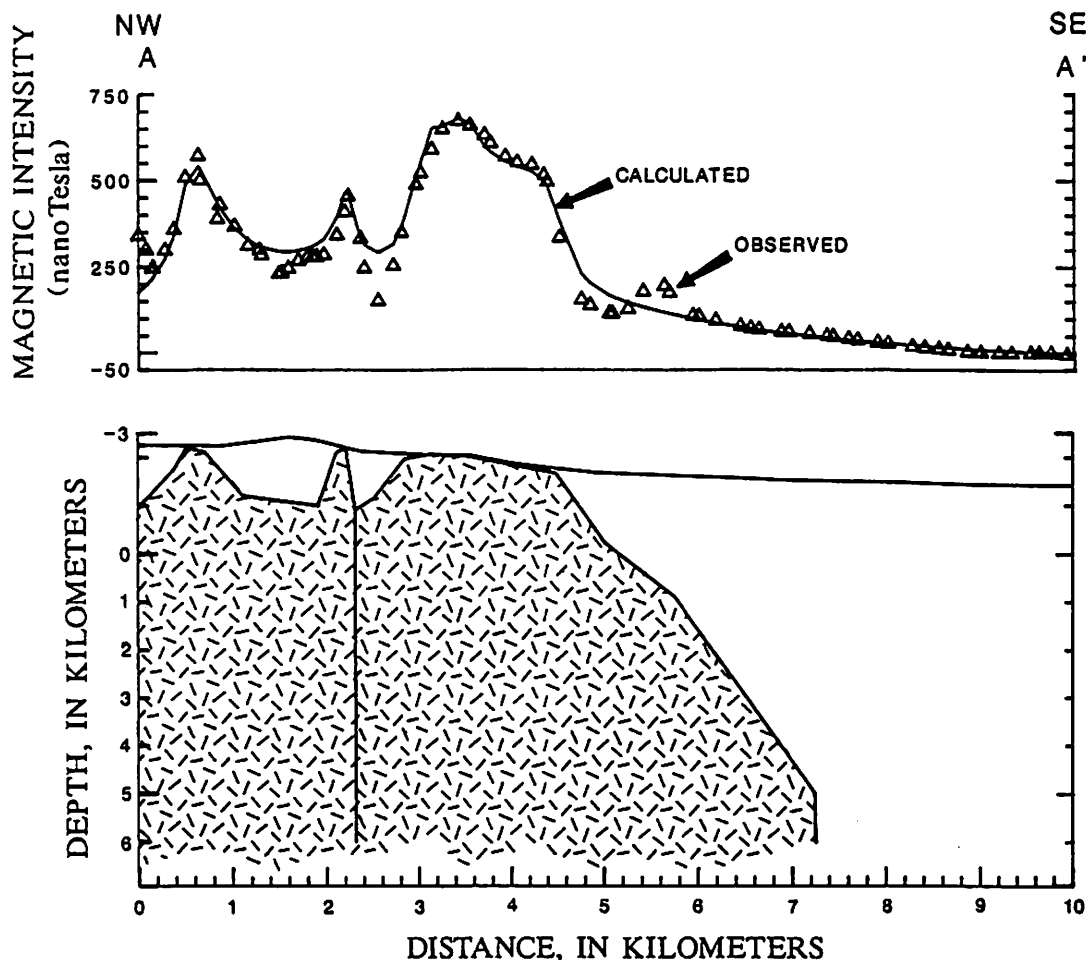


Fig. 6. Two and one-half-dimensional magnetic model of the Osgood Mountains pluton (hachured area) along line A-A' (Figs. 4, 7). The model was inverted from the data along one flight line of the contract survey using the computer program of Webring (1985). It extends to a depth of 20 km, an estimate of the depth to the Moho in the Basin and Range province. Magnetization is assumed to be completely induced. Misfits between the observed and calculated values for the magnetic field are mainly due to the true three dimensionality of the pluton. The model requires a slight increase in susceptibility of the totally buried western half (2.626×10^{-2} SI), as compared to the partly exposed eastern half (2.224×10^{-2} SI). The change in susceptibility, which would be more gradual in real-life, is represented by the almost vertical line at 2.4 km. On the other hand, a broad, regional magnetic field, produced by deep crustal features unrelated to the pluton, could also produce the higher magnetic values on the west. Future modelling should tighten the results. The susceptibility values are reasonable as compared to measurements made on outcrops that average 1.759×10^{-2} (SI) and allowing for some contribution from remanent magnetization. The Earth's field is assumed to be 53,600 nT, with declination of 16° E. and inclination 66° .

depth. Hydrothermal fluids did not affect as much volume of rock in area A3.

Contact metasomatism is widespread around the edges of the exposed Osgood Mountains pluton (Hortz and Willden, 1964), as evidenced by the number of tungsten deposits around it (Fig. 2). Field susceptibility measurements indicate very little magnetization within the granodiorite and the exoskarns near the pluton contacts. Geochemical sampling of the granodiorite also shows a significant decrease in magnetite content within 300 m or less of the contacts (Neuerberg, 1966). Thus, unlike the more common situation where secondary magnetite in skarns produces significant magnetic anomalies, contact metasomatism in this area probably is not associated aeromagnetic anomalies.

Synthesis

The results of transforming the aeromagnetic data to pseudogravity and then applying the terracing operator of Cordell and McCafferty (1989), called a terrace map, is shown on Figure 5. Terrace maps more closely resemble a map of magnetic sources and their relative magnetizations than do the original aeromagnetic maps. They are useful for those who are more familiar with geologic maps than aeromagnetic maps.

The primary purpose of a terrace map is to delineate blocks of differing magnetizations, but terrace maps can also be used to estimate relative depths of bodies with uniform magnetization. Therefore, if we assume that the magnetization of the Osgood Mountains pluton

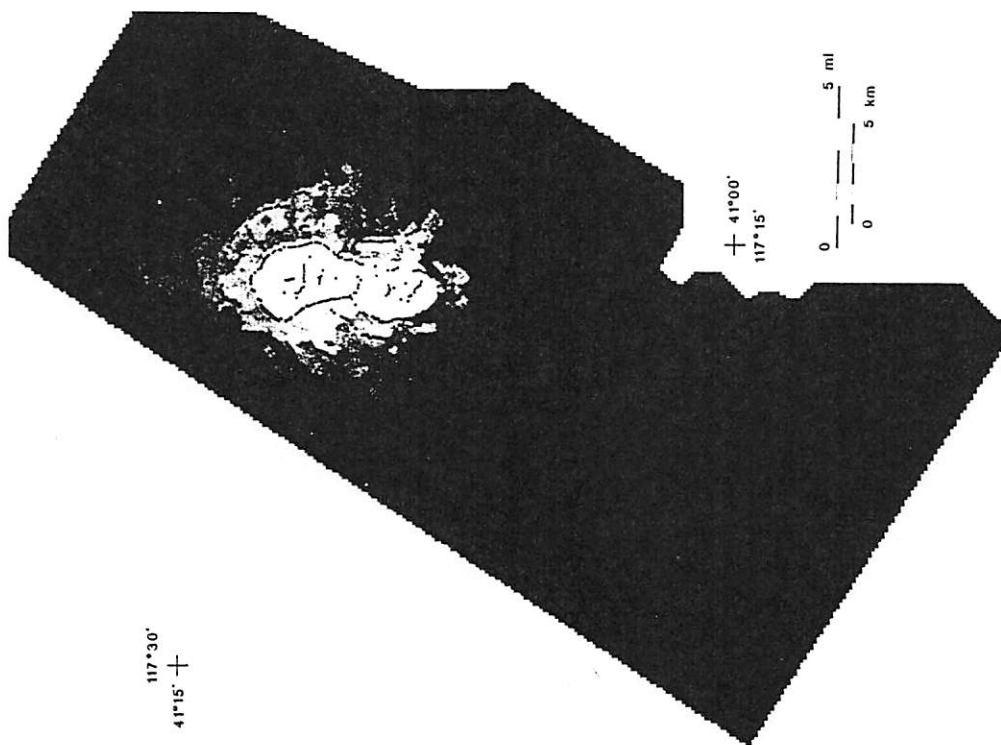


Fig. 5. Terrace map, shown in shades of gray, resulting from transforming the magnetic data to pseudogravity data and applying the terracing operator of Cordell and McCafferty (1989). The primary purpose of the terrace map is to delineate blocks of differing magnetizations, but it can also estimate relative depths of bodies having uniform magnetization. Thus, the blocks of varying values reflect the differing magnetizations of discrete lithologies (such as between volcanic and sedimentary rocks) or the differing depths of one lithology (such as the Osgood Mountains pluton). In this figure, the shades of gray have been chosen to enhance details of the pluton shape, which diminishes details in the rest of the area. Units are in milligals due to the pseudogravity

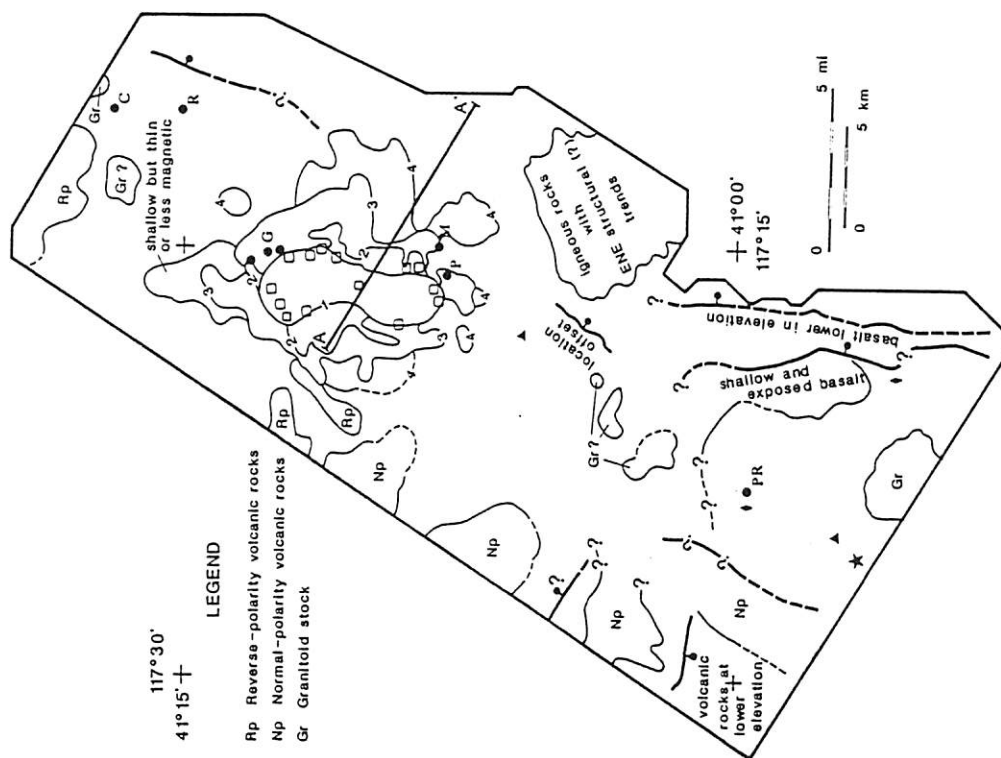


Fig. 7. Schematic diagram showing faults and surface and subsurface extent of plutonic and volcanic rocks as interpreted from the aeromagnetic data and the terrace map. The ore deposits are symbolized as in Figure 2, and labeled as in Figure 4. The Osgood Mountains pluton is shown diagrammatically; contours increase in relative depth from 1 (shallow) to 4 (deep) and coincide with interpreted normal faults in many places. However, only main features of the contours should be considered. Line A-A' refers to the model shown in Figure 6. The offset in location between Hotz and Willden's mapped fault (Fig. 2) and its expression in the magnetic data may be due to incorrect assumptions about the magnetization direction in that area. The over

is fairly uniform (i.e., having a range of susceptibility within an order of magnitude), then the areas of lower value on the terrace map surrounding the higher values over the exposed pluton indicate areas where the pluton is deeper rather than areas where its magnetization is less. The assumption of uniform magnetization for the pluton is fairly reasonable, considering the relatively uniform distribution of magnetite (except near its edges) reported by Neuerberg (1966). The shapes of the terraced areas (Fig. 5) indicate irregularities in the subsurface outline of the pluton. Protuberances are distinct south of the exposed pluton.

A magnetic model of the pluton along a flight line of the contract survey is shown in Figure 6. Using the simplifying assumptions that the pluton is fairly homogeneously magnetized and two and one-half dimensional (varying only in the profile direction) allows a rough fit of the calculated and observed magnetic data. The misfits are mainly due to the true three dimensionality of the pluton shape. The model suggests that the western, buried half of the pluton is slightly more magnetic than the eastern half. On the other hand, a broad, regional magnetic field, produced by deep crustal features unrelated to the pluton, could also produce the higher magnetic values on the west. Future modelling should tighten the results.

The considerable irregularity in the top of the buried part of the pluton is expected from the pattern of magnetization boundaries on Figures 3 and 5. Perhaps other irregularities in the exposed northwestern pluton contact explain why, at the same mine, Horz and Willden (1964) found a steep eastward dip but Stager and Tingley (1988) found a steep westward dip.

Information from the terrace and aeromagnetic maps has been synthesized into a preliminary interpretation of plutonic and volcanic rocks and possible faults (Fig. 7). Only major features are represented at this scale. The Osgood Mountains pluton is schematically represented in three dimensions by depth contours having only relative significance. These contours were interpreted from the terrace map (Fig. 5) and guided by the magnetization boundaries (Fig. 3), which may coincide with normal faults, as discussed earlier. Considering the assumptions made, only gross features of the contouring should be considered credible. In addition, the protuberance on Figure 5 on the southwestern side of the pluton (where the contour is dashed on Fig. 7) may be artificial. In this area, the terracing operator has connected magnetically moderate values from the western side of the pluton and similar values produced by volcanic rocks further west. This connection, only vaguely obvious on Figure 3, may be inaccurate because it spans the merge boundary between the two surveys.

A few general observations are evident from Figure 7; the individual features have already been examined. Volcanic rocks wrap around a large "hole" filled with nonmagnetic Paleozoic rocks in the southern part of the area, where the Preble deposit is located. On the magnetic map, this feature is almost circular (Fig. 3). The difference

in polarity of volcanic rocks mapped as Tertiary basalt and basaltic andesite along the western side of Osgood Mountains (Tba on Fig. 2) suggests at least two separate eruptive episodes. Possibly structurally controlled east-northeast trends just southeast of the center of the study area are contrary to the northeasterly and northwesterly trends of fault strikes and anomaly patterns.

The aeromagnetic data have no consistent signature over the disseminated gold deposits; however, the Pinson and Mag deposits and the northernmost Getchell pit occur near the edge of pluton protuberances, which might be normal faults, as interpreted from the magnetic data (Fig. 7). The Rabbit Creek, Chimney, and Preble deposits are in aeromagnetically nondescript areas; either they are surrounded laterally and vertically by Paleozoic rock units or igneous rocks in their vicinity have negligible magnetization. If the latter is true, the igneous rocks have either undergone extensive hydrothermal alteration that has destroyed magnetization, or they are not related to the highly magnetic igneous rocks characteristic of the rest of the area.

Acknowledgements

We are indebted to Eric Livo for the gray-tone images, which are the best reproducible display that black and white can do. We are also grateful to John Cady, whose criticisms substantially improved this paper, and to Rick Blakely and two anonymous reviewers for their helpful comments.

References

- Bagby, W. C. and Berger, B. R., 1985, Geologic characteristics of sediment-hosted disseminated precious-metal deposits in the western United States, in Berger, B. R., and Bethke, P. M., eds., *Reviews in economic geology* vol. 2—Geology and geochemistry of epithermal systems: El Paso, Society of Economic Geologists, p. 169-232.
- Baranov, V., 1957, A new method for interpretation of aeromagnetic maps: pseudo-gravimetric anomalies: *Geophysics*, v. 22, p. 359-383.
- Berger, B. R., 1985, Geologic-geochemical features of hot-spring precious-metal deposits: U.S. Geological Survey Bulletin 1646, p. 47-53.
- Berger, B. R., and Taylor, B. E., 1980, Pre-Cenozoic normal faulting in the Osgood Mountains, Humboldt County, Nevada: *Geology*, v. 8, p. 594-598.
- Blakely, R. J., and Simpson, R. W., 1986, Locating edges of source bodies from magnetic or gravity anomalies: *Geophysics*, v. 51, p. 1494-1498.
- Cordell, Lindrich, 1985, Techniques, applications, and problems of analytical continuation of New Mexico aeromagnetic data between arbitrary surfaces of very high relief [abs.]: *Proceedings of the International Meeting on Potential Fields in Rugged Topography*, Institute of Geophysics, University of Lausanne, Switzerland, Bulletin no. 7, p. 96-99.
- Cordell, Lindrich, and Grauch, V. J. S., 1985, Mapping basement magnetization zones from aeromagnetic data in the San Juan Basin, New Mexico, in Hinze, W. J., ed., *The utility of regional gravity and magnetic anomaly maps*: Tulsa, Society of Exploration Geophysicists, p. 181-197.
- Cordell, Lindrich, and McCafferty, A. E., 1989, A terracing operator

- for physical property mapping with potential field data: *Geophysics*, v. 54, no. 5, p. 621-634.
- Dobrin, M. B., 1976, *Introduction to geophysical prospecting*: New York, McGraw-Hill, 630 p.
- Erickson, R. L. and Marsh, S. P., 1974, Geologic map of the Iron Point quadrangle, Humboldt County, Nevada: U. S. Geological Survey Geologic Quadrangle Map GQ-1175, scale 1:24,000.
- Erickson, R. L. and Marsh, S. P., 1974, Geologic map of the Golconda quadrangle, Humboldt County, Nevada: U. S. Geological Survey Geologic Quadrangle Map GQ-1174, scale 1:24,000.
- Hildenbrand, T. G., and Kucks, R. P., 1988, Total intensity magnetic anomaly map of Nevada: Nevada Bureau of Mines and Geology Map 93A, scale 1:750,000.
- Hotz, P. E., and Willden, Ronald, 1964, Geology and mineral deposits of the Osgood Mountains quadrangle Humboldt County, Nevada: U. S. Geological Survey Professional Paper 431, 128 p.
- Joralemon, Peter, 1975, K-Ar relations of granodiorite emplacement and tungsten and gold mineralization near the Getchell mine, Humboldt County, Nevada: *Discussion: Economic Geology*, v. 70, p. 405-409.
- Nettleton, L. L., 1971, *Elementary gravity and magnetics for geologists and seismologists*: Tulsa, Society of Exploration Geophysicists, 121 p.
- Neuerburg, G. J., 1966, Distribution of selected accessory minerals in the Osgood Mountains stock, Humboldt County, Nevada: U. S. Geological Survey Miscellaneous Investigations Map I-471, scale 1:24,000.
- Silberman, M. L., Berger, B. R., and Koski, R. A., 1974, K-Ar age relations of granodiorite emplacement and tungsten and gold mineralization near the Getchell Mine, Humboldt County, Nevada: *Economic Geology*, v. 69, p. 646-656.
- Stager, H. K., and Tingley, J. V., 1988, Tungsten deposits in Nevada: Nevada Bureau of Mines and Geology Bulletin 105, 205 p.
- U. S. Geological Survey, 1968, Aeromagnetic map of the southern part of Norths Ranch quadrangle, Humboldt County, Nevada: U. S. Geological Survey Open-File Report 68-290, scale 1:62,500.
- U. S. Geological Survey, 1989, Potential field geophysical programs for VAX 7xx computers: U. S. Geological Survey Open-File Report 89-115, A-D, 3 floppy disks, 21 p.
- Webring, Michael, 1985, SAKI—A Fortran program for generalized linear inversion of gravity and magnetic profiles: U. S. Geological Survey Open-File Report 85-122, 104 p.
- Willden, Ronald, 1964, Geology and mineral deposits of Humboldt County, Nevada: Nevada Bureau of Mines and Geology Bulletin 59, 154 p.

Getchell Trend Airborne Geophysics An Integrated Airborne Geophysical Study Along the Getchell Trend of Gold Deposits, North Central Nevada

D.B. Hoover, V.J.S. Grauch, J.A. Pitkin, D. Krohn, and H.A. Pierce

U.S. Geological Survey Box 25046, Federal Center, MS 964, Denver, Colorado 80225

Abstract

The U.S. Geological Survey has recently completed acquisition of detailed, high quality, multi-sensor, airborne geophysical data in the vicinity of the Osgood Mountains, Humboldt County, Nevada. These data were acquired to demonstrate the utility of such data for assessment of and exploration for mineral deposits in covered terrains. Remote sensing, gamma-ray, magnetic, and electromagnetic instruments were flown, providing measurements of a variety of basic physical properties of earth materials.

The Osgood Mountains region was chosen because of the variety of known mineral deposits in the area and the presence of active gold exploration and mining of gold at six deposits in the study block. One of these, the Rabbit Creek deposit, had been identified below cover, but mining had not begun at the time of flying. This provided a unique opportunity to test the combined methods.

Integration of the data from the four principal geophysical methods used contributes to an understanding of the lithologic units, identification of alteration, structural interpretation, and characterization of deposit models. Important new lithological information resulting from this preliminary work is the three-dimensional definition of the Osgood Mountains pluton, which was responsible for significant tungsten mineralization and which may have played a role in the extensive gold mineralization in the district. Several types of alteration assemblages, probably of more than one age, can be seen in the data, and some of these are in areas not previously known to be altered.

The geophysical data are effective for identification of structures in alluvial cover that are believed related to high angle faults important in the control of mineralizing hydrothermal systems. A preliminary map of these interpreted structures can be used as a guide for exploration.

Introduction

The quest for minerals, particularly in the developed nations, is increasingly focusing on exploration in covered terrains as the probability of new discoveries in exposed areas diminishes. The problems posed by cover require more sophistication in the application of existing technology and the development of new techniques. Improvements may involve better ways of looking through cover rocks or better methods for identifying subtle differences within the cover arising from buried structures or mineralized rocks at depth. Geophysical methods will play an increasingly important role in integrated exploration programs in the future because of their ability to directly address the problems presented by covered deposits.

The U.S. Geological Survey (USGS), in its minerals assessment programs is facing the same problems as industry in the evaluation of the potential of covered areas for mineral commodities. The work presented in this paper describes some of the geophysical investigations of the USGS that are part of an integrated geologi-

cal, geochemical, and geophysical study which addresses the problems of covered areas. In 1988 funding was made available for several airborne geophysical demonstration programs that were intended to show the application of multi-sensor surveys. The authors proposed an integrated airborne program along the Getchell trend, Humboldt County, Nevada, as part of ongoing research on assessment methods that was already underway in the area. Funding became available in April; flying began in August and was completed in early November 1988.

The Getchell trend Airborne Demonstration Program was designed to illustrate the potential of an integrated and comprehensive airborne geophysical surveying program for exploration or assessment in covered terrains. Additionally, it would provide data on the geophysical signatures, and their variability for a variety of different types of deposits that were known in the area. Four distinct geophysical methods were employed: infrared and visible multispectral imaging (remote sensing), gamma-ray spectrometry, magnetics, and electromagnetics. Each technique measures distinctly

different physical properties of the earth that are useful for constraining interpretations based on only one method. The remote sensing and gamma-ray methods map properties of very-near-surface materials, that reflect surficial lithologies and subtle mineralogical or chemical variations within and between units. Electromagnetic methods provide information on electrical resistivity to depths of about 100 m with commercially available instrumentation, whereas magnetics respond to magnetic sources at any depth. This paper will review preliminary results of the airborne surveys, concentrating on the areas where multiple methods complement each other to improve the interpretation of the geologic setting. Companion papers in this volume discuss the individual airborne techniques that were used (Pirkin, 1990, gamma-ray data; Grauch and Bankey, 1990, magnetics; and Pierce and Hoover, 1990, electromagnetics).

The Getchell trend was chosen for this study because of

the presence of a variety of known types of mineral deposits, including bedded barite, skarn tungsten, tungsten-bearing manganese, silver, and disseminated gold. Active gold mines include those at the Preble, Pinson, Mag, Getchell, Rabbit Creek, and Chimney deposits. These known deposits provide a means for testing methods and models. The Rabbit Creek deposit was of particular interest. At the time of the flying, it was a blind deposit with over 100 m alluvial of cover; it was being drilled, but stripping of the cover had not yet begun.

This provided a unique opportunity to test a combination of methods. The cooperation of most of the mining companies in providing access to their properties for ground studies also was an important factor in selecting this study area.

The area surveyed lies principally on the eastern flank of the Osgood Mountains (Fig. 1), and covers an area of about 450 km². In general, the northern margin is at the Chimney deposit, and the southern boundary lies along Interstate

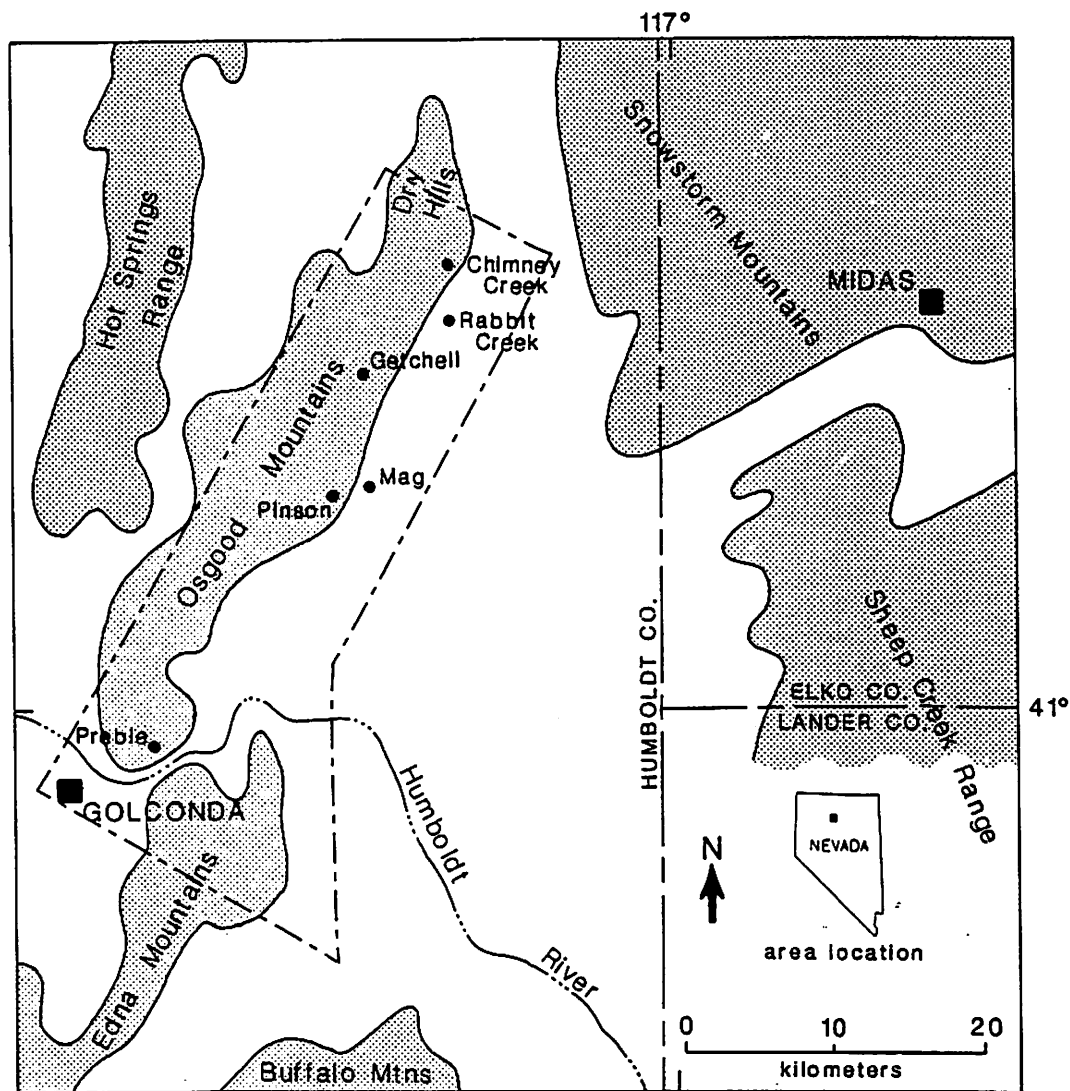


Fig. 1. Sketch map of the Osgood Mountains area, Humboldt County, Nevada, showing location of airborne surveys discussed in this paper by heavy outline

different physical properties of the earth that are useful for constraining interpretations based on only one method. The remote sensing and gamma-ray methods map properties of very-near-surface materials, that reflect surficial lithologies and subtle mineralogical or chemical variations within and between units. Electromagnetic methods provide information on electrical resistivity to depths of about 100 m with commercially available instrumentation, whereas magnetics respond to magnetic sources at any depth. This paper will review preliminary results of the airborne surveys, concentrating on the areas where multiple methods complement each other to improve the interpretation of the geologic setting. Companion papers in this volume discuss the individual airborne techniques that were used (Pickin, 1990, gamma-ray data; Grauch and Bankey, 1990, magnetics; and Pierce and Hoover, 1990, electromagnetics).

The Getchell trend was chosen for this study because of

the presence of a variety of known types of mineral deposits, including bedded barite, skarn tungsten, tungsten-bearing manganese, silver, and disseminated gold. Active gold mines include those at the Preble, Pinson, Mag, Getchell, Rabbit Creek, and Chimney Creek deposits. These known deposits provide a means for testing methods and models. The Rabbit Creek deposit was of particular interest. At the time of the flying, it was a blind deposit with over 100 m alluvial of cover; it was being drilled, but stripping of the cover had not yet begun.

This provided a unique opportunity to test a combination of methods. The cooperation of most of the mining companies in providing access to their properties for ground studies also was an important factor in selecting this study area.

The area surveyed lies principally on the eastern flank of the Osgood Mountains (Fig. 1), and covers an area of about 450 km². In general, the northern margin is at the Chimney Creek deposit, and the southern boundary lies along Interstate

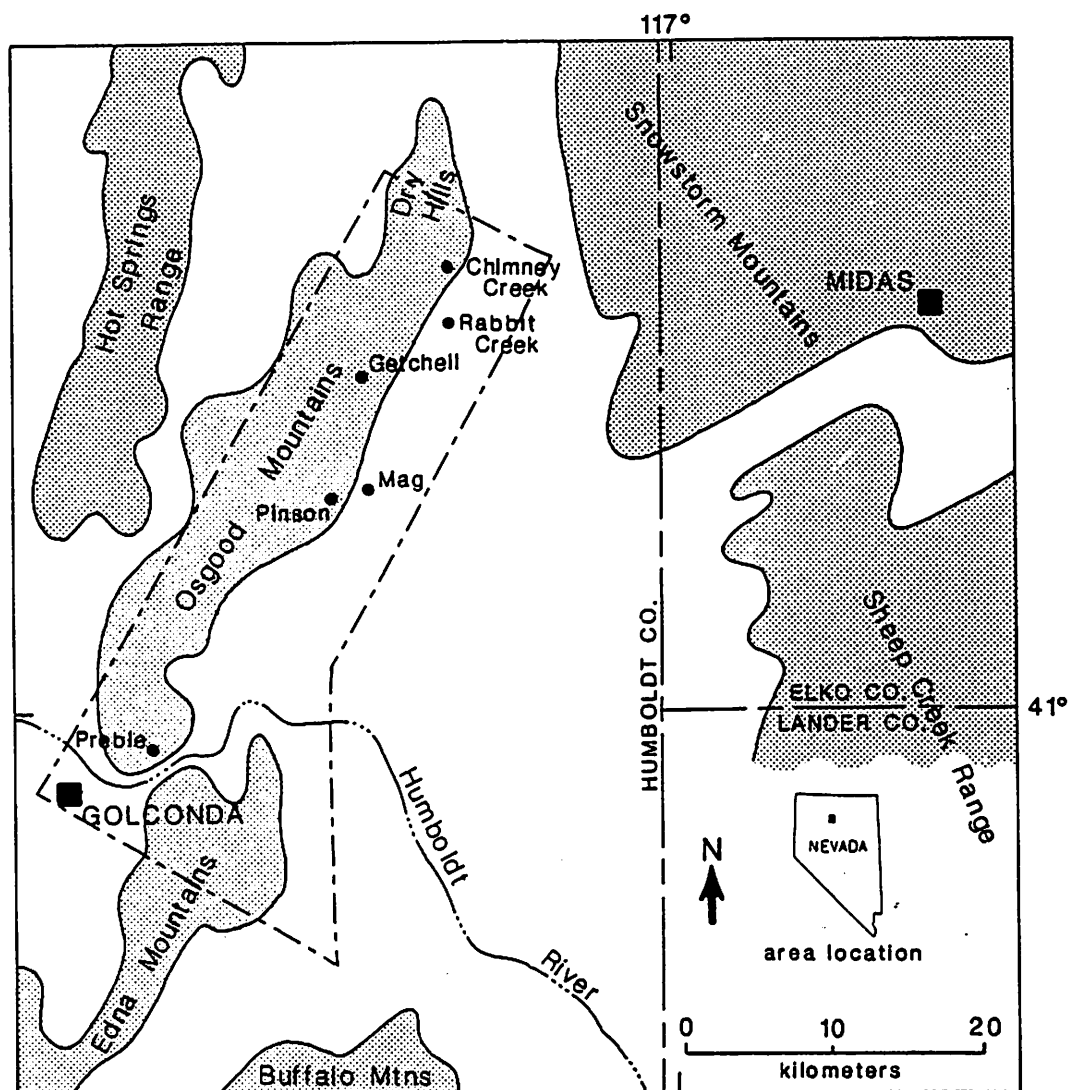


Fig. 1. Sketch map of the Osgood Mountains area, Humboldt County, Nevada, showing location of airborne surveys discussed in this paper by heavy outline

Highway 80. The western boundary is the crest of the Osgood Mountains. From the crest of the range the survey area extends east about 12 km to where the cover rocks are believed too thick for present exploitation. For practical reasons, the coverage of individual airborne surveys varied. Details are given in the companion papers.

Two strips of 63-channel airborne imaging spectrometer data in the near infrared and visible region were acquired specifically for this project, by

Geophysical Environmental Research Corporation (GER). Previously acquired remote sensing data from the Landsat Thematic Mapper (TM) satellite and the Thermal Infrared Multispectral Scanner (TIMS) system of the Stennis Space Center at NASA were also available. The TIMS system was reflown for this project, but extensive cloud cover made the data unusable. Gamma-ray data were acquired by Terrasense, Inc. using a complete calibrated system for quantitative measurement of the radioelements, uranium, thorium, and potassium, using a helicopter platform. Combined magnetic and electromagnetic data were contracted for from DIGHEM, Inc. again using a helicopter. To supplement the magnetic data acquired by DIGHEM, the USGS flew additional areas using its in-house system and a fixed-wing platform. The magnetic, gamma-ray, and electromagnetic data were acquired with a maximum flightline spacing of 400 m (1/4 mile).

These airborne and satellite data sets are useful for distinguishing lithologies, identifying areas and types of alteration, mapping structures, and characterizing geophysical signatures of deposits. In the following discussion the contribution of each of the geophysical methods to understanding of these geological features will be explained by integration of the geophysical data, rather than discussing each method separately. To illustrate the utility of these data to exploration in the Getchell area the discussion will focus on aspects that show the application of multi-disciplinary data. Analysis of these data is still preliminary and will require additional time for a complete synthesis.

The black and white, page-sized illustrations of the geophysical data shown in this paper are adequate only to show major, high-contrast features in the data. Many important features evident in larger scale color maps become obscure or impossible to illustrate at page size. In the case of the TIMS data only topographic and some linear features are evident. Because the lithologic discrimination based on spectral properties cannot effectively be shown in black and white these data are not shown. Because of the interest by the mining community in these airborne data sets, the digital data have been released through the National Oceanic and Atmospheric Administration's Geophysical Data Center, Boulder, Colorado. Colorshaded-relief maps of these data at 1:100,000 scale also can be seen at the Nevada Bureau of Mines in Reno, and at USGS offices in Menlo Park, California, Tucson, Arizona, Spokane, Washington, Denver, Colorado, Salt Lake City, Utah, and Reston, Virginia. The reader interested in more detail is referred to one of the above sources.

Geologic Setting

The Osgood and Edna Mountains region has undergone repeated episodes of structural deformation particularly during the Paleozoic. Mesozoic and Cenozoic extrusive and intrusive rocks further complicated or masked relationships. The following geological summary is based on mapping by Hartz and Willden (1964), Willden (1964), and Erickson and Marsh (1974a, 1974b), and unpublished mapping by A. R. Wallace and D. M. McGuire, both of the USGS.

Extensive new mapping is currently being conducted by mining companies in the region. As additional information becomes available, changes in the interpretation of the geological, geochemical, and geophysical data can be expected.

Lithology

The oldest units shown on the geologic map (Fig. 2) are Paleozoic quartzite, shale, limestone, and sandstone deposited in shallow shelf to eugeosynclinal environments. The Osgood Mountain Quartzite (ϵ_{om}), of Early Cambrian(?) age, is the oldest of these units and is overlain by Middle and Upper Cambrian shales and limestones of the Preble Formation (ϵ_p). Middle and Upper Ordovician Comus Formation (Oc) carbonates and shales were deposited directly on the Preble Formation. Overlying this are Ordovician cherts, greenstones, and argillites of the Valmy Formation (Ov). Only minor exposures of the latter unit occur in the area studied. Silurian to Early Mississippian units are missing in this area as a result of disturbances of the Early Mississippian Antler orogeny, but a return to shelf-type sedimentation resulted in the deposition of the Antler-age sequence, which in the study area includes limestone, shale, and sandstone of Pennsylvanian to Permian age. The only known Mesozoic units in the area are intrusive rocks of granodiorite composition, which were responsible for tungsten mineralization, and possibly for gold mineralization (Silberman et al., 1974). The most prominent exposure is the Osgood Mountains pluton in the northern part of the Osgood Mountains. In outcrop the pluton appears as two ovoid bodies joined by a narrow septum to form an hour glass-shaped body. This body appears prominently in all the geophysical data. A smaller granodiorite pluton is present in the Edna Mountains east of Golconda, with most exposures north of the interstate highway. Skarns and hornfels developed in carbonate rocks on the margins of the plutons host all but one of the tungsten deposits.

Cenozoic rocks of the region consist principally of basalt and basaltic andesite flows and Neogene to Quaternary fanglomerates. Rhyolites and tuffs are present to the east and southwest of the survey area and they are source rocks for some of the alluvial material in the area. Only minor amounts of rhyolites and tuffs are known in the study area.

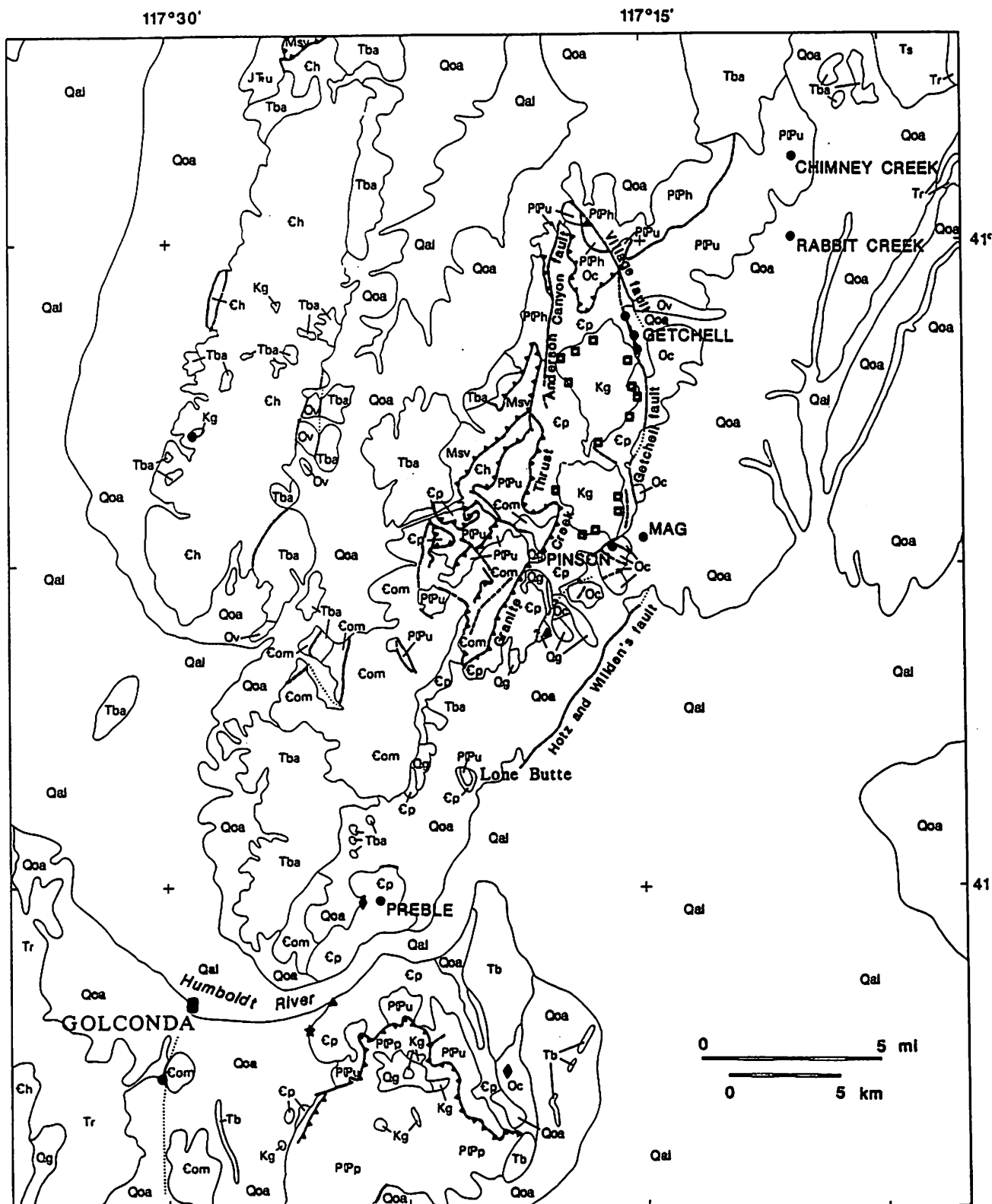


Fig. 2. Geological map of the Osgood Mountain area, Humboldt County, Nevada adopted from Willden (1964), Hotz and Willden (1964), and Erickson and Marsh (1974a, 1974b).

DESCRIPTION OF MAP UNITS
(Listed in approximate stratigraphic order)

- Qal - Quaternary alluvium
- Qoa - Older Quaternary alluvium
- Qg - Quaternary gravel
- Tb - Pliocene basalt
- Tr - Miocene rhyolite flows and tuffs
- Ts - Miocene clastic rocks and tuffs
- Tba - Miocene basalt and basaltic andesite
- Kg - Cretaceous granodiorite (about 90 Ma)
- JTu - Jurassic and Triassic metaclastic rocks, undivided
- PPu - Permian and Pennsylvanian clastic and carbonate rocks, undivided. Includes Edna Mountain Formation (Permian), Antler Peak Limestone (Pennsylvanian and Permian), Highway Limestone (Pennsylvanian), and Battle Formation (Pennsylvanian). In the Osgood Mountains, includes the Etchart Limestone (Pennsylvanian and Permian) and the Adam Peak Formation (Pennsylvanian and Permian).
- PPp - Pumpernickel Formation (Pennsylvanian and Permian)--siliceous sedimentary and volcanic rocks
- PPh - Pennsylvanian and Permian siliceous sedimentary and volcanic rocks, undivided. Includes the Havallah Formation (Pennsylvanian and Permian), rocks similar to the Havallah and Pumpernickel Formations in the Hot Springs range, and the Farrel Canyon Formation (Pennsylvanian and Permian) in the Osgood Mountains.
- Msv - Mississippian siliceous sedimentary and volcanic rocks. In the Osgood Mountains includes the Goughs Canyon Formation.
- Ov - Valmy Formation (Ordovician)--Chert and greenstone
- Oc - Comus Formation (Ordovician)--Carbonate rocks and sandstone
- Ch - Harmony Formation (Cambrian)--Sandstone and shale. Includes small exposures of Paradise Valley Chert (Cambrian) on the west side of the Hot Springs Range.
- Cp - Preble Formation (Cambrian)--Shale and limestone
- Com - Osgood Mountain Quartzite (Cambrian)
- Contact
- - - Fault, dashed where approximately located, dotted where concealed
- ▶ Thrust fault, sawteeth on upper plate
- MAG Gold deposit; names indicate operational or developing mines
- Tungsten deposit
- ◆ Silver deposit
- ▲ Barite deposit
- ★ Manganese deposit

The Paleozoic rocks in this area were extensively deformed during three pre-Tertiary tectonic events. Thrusting during the Antler and Sonoma orogenies brought western facies deep-water units over or interleaved them with, eastern facies, shallow-water units in a complex assemblage. This can be seen in the Osgood and Edna Mountains (Fig. 2) where exposures are good.

These thrusts are generally north or northeast striking. The Paleozoic units are tilted and folded, often isoclinally, and steeply dipping. Bedding strikes generally north or northeast and dips generally east to southeast.

Mesozoic faults have been identified only adjacent to the Osgood Mountains pluton. These are normal, north to northeast striking faults, and include the Anderson Canyon, Getchell, and Village faults (Fig. 2).

Cenozoic Basin-and-Range extension reactivated north-striking normal faulting and produced the Osgood and Edna Mountains horst blocks. During the Basin-and-Range extension, mafic and felsic dikes were intruded along many of these reactivated zones. The high angle faults here, and as Percival and others (1988) point out for most sediment hosted gold deposits, were important ore controls, a control important on both regional and deposit scales.

Mineral Deposits

A variety of types of mineral deposits are present in the area shown (Fig. 2). Gold is of primary interest today, and it is being actively mined at the Preble, Pinson, Mag, Getchell, Rabbit Creek, and Chimney deposits (Fig. 2). During the period 1939-1941, the Getchell mine was the leading gold producer in Nevada. Exploration in the area now is entirely focused on gold, with private industry having extensive exploration programs on all available land.

Bedded barite has been mined from four deposits in the Preble and Comus Formations in the southern half of the study area. None of these are presently active. Scheelite was mined from numerous skarn deposits surrounding the Osgood Mountains pluton from 1942-1962. Humboldt County ranks second in the state for production of tungsten, with the bulk of that production coming from deposits in this area (Stager and Tingley, 1988). No commercial tungsten mineralization has been found adjacent to the intrusive in the Edna Mountains.

Silver has been produced from the Silver Lode claims just west of the Preble mine and from the Silver Coin and adjacent mines in the southeast part of the survey region.

A unique tungsten-bearing manganese deposit at the Golconda mine on the west flank of the Edna Mountains was mined from 1941-1945 (Stager and Tingley, 1988). This is a Quaternary, hot-spring manganese deposit formed on steeply dipping Preble Formation and overlain by tufa (Kerr, 1940). Mineralization extends only a short distance into the underlying rocks. The spring is weakly active today.

Lithologic Characterization

Collectively, the airborne geophysical data sets are able to differentiate between some of the major lithologic units, and, at least for the Preble Formation, distinguish calcareous members from the surrounding phyllitic members. The geophysical characteristics of these major units will be described with reference to the geologic map (Fig. 2). Because this region is well mapped, there are no major discrepancies between mapped lithologies and those suggested by the airborne geophysical data. The airborne data provide an excellent example of what an integrated airborne program can do to facilitate mapping in poorly known or covered regions, permitting more efficient use of geologic staff. Of more interest to the present exploration community is the mapping of some units where they are hidden by cover, and identification of areas with anomalous physical properties.

The Osgood Mountain Quartzite (€om, Fig. 2) is defined by a high SiO₂ response in the TIMS data, very low radioelement content (Figs. 3, 4, and 5), and high resistivity (>1000 ohm-m, Fig. 6). It is transparent magnetically like all the sedimentary units in the area, so magnetic data does not help in the mapping of these units. Differentiation between the sedimentary rocks thus relies on the use of the remote sensing, gamma-ray, and electromagnetic methods. The largest exposure of the Osgood Mountain Quartzite is in a southwest-trending band about 15 km long beginning at the southwest end of the Osgood Mountains pluton. The radioelement maps (Figs. 3, 4, and 5), and the 900 Hz resistivity map (Fig. 6) show this quartzite as a band of black to dark grey tones. It can be distinguished from relatively massive limestone units, that are also low in radioelements and have high resistivities, by the high SiO₂ response shown in the TIMS data.

The Preble Formation (€p, Fig. 2) phyllites which constitute the greater thickness of the formation (Hotz and Willden, 1964) have a TIMS signature indicative of intermediate SiO₂ content, radioelements K and particularly Th (12-16 ppm) elevated above average for the area, and resistivity averaging several hundred ohm-m. The intermediate limestone member of the Preble Formation, for example near the Preble mine, has distinctly lower radioelement and SiO₂ content and higher resistivity than the phyllite. The limestone member has not been mapped separately on Figure 2.

A notable exception to the high resistivity of the middle limestone member can be seen adjacent to the Osgood Mountains pluton southwest of the Pinson mine, where it crops out over a distance of 7 km. The eastern boundary is several hundred meters west of the high angle fault that separates the Preble and Comus Formations in this area (Fig. 2). The resistivity map at 900 Hz (Fig. 6) shows a band of very low resistivities in this region, in places less than 5 ohm-m. Resistivities in this zone tend to decrease as the pluton is approached.

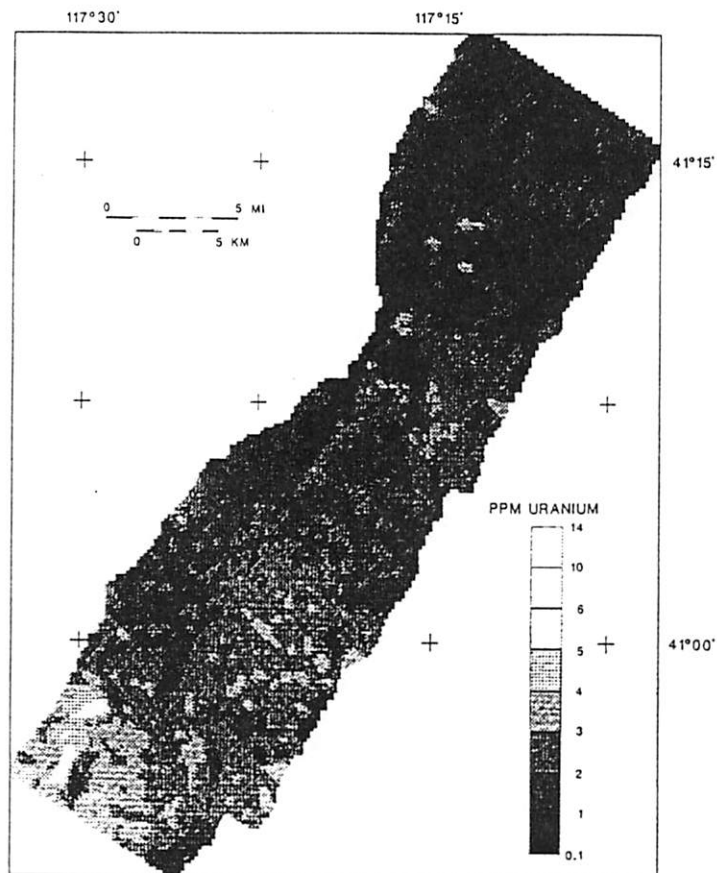


Fig. 3. Uranium concentrations map derived from an airborne gamma-ray survey of part of the Osgood Mountains, Humboldt County, Nevada.

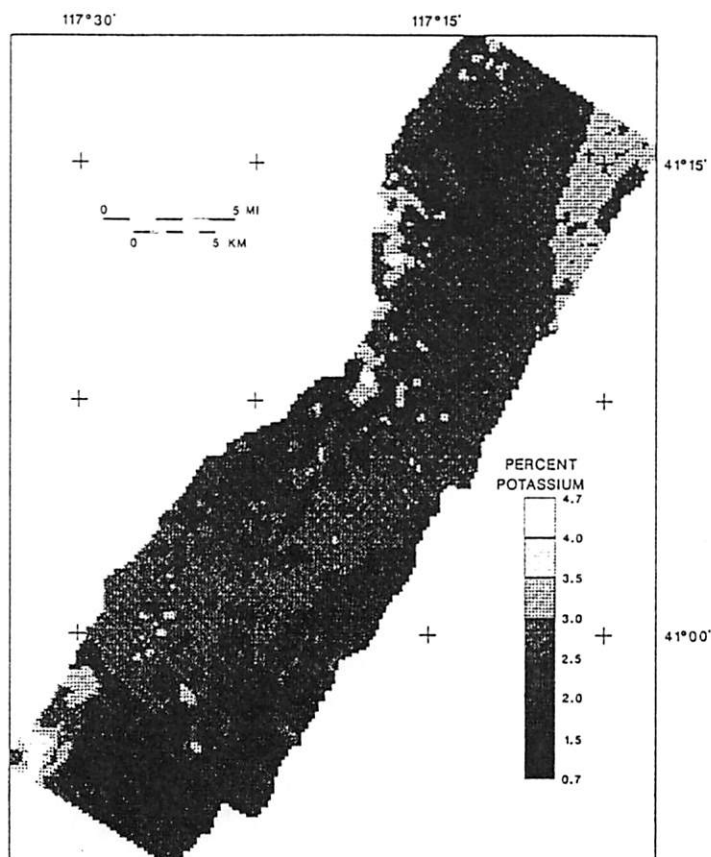


Fig. 4. Potassium concentration map derived from an airborne gamma-ray survey of part of the Osgood Mountains, 745 Humboldt County, Nevada.

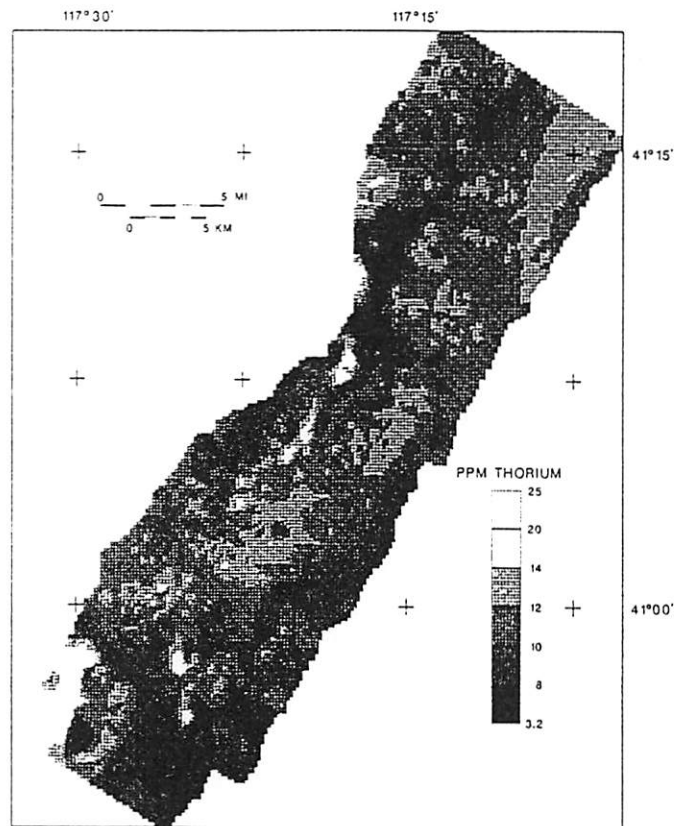


Fig. 5. Thorium concentration map derived from an airborne gamma-ray survey of part of the Osgood Mountains, Humboldt County, Nevada.



Fig. 6. Resistivity map for a frequency of 900 Hz, derived from DIGHEM* airborne electromagnetic survey of part of the Osgood Mountains, Humboldt County, Nevada.

Radioelement and TIMS data show nothing anomalous.

Resistivities computed at 56,000 Hz, the very shallow looking data, do not identify a strong conductor in this area, but the 7200 Hz data begins to reveal a conductive unit. The cause of the low resistivity is not exposed at the surface. Drilling across this anomalous zone to 160 m (500 ft) shows that the middle member of the Preble is present (E. Kretschmer, 1985, personal comm.), and that it dips steeply to the east.

Because the 900 Hz EM response comes predominantly from the upper 100 m, the anomalous response must be related to the Preble Formation. We speculate that this low resistivity may be related to the presence of sulfides and carbon, perhaps remobilized and deposited as thin films along fractures resulting from thermal or hydrothermal processes adjacent to the pluton.

Too little Comus Formation (Oc, fig. 2) is exposed and distant from mineralized areas to assign a geophysical signature. Most exposures are along the east side of the range near the Gertchell, Mag, and Pinson deposits.

The Pennsylvanian and Permian units are predominantly calcareous and have a signature similar to that of the middle member of the Preble Formation. The low radioelement values and high resistivities of these units may be seen in Figures 3, 4, 5, and 6 extending northeast from the Gertchell mine area to just west of the Chimney deposit. The Adam Peak Formation constitutes the bulk of the mapped Pennsylvanian and Permian unit 2 km west of the southern lobe of the Osgood Mountains pluton. In this area, over 50% of the formation is composed of sandstone or dolomitic sandstone; the remainder is shale, siltstone, limestone, and chert (Hotz and Willden, 1964). The beds dip steeply and strike north. Although not expected, the electrical data (Fig. 6) show that this formation also is very conductive similar to the anomalous middle member of the Preble Formation near the Pinson mine. The conductive Adam Peak Formation terminates on the southwest against a northwest-striking fault (Fig. 2). Adam Peak Formation occurs south of this fault, but it and other Pennsylvanian and Permian units are not conductive. The low resistivity associated with the main part of the Adam Peak Formation is most prominent at 900 Hz but is evident also at 7200 and 56,000 Hz, suggesting that the anomalous values are near the surface and probably not due to underlying units. As with the middle part of the Preble Formation adjacent to the granodiorite, we believe this is probably related to thermal and/or hydrothermal effects and not representative of Adam Peak Formation as such.

The Harmony Formation (E-h, fig. 2), composed principally of feldspathic sandstone, is in thrust contact with the Adam Peak Formation on its west side. The northern third of this unit also appears very conductive, again suggesting that alteration has taken place. An abrupt transition to high resistivity (from 2.5-600 ohm-m) occurs along a northwest trend suggesting fault or fracture control.

The Cretaceous granodiorite in the Osgood Mountains is prominently mapped in all four data sets. In the magnetic data (Fig. 7) it is the dominant feature. The

boundary determined by automated horizontal gradient analysis (Cordell and Grauch, 1985) computer processing conforms very well with the mapped contacts, except in the region between the two main lobes where the magnetic data shows that the body is present beneath thin cover. Hotz and Willden (1964) postulated that the granodiorite extended under shallow cover to the north, based on wide spread metamorphism in the area. The magnetic data confirm this inference. Hotz and Willden (1964) also suggest that the western boundary of the granodiorite dips steeply east. The magnetic data imply otherwise. Grauch and Bankey (1990) map the pluton as extending under cover several kilometers west of its surface expression. Inferred alteration in the Preble, Harmony, and Adam Peak, Formations and high resistivities in the Preble Formation adjacent to the west side of the pluton are consistent with a westward subsurface extension of the body.

The granodiorite has a unique signature in the TIMS data, shown as a combined response from SiO_2 and mafic minerals, and in the radioelement data. The granodiorite does not stand out directly in the individual radioelement maps of Figures 3, 4, and 5, but it becomes clearly defined in a color composite presentation where it has a dominant potassium signature.

This is due to a relative deficiency of thorium and especially uranium in the intrusive. Electrically the granodiorite is an area of high resistivity, greater than 1000 ohm-m. The resistivity map (Fig. 6) does not provide sharp definition at the contact due to the skarn zone developed along the border of the granodiorite. Resistivity of the metamorphosed sedimentary rocks approaches that of the granodiorite.

A buried outlier, inferred to be granodiorite, is evident from the geophysical data on the east side of the southern lobe of the pluton. It appears in the magnetic data as a slight high, with northwest trending boundaries on the north and south protruding southeast from the main magnetic high. This area is not evident in the resistivity maps, but a derivative map (ratio of the 7200 Hz to 900 Hz data) defines the area as anomalous. This outlier is potentially important because of the ground preparation that may have taken place. The Mag gold deposit is within this region.

The small exposures of granodiorite in the southern part of the study region are well expressed only in the magnetic data (Fig. 7). The lack of expression in the TIMS and radioelement data may be due to the few exposures. The lack of expression in the resistivity data is more surprising. This may be due to too little of the granodiorite within the exploration depth of the survey, alteration of the intrusive, or a combination of these.

The radioelement characteristics of gold-bearing granitoids that are probable source rocks for gold mineralization have been discussed by several authors (Kochetkov et al., 1987; Vasil'ev et al., 1985; Zlobin and Kurulenko, 1981). These authors indicate that low content of radioelements and low Th/U ratios (1.5-2.5) are characteristic. Radioelement data for the Osgood

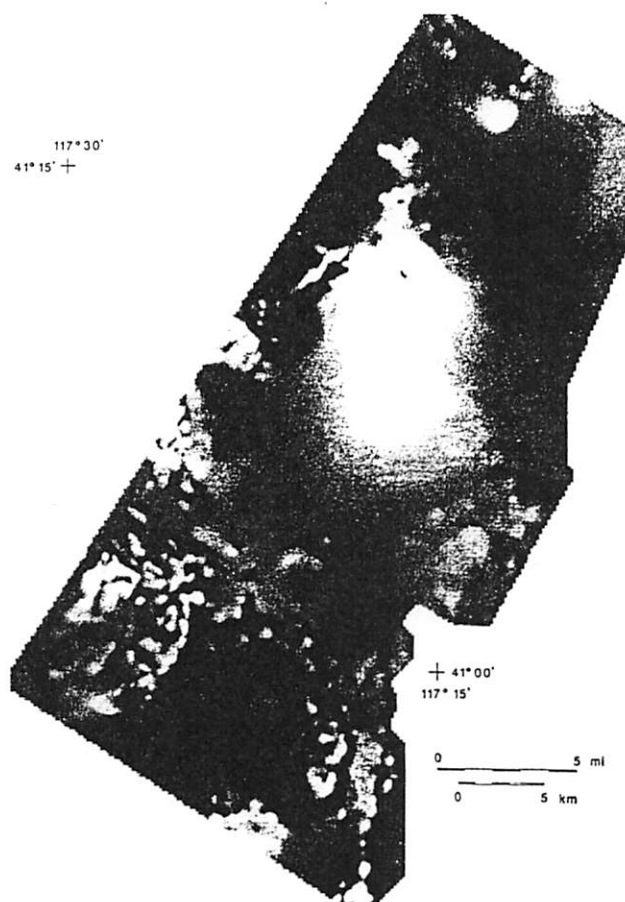


Fig. 7. Total field airborne magnetic map of part of the Osgood Mountains, Humboldt County, Nevada.

Mountains pluton shows that U is about 0.5 ppm, Th about 8 ppm, K about 2.7%, and Th/U=16. An average granodiorite would contain U=2.3 ppm, Th=9.0 ppm, K=2.55% and Th/U=4 (Clark et al., 1966). Horz and Willden (1964) give values of 2.8% for K_2O from two samples from the northern part of the pluton. The radioelement content of the pluton is average except for the greatly reduced U content. It is not clear to what extent the low U may be reflecting differential weathering, giving an anomalously high Th/U ratio. The average K, and Th contents, however, suggest that this granodiorite would not meet the criteria of the Russian authors, although Neuerburg (1966) does report higher than average gold values for the pluton.

In the northern part of the survey area, two small magnetic highs are seen: one near the Chimney mine, and another 8 km north of the Gertchell mine. These are inferred to be expressions of buried intrusives. They are not expressed in the other data sets because of their depth of burial. In the vicinity of Lone Butte, 6 km northeast of the Preble mine, interpretation of the magnetic data suggests the presence of another intrusive (Grauch and Bankey, 1990).

The Tertiary basalts are best expressed in the magnetic data. The exposed units show a short wavelength, high amplitude pattern typical of such volcanic rocks. The basalts, however, do not have a consistent radioele-

ment signature. The basalts capping a ridge in the southeast part of the area show the lowest values of potassium, about 1.5%, but not nearly as low as reported by Horz and Willden (1964) for a sample of this flow (0.6%). It is not clear to what extent the higher potassium identified in the airborne data may be due to windblown detritus. Resistivities of the basalts are variable, generally between 1000 and 100 ohm-m. Magnetic features in the area of Quaternary cover south and east of the Pinson mine are believed to be related to buried igneous rocks, some of which could be basalts within the fill. Quaternary alluvium is generally below 100 ohm-m, and in places, such as east of Lone Butte, it may reach 2 ohm-m (Fig. 6). The very low values in that area are believed to be due to clay sediments saturated with warm saline water that issues from a warm spring. Radioelement data provides the best evidence for disparate sources of the transported material. This is particularly evident in the thorium data (Fig. 5) but is also seen in the potassium data. In the northeastern part of the map, a sharp boundary is seen approximately along the trace of the Rabbit Creek drainage. High thorium east of the drainage derives from Miocene volcanic rocks exposed to the east. The low thorium material west of the drainage derives from the Pennsylvanian and Permian carbonates further west. A similar pattern can be seen in the southwestern part of the study along a drainage east of Golconda.

Alteration Patterns

The effects of alteration on the rock types in the Getchell trend are evidenced in all the geophysical data sets. The TIMS data reveal areas of silicification related to jasperoids as single pixels near the Preble mine. GER multi-spectral data, which we are just beginning to process, has revealed illite along the Getchell fault in the Getchell mine area (M.D. Krohn, 1989, personal comm.). Illite is a characteristic alteration mineral in gold deposits along the Carlin trend (Percival et al., 1988). The spectral response of the illite particularly in the longer wavelengths near 2.4 micrometers, appears related to mica polytypes (Hauff et al., in press), which in turn may be related to differences in formation of the clays. Radioelement redistribution from hydrothermal systems, particularly potassium metasomatism, is clear in the gamma-ray data. Destruction of magnetite is prominently seen in the magnetic data. Low resistivities in some areas are believed to be related to alteration, probably with introduction and redistribution of sulfides and carbon. Examples of these will be discussed below. In other areas of northern Nevada resistivity highs related to silicification have been reported (P. Hallof, 1989, personal commun., and C. Windells, 1989, personal commun.). Evidence for high resistivity silicified areas, either from the airborne or limited ground surveys, has not yet been seen in the Getchell region. This appears to be a peculiarity of this region, lack of sufficient detail near the deposits, or insufficient contrast in resistivity.

Alteration within the Preble Formation and Pennsylvanian and Permian sedimentary rocks adjacent to the Osgood Mountains pluton, evidenced by anomalously low resistivities, has already been discussed. Because of the spatial relationship to the Osgood Mountains pluton, the hydrothermal system responsible for the inferred alteration is speculated to have been derived from the cooling pluton. If these low resistivity rocks are related to alteration processes, then much additional research is needed to determine their relationship, if any, to the granodiorite, and to the presence of mineralized rocks adjacent to the pluton.

The most obvious area of alteration revealed in the airborne data is in the center of the northern lobe of the Osgood Mountains pluton. This is indicated by a large local potassium increase, and prominent local magnetic low coincident with sec. 5, T38N, R42E. Extensive alteration in the pluton within section 5 is discussed by Hotz and Willden (1964) and Neuerburg (1966). Alteration occurred during late-stage crystallization and from a post-solidus hydrothermal system. Granodiorite in the altered area was first prospected for silver, and it later produced scheelite from quartz bodies and veins. Neuerburg's (1966) accessory mineral data shows a strong northwest trend in mineral distribution suggesting that this was a preferred direction along which the hydrothermal systems developed. Magnetic data shows an elliptical low, trending northwest (Fig. 7), that corresponds with the mapped alteration in sec. 5. Whole

rock magnetite quantities within the granodiorite (Neuerburg, 1966) show that magnetite was destroyed in a northwest-trending zone through sec. 5, indicating the cause of the magnetic low. Although Neuerburg (1966) show 5 other low magnetite zones within the granodiorite, the magnetic data show that no other areas have been as extensively altered as in sec. 5.

Coincident with the magnetic low over the altered area of sec. 5 in the Osgood Mountains pluton, the radioelement data show a local, nearly circular pattern of alteration, with increases in all three elements. Uranium values are 1.5-2 ppm, thorium values are 12-14 ppm, and potassium values are 4-4.5%. Thorium and potassium are almost doubled, and uranium is tripled or quadrupled. The increased content of all three radioelements is consistent with alteration associated with late-stage cooling processes.

Resistivity data show slightly reduced values in the altered area, with a northwest alignment. This is not easily seen in Figure 6 because of the scale. The alteration is not as evident in the TIMS data, but appears as a patch of increased silica content.

The potassium map (Fig. 4) shows two other areas adjacent to the granodiorite that have distinctly anomalous potassium (>4%). Both areas are within the Preble Formation about 1 km from the granodiorite contact. One is 3 km northwest of the altered zone in the granodiorite, and the other 2.5 km west of the Pinson mine at the contact with the Granite Creek thrust (Fig. 2). Magnetic data (Fig. 7) suggest that small apophyses of granodiorite may be present below these high-potassium regions. Thorium is high in both of these areas, but uranium is increased only in the area west of the Pinson mine. Resistivity data are not available in the northern area. The area west of Pinson shows a large resistivity gradient that, at least in part, reflects the contrast between the Osgood Mountain Quartzite and Preble Formation where they are juxtaposed across the Granite Creek thrust. The high-potassium area west of the Pinson mine is the northeast terminus of a distinct southwest-trending radioelement linear feature that coincides with the Granite Creek thrust for 8 km and that continues less distinctly to the Humboldt River. The full extent of this linear feature is best expressed in the uranium data, although it appears as a prominent high in all three radioelements along the Granite Creek thrust within the Preble Formation. The quantities of radioelements tend to decrease away from the granodiorite.

Southwest of the terminus of the Granite Creek thrust electrical data identify a narrow, linear conductive zone inferred to be related to a steeply dipping fault generally coincident with the radioelement linear. This conductive zone is not evident to the northeast along the thrust because of the large contrast in resistivities between the quartzite and phyllite across the thrust. The magnetic data are very quiet along the Granite Creek thrust, but short disconnected magnetization boundaries further south (Grauch and Bankey, 1990) may

represent faulting related to this linear trend.

Figures 8, 9, and 10 show the radioelement concentrations for the southern quarter of the survey area in more detail. Two areas of high potassium and thorium are evident in this region within phyllites of the Preble Formation. One is centered 1 km east of the manganese deposit at the Golconda mine, and the other is 3 km north of the manganese deposit. This area is particularly quiet magnetically with no distinct indication of magnetic minerals associated with the increase in radioelements. These two radioelement highs are adjacent to northeast-trending electrical lows that suggest high-angle faults. The electrical low east of the Golconda mine correlates with a short northeast striking fault mapped by Erickson and Marsh (1974a) and more extensive alteration to the northeast. This electrically conductive zone can be traced to the Preble mine. We postulate that the Golconda ore body, anomalous radioelement values, and the Preble ore body are related to alteration of the Preble Formation by solutions whose paths were controlled by a high-angle fault system that is reflected in the electrical and radioelement data. The maps (Figs. 8, 9, and 10) show very high uranium and elevated potassium and thorium values associated with the Golconda hot spring just northeast of the point 40° 57' 30"N, and 117° 30'W. Other known areas of thermal water in the area do not have a similar expression. The maps also suggest that the basaltic andesite in the northwest part of the figures is anomalous in K and Th, possibly indicative of alteration. The basaltic andesite flows (andesite in Erickson and Marsh, 1974a) have a total thickness of about 62 m (200 ft) and have been dated at 22.0 ± 0.7 m.y. (Erickson and Marsh, 1974a). Underlying these flows is andesite tuff that is as much as 94 m (300 ft) thick and that was erupted onto Osgood Mountain Quartzite. The high potassium (3-3.5%) and thorium (14-20 ppm) and low uranium (1-2 ppm) in some areas is anomalous for andesite (Clark, et al., 1966). The anomalous regions are in topographically high parts of the range where wind-blown detritus is not expected to accumulate. The areas of high K and Th correlate with resistivity and magnetic lows (Figs. 6 and 7). These magnetic and resistivity lows could be responding to underlying tuffs in areas where the andesite flows are thin. However, the tuffs would not be expected to have such high K and Th contents, and, where they are exposed, they do not exhibit the high values seen over the flows. This suggests alteration but needs ground confirmation.

Discussion of Data

Structural Interpretation

Patterns in the various geophysical data sets that provide evidence of the structural setting in the area will be discussed in this section. Because the airborne data sets provide relatively little information on details of the

variation of the mapped properties with depth, low-angle structures are often difficult to define. These data are most effective at identifying lateral changes in properties that, with some knowledge of geologic relationships, may be interpreted in terms of high-angle structures or abrupt lithologic changes. This section will focus on the identification and location of near vertical structures. As Percival and others (1988) have pointed out, the high-angle structures had a primary role in localizing the flow of hydrothermal systems responsible for the deposition of gold. This is true at both regional and deposit scales.

Structural analysis using the individual airborne data sets has been based primarily on lineament identification and their relationships to known geology. A lineament map derived from the TIMS data for the east side of the Osgood Mountains (Fig. 11) shows prominent northeast and northwest trends with a less-prominent north-south set. Many of these correspond with features seen in the other airborne data sets. A good example on Quaternary cover is a 4-km-long, north-trending, broken, linear feature identified by the letter A in Figure 11. The northern trending TIMS linear feature correlates directly with a north-trending, resistivity boundary high on the west, inferred to be due to faulting.

Visual examination of the airborne data shows that north-south and northeast-southwest trends are the most prominent. Figure 12 is a preliminary interpretation of the major structural breaks derived from the new airborne data. Other constraints on the interpretation are from the geologic data presented in Figure 2, and from limited ground geophysical data. Previously known faults, including the Getchell fault zone, the Hotz and Willden fault, and the Granite Creek thrust, are well defined and extended by the airborne data. Major new features are informally called the Rabbit Creek, the Getchell east, Silver King, Iron Point, Golconda, Preble east, and Red House Flat geophysical structures (Fig. 12). These are inferred to be faults or fault zones.

The Getchell fault is best identified in the 900 Hz resistivity data as a zone of low resistivity along the east side of the Osgood Mountains pluton.

The low resistivities closely follow the fault as mapped by Hotz and Willden (1964) to just north of the Mag deposit. They suggest that the Ogee and Pinson fault at the Pinson mine may be a southwest extension of the Getchell fault. The geophysical data, however, suggest that the Getchell fault extends due south through the Mag deposit to the Hotz and Willden fault. Operations at the Mag deposit have clearly shown a major steeply dipping fault within the pit (E. Kretschmer, 1989, personal comm.); the electrical data indicate that this is the Getchell fault zone. The Ogee and Pinson fault to the west of this may be a splay fault from the main structure.

The informally named Hotz and Willden fault is defined geologically by a scarp in the Quaternary alluvium southeast of the Pinson mine. The southwestern half is defined by a magnetic lineation that is offset from the mapped fault slightly to the west. There is no

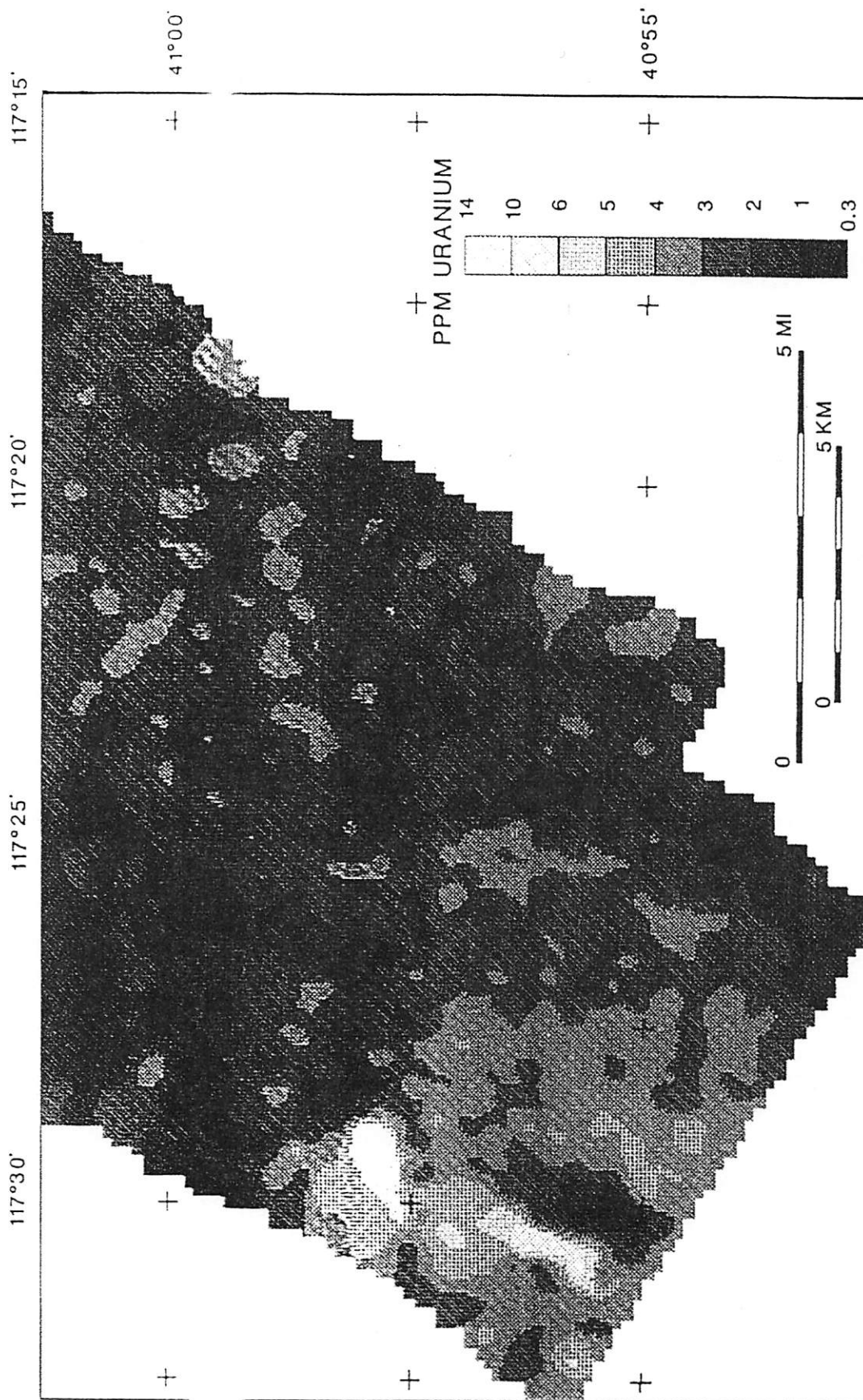


Fig. 8. Detail of the southern quarter of the uranium concentration map of Figure 3.

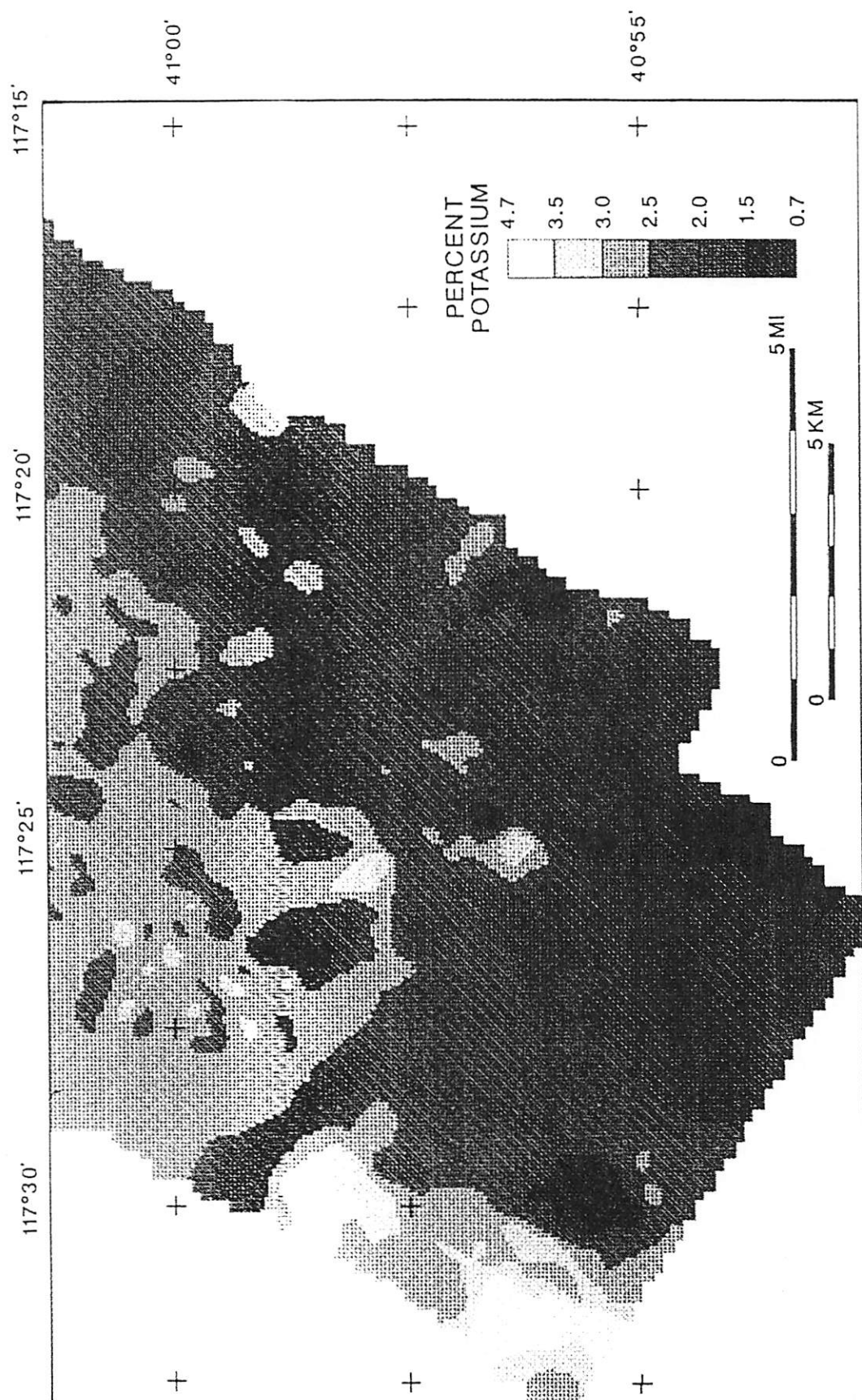


Fig. 9. Detail of the southern quarter of the potassium concentration map of Figure 4.

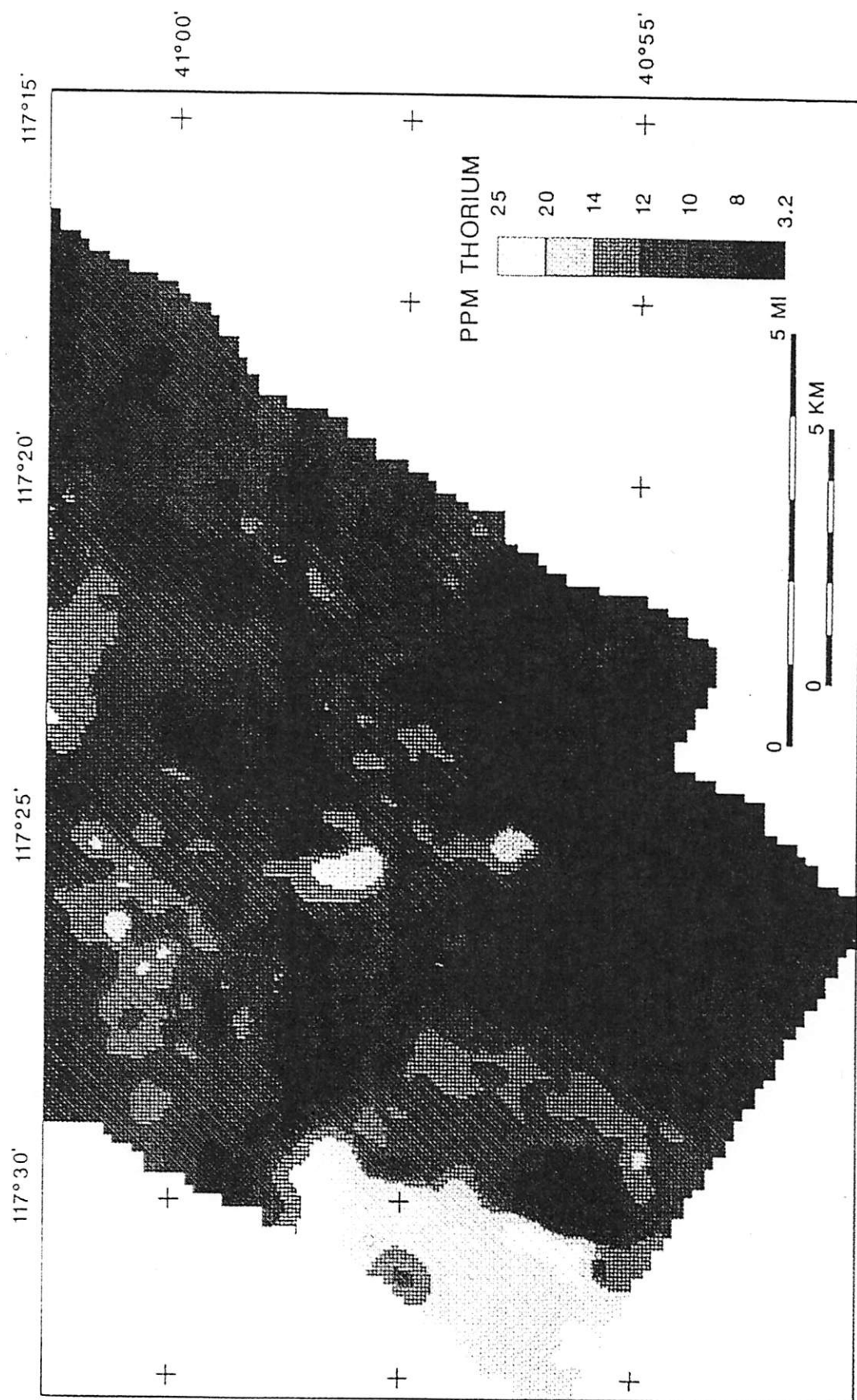


Fig. 10. Detail of the southern quarter of the thorium concentration map of Figure 5.

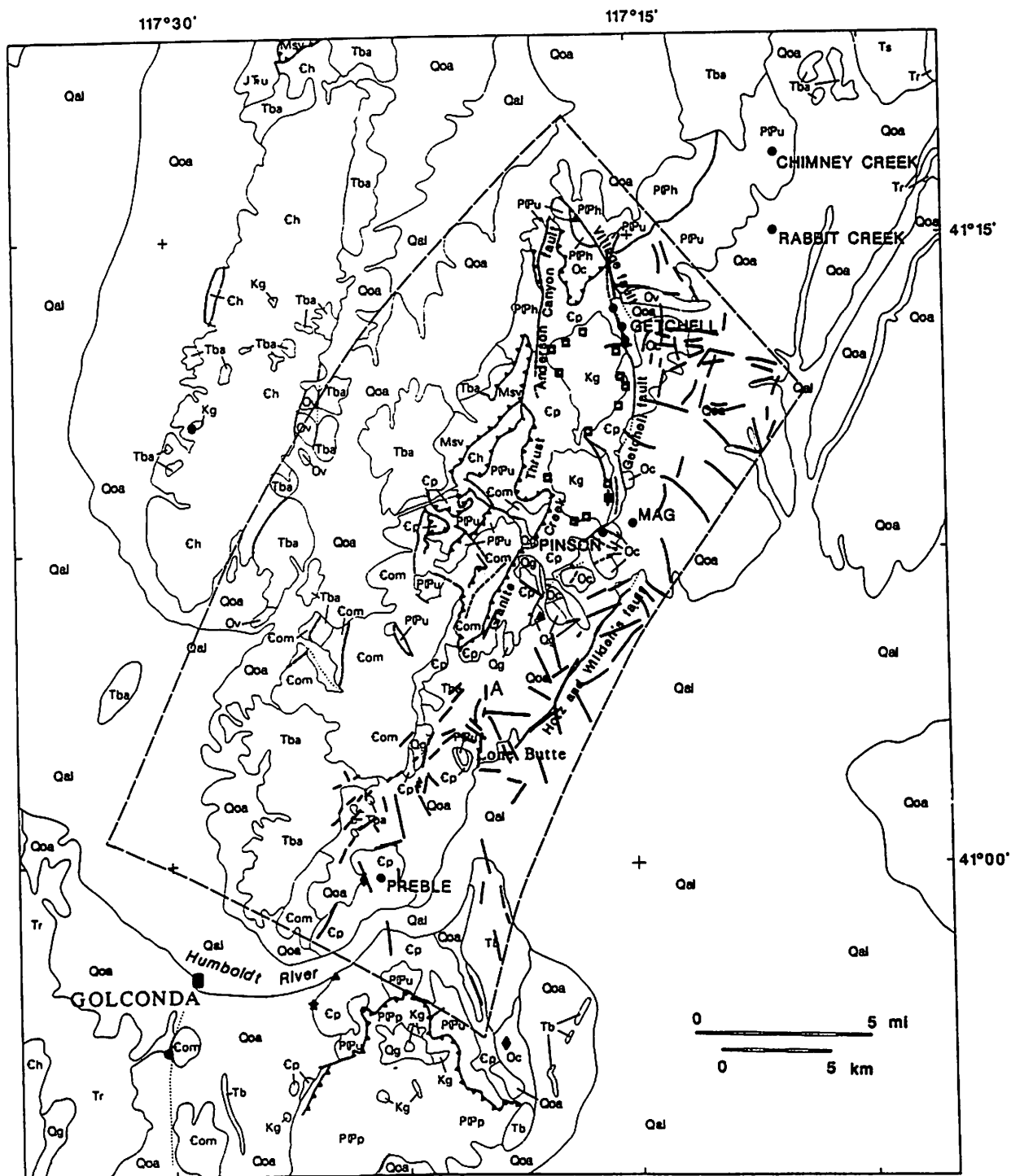


Fig. 11. Lineament map for the eastern margin of the Osgood Mountains, Humboldt County, Nevada, derived from a TIMS image.

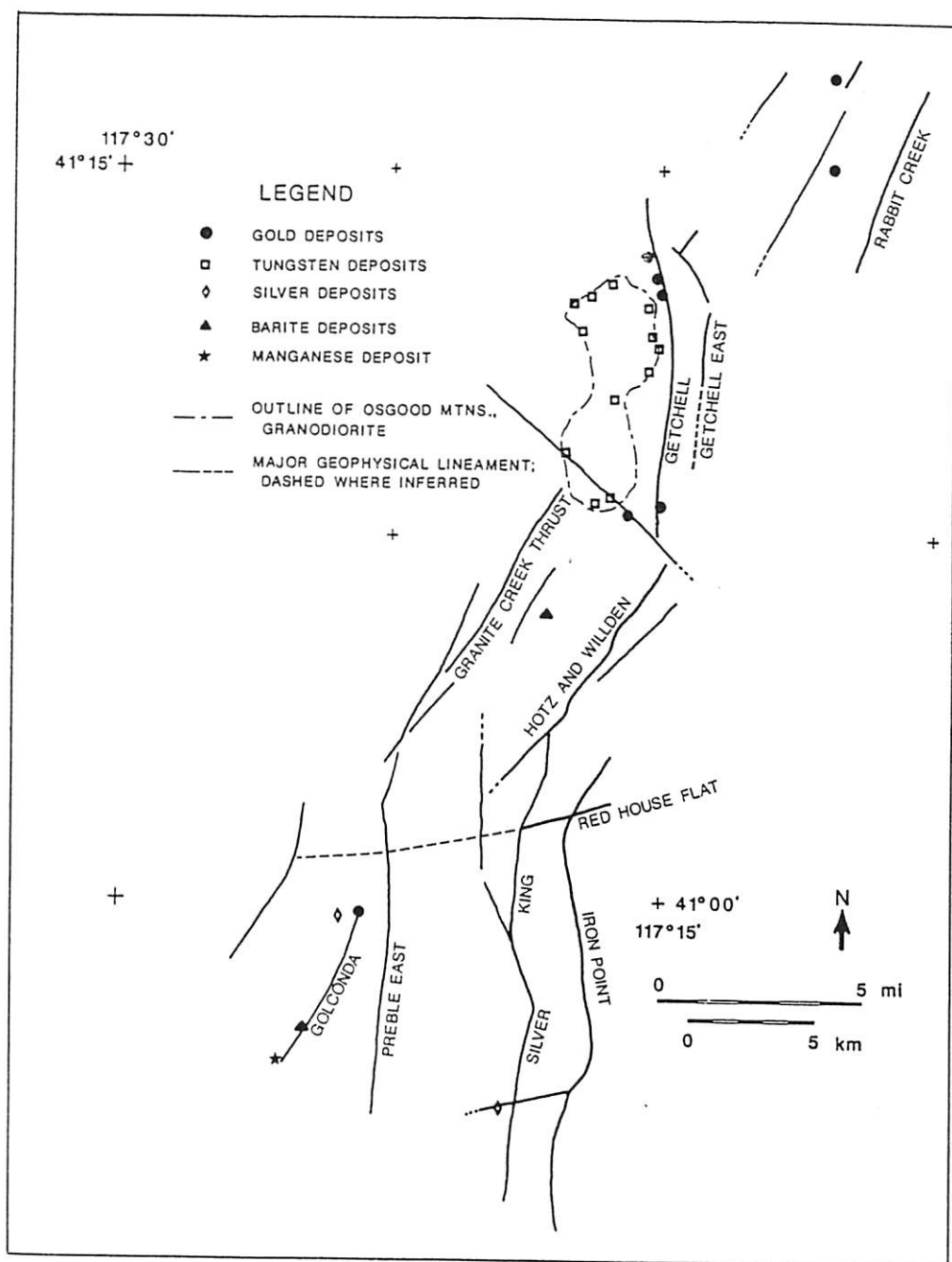


Fig. 12. Interpretive map showing major geophysical lineaments in the Osgood Mountains, Humboldt County, Nevada. Most of the lineaments are inferred to be related to steeply dipping fault or fracture zones.

magnetic expression on the northeastern half. Electrical data, however, provide definition over most of its length. The resistivity maps by themselves do not clearly identify the fault. However, a derivative map, made by taking the ratio of the 7200 Hz to 900 Hz maps (Pierce and Hoover, 1990), does define the fault due to differences in the thickness of fill on either side.

The Rabbit Creek structure was first recognized in the magnetic data. It is a distinct, linear, 6-km-long feature along the western bank of the Rabbit Creek drainage, east of the Rabbit Creek deposit. The mag-

netization boundary map of Grauch and Bankey (1990) shows this as the most prominent magnetic feature in the area and suggests it is derived from a shallow source. The magnetic boundary correlates exactly with a small, linear resistivity low best seen in the 900 Hz data. The southern end of both the magnetic and electrical linears terminates abruptly at the same point, as if cut off by another structure. At this point the 56,000 Hz resistivity map, the shallowest-looking of the electrical data sets, shows a pronounced, very local drop in resistivity to 2 ohm-m. This local low resistivity zone is on the western

margin of Rabbit Creek and not within the flat drainage area. The low resistivity zone may be related to thermal and/or saline water slowing near the surface along the intersection of the Rabbit Creek structure with a cross structure.

The radioelement data shows no local anomaly related to the low resistivity zone at the south end of the Rabbit Creek structure. A lithologic boundary defined by the radioelements along the Rabbit Creek drainage was mentioned in the section on lithologic mapping. A strong gradient in potassium and thorium values correlates with the Rabbit Creek structure to its southern end and then bends south to follow the drainage. These data imply that the Rabbit Creek geophysical structure is a fault that controls the location of the drainage and is responsible for contrasts in lithologies revealed by the geophysical data across the feature. Reconnaissance mapping (A. Wallace, 1989, personal commun.) suggests the presence of a normal fault with significant offset down to the east. Unfortunately, no TIMS or GER remote sensing data are available in this part of the survey area.

The Getchell east structure is subparallel to the Getchell fault approximately 1.5 km to the east. It is defined by an arcuate trend of low resistivity zones, discrete magnetization boundaries, and multiple linear features observed on TIMS data. It was first identified by ground electrical surveys (Hoover et al., 1984), but not well defined until acquisition of the airborne data.

The Silver King structure passes adjacent to the Silver King and Silver Coin mines where it is defined by a large topographic escarpment. The structure is clearly defined by electrical and magnetic data, particularly on the east side of the Edna Mountains where a basalt cap provides a large contrast in physical properties. This structure trends irregularly north, beneath alluvium to where it meets an east-northeast striking feature, the Red House Flat structure, at which point it turns northeast and appears to intersect the Hertz and Willden fault. The geophysical and geologic data suggest that the basalt that caps the plateau on the west has been downdropped on the east and is now covered by alluvium.

About 2 km east of the Silver King structure, a subparallel structure, the Iron Point structure, is also clearly seen in the magnetic and electrical data, suggesting an additional step fault, down to the east, that closely parallels the Silver King structure. Both structures bend to the northeast where they are crossed by the Red House Flat feature. Relationships within this area of crosscutting features are complex and not entirely clear at this time.

The Red House Flat structure is best defined by an extremely low resistivity zone, 2 ohm-m, with an abrupt gradient on the north (Fig. 6). A warm spring occurs where this linear gradient crosses the southern end of a small outcrop of Preble Formation (not shown on Fig. 2). This linear feature also is defined in the electrical and magnetic data by changes in the trend of linear features from approximately north-south on the south to northeast on the northern side.

In the vicinity of the Preble mine, two long trends of low resistivity can be seen. This is an area that is generally very quiet magnetically so that there are no corresponding magnetic features. The Golconda structure is an interrupted zone of conductive rock, as low as 15 ohm-m in places, that trends northeast from the Golconda mine to the Preble mine. The low resistivity zone correlates well with a small fault and alteration just east of the manganese deposit. The Preble mine, at the northeast end of this trend, is also expressed as a distinct low in resistivity. Ground electrical data obtained at the Preble deposit prior to mining also shows a conductive zone which correlates directly with the ore and which matches well, in position, with the airborne data. We infer that the Golconda geophysical structure identifies a zone along which hydrothermal systems that fed the Preble and Golconda deposits were constrained.

The Preble east structure trends to the north for 14 km, passing 1 km east of the Preble mine. It is one of the more prominent electrical features in the southern part of the study area. We are not aware of any mineralization or alteration related to this feature.

Near the southern end of the Osgood Mountain pluton, an interrupted northwest trend in the resistivity data aligns with mineralogical trends within the pluton presented by Neuerburg (1966). Trends along this direction are difficult to define in the airborne data because they are subparallel to the flight-line directions. Several tungsten deposits exposed on the southern border of the pluton are aligned on this trend. Resistivity data also suggest alteration along this trend extending as far northwest as the sharp resistivity gradient in the Harmony Formation described earlier.

Deposit Models

An important goal of the airborne study was to be able to help characterize the geophysical signature of the various types of mineral deposits in the area. It was also hoped that, from the disseminated gold deposits in the area, recognition of a characteristic signature might make it possible to identify the Rabbit Creek deposit below its thick cover.

Examination of these airborne data shows that there are no definitive signatures associated with either the tungsten skarn or the disseminated gold deposits. As a result, this preliminary analysis of the data fails to identify the Rabbit Creek deposit. We do not, however, preclude the possibility that further processing of the data sets will define or narrow the exploration region for deeply buried deposits such as Rabbit Creek. There also are too few manganese, silver, and barite deposits, and no clear signatures to permit more than speculation on those deposit types.

The gamma-ray data provide airborne geochemical information on the deposits. The Russians have been using this technique extensively in their gold exploration program, and they typically find elevated potassium values and lower thorium in many deposits

(Krendelev and others, 1976). We hoped that the Getchell trend deposits would reveal a typical signature; Hoover and others (1987) reported high radioelements in the Mag deposit and in the south pit at Getchell, and Berger (1985) reported elevated thorium at Getchell. The airborne data show no consistent radioelement signature. The south pit at Getchell is the only one showing elevated uranium. Although the uranium at 3.5-4 ppm is elevated above local background at the Getchell south pit, this is at or below values common in shales and below that of acid igneous rocks (Clark and others, 1966). The Pinson mine is on the edge of a potassium high, but all other deposits show no radioelement features that alone permit them to be differentiated from the background.

Magnetic, remote sensing, and electrical data individually give no prominent clues as to the exact location of any of the deposits. However, all the deposits are located on steeply dipping fault zones, and the geophysical data provide important clues as to the location of these features. The larger and longer faults played an important role in localizing the hydrothermal systems responsible for ore deposition, and it is these large features that are more easily defined by the airborne data. Identification of these features while not directly indicative of mineralization, considerably restricts the area for detailed exploration. Because they look below the surface, magnetic and electrical methods are the more definitive tools in covered areas. Within this study area, the resistivity map appears to be the single most useful tool for identifying structures along which deposits are located. All the known deposits are centered on or immediately adjacent to a linear conductive zone, except for Rabbit Creek. Rabbit Creek was not clearly identified by the airborne data because the alluvial cover was too thick.

Ground electrical data obtained prior to mining confirm that cover is too thick and conductive for direct detection of basement features from the air.

The ground data do show that deeper looking electrical methods would identify a conductive zone associated with ore. This is not meant to imply that electrical methods can or should be used alone.

We do not yet know enough about leakage haloes that may develop in cover rocks above ore deposits to make any reasonable predictions from the TIMS or gamma-ray data of such features in this area. However, at the Hot Springs Ranch south of the study area, a potassium anomaly has been defined by ground surveys in thick cover over an inferred basement fault (D. Hoover, unpublished data). Also to be noted is an area of high potassium values where the Hotz and Willden and Getchell faults and a northwest-trending feature through the Pinson mine intersect. This potassium high may only be due to windblown detritus, but additional ground studies are needed to verify this.

Summary

The airborne remote sensing, gamma-ray, magnetic, and resistivity data sets obtained along the Getchell trend of gold deposits used together provide a synoptic view of physical property variations that may be used to map lithologies, identify areas of alteration, map structures and contribute to knowledge of the geophysical characterization of mineral deposit models. The analysis of these large multiple data sets that has been presented here is very preliminary and summarizes the work to date. Since receiving the data, there has been limited opportunity for ground investigations that would assist in understanding many of the subtleties in the data. Additional ground data should help significantly in refining the interpretation and predicting possible mineralized areas. Integration of all the data is effective for mapping many individual lithologies in the region flown. Because the region is well mapped, the geophysical data suggested only minor changes in some contacts. An integrated program such as this, however, could be very effective in areas where the surficial geology is not as well known. Of more importance in this area is the mapping of units below cover. The subsurface extent of the Cretaceous granodiorite in the Osgood Mountains has been defined for the first time and has been shown to be more extensive than previously believed. This provides three-dimensional information on terrains favorable for tungsten skarn mineralization. Several of the gold deposits in the area are adjacent to the granodiorite. Although the existence of a genetic relationship between the deposits and the granodiorite is still contested, the new knowledge of its three-dimensional configuration does put additional constraints on locations for potential mineralization. This is also true for the other blind intrusive bodies inferred in this study.

Mapping of lithologies, such as the alluvial covered, down-faulted block of basalt between the Silver Coin and Iron Point structures in the southeast part of the study area, helps decipher the structural relationships that might be important in localizing mineralization in this area.

Identification of alteration zones provides direct indication of hydrothermal activity that may have produced economic mineral deposits. Our understanding of the nature of alteration effects suggested by the data is very rudimentary at this time due to a lack of field checking. This work has revealed several areas with different signatures that appear to be the result of alteration and which have not previously been identified as such. Additional geological, geochemical, and geophysical studies will be required to understand the relationship between these alteration features and mineral deposits. For exploration in covered regions we need to understand how haloes within cover, such as that suggested southeast of the Pinson mine, are formed.

Structures play an important part in localizing mineralization. The use of high-quality multisensor surveys, as done in this study, and integration of those

data can significantly improve our understanding of the structural setting. These integrated methods become particularly effective in covered areas. The preliminary structure map resulting from this work identifies several features hidden by alluvial cover that had not previously been identified. Rapid and detailed data acquisition over a large region can provide a framework for structural interpretation in covered areas. This can enhance ground exploration and drilling programs and speed the process towards discovery. As additional ground information becomes available, the airborne data can be reevaluated and interpretations improved.

There are no clearly evident geophysical signatures for either tungsten skarn or sediment-hosted gold deposits that permit us to identify the individual deposits on the basis of an airborne geophysical survey. We believe, however that with a more detailed analysis we will be able to considerably restrict and map the favorable ground in which to explore for these commodities. An important aspect of this work is that the known gold deposits are all on or very close to major lineaments in the airborne geophysical data. Through more detailed analysis of these data means to identify those segments of the lineaments that are most favorable may be developed.

References

- Berger, B.R., 1985, Geological and geochemical relationships at the Getchell mine and vicinity, Humboldt County, Nevada; in Hollister, V.F., ed., *Discoveries of epithermal precious metal deposits: American Institute of Mining and Metallurgical Engineers*, v. 1., p. 51-59.
- Clark, S.P., Jr., Peterson, Z.E., and Heier, K.S., 1966, Abundance of uranium, thorium, and potassium; in Clark, S.P., ed., *Handbook of Physical Constants: Geological Society of America Memoir 92*, p. 521-541.
- Cordell, Lindrith, and Grauch V.J.S., 1985, Mapping basement magnetization zones from aeromagnetic data in the San Juan Basin, New Mexico, in Hinze, W.J., ed., *The utility of regional gravity and magnetic anomaly maps: Society of Exploration Geophysicists, Tulsa, Oklahoma*, p. 181-197.
- Erickson, R.L., and Marsh, S.P., 1974a, Geologic map of the Golconda Quadrangle, Humboldt County, Nevada: U.S. Geological Survey Geol. Quad. Map GQ 1174, scale 1:24,000.
- Erickson, R.L., and Marsh, S.P., 1974b, Geologic map of the Iron Point Quadrangle, Humboldt County, Nevada: U.S. Geological Survey Geol. Quad. Map GQ 1175, scale 1:24,000.
- Grauch, V.J.S., and Bankey, Viki, 1990, Preliminary results of aeromagnetic studies of the Getchell disseminated gold deposit trend, Osgood Mountains, North-Central Nevada, in Schafer, R.W., and Wilkinson, W.H., eds., *Geology and Ore Deposits of the Great Basin, Symposium Proceedings: Geological Society of Nevada*, _____.
- Hoover, D.B., Pierce, H.A., and Abrams, G.A., 1984, Telluric traverse data release for the Getchell and Preble disseminated gold deposits, Humboldt County, Nevada: U.S. Geological Survey Open-File Report 84-846, 13 p.
- Hoover, D.B., Smith, B.D., Grauch, V.J.S., and Podwysocki, M.H., 1987, Geophysical studies in the vicinity of the Getchell Fault system, Humboldt County, Nevada [abs.]: 3rd Annual McKelvey Forum, Denver, Colorado, March 1987, p. 31.
- Hotz, P.E., and Willden, Ronald, 1964, Geology and mineral deposits of the Osgood Mountains Quadrangle, Humboldt County, Nevada: U.S. Geological Survey Professional Paper 431, 128 p.
- Houff, P.L., Kruse, F.A., and Madrid, R.A., in press, Gold exploration using illite polytypes defined by x-ray diffraction and reflectance spectroscopy: World Gold '89', *Proceedings of the Society of Mining Engineers*, 7 p.
- Kerr, P.F., 1940, Tungsten-bearing manganese deposit at Golconda, Nevada: *Geological Society of America Bulletin*, v. 51, p. 1359-1390.
- Kochetkov, A.Ya., Zlobin, V.A., and Popov, A.B., 1987, Radioactive elements and gold in Mesozoic magmatic rocks of central Aldan: *Soviet Geology and Geophysics*, v. 28, no. 12, p. 34-42.
- Krendele, F.P., Mironov, A.G., and Gofman, A.M., 1976, Use of gamma-ray spectrometric methods in contouring ore zones in the Trans-Baikal region: *Geology Institute Ulan-Ude, USSR, Geol. Geofiz. v. 8*, p. 67-75 (Russian).
- Neuerburg, G.J., 1966, Distribution of selected accessory minerals in the Osgood Mountains stock, Humboldt County, Nevada: U.S. Geological Survey Miscellaneous Geologic Investigations Map I-471, scale 1:24,000.
- Osterberg, Mark, 1988, Geology of the Chimney Creek sediment-hosted gold deposit Osgood Mountains, Nevada: *Geological Society of Nevada Newsletter*, v. 1, no. 2, p. 4-6.
- Percival, T.J., Bagby, W.C., and Radtke, A.S., 1988, Physical and chemical features of precious metal deposits hosted by sedimentary rocks in the Western United States; in Schafer, R.W., Cooper, J.J., and Vikre, P.G., eds., *Bulk Mineable Precious Metal Deposits of the Western United States: Geological Society of Nevada*, p. 11-34.
- Pierce, H.A., and Hoover, D.B., 1990, Airborne electromagnetic applications—mapping structure and electrical boundaries beneath cover along the Getchell trend, Nevada, in Schafer, R.W., and Wilkinson, W.H., eds., *Geology and Ore Deposits of the Great Basin, Symposium Proceedings: Geological Society of Nevada*, _____.
- Pitkin, J.A., 1990, Radioelement data for the Getchell trend, Humboldt County, Nevada—geologic discussion and possible significance for gold mineralization, in Schafer, R.W., and Wilkinson, W.H., eds., *Geology and Ore Deposits of the Great Basin, Symposium Proceedings: Geological Society of Nevada*, _____.
- Silberman, M.L., Berger, B.R., and Koski, R.A., 1974, K-Ar relations of granodiorite emplacement and tungsten and gold mineralization near the Getchell mine, Humboldt County, Nevada: *Economic Geology*, v. 69, p. 646-656.
- Stager, H.K., and Tingley, J.V., 1988, Tungsten deposits in Nevada: Nevada Bureau of Mines and Geology Bulletin 105, 205 p.
- Vasil'ev, B.D., Zlobin, V.A., Pavlova, L.K., Ponomareva, A.P., and Shirokikh, I.N., 1985, Radiogeochemical properties of magmatic rocks in gold regions of Kuznets Alatau: *Soviet Geology and Geophysics*, v. 26, no. 1, p. 45-54.
- Willden, Ronald, 1964, Geology and mineral deposits of Humboldt County, Nevada: Nevada Bureau of Mines and Geology Bulletin 59, 154 p.
- Zlobin, V.A., and Kurulenko, R.S., 1981, Formation conditions and features of gold-containing granitic rocks on the basis of radiogeochemical data: *Ins Geol Geofiz. Novosibirsk USSR, Geol. Geofiz.*, v. 4, p. 68-74 (Russian).

Airborne Electromagnetic Applications – Mapping Structure and Electrical Boundaries Beneath Cover Along the Getchell Trend, Nevada

Herbert A. Pierce and Donald B. Hoover

U.S. Geological Survey, Denver Colorado

Introduction

The use of geophysical techniques to explore for covered mineral deposits will become more common as the remaining exposed deposits are located and developed. Airborne methods will play an increasingly important role for regional to district scale studies. Airborne geophysical techniques allow geoscientists to investigate different physical characteristics of the earth not only at the surface, but to varying depths. For example, satellite and airborne spectral remote sensing techniques sense only variations of properties at the earth's surface. Airborne radiometrics sense from the earth's surface to a depth of about 50 centimeters. Magnetic techniques are able to sense from the earth's surface to deeply (> 10 km) buried structures, however, as the depth increases resolution decreases. Multi-frequency airborne electromagnetics, in contrast to the other airborne techniques, can sense to different depths depending on the frequency used and the resistivity of the rocks. Using different frequencies to sense to different depths gives better definition of the structural setting by allowing investigations to different depths. Better definition of structures increases the probability of success in exploration, especially true where mineral-bearing rocks are covered by alluvium.

In 1988, the U.S. Geological Survey funded a multi-sensor airborne-geophysical program to demonstrate the use of geophysics in exploration for covered mineral deposits. A progress report of the airborne electromagnetic survey portion of the study is reported here. Companion papers in this volume discuss the other geophysical techniques that are part of the Getchell trend airborne demonstration project.

Geologic Setting

The Getchell trend lies north of the Humboldt River, in Humboldt County, on the east side of the Osgood Mountains in the Basin and Range Province, Nevada. The trend is generally NNE and six active low-grade-high-tonnage gold mines roughly define the trend (Figure 1). The area covered by the airborne electromagnetic (AEM) survey is composed of Paleozoic sedimentary rocks, Cretaceous granodiorite, and Tertiary extrusive rocks. Distribution of these rock units are shown on

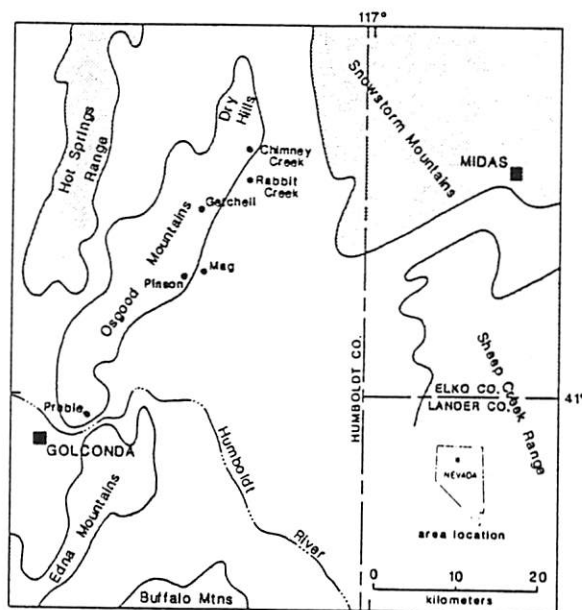


Fig. 1. The Getchell trend airborne demonstration project location map. The dark solid line is approximately the boundary for the airborne electromagnetic survey. The dark square is the town of Golconda on the southwest, to the northeast, the dark square is the town of Midas. The dots indicate several disseminated bulk-mineable gold deposits within the survey area.

Figure 2, the geologic map. Figure 2, a simplified compilation of geologic information, compiled from Horz and Willden (1964), and Erickson and Marsh (1974a,b). A detailed summary of the thrusting, faulting, intrusive, and extrusive events is given in Hoover et al., (this volume).

Data Acquisition

1150 line-miles of digital multi-frequency airborne electromagnetic (AEM) survey were flown using a DIGHEM IV system in November, 1988, along the east side of the Osgood Mountain Range, Nevada (Figure 1). Use of brand names and model numbers in this report is for the sake of description only, and does not constitute endorsement by the U.S. Geological Survey. The Osgood Mountains are part of the gold-bearing Getchell trend, northeast of the town of Golconda, Nevada. The airborne data were acquired at a flight-line spacing of 1/4

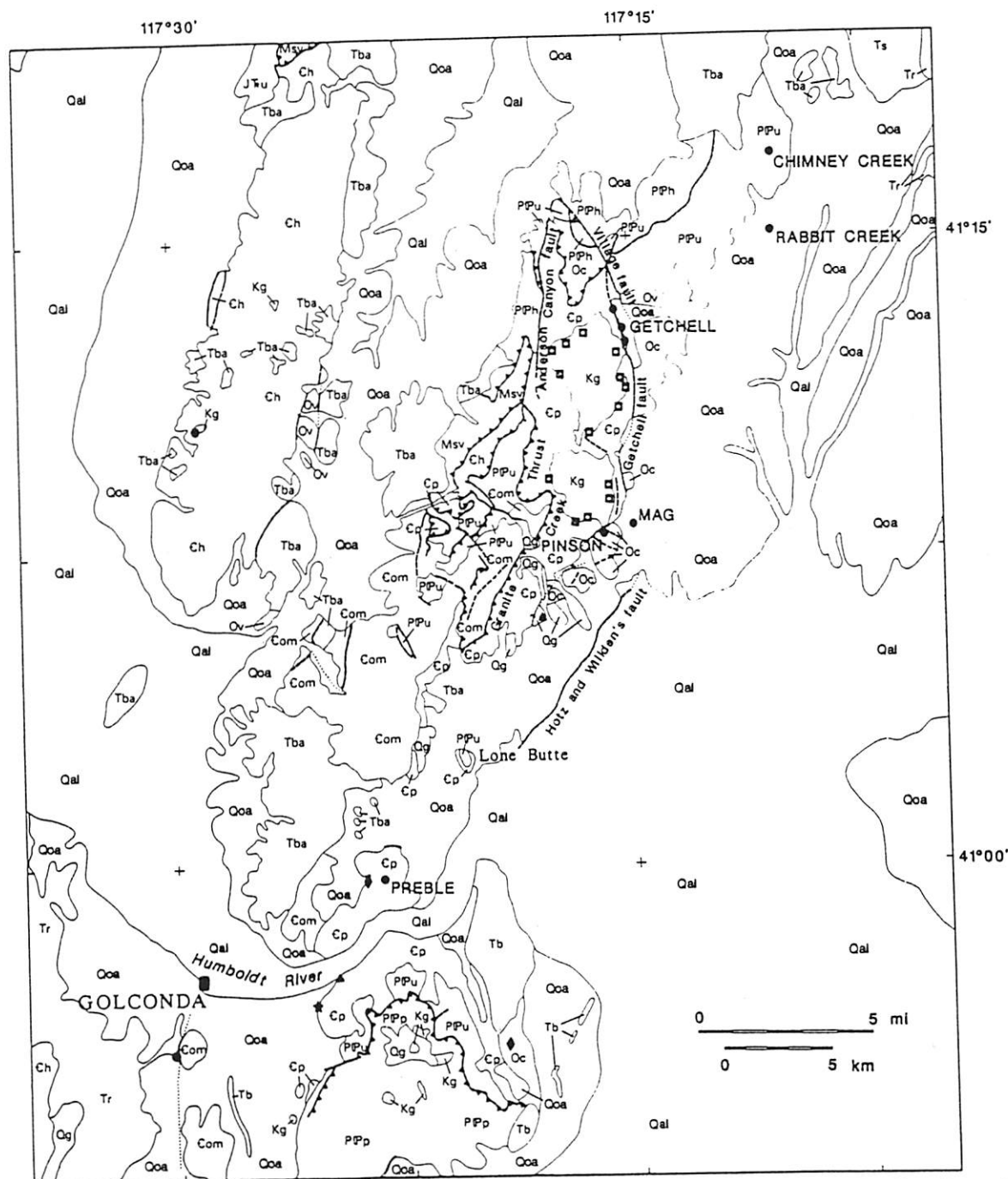


Fig. 2. The geologic map of the Osgood Mountains and vicinity. This map is a compilation of the geologic data from Hotz and Willden (1964), and Erickson and Marsh (1974a,b).

mile (402 m) using a helicopter with the instrument sensors flown at a nominal 100 feet (30.5 m) altitude above ground surface. Selected areas about 2 by 3 miles on a side (3.2 x 4.8 km) over the Preble, Mag, Pinson, Getchell, Rabbit Creek, and Chimney deposits were flown at 1/8 mile (201 m) flight-line spacing. Flight-line azimuth was approximately 121 degrees. AEM frequencies used for this survey were 56,000, 7,200, and 900 Hertz. Figure 3 shows the DIGHEM IV electromagnetic 4-coil pair system configuration (3 coplanar, 1 coaxial). The three horizontal coil pairs are used for

resistivity mapping because of large signal and low noise levels (Fraser, 1986). The sensor is flown 30.5 m above ground and the DIGHEM IV transmitter-receiver coil separation is 8 m. VHF transponders in the Osgood Mountain Range and in the valley between the Osgood Mountains and Sheep Creek Ranges (Figure 1) were used for precise location and navigation of the helicopter carrying the instruments. Where VHF transponder coverage was not available, a continuously operating VHS video recorder camera were used to record and recover the flight path.

DESCRIPTION OF MAP UNITS
(Listed in approximate stratigraphic order)

- Qal - Quaternary alluvium
- Qoa - Older Quaternary alluvium
- Qg - Quaternary gravel
- Tb - Pliocene basalt
- Tr - Miocene rhyolite flows and tuffs
- Ts - Miocene clastic rocks and tuffs
- Tba - Miocene basalt and basaltic andesite
- Kg - Cretaceous granodiorite (about 90 Ma)
- JTu - Jurassic and Triassic metaclastic rocks, undivided
- PPu - Permian and Pennsylvanian clastic and carbonate rocks, undivided. Includes Edna Mountain Formation (Permian), Antler Peak Limestone (Pennsylvanian and Permian), Highway Limestone (Pennsylvanian), and Battle Formation (Pennsylvanian). In the Osgood Mountains, includes the Etchart Limestone (Pennsylvanian and Permian) and the Adam Peak Formation (Pennsylvanian and Permian).
- PPp - Pumpernickel Formation (Pennsylvanian and Permian)--siliceous sedimentary and volcanic rocks
- PPh - Pennsylvanian and Permian siliceous sedimentary and volcanic rocks, undivided. Includes the Havallah Formation (Pennsylvanian and Permian), rocks similar to the Havallah and Pumpernickel Formations in the Hot Springs range, and the Farrel Canyon Formation (Pennsylvanian and Permian) in the Osgood Mountains.
- Msv - Mississippian siliceous sedimentary and volcanic rocks. In the Osgood Mountains includes the Goughs Canyon Formation.
- Ov - Valmy Formation (Ordovician)--Chert and greenstone
- Oc - Comus Formation (Ordovician)--Carbonate rocks and sandstone
- Ch - Harmony Formation (Cambrian)--Sandstone and shale. Includes small exposures of Paradise Valley Chert (Cambrian) on the west side of the Hot Springs Range.
- Cp - Preble Formation (Cambrian)--Shale and limestone
- Com - Osgood Mountain Quartzite (Cambrian)
- Contact
- - - Fault, dashed where approximately located, dotted where concealed
- - - Thrust fault, sawteeth on upper plate
- Gold deposit; names indicate operational or developing mines
- ◻ Tungsten deposit
- ♦ Silver deposit
- ▲ Barite deposit
- ★ Manganese deposit

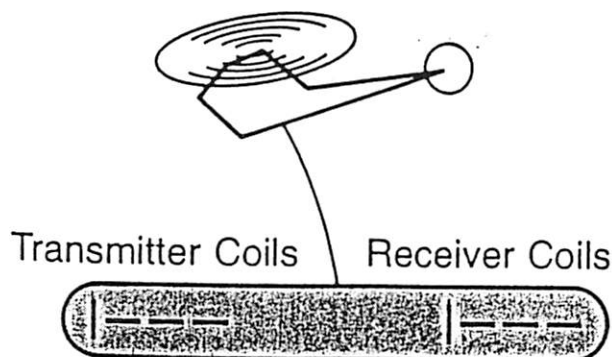


Fig. 3. The helicopter-borne DIGHEM IV system. The three horizontal (coplanar) and one vertical (coaxial) transmitter-receiver coils are carried in a bird below the helicopter.

Airborne Resistivity Mapping

AEM methods for mineral exploration were developed in Canada in the 1950's and for many years, the methods were used primarily to find and identify conductive targets within the earth. During the 1970's the use of AEM techniques was further extended to produce resistivity maps that gave a quantitative measure of the earth's resistivity (Fraser, 1978). An excellent summary of instrumentation, theory, and applications of AEM resistivity mapping is provided in the proceedings of a workshop held in Ottawa, Canada, October 1985, entitled "Airborne Resistivity Mapping (Palacky, ed., 1986).

The transmitter coils carried by the helicopter are used to induce electric currents in earth's surface. These electric currents produce varying magnetic fields which are then recorded by a series of receiver coils in the DIGHEM IV bird. The receiver-coil signals are then used to compute the apparent resistivities of the rocks. The DIGHEM IV system uses the inphase/quadrature algorithm of the "pseudo-layer half space model" described in Fraser (1978) to compute apparent resistivities. This algorithm corrects apparent resistivity variations caused by altitude errors. Multiple frequencies are used because depth-of-exploration is a function of frequency as well as resistivity, with lower frequencies giving greater depth of penetration (see Palacky, ed., 1986). As a rule-of-thumb, for the average resistivities seen in this survey, the depth-of-exploration is on the order of 10 m (32 feet) at 56,000 Hz, 30 m (96 feet) at 7,200 Hz, and 90 m (288 feet) at 900 Hz.

The resistivity of earth materials is primarily determined by the porosity, and the amount and quality of water contained in the rocks, except where there are significant quantities of electrically conductive minerals, such as pyrite. Igneous and metasedimentary rocks tend to have high resistivities, porous sandstone has intermediate resistivity, and shale has low resistivity, especially when water-saturated. Because electrical conduction takes place primarily through ions in the free water of earth materials, water quality can also play an important role in determining resistivity. Saline connate waters generally result in lower resistivity values. Clays have quite low resistivity values because of their porosity and their surface conduction properties. The range of resistivities encountered by in-situ measurement of earth materials varies by about five orders of magnitude. For example, graphitic schists may have resistivity values less than 0.5 ohm-meters and dry volcanic rocks may have resistivity values more than 50,000 ohm-meters. This wide range of values permits discrimination between various rock units and identification of structures such as faults and lithologic contacts.

Data Description

Three apparent resistivity shaded relief maps (figs. 4 to 6), one for each frequency sampled, were plotted using

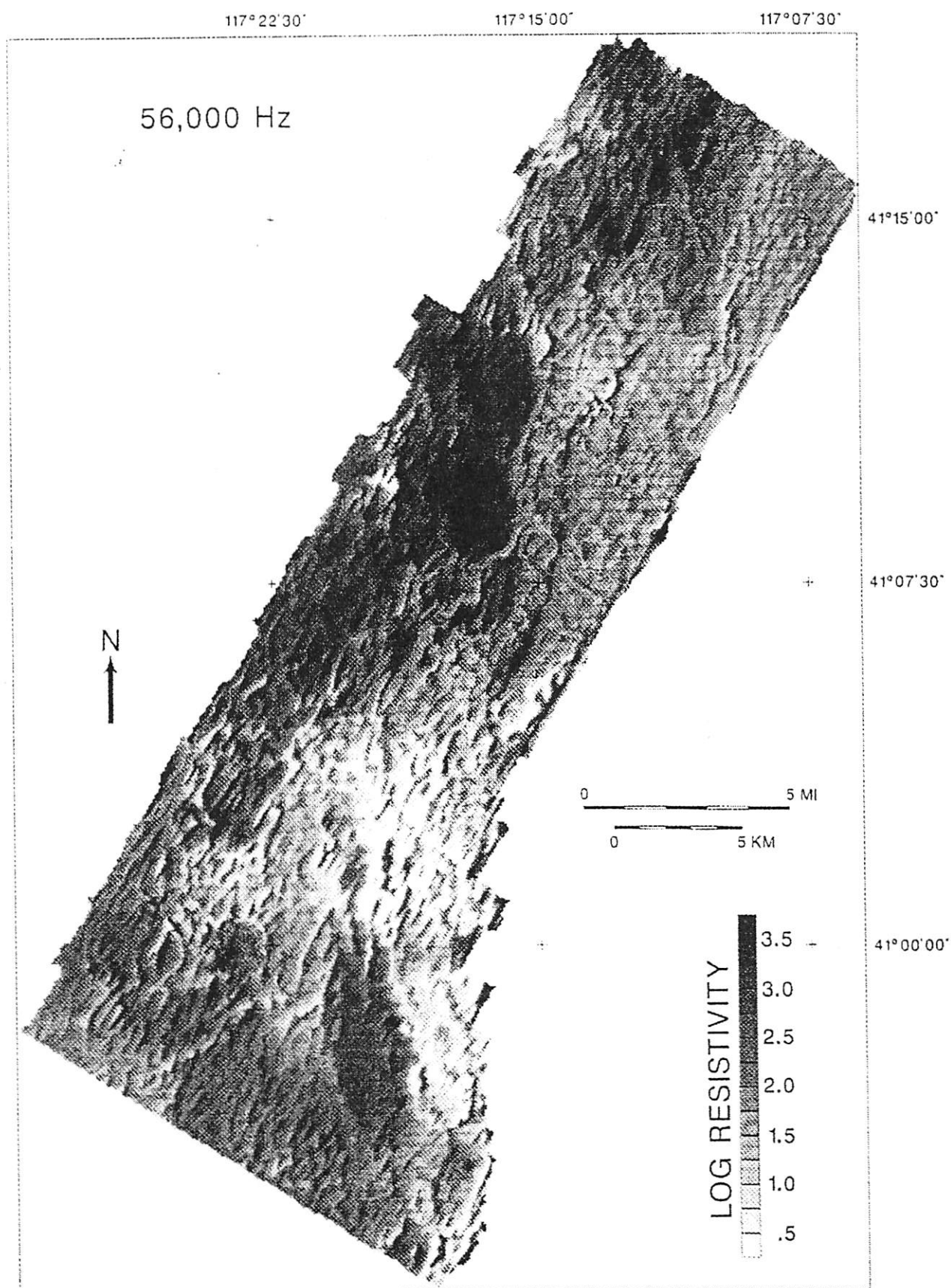


Fig. 4. 56,000 Hz resistivity shaded relief map of the Gatchell trend.

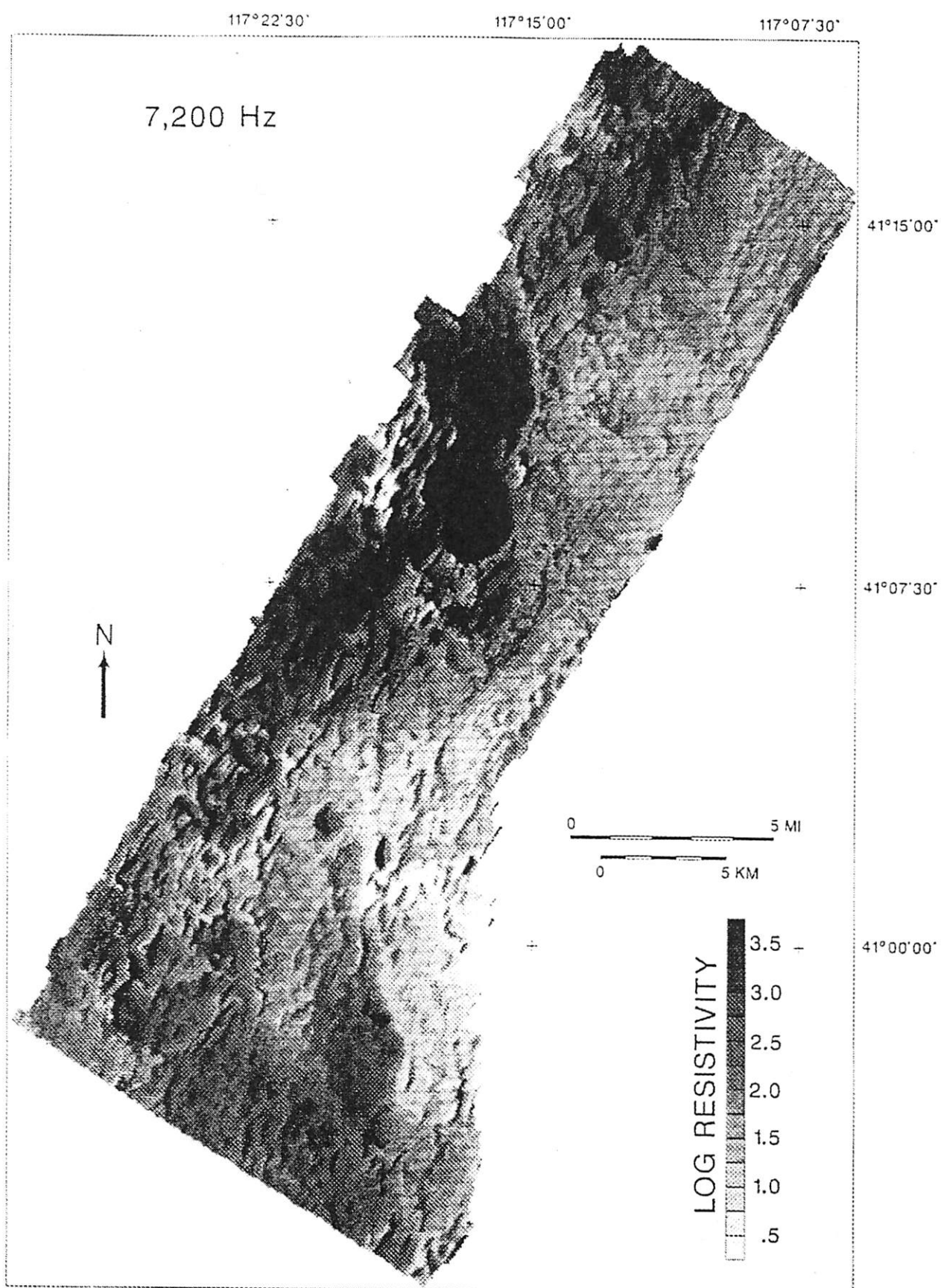


Fig. 5. 7,200 Hz resistivity shaded relief map of the Gatchell trend.

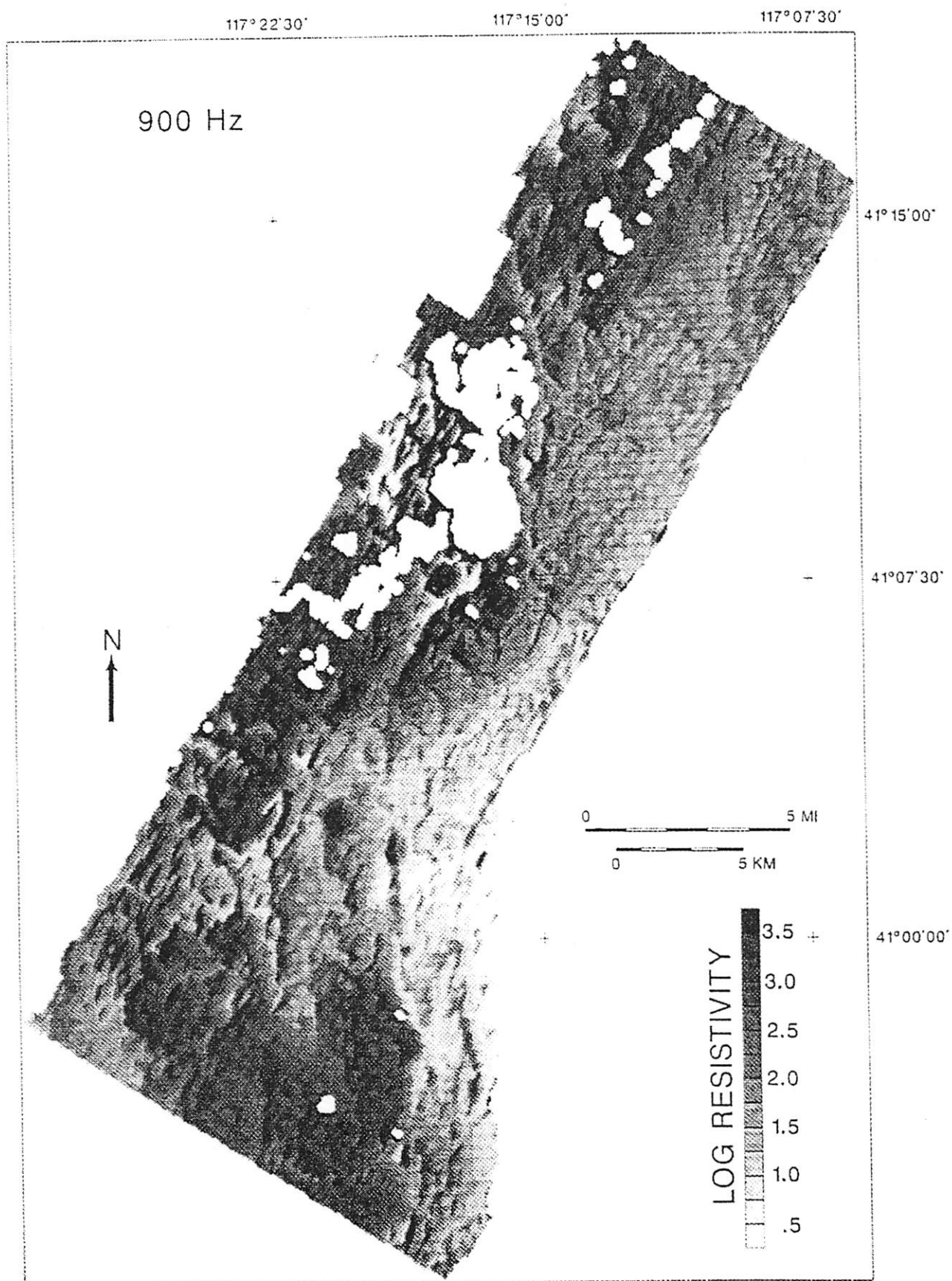


Fig. 6. 900 Hz resistivity shaded relief map of the Getchell trend.

apparent resistivities from a DIGHEM IV system, calculated using algorithms described by Fraser (1986). These general features appear on the maps (1) the entire southeast side shows conductive alluvial cover; (2) the northwestern quarter exhibits high frequency and relatively resistive Paleozoic sediments of the Dry Hills; (3) the hour glass resistive block is the Cretaceous granodiorite of the Osgood Mountains; (4) south, and still on the west side of the map are the resistive quartzites of the Osgood Mountains and, (5) in the southern quarter, the Paleozoic sedimentary rocks and basalts are resistive. These five features carry through for all three frequencies, however, as the frequency is lowered and the depth of penetration increases, effects of structural blocks defined by faults and lithologic boundaries may be interpreted. For example, on the 900 Hertz map, the low on the east side of the Cretaceous granodiorite is most certainly caused by the Getchell fault. The apparent flat topped look of the granodiorite is caused by the limited range of resistivities that can be recorded. For the 900 Hertz AEM map, the highest resistivity that can be recorded is 1000 ohm-meters, however, from ground resistivity techniques and from the other two resistivity maps with a larger dynamic range the actual apparent resistivity value is on the order of 4000 ohm-meters.

Discussion of the AEM Maps

The real power of the high resolution AEM maps is that the geoscientist can interpret lithologies, alteration zones, and faults. The three AEM resistivity maps are best viewed in color at a larger scale. Black and white page-sized copies do not adequately represent important subtle features. Colored shaded relief maps at 1:100,000 are available at the Nevada Bureau of Mines in Reno, and at USGS offices in Menlo Park, CA; Tucson, AZ; Spokane, WA; Denver, CO; Salt Lake City, UT; and Reston, VA.

To help focus on several large areas and major electrical lineaments we have sketched an area/lineament map (Figure 7). This map was compiled from the 900 Hz apparent resistivity map, but represents features seen in all three resistivity maps. Figure 7 shows areas with a similar signature (i.e., resistivities and anomaly wavelengths). Letters (A, B, C) are used to designate areas, and numbers are used to designate electrical lineaments.

A good example of how electrical lineaments on these maps relate to mapped geologic features can be seen by comparing the lineament, line 8, Figure 7, to the Getchell fault zone. The Getchell fault zone, on the east side of the granodiorite (Figure 2) is represented by a narrow conductive trough-line seen on any of the three resistivity maps. This fault juxtaposes Cretaceous granodiorite against the Paleozoic sedimentary rocks of the Preble Formation. The resistivity contrast between formations is about 40 to 1. The low resistivity values along the trough are attributed to an increase in fracture porosity and clay minerals developed along the fault zone.

Another example of electrical lineaments from the

AEM maps relating to faults in cover rocks is the northeast-trending Hotz and Willden fault east of the Pinson mine, shown on Figure 2. This fault is down-dropped on the southeast with less than 90 m of alluvium on the up-thrown side. This fault is coincident with an electrical lineament, Figure 7, line 6.

A good example of how areas from the AEM maps complement the mapped geology is displayed by the Cretaceous granodiorite of the Osgood Mountains. The dumbbell-shaped area of high resistivity rocks in the northern half of all three resistivity maps is sketched in Figure 7 as area A. The 56,000 Hz resistivity map, Figure 4, shows variations in apparent resistivity in the near-surface material. The 7,200 Hz resistivity map looks deeper, but surficial features are still apparent. For instance, an area of alteration centered in the northern lobe of the granodiorite body, an old silver prospect called the Getchell section 5 pit, shows up as a low on the AEM maps. The 900 Hz resistivity map, because of the instrument limitations previously mentioned, is saturated at 1000 ohm-meters for most of the resistive granodiorite body. Other major areas of resistive rock adjacent to and south of the granodiorite (area B, Figure 7) correlate with exposures of quartzites and calcareous Paleozoic sedimentary rocks (Hotz and Willden, 1964). Areas J and K (Figure 7), adjacent to the granodiorite are mapped as shales (Preble Formation) have much lower resistivities than similar rocks in areas I and L. The reason for the very low resistivity values in areas J and K is not understood, but may be related to hydrothermal alteration of these sedimentary rocks during the intrusion of the adjacent granodiorite stock. Resistive rocks in the southern part of the survey area (area G) correlate with extrusive volcanic rocks and with resistive Paleozoic sedimentary rocks. Area M coincides with mapped outcrops of Miocene basalts and basaltic andesite.

Areas C, D, E, and F are mapped as alluvium and from the AEM maps generally have resistivities less than 100 ohm-meters. Approximately one half of the study area is mapped as alluvial rocks. Variations in resistivities of alluvial areas may reflect changes in resistivity entirely within the alluvium, or may reflect a change in thickness of the alluvium where the cover is thin enough that bedrock resistivity is being measured. Areas D and E represent very conductive alluvial areas where values approach 0.5 ohm meters. A warm spring is present on the northeast side of the area D indicating that thermal zones may be recognized as anomalous conductive values. The trend of area D is parallel with the NE-trending Midas Trough (Wallace, 1989). Areas D and E are bounded by north-trending electrical lineaments, as shown on Figure 7, and may be down-dropped relative to area G. This is consistent with the interpretation from the magnetic data (V.J.S. Grauch, oral commun., 1989).

Major lineaments seen in the 900 Hz resistivity map are identified by number in Figure 7. These identify breaks or changes in resistivities. Two trend directions are clear from the resistivity data, the first is a north-trending set of electrical lineaments. Examples of this

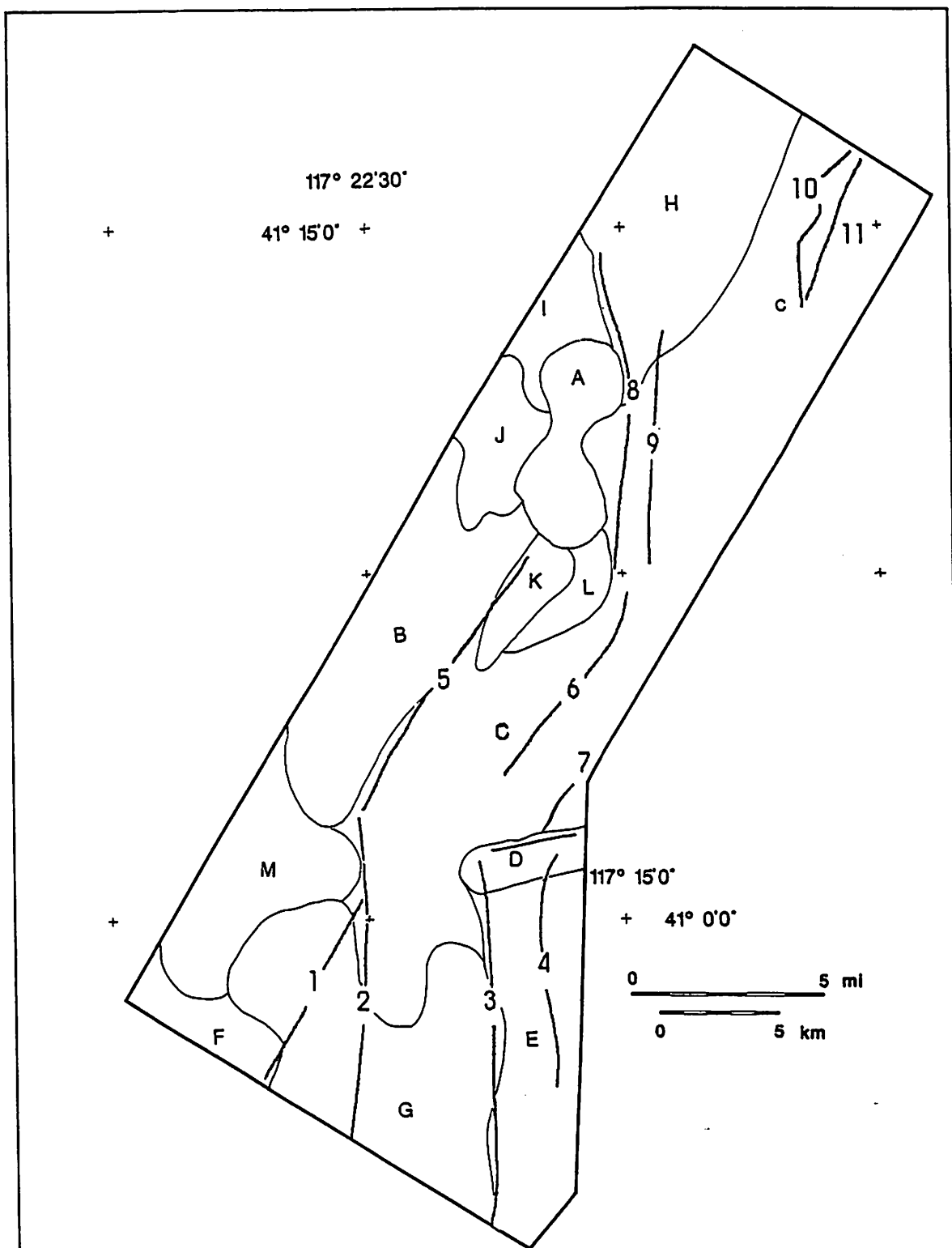


Fig. 7. Sketch map derived from the 900 Hz resistivity map showing areas with gross similarities, such as resistivities and anomaly wavelengths, labeled A, B, C, etc., as well as major electrical lineaments labeled 1, 2, 3, etc.

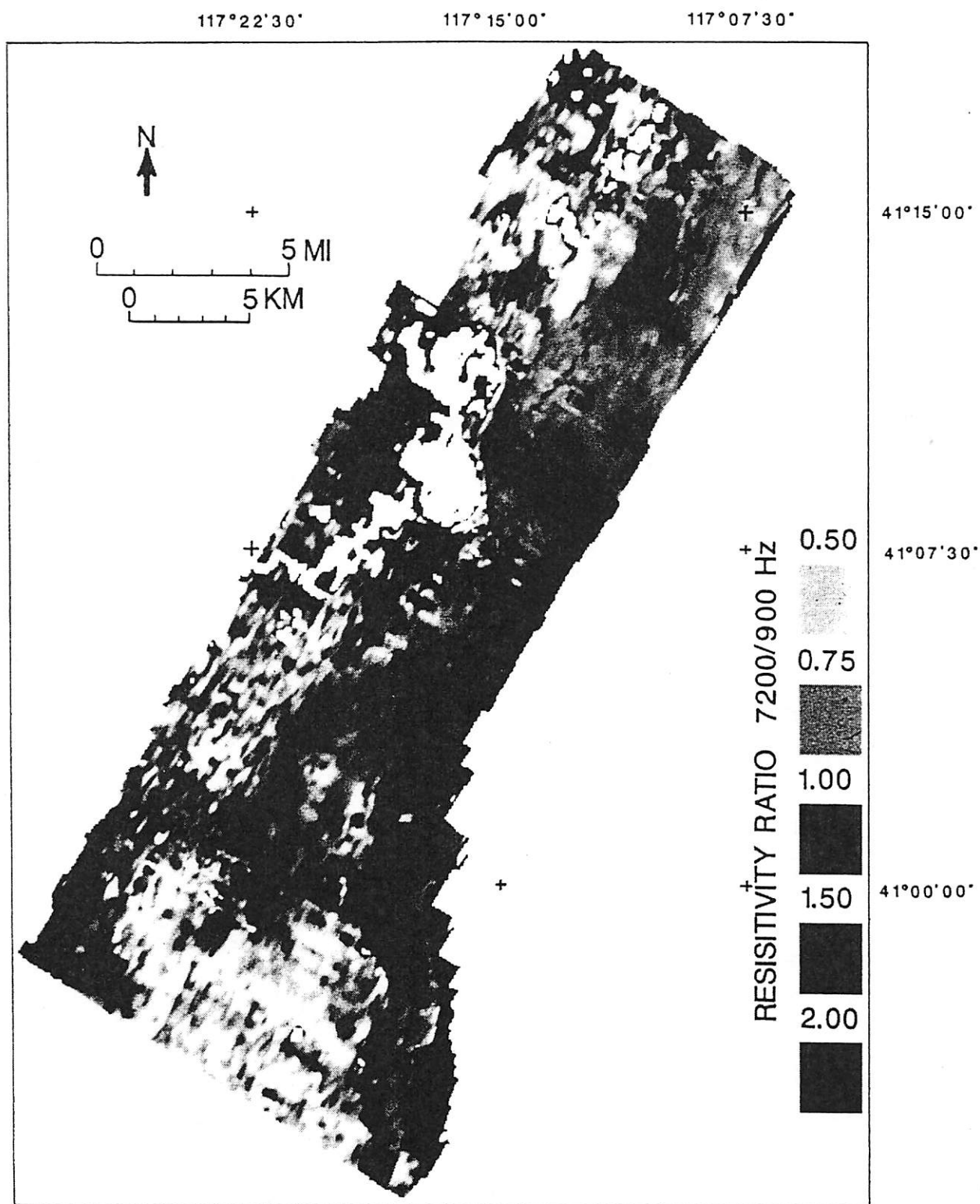


Fig. 8. Resistivity ratio shaded relief map produced by dividing the 7,200 Hz grid by the 900 Hz grid. Values larger than one indicate resistivity decreasing with depth, values smaller than one indicate areas with resistivity increasing with depth. Note that several areas in the Dry Hills, the Cretaceous granodiorite, and the quartzites (see location and geology maps, figs. 1 & 2) are left blank due to resistivity values larger than the DIGHEM instrument can resolve at 900 Hertz.

trend direction are shown by lines 2, 3, 4, 8, and 9. The second is a northeast-trending set shown by lines 1, 5, 6, and 11. The disseminated gold deposits at Preble, Mag, and Getchell are all located near one or more of the electrical lineaments. The Rabbit Creek and Chimney deposits are 1 mile from one of these major AEM electrical lineaments. In the case of Rabbit Creek, the AEM data do not "see" deep enough to pick up any electrical lineaments associated with this deposit. More likely, however, is that the lineaments are subtle features that are masked by the compilation of the data. For example, gridding the original data has a filtering effect that tends to smooth out the subtle features. Also, near these deposits a powerline affects the data by adding noise to the recorded signal. Individual flight-line profiles must be carefully reviewed and caution exercised when interpreting data near powerlines.

A second lineament line (line 9) about 1.5 km east and parallel to the Getchell fault was originally suggested by a single point low on a ground electrical traverse. Here, again, special care must be taken because of the proximity to a powerline. Further ground investigations during 1989 may improve our understanding of the electrical signature of this lineament.

Another aid to the interpretation of these data is a ratio-shaded relief map (Figure 8). For this map, the 7,200 Hz map was divided by the 900 Hz map on a grid-cell by grid-cell basis and the resultant grid displayed. Where the rocks become more conductive with increasing depth, the map values are greater than 1; where the rocks are more resistive with increasing depth, the map values are less than unity. This is true for most of the map with exceptions where the 900 Hertz resistivity map exceeds 1000 ohm-meters. To reduce the chance of misinterpretation of the ratio map, default values were inserted into the Hertz grid where resistivities were greater than 900 ohm-meters. The resulting ratio map has no data where the 900 Hertz resistivity values are greater than 900 ohm-meters.

An observation that seems to hold for all but the central and south pits of the Getchell mine is the deposits appear to be located where the resistivities at depth are lower than at the surface. The central and south Getchell pits do not follow this observation possibly because these deposits are closer to the surface. That is, there is little resistivity contrast because there is little or no resistive cover above the deposit.

An area of ratios greater than one starts at the extreme southeast corner of the survey area and proceeds north to just north of the Mag deposit. Just south of the Mag deposit this area seems to be bounded on the west by the Hotz and Willden fault. South of the mapped extent of the Hotz and Willden fault electrical lineament 3, Figure 7, bounds the area on the west. Though this area is covered by alluvial rocks, it may be an area for further exploration. Another zone of interest is a NW-trending zone of ratios > 1 in the southern quarter of the survey area. This zone cuts across alluvial cover and Tertiary basalts. The zone also cuts across areas E, C, and M (Figure 7). The Preble mine is roughly on the southwestern boundary of this zone. What relationships this cross-cutting zone of conductive rocks with increasing

depth has to the Preble mine is not understood.

The last area of interest is just south of the Rabbit Creek deposit. This area of ratios greater than 1 has a fairly thick (about 125 m) alluvial overburden. The overburden is greater than the maximum depth-of-exploration for the AEM survey. Therefore, the difference between the two frequencies is caused by the lower rocks. It may be that we are seeing effects in the overburden caused by hydrothermal leakage along a fault or a deposit at depth.

Summary

These digital resistivity maps show several electrical lineaments that are lithologic, structural, or topographic in nature. Several of these boundaries have been mapped on the surface by conventional geologic mapping techniques (Figure 2). The AEM resistivity maps help geoscientists extrapolate surficial features into areas covered by alluvium. Using the AEM 900-Hertz frequency, which is the deepest penetrating of the three AEM frequencies, helps locate inferred structures associated with disseminated-gold deposits covered by alluvium. Conductive lineaments identified by the AEM survey coincide with mapped faults associated with known disseminated-gold deposits traced from the ranges where they are exposed into the basins where they are covered, thus delineating areas for further exploration. Buried conductive lineaments related to known faults can improve interpretation of the structural setting. Combining electrical structures identified by the AEM surveys with existing geologic maps of permissive host rocks may prove to be a powerful tool in disseminated-gold exploration.

References

- Erickson, R.L., and Marsh, S.P., 1974a, Geologic map of the Golconda quadrangle, Humboldt County, Nevada: U.S. Geological Survey Geologic Quadrangle Map GQ-1174, scale 1:24,000.
- _____, 1974b, Geologic map of the Iron Point quadrangle, Humboldt County, Nevada: U.S. Geological Survey Geologic Quadrangle Map GQ-1175, scale 1:24,000.
- Fraser, D.C., 1978, Resistivity mapping, with an airborne multi-coil electromagnetic system: *Geophysics*, v. 43, p. 144-172.
- _____, 1978, The multi-coil II airborne electromagnetic system: *Geophysics*, v. 44, p. 1367-1394.
- _____, 1986, DIGHEM resistivity techniques in airborne electromagnetic mapping in Palacky, G.J., ed., *Airborne resistivity mapping: Geological Survey of Canada Paper 86-22*, 523 p.
- Hoover, D.B., Grauch, V.J.S., Pitkin, J.A., Krohn, Dennis, and Pierce, H.A., 1990, An integrated airborne geophysical study along the Getchell trend of gold deposits, north-central Nevada: to be published in the *Proceedings of the Geological Society of Nevada Great Basin Symposium*, April 1990.
- Hotz, P.E., and Willden, Ronald, 1964, *Geology and mineral deposits of the Osgood Mountains quadrangle, Humboldt County, Nevada*: U.S. Geological Survey Professional Paper 431, p. 128.
- Palacky, G.J., ed., 1986, *Airborne resistivity mapping: Geological Survey of Canada Paper 86-22*, 523 p.
- Wallace, A.R., 1989, Coeval Miocene volcanism, extension, and precious-metal mineralization in northern Nevada: *Geological Society of America Abstracts with Programs*, v. 21, no. 5, p. 155.

Structurally Controlled Gold Trends Imply Large Gold Resources in Nevada

Daniel R. Shawe

U.S. Geological Survey, MS 905, Box 25046 Federal Center, Denver, Colorado 80225

Abstract

Numerous gold deposits aligned along the regional Battle Mountain-Eureka, Carlin, and other trends in Nevada coincide with zones of faults, intrusive igneous rocks, and (or) geophysical discontinuities, indicating that mineralization was localized along major crustal structures. These structures, which penetrate deep into or through the crust, controlled emplacement of magmas into the upper crust, and guided dispersal of hydrothermal solutions derived from the intrusions or formed from heated ground waters. Deformation along the regional structures shattered upper crustal rocks, providing local permeable zones favorable for solution flow and precipitation of gold ores.

The 200 km-long Battle Mountain-Eureka structural trend is marked by gold deposits associated with hypabyssal stocks, although other types also are present. These deposits were formed at depths perhaps as great as 5 km. K-Ar studies at some stock-associated deposits indicate that they formed at about 40-38 Ma; others are as old as about 100 Ma. Deep erosion has removed much of the Tertiary volcanic cover that blanketed the Battle Mountain-Eureka trend at the time of intrusion and mineralization.

In contrast, the Carlin structural trend, about 80 km long, is characterized mostly by sedimentary rock-hosted disseminated-type gold deposits. These formed at depths probably no greater than about 3 km, and above the level of hypabyssal stock emplacement. K-Ar studies at the Gold Quarry deposit in the Carlin trend indicate that some mineralization may have occurred at about 29 Ma(?), later than the dated deposits in the Battle Mountain-Eureka trend. The Carlin trend has been less deeply eroded than has the Battle Mountain-Eureka trend, and volcanic rocks are still abundant. The recent discovery of a deep-level gold deposit beneath the Post disseminated deposit in the Carlin trend suggests that deeper gold deposits similar to those exposed in the Battle Mountain-Eureka trend may be present beneath other disseminated ores.

The great linear extent of the Battle Mountain-Eureka and Carlin gold trends, the large number of deposits in each trend, and the evidence for a large vertical range of gold deposition indicate that extremely large hydrothermal systems may have been concentrated along these trends. Numerous other gold deposits of many types occur throughout Nevada, commonly in geologic settings similar to those just described, and regional structures likely controlled major gold deposition in those areas as well. Probably many deposits remain to be discovered, and the potential for additional resources of gold in the State appears to be large.

Introduction

Regional alignments of ore deposits such as the Battle Mountain-Eureka, Carlin, and other trends in Nevada have long been postulated (especially for example Roberts, 1966). The belts, or trends of ore deposits, many mined for gold, coincide with zones of faults, intrusive igneous rocks, and (or) geophysical discontinuities, indicating that mineralization was localized along major crustal structures. Regional considerations suggest that these structures penetrate deep into or through the crust, controlled emplacement of magmas into the upper crust, and guided dispersal of hydrothermal solutions derived from the intrusions or formed from heated ground waters. Deformation along the regional structures shattered upper crustal rocks, providing local permeable zones favorable for solution flow and precipitation of gold ores.

A great variety of gold deposits in varied geologic environments occur in the different structural trends, and these vary in age and level of exposure. Deposits of

similar type and age tend to occur in a particular gold trend, although deposits may make up groups of different ages in a single trend. These relations reflect differences in level of exposure of the different gold trends or parts of gold trends. A trend thus represents a limited part of a large mineralized system that originally contained in total most or all of the various types of deposits, or it may exhibit different parts of more than one mineralized system.

This analysis of geologic and geophysical discontinuities, and of the character of varied gold deposit types, provides insight into the interrelationships among major structural zones, igneous rocks, and the gold deposit trends, and the mechanisms of deposit genesis.

Geophysical and Geological Discontinuities

Significant gold deposits (those that have produced or have reserves of 10,000 oz of gold or more) are closely

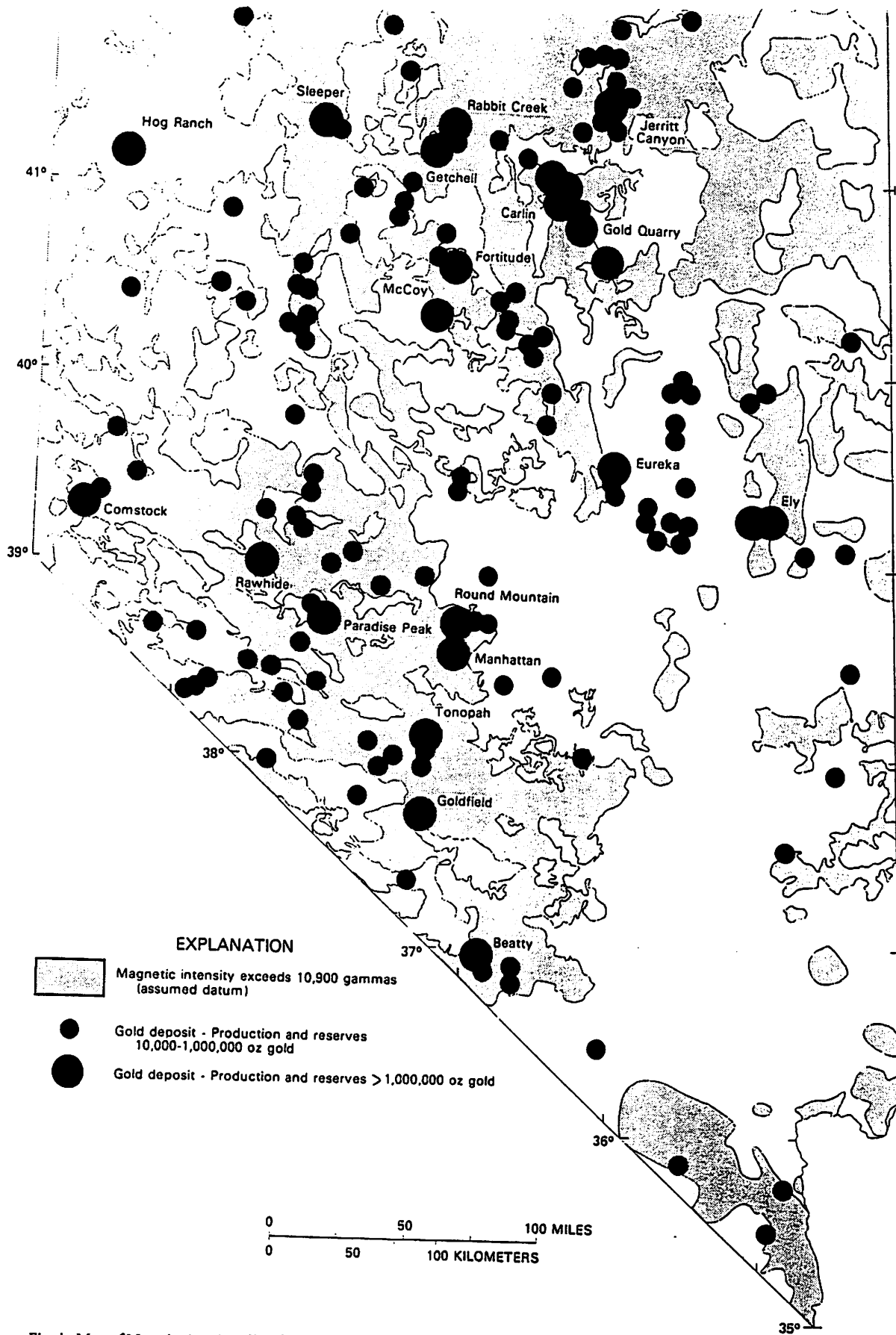


Fig. 1. Map of Nevada showing distribution of significant gold deposits (from Bonham, 1967; 1989; other sources) and areas of magnetic intensity greater than 10,900 gammas (Zietz and others, 1978).

associated with zones of high magnetic intensity throughout the state (fig. 1). Of about 145 such deposits 87 percent lie within or no more than about 5 km from areas of 10,900 gammas or higher magnetic intensity (relative to an assumed datum, Zietz and others, 1978). The 10,900-gamma contour was selected as it encloses most of the areas of gold deposits in Nevada, and it divides the state into roughly 50 percent "high" magnetic intensity and 50 percent "low" magnetic intensity. All of the nearly two dozen major deposits (production and reserves greater than 1 million oz of gold) are in areas of high magnetic intensity. The areas of high magnetic intensity in general outline areas of intrusive igneous rocks, and the gold deposits are closely associated spatially with those igneous rocks. Recently published magnetic maps for Nevada (Hildenbrand and Kucks, 1988a, 1988b) show some of the gold deposit-high magnetic intensity relations more clearly than does the map of Zietz and others (1978), but general relations appear the same on the recent maps.

The zones of high magnetic intensity commonly form well defined alignments that represent linear arrays of igneous intrusive bodies. The linearity of such arrays suggests that the igneous bodies were emplaced along major structural breaks in the crust. Axes of the elongated zones of high magnetic intensity therefore may approximate the positions of such structural breaks, or fault zones (fig. 2). In figure 2 the alignments of igneous rocks are characterized as of either Precambrian, Mesozoic, or Tertiary age on the basis of the dominant age of the igneous rocks in the alignments. From figure 2 it is apparent that northwesterly and northeasterly alignments are common, but several northerly and easterly trends also are evident. All of the variously oriented trends are represented in both the Mesozoic and Tertiary igneous rock alignments, indicating that the trends had been established as early as Mesozoic time.

Broad gravity features of Nevada are bounded by an orthogonal system of mostly northeast- and northwest-trending lines, as shown in figure 3. The pattern suggests that major crustal blocks of differing density may be bounded by northeasterly and northwesterly structural zones (see also, Wallace, 1984) that parallel or coincide with some of the structural zones indicated by the magnetic data. Superimposed on the gravity patterns of figure 3 is a greatly generalized outline of major geologic terranes (fig. 4), the boundaries of which again show a tendency toward northeasterly and northwesterly orientations. Recently published gravity maps of Nevada (Saltus, 1988a, 1988b) show some gravity discontinuities more clearly than does the map of Eaton and others (1978) from which figures 3 and 4 were drawn, although general relations appear unchanged.

The characteristic northerly orientation of mountain ranges in Nevada is disrupted significantly by numerous transverse geologic breaks. These breaks, either prominent mapped faults or pronounced topographic discontinuities that reflect geologic breaks, tend to fall into two groups, one of northeasterly trend and one of

northwesterly trend. Major transverse structures so defined are shown on figure 5. The near coincidence and (or) parallelism of several of these major structural breaks with significant magnetic and gravity trends again suggest that large structures have controlled disruption of the crust and emplacement of igneous rocks in the upper part of the crust.

I believe that the transverse structures depicted on figure 5, although they may in general reflect directions of Neogene and younger extension, are controlled more fundamentally by a preexisting orthogonal structural grain.

In summary, a long established structural framework of northeasterly, northwesterly, northerly, and easterly fault zones has controlled emplacement of magmas into the upper part of the crust during Mesozoic and Tertiary time. Deposition of gold ores was related spatially and probably genetically to emplacement of the magmas.

Battle Mountain-Eureka Gold Trend

The Battle Mountain-Eureka gold trend, about 200 km long in north-central Nevada (fig. 6), is marked by skarn gold deposits associated with hypabyssal stocks, vein and stockwork deposits, and disseminated types. The Fortitude deposit in Copper Canyon near Battle Mountain (Wotruba and others, 1988) formed at the contact between upper Paleozoic carbonate and clastic rocks and a 38.5 Ma granodiorite stock. North-trending faults constitute the dominant structural element in the vicinity of the deposit. Pyrrhotite, pyrite, chalcopyrite, marcasite, arsenopyrite, sphalerite, galena, and gold are associated with calc-silicate minerals such as actinolite, garnet, diopside, and epidote as replacements of carbonate rocks. Gold grade is about 0.2 oz Au/ton. Early stages of mineralization were at temperatures of about 500 C, cooling to about 250 C in late stages. The Fortitude deposit is part of a zoned mineralized system centered on the Copper Canyon stock (Theodore and others, in press).

The Hilltop deposit is in the Shoshone Mountains about 25 km southeast of Battle Mountain (fig. 6). Mineralized breccias and veins are hosted in lower Paleozoic silicic rocks which are altered to a quartz-sericite-pyrite assemblage in the vicinity of granodiorite porphyry plugs, dikes, and sills dated at about 38 Ma (Lisle and Desrochers, 1988). A north-striking, shallowly west-dipping fault was the major control on mineralization. Pyrite, molybdenite, chalcopyrite, sphalerite, galena, tetrahedrite, stibnite, marcasite, and gold are associated with quartz and chalcedonic quartz in the deposits. Gold grade is about 0.08 oz Au/ton. Deposition took place in stages beginning at a temperature of about 250 C and ending at a temperature of about 120 C.

Although not in the Battle Mountain-Eureka trend, the nearby McCoy and Cove deposits, about 45 km southwest of Battle Mountain (fig. 6), are in part similar to the Fortitude deposit. The McCoy deposit (Kuyper, 1988) is a skarn deposit hosted in Triassic carbonate and

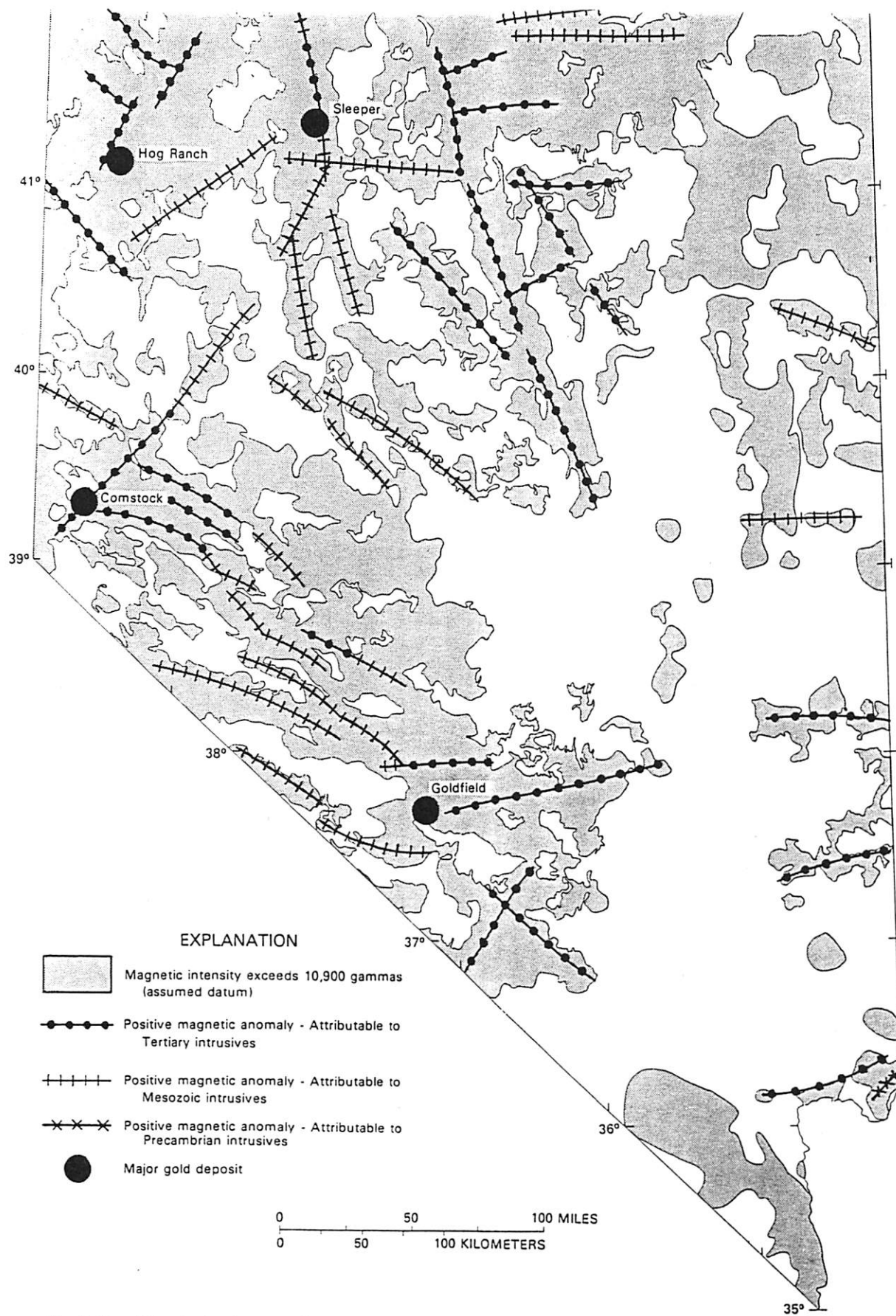


Fig. 2. Map of Nevada showing areas of magnetic intensity greater than 10,900 gammas (Zietz and others, 1978), and alignments of Tertiary, Mesozoic, and Precambrian intrusives (based on Stewart and Carlson, 1978; some Tertiary intrusive alignments in areas of Tertiary volcanics are inferred).

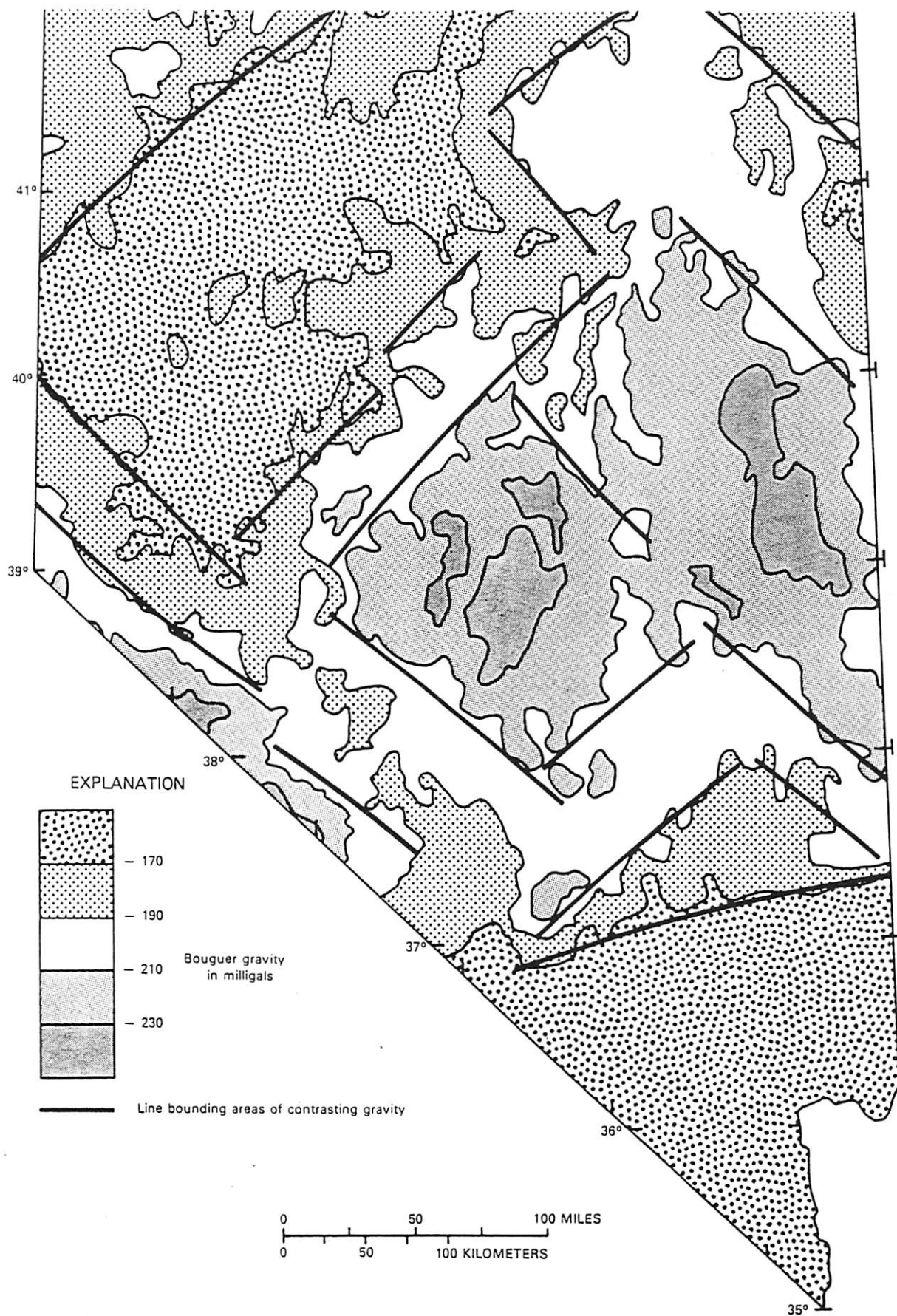


Fig. 3. Simple Bouguer gravity map of Nevada (from Eaton and others, 1978, plate 3-1) showing orthogonal pattern of lines bounding areas of contrasting gravity.

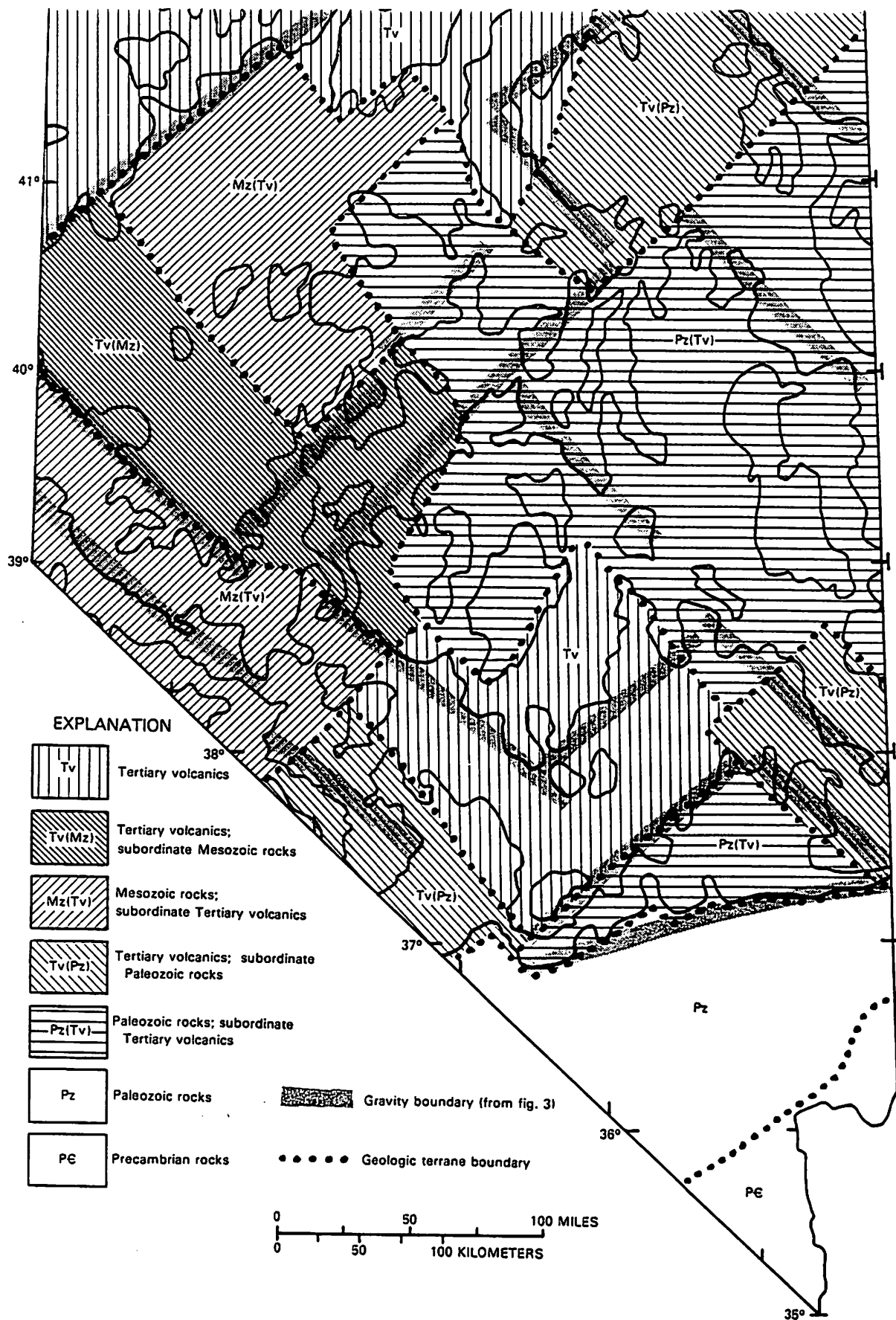


Fig. 4. Simplified geologic map of Nevada showing major geologic terranes and gravity boundaries. Minor rock associations are not indicated.

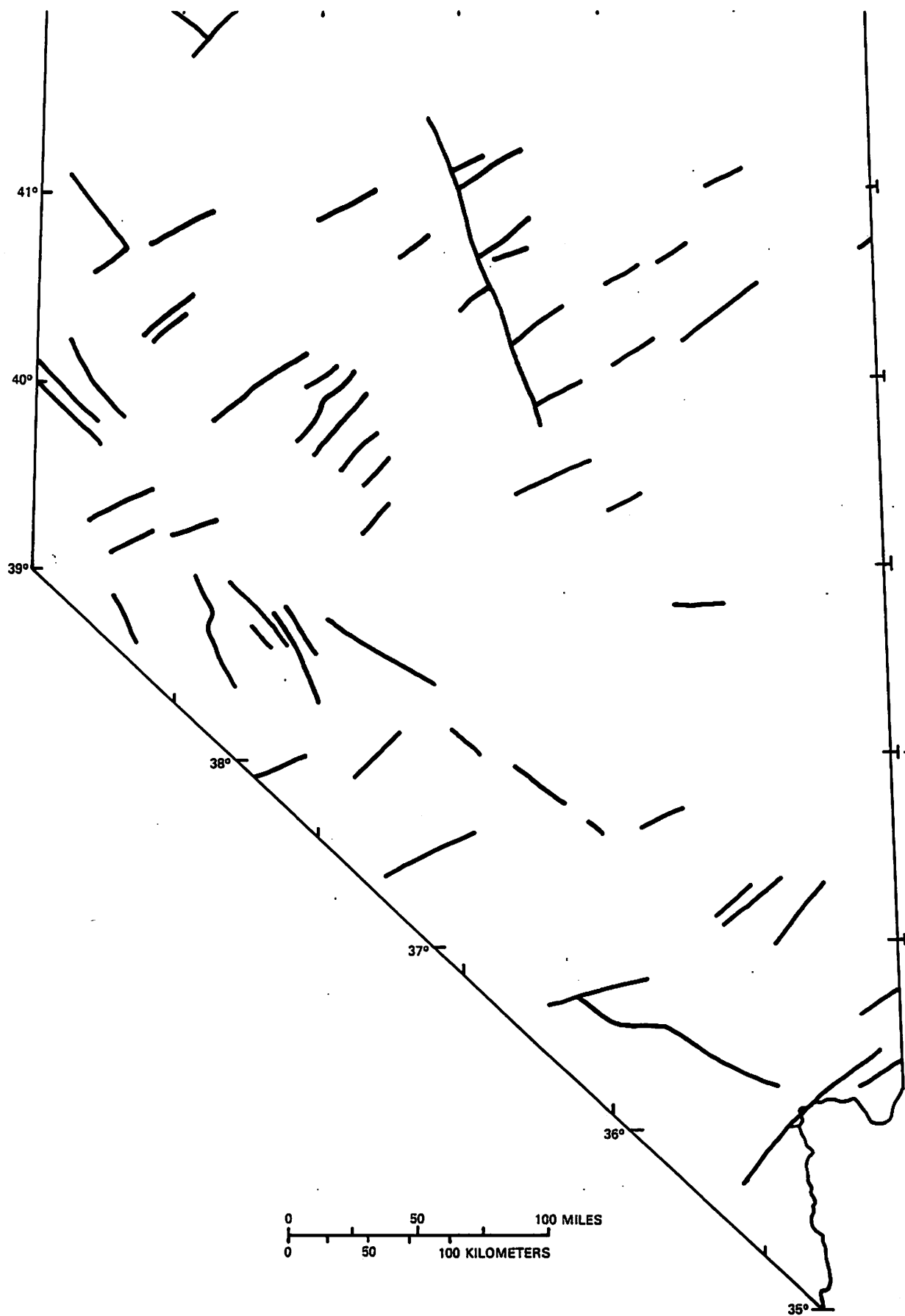


Fig. 5. Map of Nevada showing significant transverse geologic breaks, either prominent mapped faults (Stewart and Carlson, 1978) or pronounced topographic discontinuities.

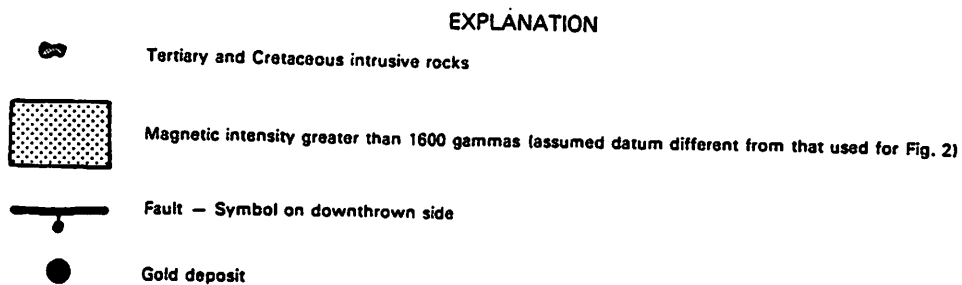
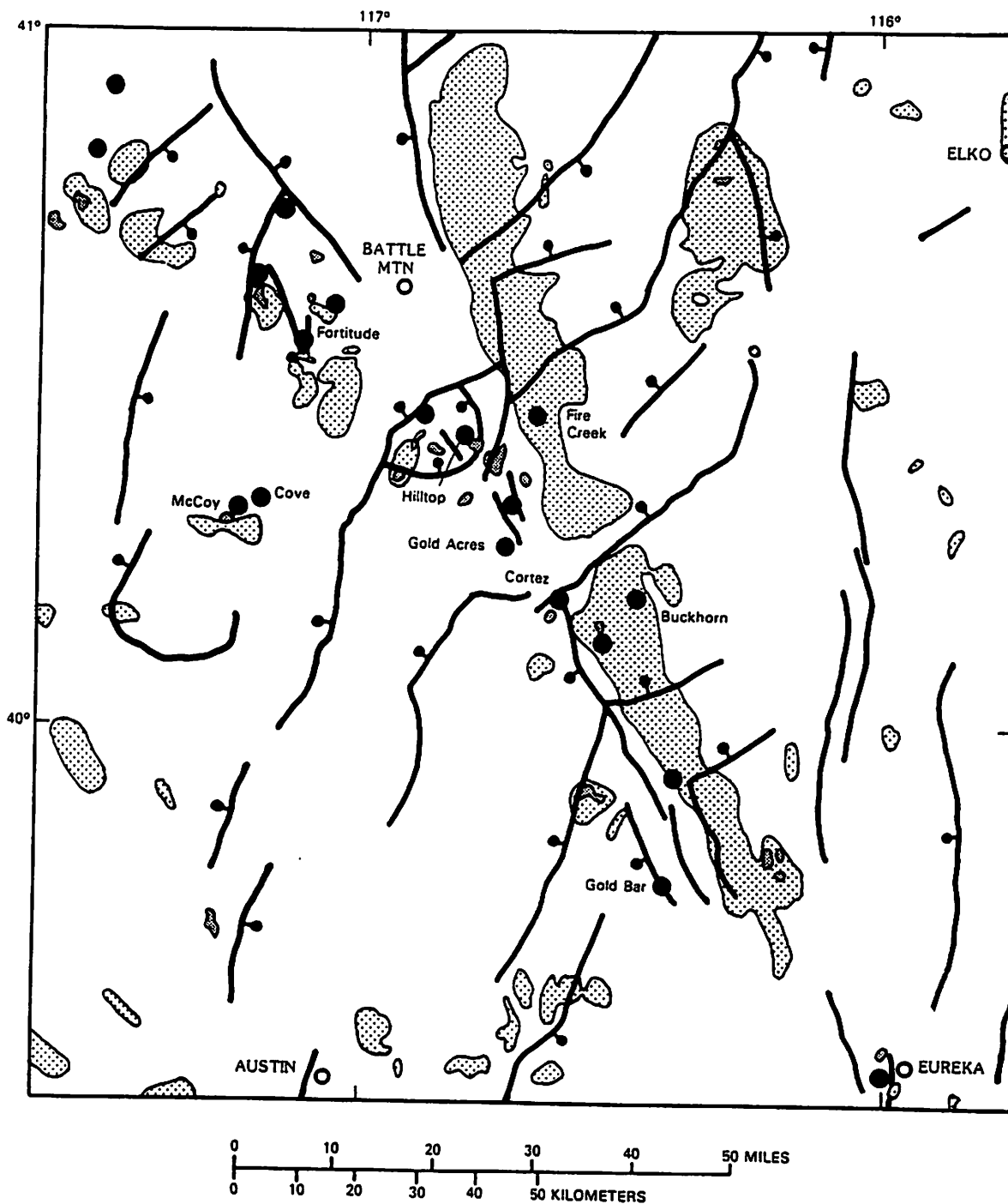


Fig. 6. Map showing gold deposits of the Battle Mountain-Eureka trend (from Bonham, 1967; 1989; named deposits are referred to in the text), major faults (Stewart and Carlson, 1978), early Tertiary and Cretaceous intrusive rocks (Stewart and Carlson, 1978; Silberman and McKee, 1971), and positive magnetic anomalies (greater than 1600 gammas: Stewart and others, 1977).

silici-clastic rocks in the contact zone adjacent to a 40 Ma quartz monzonite-granodiorite porphyry stock. Northeast-trending faults controlled emplacement of the igneous rocks; this set is cut by a younger set of northwest-trending faults. Pyrite, chalcopyrite, and pyrrhotite occur with orthoclase, epidote, actinolite, garnet, and diopside in gold-bearing rock. Gold grade is about 0.09 oz Au/ton. Adularia from gold-bearing quartz-pyrite rock has been dated at about 39 Ma (Kuyper, 1988). The Cove deposit, about 1 km northeast of McCoy, consists of two elements, a deep sulfide-rich mineralized zone mostly in Triassic conglomerate and a shallower zone in carbonate rock characterized by jasperoid and abundant manganese oxide. A locally mineralized porphyry dike at the Cove deposits has been dated at about 39 Ma.

At Eureka, at the southeast end of the gold trend, sulfide-rich replacement deposits, locally associated with jasperoid, formed in lower Paleozoic carbonate rocks near a Cretaceous quartz diorite porphyry dated at about 100 Ma (Marvin and Cole, 1978; Silberman and McKee, 1971). A major north-striking fault was the principal control of mineralization in the district. Near the stock contact mineralized zones are characterized by pyrite, pyrrhotite, and magnetite in association with biotite, garnet, diopside, chlorite, and epidote. The adjacent stock is laced with quartz veinlets that carry molybdenite and other sulfides. Manto deposits in carbonate rocks farther from the stock carry abundant sphalerite and galena as well as silver minerals and gold. Gold grade ranges from 0.15-0.20 oz Au/ton in large tonnages to as high as 1.33 oz Au/ton in parts of the mantos (Shawe and Nolan, 1989). Most of the ore mined at Eureka was at the surface and strongly oxidized. Gold grades averaged about 1 oz Au/ton.

Several low-grade disseminated gold deposits in the south part of the Eureka district occur in lower Paleozoic carbonate rocks. They are characterized by abundant jasperoid and the presence of realgar. One of the deposits is associated with an Oligocene rhyodacite dike (Oligocene intrusives in the area have been dated at about 39-34 Ma; Blake and others, 1975; Nolan and others, 1974; Jaffe and others, 1959).

The Cortez and Gold Acres low-grade disseminated gold deposits in the central part of the gold trend about 50 km southeast of Battle Mountain, are similar in many ways to low-grade disseminated gold deposits in the Carlin trend. The Cortez deposit (Wells and others, 1969) is in jasperized lower Paleozoic carbonate rocks and it envelops a biotite-quartz-sanidine porphyry dated at 34 Ma. A major north- to north-northwest-trending fault may have been the principal control on localization of the Cortez deposit. Gold occurs as micron-size particles in hematite-goethite pseudomorphs after pyrite in the silicified carbonate rocks. Anomalous amounts of mercury, arsenic, antimony, tungsten, copper, and nickel accompany the gold.

The Gold Acres deposit (Wrucke and Armbrustmacher, 1975) was mined in the 1940s and 1950s as one

of the earliest of the so-called Carlin type of disseminated gold deposit. It formed in lower Paleozoic carbonate, chert, and silici-clastic rocks near a Cretaceous granite porphyry intrusive dated at about 99 Ma. Low-angle faults dominate the setting at Gold Acres. Perhaps a major northwesterly structure, not evident at the surface, controlled mineralization, inasmuch as the deposit lies in a narrow well defined northwesterly zone of deposits that crosses the northern Shoshone Mountains. Three main stages of mineralization took place at the mine. Garnet-bearing tactite characterized by molybdenite formed at about 380 C, followed by a sulfide stage at about 265-150 C. A final stage saw deposition of gold with associated metals arsenic, mercury, antimony, tungsten, and silver, at about 150 C.

The Gold Bar deposit (Broili and others, 1988) lies along a major range-bounding northwest-trending fault about 50 km northwest of Eureka. The deposit is hosted by upper Paleozoic carbonate rocks that have been locally brecciated, jasperized, sanded, and argillized. The deposit lies along a major north-northwest-striking fault. Early deposition of calcite was followed by pyrite and quartz in veins, widespread silicification (formation of jasperoid), and disseminated deposition of realgar, orpiment, and gold. In addition to arsenic and gold, antimony and mercury are also anomalous in the deposit. High-grade gold zones formed along fault intersections. Carbonaceous ores in the deposit contain about 0.2 oz Au/ton, about twice the grade of the jasperoid and oxidized ores in the deposit. Nearby volcanic rocks dated at about 24 Ma have been hydrothermally altered, implying that the Gold Bar deposit may be younger than 24 Ma, an inference supported by the occurrence of the deposit along a range-front fault of probable Miocene or younger age.

The Buckhorn gold deposit (Monroe and others, 1988) is in Miocene basalt (about 16 Ma) just east of the Battle Mountain-Eureka trend about 65 km southeast of Battle Mountain. It is localized along north-northwesterly faults within and parallel to the large positive magnetic anomaly that marks a regional zone of Miocene basalt intrusion and extrusion. Development of argillic alteration and associated opaline quartz (including some nearby hot springs sinter), quartz, adularia, calcite, and gypsum indicates a near-surface, hot springs origin for the deposit. Very fine grained pyrite occurs in cryptocrystalline quartz. Anomalous metals present in the low-grade gold ore (average about 0.04 oz Au/ton) are silver, arsenic, antimony, mercury, thallium, copper, zinc, lead, molybdenum, and tungsten. Temperatures of deposition ranged from about 290 C down to 150 C. Adularia in the deposit has been dated at about 15 Ma (Wells and Silberman, 1973).

The gold deposit at Fire Creek 30 km southeast of Battle Mountain also is in Miocene basalt and lies along the north-northwesterly regional magnetic anomaly.

In summary, the Battle Mountain-Eureka gold trend consists of several components. The earliest is represented by the high-temperature skarn and manto deposits at

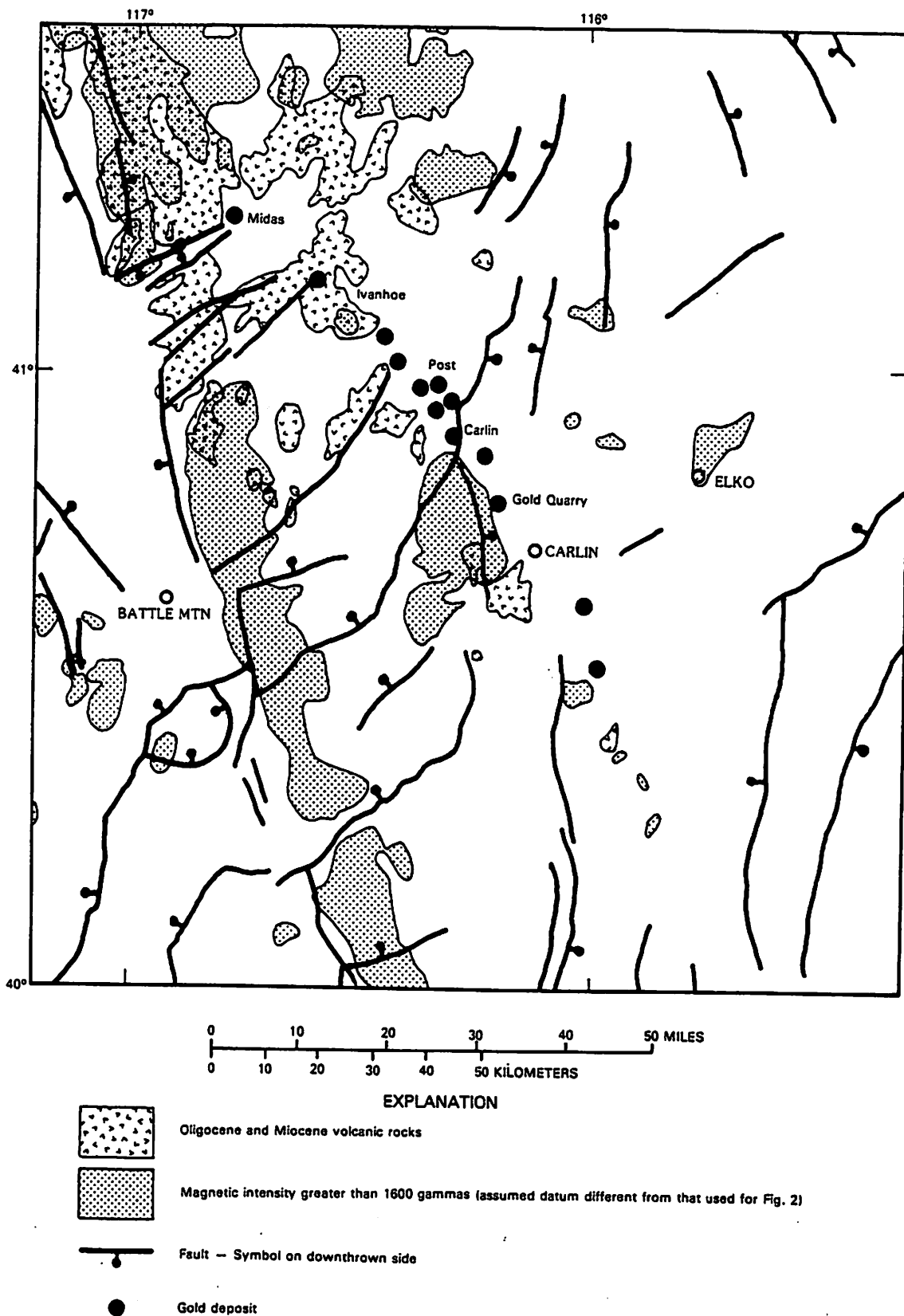


Fig. 7. Map showing gold deposits of the Carlin trend (from Bonham, 1967; 1989; the Midas and Ivanhoe deposits, about 15 Ma, may not be part of the Carlin trend proper; the other named deposits are referred to in the text), major faults (Stewart and Carlson, 1978), Oligocene and Miocene volcanic rocks (Stewart and Carlson, 1978; McKee and others, 1971; Miocene basalts related to the prominent north-northwesterly magnetic anomaly are not shown), and positive magnetic anomalies (greater than 1600 gammas: Stewart and others, 1977).

Eureka and the tectite deposit at Gold Acres, each related to 100 Ma porphyry intrusives. The main element of the trend, and by far the most important in terms of amount of gold deposited, was related to hypabyssal igneous rocks that were emplaced about 40-34 Ma. The deposits include the Fortitude skarn deposit, Hilltop breccias and veins, the Cortez disseminated deposit, and probably low-grade disseminated deposits at Eureka. The Fortitude and Hilltop deposits may have formed at depths as great as about 4-5 km, based on estimates of the general level of stock emplacement (for example, Bodnar and Beane, 1977; Cornwall, 1982), and the Cortez and Eureka disseminated deposits formed at probably shallower depth. Just southwest of the gold trend the McCoy skarn and Cove sulfide and jasperoid ores also formed during this period of magmatic activity. The gold mineralization at Gold Acres also may have occurred during this Oligocene episode. The alignment of Oligocene intrusives and associated positive magnetic anomalies in the Battle Mountain-Eureka trend and the closely parallel array of Oligocene gold deposits is apparent on figure 5. Younger gold mineralization that occurred during the Miocene (probably about 15 Ma) such as at Buckhorn, Fire Creek, and perhaps at the Gold Bar deposit, may have been controlled by the north-northwesterly zone of basalt intrusion, and was unrelated to the earlier mineralization along the Battle Mountain-Eureka gold trend. On the other hand, continued mineralizing activity along the older gold trend may have taken advantage of the younger structural trend that controlled basalt emplacement, to form the Buckhorn and other younger gold deposits.

Carlin Gold Trend

The Carlin gold trend, about 80 km long and subparallel with and 75 km northeast of the Battle Mountain-Eureka trend (fig. 7), is characterized by low-temperature disseminated gold ores mostly in Paleozoic carbonaceous carbonate rocks. Intrusive rocks are sparse in the trend; dated intrusives are about 130-106 Ma and about 37 Ma (Silberman and McKee, 1971; McKee and others, 1971; Evans, 1974). Volcanic rocks along the trend have been dated at about 39-36 Ma (McKee and others, 1971) and about 14 Ma (McKee and others, 1971). Volcanic rocks of these age groups are particularly abundant along the northwest part of the Carlin trend (Stewart and Carlson, 1976) (fig. 7). A parallel alignment of positive magnetic anomalies lying a few kilometers southwest of the Carlin trend (fig. 7) probably reflects buried intrusive rocks related to the exposed Cretaceous and Oligocene-Miocene igneous rocks along the trend.

The Carlin gold deposit (Hardie, 1966; Hausen and Kerr, 1968; Noble and Radtke, 1978; Radtke and others, 1980; Radtke, 1985; Bakken and Einaudi, 1986), famous as the first large deposit of disseminated (or "invisible") gold mined in Nevada, is hosted by Silurian and Devonian silty, organic-rich carbonate rocks. Host

rocks in the mine area were intruded mostly along northwest- to north-northwest-trending faults by several granodiorite dikes, one of which was dated as 128 Ma (Radtke and others, 1980). In places the host rocks were intensely silicified (jasperized) and argillized, and mineralized with a variety of metallic minerals. Principal controls on mineralization were northeast- and north-northwest-striking faults (Bakken and Einaudi, 1986). In addition to abundant pyrite, also present are realgar, stibnite, sphalerite, galena, molybdenite, chalcopyrite, cinnabar, gold, and several other sulfide and sulfosalt minerals that contain mercury, antimony, and thallium. Other minerals are barite, quartz, potassium clays, sericite, anhydrite, kaolinite, calcite, and dolomite. Metals that are anomalously enriched in the deposit include gold, iron, arsenic, antimony, mercury, thallium, lead, zinc, and copper. (Radtke and others, 1980). Gold grades in the Carlin deposit average about 0.32 oz Au/ton. Main gold-stage mineralization took place at about 175-200 °C, and some later-stage hydrothermal activity was at higher temperatures. Mineralization probably took place at a depth of about 3 km (Rose and Kuehn, 1987). The deposit has not been radiometrically dated; Radtke and others (1980) suggested a late Tertiary age whereas Bakken and Einaudi (1986) suggested a pre-late Tertiary age.

The Gold Quarry deposit, largest of the Nevada disseminated gold deposits, is hosted in transitional facies siltstone, shale, silty limestone, and chert of Ordovician age (Rota, 1988). Silicification, alunitization, and argillization affected the host rocks in the vicinity of mineralized rock. Mineralization was controlled principally by north-northwest-trending faults. Unoxidized mineralized rock is characterized by sulfides; anomalous amounts of gold, silver, arsenic, antimony, copper, lead, nickel, zinc, and mercury occur in ore. Average gold grade in the deposit is 0.049 oz Au/ton. Alunite from the Gold Quarry deposit has been dated at about 29 Ma (Rota, 1989; Rota and Hausen, in press), a minimum age that may also represent a possible resetting event.

Most other deposits in the Carlin trend consist of disseminated ores in Paleozoic sedimentary rocks and are similar in many ways to either the Carlin or the Gold Quarry deposits. The Deep Post high-grade gold deposit, however, recently discovered underlying the Post deposit near the north end of the Carlin trend, appears to be different from the other deposits. It is a sulfide-rich deposit hosted in Devonian calcareous and siliciclastic sedimentary rocks that have been hydrothermally argillized, silicified, and brecciated (Zimmerman and others, 1989); gold values reported for one drill interval of about 155 m average 0.93 oz Au/ton (Newmont Gold Company Annual Report, 1987). Some gold occurs in a nearby Jurassic or Cretaceous stock and associated skarns. According to Zimmerman and others (1989) the Deep Post deposit is cut by a late-mineral or post-mineral dike that is dated by the K-Ar method as about 40 Ma. The deposit may be similar to the sulfide-rich deep deposit at Cove south of Battle Mountain, or to parts of the sulfide-rich mantos at Eureka.

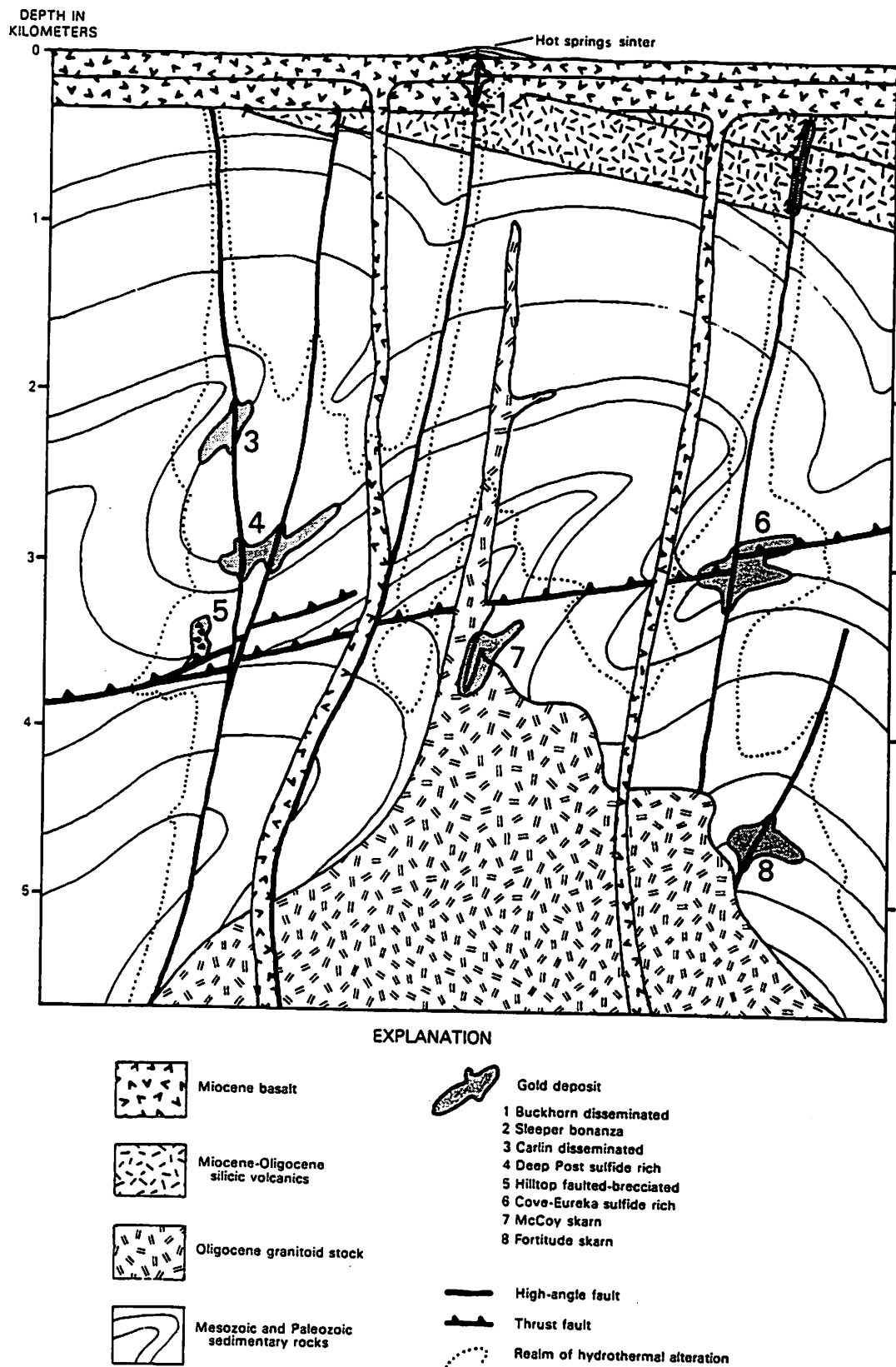


Figure 8. Idealized cross-sectional diagram showing environments of some Nevada gold deposits. The deposits shown are not all parts of the same system, but analogous deposits may have formed during specific mineralizing events.

In summary, the Carlin trend is made up mostly of disseminated gold deposits in Paleozoic sedimentary rocks; the deposits form a remarkably linear north-northwest-trending array. The trend is centered on an area of igneous rocks that range in age from about 37-14 Ma. The presence of abundant volcanic rocks at the surface, in contrast to sparse volcanics associated with the Oligocene intrusives of the Battle Mountain-Eureka trend, suggests that the Carlin trend is less deeply eroded and hence younger than the Battle Mountain-Eureka trend. The age of mineralization in the Carlin trend is poorly established; as in the Battle Mountain-Eureka trend, mineralization may have occurred in multiple episodes. One deposit (Gold Quarry) is evidently no younger than about 29 Ma. The Deep Post deposit in the northern part of the Carlin trend apparently is at least 40 Ma and is a sulfide-rich deposit which may be similar to the deep deposit at Cove, or to parts of the Eureka sulfide-rich ore bodies, which were formed at depth outward from skarn zones that are adjacent to porphyry stocks. Its presence suggests a deeper-level part to the Carlin trend hydrothermal system that is analogous to the deeper-level deposits of the Battle Mountain-Eureka gold trend.

Discussion and Conclusions

The linearity of the gold trends and concentration of igneous rocks along them suggest that deep-penetrating regional structures controlled the emplacement of magmas generated in the lower part of the crust or upper mantle. The magmas served as heat source and either provided hydrothermal fluids or caused heating of ground waters that were responsible for transport and deposition of the gold ores. Deformation of the structures resulted in extensive fracturing of shallow crustal rocks, providing permeable zones for solution flow and ore deposition in a variety of rock types. Varied rock compositions likely afforded local chemically favorable sites for deposition, and formation of deposits that exhibit a variety of morphologies and styles of mineralization.

The great linear extent of the Battle Mountain-Eureka and Carlin gold trends, the large number of deposits in each trend, and the evidence for a large vertical range of gold deposition indicate that extremely large hydrothermal systems were concentrated along these trends. Although several episodes of mineralization may have taken place along the trends, a major episode occurred in the Battle Mountain-Eureka trend at about 40-35 Ma during which time deposits formed at different structural levels and in different geologic environments. Apparently a similar major episode took place in the Carlin trend, but possibly of a somewhat younger age. A wide range of deposits is evident in the Battle Mountain-Eureka trend, but only the upper levels of large hydrothermal systems are exposed in the Carlin trend. Figure 8 is an idealized diagram drawn to represent the principal elements of the envisaged large hydrothermal systems.

The numerous other gold deposits throughout Nevada are of many types, including the types that have been described here in the Battle Mountain-Eureka and Carlin trends, and they occur commonly in geologic settings similar to those of the two described trends. As was the localization of the deposits of those two trends, the localization of many of the other gold deposits throughout Nevada likely was controlled by regional structures.

Probably many gold deposits remain to be discovered throughout the state, and the potential for additional resources of gold appears to be large. Possible examples of localities where new gold deposits will be found are the following. In northwestern Nevada the Hog Ranch deposit lies close to the axis of a prominent northeasterly positive magnetic anomaly that likely reflects a linear trend of buried Tertiary intrusive rocks. Exploration along that trend could reveal additional deposits. An alignment of Tertiary intrusives northeasterly from the Comstock Lode district may indicate the site of yet undiscovered gold deposits. A trend of Tertiary intrusives extending northward from the Sleeper deposit likewise suggests a zone where gold exploration might be successful. Goldfield lies near the west end of an east-trending alignment of Tertiary intrusives that may warrant exploration. Of course exploration in any of these areas would require application of sound geologic knowledge as well as detailed geochemical and geophysical information. I hope exploration geologists familiar with the state of Nevada will find the suggestions in this paper useful.

Acknowledgements

This paper has been improved by valuable reviews by Alan Wallace and Ted Armbrustmacher of the U.S. Geological Survey, and by Lew Gustafson and an anonymous reviewer of the Geological Society of Nevada.

References

- Bakken, B.M., and Einaudi, M.T., 1986, Spatial and temporal relations between wall rock alteration and gold mineralization, main pit, Carlin gold mine, Nevada, U.S.A.: in MacDonald, A.J., ed., *Gold '86, an international symposium on the geology of gold deposits: Proceedings Volume*, Toronto, p. 388-403.
- Blake, M.C., Jr., McKee, E.H., Marvin, R.F., Silberman, M.L., and Nolan, T.B., 1975, The Oligocene volcanic center at Eureka, Nevada: *U.S. Geological Survey Journal of Research*, v. 3, no. 5, p. 605-612.
- Bodnar, R.J., and Beane, R.E., 1977, Temperature variations in pre-intrusive cover over a buried pluton: *Geological Society of America Abstracts with Programs*, v. 9, no. 7, p. 903-904.
- Bonham, H.F., 1967, Gold producing districts of Nevada: Nevada Bureau of Mines Map 32.
- , 1989, Bulk-mineable precious-metal deposits and prospects in Nevada: Nevada Bureau of Mines and Geology Map 91.
- Broili, Chris, French, G. McN., Shaddrick, D.R., and Weaver, R.R., 1988, Geology and gold mineralization of the Gold Bar deposit, Eureka County, Nevada, in Schafer, R.W., Cooper, J.J., and Vikre, P.G., eds., *Bulk mineable precious metal deposits of the western United States: Symposium Proceedings*, Geological Society of

- Nevada, Reno, p. 57-72.
- Cornwall, H.R., 1982, Petrology and chemistry of igneous rocks, Ray porphyry copper district, Pinal County, Arizona, in Titley, S.R., ed., *Advances in geology of the porphyry copper deposits, southwestern North America*: Tucson, University of Arizona Press, Chapter 11.
- Eaton, G.P., Wahl, R.R., Prostka, H.J., Mabey, D.R., and Kleinkopf, M.D., 1978, Regional gravity and tectonic patterns: Their relation to late Cenozoic epeirogeny and lateral spreading in the western Cordillera, in Smith, R.B., and Eason, G.P., eds., *Cenozoic tectonics and regional geophysics of the western Cordillera*: Geological Society of America Memoir 152, p. 51-91.
- Evans, J.G., 1974, Geologic map of the Welches Canyon quadrangle, Eureka County, Nevada: U.S. Geological Survey Geologic Quadrangle Map GQ-1117, scale 1:24,000.
- Hardie, B.S., 1966, Carlin gold mine, Lynn district, Nevada: Nevada Bureau of Mines Report 13, p. 73-83.
- Hausen, D.M., and Kerr, P.F., 1968, Fine gold occurrence at Carlin, Nevada, in Ridge, J.D., ed., *Ore deposits of the United States, 1933-1967* (Graton-Sales vol.): New York, American Institute of Mining, Metallurgical, and Petroleum Engineers, v. 1, p. 908-940.
- Hildenbrand, T.G., and Kucks, R.P., 1988a, Total intensity magnetic anomaly map of Nevada: Nevada Bureau of Mines and Geology Map M93A, scale 1:750,000.
- _____, 1988b, Filtered magnetic anomaly maps of Nevada: Nevada Bureau of Mines and Geology Map M93B, 4 maps at scale 1:1,000,000; 2 maps at scale 1:2,000,000.
- Jaffe, H.W., Gottfried, David, Waring, C.L., and Worthing, H.W., 1959, Lead-alpha age determinations of accessory minerals of igneous rocks (1953-1957): U.S. Geological Survey Bulletin 1097-B, p. 65-148.
- Kuyper, B.A., 1988, Geology of the McCoy gold deposit, Lander County, Nevada, in Schafer, R.W., Cooper, J.J., and Vikre, P.G., eds., *Bulk minable precious metal deposits of the western United States: Symposium Proceedings*, Geological Society of Nevada, Reno, p. 173-185.
- Lisle, R.E., and Desrochers, G.J., 1988, Geology of the Hilltop gold deposit, Lander County, Nevada, in Schafer, R.W., Cooper, J.J., and Vikre, P.G., eds., *Bulk minable precious metal deposits of the western United States: Symposium Proceedings*, Geological Society of Nevada, Reno, p. 101-117.
- Marvin, R.F., and Cole, J.C., 1978, Radiometric ages—Compilation A, U.S. Geological Survey: *Isochron/West*, no. 1, p. 15-32.
- McKee, E.H., Silberman, M.L., Marvin, R.F., and Obradovich, J.D., 1971, A summary of radiometric ages of Tertiary volcanic rocks in Nevada and eastern California. Part 1—Central Nevada: *Isochron/West*, no. 2, p. 21-42.
- Monroe, S.C., Godlewski, D.W., and Plahuta, J.T., 1988, Geology and mineralization at the Buckhorn mine, Eureka County, Nevada, in Schafer, R.W., Cooper, J.J., and Vikre, R.G., eds., *Bulk minable precious metal deposits of the western United States: Symposium Proceedings*, Geological Society of Nevada, Reno, p. 273-291.
- Newmont Gold Company, 1987, Annual Report, 24 p.
- Noble, L.L., and Radtke, A.S., 1978, Geology of the Carlin disseminated replacement gold deposit, Nevada, in Shawe, D.R., ed., *Guidebook to mineral deposits of the central Great Basin*: Nevada Bureau of Mines and Geology Report 32, p. 40-44.
- Nolan, T.B., Merriam, C.W., and Blake, M.C., Jr., 1974, Geologic map of the Pinto Summit quadrangle, Eureka and White Pine Counties, Nevada: U.S. Geological Survey Miscellaneous Investigations Map I-793, scale 1:31,680.
- Radtke, A.S., 1985, Geology of the Carlin gold deposit: U.S. Geological Survey Professional Paper 1267, 124 p.
- Radtke, A.S., Rye, R.O., and Dickson, F.W., 1980, Geology and stable isotope studies of the Carlin gold deposit, Nevada: *Economic Geology*, v. 75, p. 641-672.
- Roberts, R.J., 1966, Metallogenic provinces and mineral belts in Nevada: Nevada Bureau of Mines Report 13, p. 47-72.
- Rose, A.W., and Kuehn, C.A., 1987, Ore deposition from acidic CO₂-rich solutions at the Carlin gold deposit, Eureka County, Nevada: Geological Society of America Abstracts with programs, p. 824.
- Rota, J.C., 1988, The Gold Quarry mine: history and general geology, in Schafer, R.W., Cooper, J.J., and Vikre, P.G., eds., *Bulk minable precious metal deposits of the western United States: Symposium Proceedings*, Geological Society of Nevada, Reno, p. 49-56.
- Rota, J.C., and Hausen, D.M., 1989, Geology of the Gold Quarry mine—1988 (abs.): American Institute of Mining, Metallurgical, and Petroleum Engineers Annual Meeting program, p. 40.
- Salts, G.V., 1988a, Bouguer gravity map of Nevada: Nevada Bureau of Mines and Geology Map M94A, scale 1:750,000.
- _____, 1988b, Regional, residual, and derivative gravity maps of Nevada: Nevada Bureau of Mines and Geology Map M94B, 4 maps at scale 1:1,000,000, 2 maps at scale 1:2,500,000.
- Shawe, D.R., and Nolan, T.B., 1989, Gold in the Eureka mining district, Nevada, in Shawe, D.R., Ashley, R.P., and Carter, L.M.H., eds., *Geology and resources of gold in the United States*: U.S. Geological Survey Bulletin 1857-C, p. C29-C39.
- Silberman, M.L., and McKee, E.H., 1971, K-Ar ages of granitic plutons in north-central Nevada: *Isochron/West*, no. 1, p. 15-32.
- Stewart, J.H., and Carlson, J.E., 1978, Geologic map of Nevada: U.S. Geological Survey, scale 1:500,000.
- Stewart, J.H., and Carlson, J.E., 1976, Cenozoic rocks of Nevada: four maps (scale 1:1,000,000) and brief description of distribution, lithology, age, and centers of volcanism: Nevada Bureau of Mines and Geology Map 52.
- Stewart, J.H., Moore, W.J., and Zietz, Isidore, 1977, East-west patterns of Cenozoic igneous rocks, aeromagnetic anomalies, and mineral deposits, Nevada and Utah: Geological Society of America Bulletin, v. 88, p. 67-77.
- Theodore, T.G., Howe, S.J., and Blake, D.W., in press, The Tomboy-Minnie gold deposits at Copper Canyon, Lander County, Nevada, in Shawe, D.R., Ashley, R.P., and Carter, L.M.H., eds., *Geology and resources of gold in the United States*, U.S. Geological Survey Bulletin 1857-E.
- Wallace, R.E., 1984, Patterns and timing of late Quaternary faulting in the Great Basin province and relation to some regional tectonic features: *Journal of Geophysical Research*, v. 89, p. 5763-5769.
- Wells, J.D., and Silberman, M.L., 1973, K-Ar age of mineralization at Buckhorn, Eureka County, Nevada: *Isochron/West*, no. 8, p. 37-38.
- Wells, J.D., Stoiser, L.R., and Elliott, J.E., 1969, Geology and geochemistry of the Cortez gold deposit, Nevada: *Economic Geology*, v. 64, p. 526-537.
- Wotruba, P.R., Benson, R.G., and Schmidt, K.W., 1988, Geology of the Fortitude gold-silver skarn deposit, Copper Canyon, Lander County, Nevada, in Schafer, R.W., Cooper, J.J., and Vikre, P.G., eds., *Bulk minable precious metal deposits of the western United States: Symposium Proceedings*, Geological Society of Nevada, Reno, p. 159-171.
- Wrucke, C.T., and Armbrustmacher, T.J., 1975, Geochemical and geologic relations of gold and other elements at the Gold Acres open-pit mine, Lander County, Nevada: U.S. Geological Survey Professional Paper 860, 27 p.
- Zietz, Isidore, Gilbert, F.P., and Kirby, J.R., 1978, Aeromagnetic map of Nevada: color coded intensities: U.S. Geological Survey Geophysical Investigations Map GP-922, scale 1:1,000,000.
- Zimmerman, C.J., Walck, C.M., Vaillancourt, D., and Hausen, D.M., 1989, Geology and process mineralogy of the Deep Post gold deposit (abs.): American Institute of Mining, Metallurgical, and Petroleum Engineers Annual Meeting program, p. 40.

Multivariate statistical analysis of geophysical data in Nevada

Uzi Vulkan* and Joseph S. Duval†

ABSTRACT

Regional magnetic, gravity, and gamma-ray data in Nevada were analyzed using a multivariate statistical method. The algorithms used are part of the public-domain Geographical Resource Analysis Support System (GRASS). Twenty-seven statistical groups (clusters) were found to be the optimum number that best represents the geophysical data. The resulting map of the distribution of these groups shows linear features which define a geophysical trend not previously recognized. This trend is clearly related to the northern Nevada rift and extends from near the northern border of Nevada to the southern part of the State with a northwest-southeast trend to about 37°N latitude,

where a change of direction occurs to a northeast-southwest trend. Although not spatially coincident, the Roberts Mountains Thrust, the Golconda Thrust, and the 0.706 contour of the $^{87}\text{Sr}/^{86}\text{Sr}$ ratio exhibit similar trends over part of their lengths. The significance of this geophysical trend is uncertain. One possible interpretation is that it corresponds to the central graben of a rift system larger than previously postulated. The classified data were also compared to a digital geologic map, and the results show that, for some areas of the state, mapped geology and specific groups do have a clear relationship. In general, however, mapped geologic units and the groups have no unique relationships.

INTRODUCTION

The regional data sets used in this study are residual magnetic data (Hildenbrand and Kucks, 1988), isostatic gravity (Saltus, 1988), and gamma-ray spectrometric data (Duval, 1988). The magnetic, gravity, and gamma-ray data have been examined and interpreted separately (e.g., Blakely, 1988; Blakely and Jachens, 1991; Duval and Pitkin, 1988), but all three data sets have not been analyzed together.

Statistical techniques have been applied to gamma-ray data (Grant et al., 1978; Newton and Slaney, 1978; Duval, 1976, 1977, 1983; Pirkle et al., 1984; Pires and Harthill, 1989). The results of these studies indicate that statistical grouping of the data aids in the identification of features related to geological processes. These previous studies have used only gamma-ray data and have not included other geophysical information. In this work, we include the gravity and magnetic anomalies in addition to the gamma-ray data in order to test the relationships among them. The Geographical Resource Analysis Support System (GRASS) described

by Lozar (1989), Lozar and Goran (1987), and Hastings (1988) was used.

DATA ANALYSIS

The geophysical data set includes both surface and sub-surface information. The aeroradiometric data reflect near-surface concentrations of potassium (K), equivalent uranium (eU), and equivalent thorium (eTh) (Duval, 1988). Isostatic gravity (Saltus, 1988) and the residual magnetic field (Hildenbrand and Kucks, 1988) reflect mass and magnetization variations throughout the crustal section. All of these data are in the form of regional maps produced by gridding the data to a grid cell size of 1.0 kilometer.

The magnetic data were filtered with a pseudogravity operator (Baranov, 1957) in order to permit more direct comparison with gravity data. The pseudogravity anomaly magnitudes were not rescaled to milligals. The isostatic and pseudogravity data were processed with a terracing operator (Cordell and McCafferty, 1989). The terracing operator produces a field composed of uniform domains separated by

Manuscript received by the Editor August 22, 1991; revised manuscript received October 13, 1992.

*formerly U.S. Dept. of the Interior, Geological Survey, Reston, VA.; presently SOREQ Nuclear Research Center, Israel Atomic Energy Commission, Yavne 70600, Israel.

†U.S. Dept. of the Interior, Geological Survey, MS 927, Reston, VA 22092.

Prepared by an agency of the U.S. government.

abrupt domain boundaries. The resulting map is crudely proportional to a physical-property map although no attempt was made to represent the data as densities. The terracing operation provides an effective means to compare data sets directly.

All the geophysical data were converted to raster cell maps with a cell size of 1.0 sq km. All of the data sets were converted to values of 1-240 using a linear scaling transformation. The minimum data values were set equal to 1 and the maximum values to 240. The effect of these transformations is to standardize the variables to the same range so that Euclidian measures can be used.

Our data analysis method is a multivariate statistical technique which uses a clustering algorithm to define signatures for statistically distinct data classes (groups). This method uses the mean vector and the covariance matrix of groups of data points which are statistically similar to define data signatures (Richards, 1986). The data signatures obtained from the clustering algorithm were used in a classification algorithm to classify the individual pixels within the data set. The clustering algorithm used to define the groups in GRASS is known as an unsupervised clustering method because it does not use predetermined groups and bases all decisions upon statistical criteria.

Nevertheless, we achieved supervised classification by identifying groups of pixels which were consistently grouped together when the clustering parameters (number of initial groups, minimum group separation, percent convergence, and sample size) were changed. A sample size of 2 data cells was used, and the percent convergence was required to be 95 percent. The choice of a sample size of 2 was mandated by the size of the data set and the limitations of the data processing algorithm. Other values (80-98 percent) for the convergence parameter were tried, but the algorithm was not found to be particularly sensitive to this parameter except for the total calculation time. We found that 95-percent convergence produced good results in a reasonable time (less than 30 minutes elapsed time for these data using a 2 MIP workstation). The minimum separation was varied from 0.4 to 0.7 nondimensional units and the number of initial groups from 10 to 30.

After the group signatures were calculated for each of the combinations of parameters, the maximum-likelihood algorithm was used to classify the data. All of the resulting maps were compared to one another to identify pixels which were consistently grouped together. The masking capabilities of GRASS were then used to isolate one particular set of such pixels and the clustering algorithm was used to calculate the signature for that group. Twenty-seven distinct groups were identified. The signatures of these groups were used to calculate the classification map shown in Figure 1. Table 1 lists the 27 groups used, and although the range of numbers used in the analysis was 1-240, the values in the table are given as the corresponding values of the data prior to conversion to GRASS cell maps.

RESULTS

The aeromagnetic map (Hildenbrand and Kucks, 1988) shows a narrow anomaly with a north-northwest trend extending 280 km through north-central Nevada. This fea-

ture, which has been interpreted as a rift zone called the northern Nevada rift (Zoback and Thompson, 1978; Blakely, 1988), is shown schematically in Figure 2 (marked as "Mag"). On the basis of the gravity data, Blakely (1988) drew a line that extended the northern Nevada rift zone considerably farther to the south-southeast, to about 36°N. The trace of the proposed rift zone and the possible extension of it are seen in Figure 1 as the straight line portion of Line 1 which is a linear feature defined by boundaries between different groups. The classification map (Figure 1) also suggests another parallel linear feature about 90 km west of the eastern linear feature (refer to Figures 2 and 3). In the northern part of the state, two approximately linear magnetic anomalies (not indicated in Figure 2) occur near and along the western feature. Blakely (1988) noted that these anomalies are associated with isostatic gravity anomalies, and he identified these as reflecting subparallel rifts.

To emphasize the linear features identified in this study, the classification map was converted into a binary map (Figure 3) showing pixel groups "within the lines" and "outside the lines." The "inside groups" are marked with an asterisk in Table 1. The last column in Table 1 shows the percentage of pixels "inside the lines" for each group. The choice of which groups are "inside groups" was based upon a subjective determination of the groups defining the linear features. The selected groups have 30 percent or more pixels inside the lines, except for group 18, which has only 26.2 percent of its pixels inside the lines. Group 18 was chosen because it is associated with group 20 in the northern part of Nevada (see Figure 1).

On the basis of the gamma-ray data the "inside groups" can be separated into two supergroups: one supergroup (groups 5, 11, and 16) has high concentrations of the radioactive elements and the other has moderate concentrations (groups 12, 18, and 20). All areas of low radioactivity (less than 1.7 percent K, less than 8.5 ppm eTh, and less than 2.3 ppm eU) are associated with groups that are outside of the linear features shown in Figure 2. The magnetic values inside the lines are not high (only low- to medium-range magnetic values are included in the "inside groups"), while areas of high magnetic values are always outside of the lines. The same is true for the gravity data, excepting one group (20) with high gravity values located in the northern part of the State.

Two west-east profiles of the data (A-A' and B-B', in Figure 2) are shown in Figures 4 and 5, respectively. These profiles show the data used for analysis and not the results of the analysis. On profile A-A', the "inside" is characterized by relatively high concentrations of K, eU, and eTh, low gravity values, and medium magnetic values. On profile B-B', indications of the linear features are not as evident as for A-A', but still the radiometric data are high and the gravity and residual magnetic data are low to medium. The linear feature can be seen clearly in profile A-A', but only by the combination of all the data sets can it be detected in the data along profile B-B'. This underscores the fact that the identification of these linear features is dependent upon the combination of all of the geophysical data sets and upon using something other than visual interpretation.

We did perform an analysis of other combinations of the data, for example magnetic and gravity, magnetic and radio-

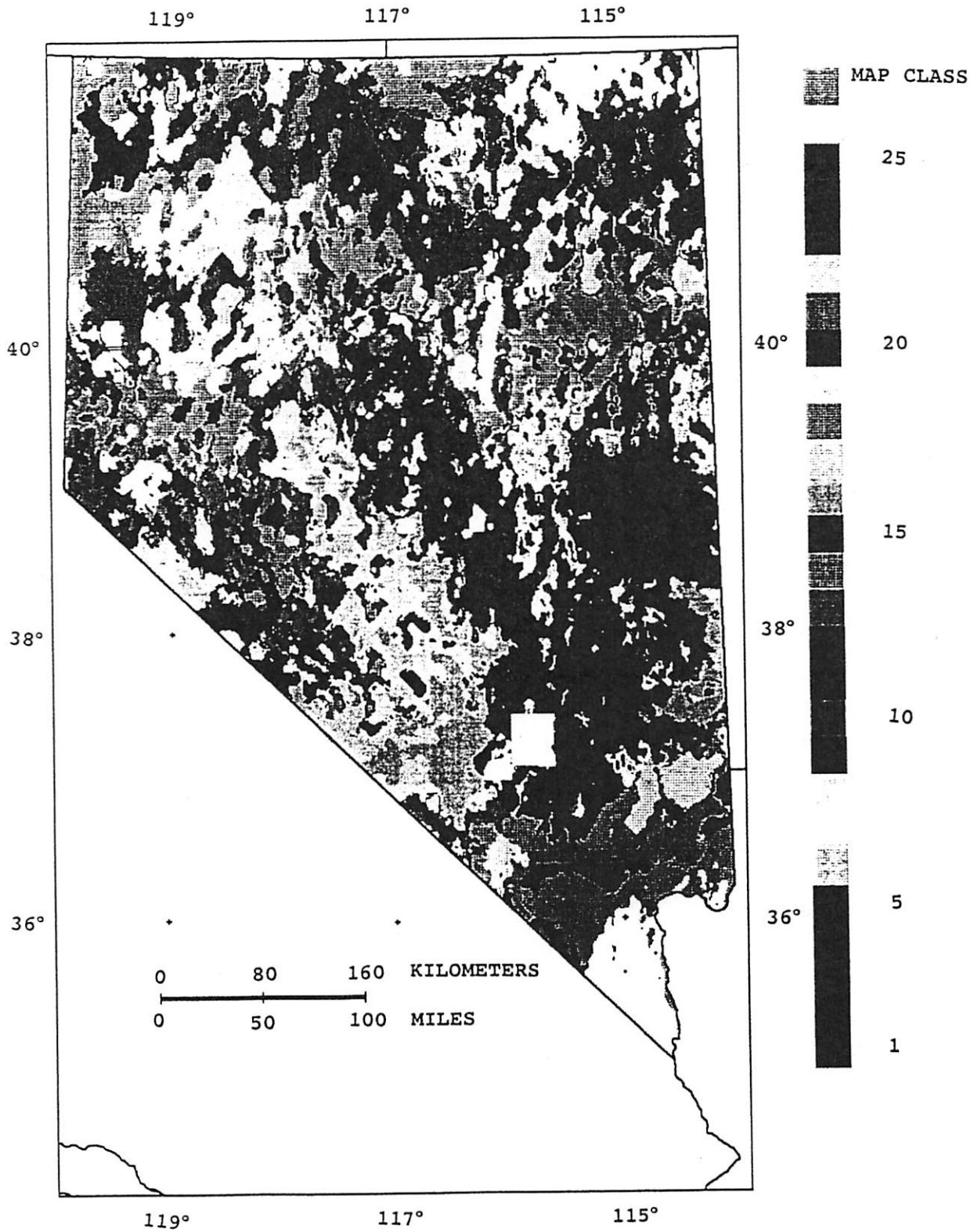


FIG. 1. Map showing the distribution of the 27 statistical groups identified in this study. Map class is the same as the group number listed in Table 1.

metric, gravity and radiometric, and radiometric. In all cases the resulting classification maps showed parts of the linear features seen in Figure 1 but in no instance was the complete feature evident (as shown in Figures 1 and 3).

INTERPRETATION

The Consortium for Continental Reflection Profiling (COCORP) obtained deep seismic reflection data across the central part of Nevada, around latitude 40°N (Hauge et al., 1987; Potter et al., 1987). The eastern linear feature (Figure 2) crosses COCORP line 6 at about vibration point VP-320 as numbered on the stacked profile of the COCORP Seismic Atlas. Potter et al. (1987) showed that near this point there is a change in the density of reflectors (Potter et al., 1987, Figure 2) and that there are some reflectors that dip gently westward at about 13 degrees at a depth of about 13 km. The change in the density of reflectors is a strong feature of the seismic data, and it cannot be explained as a loss of reflected energy caused by attenuation because strong reflectors identified by Potter et al. (1987) as the Moho are present. The western feature crosses COCORP line 3 at about VP-320. Hauge et al. (1987) showed some dipping reflectors around this point, which they assume may be connected to the Golconda Thrust or the Roberts Mountain Thrust. The character of these dipping reflectors suggests the presence of faulting, but the seismic data in the vicinity of VP-320 on line 3 do not suggest any major differences between the subsurface materials to the east and west of this location. Catchings

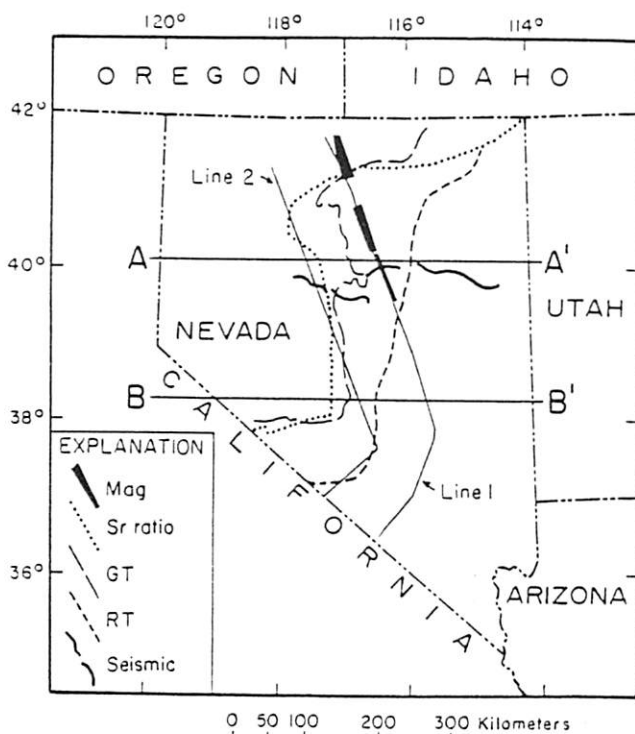


FIG. 2. Some features in Nevada: residual magnetic anomaly (Mag), 0.706 $^{87}\text{Sr}/^{86}\text{Sr}$ ratio line, the parallel features (lines 1 and 2), COCORP seismic lines, Golconda Thrust (GT), Roberts Mountains Thrust (RT), and cross sections A-A' and B-B', which are shown in Figures 4 and 5.

and Mooney (1991) present an interpretation of combined seismic reflection and refraction data which includes a model that shows a deepening of the midcrustal layers (10 to 15 km in depth) in the area of the 0.706 $^{87}\text{Sr}/^{86}\text{Sr}$ contour.

Babaie (1987) used the $^{87}\text{Sr}/^{86}\text{Sr}$ ratio in his research on the Golconda Thrust. The interpretation of the line following the ratio value of 0.706 is that it represents the edge of the North American continent (Armstrong et al., 1977). This line is shown plotted in Figure 2, and it is partially coincident with the western linear feature identified in this study.

We obtained digitized geology (Turner and Bawiec, 1991) based upon the 1:500,000 scale Geologic Map of Nevada (Stewart and Carlson, 1978). The digitized geology was converted to a GRASS cell map with the same cell size as the geophysical data. This conversion process resulted in the omission of geologic units that had a surface area less than about 0.5 sq km. The geologic grid was compared to the classification map (Figure 1) by use of a cell crosscorrelation method. The results of the comparison showed no unique relationship between any one geologic unit and an individual group. Nonetheless, specific areas in the State show a clear relationship between the mapped geology and specific groups.

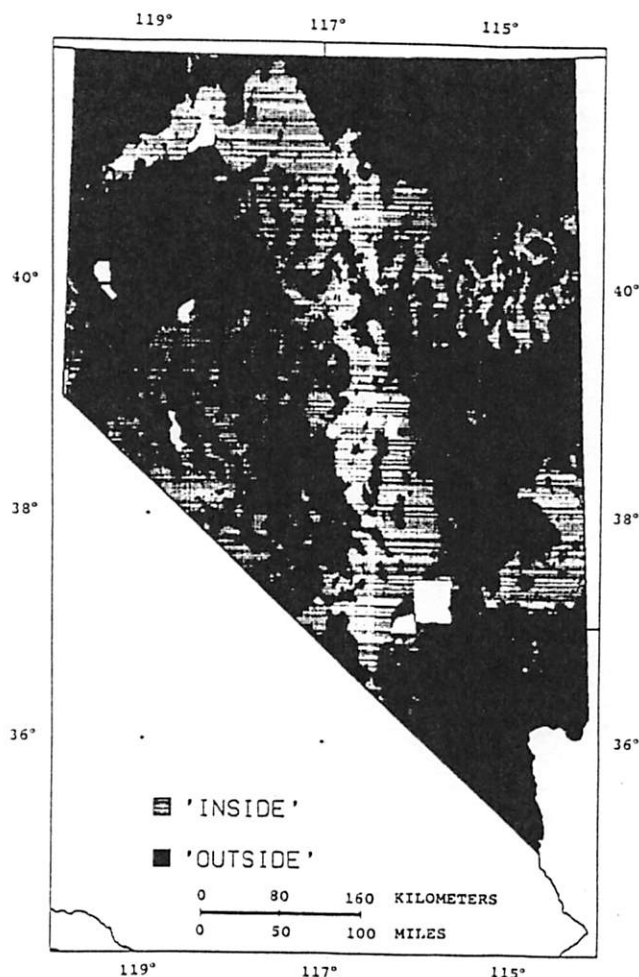


FIG. 3. Binary map showing groups identified as "inside groups" (light gray, refer to Table 1) and "outside groups" (dark gray).

One example of such a relationship is in the southern part of the state. The most southern part of Nevada is classified into 2 groups (26 and 27) both of which have some of the highest magnetic and gravity values present in the data. However, these groups have very different radioelement concentrations. The most southern group (26) has relatively high radioelement concentration, whereas the other (27) has relatively low radioelement concentrations. The areas of higher radioactivity correspond to areas of exposed Precambrian granitoids. The areas of low radioactivity correspond to exposed carbonate rocks and sediments derived from them. The high magnetic and gravity values are associated with the Precambrian rocks, and group 27 shows the extent of these rocks beneath the carbonate rocks. Blank (1988) interpreted the magnetic anomaly associated with group 27 as reflecting the presence of a domal form upwarp of the Precambrian basement.

Groups 26 and 27 are also present in northern Nevada. Group 26 occurs in a large area of northeastern Nevada. In this area the 1:500000-scale geology (Stewart and Carlson, 1978) is predominantly Tertiary silicic ash-flow tuffs, rhyolitic flows, and shallow intrusive rocks. Group 27 occurs in two large areas, one in the northwestern part of the State in the vicinity of the border with Oregon and the other in the north-central part along the border with Oregon and Idaho. In the northwestern area, group 27 is associated with Tertiary basalt flows, and in the north-central area, it is associated with basalt and other volcanic rocks.

Another distinctive pattern seen in Figure 1 is a crescent-shaped pattern along the eastern border of the state near 38°N latitude. This crescent-shaped area is defined primarily by group 16 with an apparent association of groups 5, 9, and 11. In the crescent area of group 16, the primary geologic units are silicic ash-flow tuffs and tuffaceous sedimentary rocks (48 percent), rhyolite flows and shallow intrusive rocks (17 percent), andesite and related rocks of intermediate composition (8 percent), and alluvium (27 percent). Group 16 is characterized by moderate magnetic values (-62.1 nT), low gravity (-17.8 mGal), and relatively high radiometric values (2.8 percent K, 3.7 ppm eU, and 18.7 ppm eTh). Stewart et al. (1977) considered this crescent pattern to be part of a larger east-west pattern of aeromagnetic anomalies related to calc-alkalic volcanic rocks. They interpreted this larger pattern as defining a zone corresponding in part to the Wah Wah-Tushar mineral belt of Hilpert and Roberts (1964). This study does not provide any information relevant to this interpretation, but the crescent pattern shown here is more coherent than the pattern of magnetic highs shown by Stewart et al. (1977).

CONCLUSIONS

Multivariate analysis of magnetic, gravity, and gamma-ray data for Nevada has resulted in the recognition of a linear geophysical trend which has not been recognized by other techniques. Because the major trends of this feature are

Table 1. Data groups, total number of grid cells (pixels) in each group and the statistical means given by the clustering algorithm for the magnetic (pseudogravity filtered data) (nanoteslas, nT), gravity (milligals, mGal), potassium (percent, pct) thorium (parts per million, ppm), and uranium (ppm) data. The last column lists the percentage of the pixels which lie "inside" the linear features drawn in Figure 2. The groups marked by an asterisk are those groups identified as "inside groups."

Group no.	No. pixels	Magnetic (nT)	Gravity (mGal)	K (pct)	Th (ppm)	U (ppm)	Percent "inside"
1	5374	-198.1	-6.9	1.5	9.6	2.4	4.3
2	3375	-196.6	-5.0	2.4	17.7	3.8	20.6
3	6389	-191.5	-14.8	1.5	9.0	2.5	7.2
4	11954	-173.6	-0.5	0.9	4.9	1.6	0.5
5*	3917	-163.0	-9.4	2.6	18.0	3.6	53.9
6	3759	-144.1	0.4	1.6	8.5	2.6	2.7
7	4538	-143.0	-0.5	1.9	10.8	3.0	14.5
8	4498	-141.0	2.4	1.4	7.1	2.1	1.3
9*	5965	-139.8	-14.8	2.6	17.2	3.7	53.9
10	4176	-113.2	-5.6	1.3	6.3	2.0	6.3
11*	4427	-104.8	-16.2	2.5	14.8	3.5	45.0
12*	3366	-87.0	-8.1	1.9	10.1	2.6	30.0
13	5797	-73.5	0.3	2.2	12.1	3.0	16.4
14	4259	-70.5	2.2	1.1	5.5	1.7	18.0
15	5834	-66.5	-0.9	2.6	15.6	3.5	23.5
16*	11685	-62.1	-17.8	2.8	18.7	3.7	54.7
17	7158	-55.5	8.3	1.2	6.3	1.9	12.1
18*	4292	-51.3	-4.1	1.8	8.9	2.4	26.2
19	12121	-42.5	-9.9	2.8	15.8	3.4	18.6
20*	9831	-12.2	6.5	1.8	9.0	2.4	36.3
21	8392	22.1	-6.5	1.0	4.5	1.6	1.9
22	3409	50.7	-2.6	1.9	9.5	2.3	0.3
23	4884	65.9	4.5	1.7	9.4	2.3	0.8
24	5769	66.3	-8.3	1.8	8.3	2.3	0.3
25	7620	80.9	7.8	1.2	6.6	2.1	0.0
26	8316	123.7	0.9	2.4	15.9	3.3	0.6
27	10647	138.1	2.2	1.0	5.2	1.9	0.0

similar to the $^{87}\text{Sr}/^{86}\text{Sr}$ 0.706 contour, the Golconda Thrust, and the Roberts Mountains Thrust, we believe that they are all related. One possible interpretation is that the western edge of the sialic craton has affected the shape of the thrusts by creating a zone of weakness along which the Golconda and Roberts Mountains allochthons broke. However, this relationship seems to break down to the north where the geophysical zone crosses the other features. Part of the eastern edge of the geophysical zone is coincident with the northern Nevada rift and supports the suggestion of Blakely (1988) and Blakely and Jachens (1991) that the rift extends to southern Nevada. Indeed, the geophysical characteristics of the zone identified in this study are somewhat similar to the geophysical characteristics of the Rio Grande rift in New Mexico (Cordell, 1978). In both cases the data show extensive linear features which are several tens of kilometers wide and which are characterized by relatively low gravity and residual magnetic values. The low gravity values suggest the presence of low density materials filling a rift related graben. This geophysical zone, identified using multivariate statistical analysis, suggests that the Nevada rift zone extends to the southern part of the state and suggests a westward expansion of the rift zone to a width of about 90 km. These results also suggest that the southern part of the rift trends to the southwest and may extend into California.

The magnetic and gravity measurements are bulk property measurements, whereas the gamma-ray data reflect the radioelement concentrations in the top few inches of rock or soil. Because the results of this study indicate that the geophysical feature identified could not be identified using gravity and magnetic data alone, the gamma-ray data are correlated with the potential field data. In order to explain this correlation, we postulate that the subsurface processes affecting the potential field data have also affected the near-surface processes which determine the gamma-ray signatures. The mechanisms by which this might occur are not known.

The use of the GRASS GIS programs on geophysical data has proven beneficial. The GRASS system enables the user to work with raster and vector data layers. GRASS is user friendly and versatile. The approach used in this study, to define "training sets," enables the user to identify groups of data which result in well-defined classification signatures even though a priori definitions of the training sets were not possible.

ACKNOWLEDGMENT

We would like to thank Robert M. Turner, Branch of Resource Assessment, U.S. Geological Survey for providing the digitized geology.

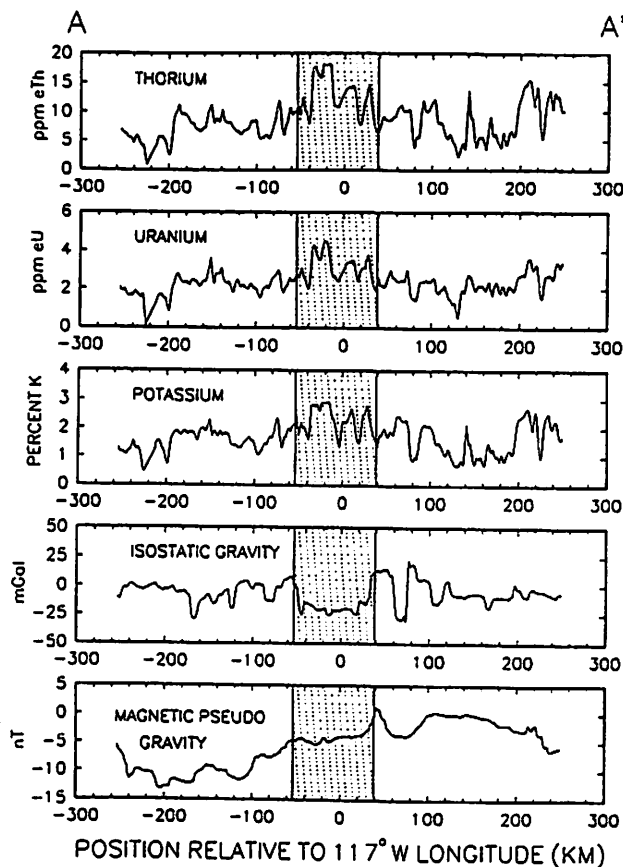


FIG. 4. Stacked profiles of the geophysical data along cross section A-A'. The x-axis is the position relative to 117°W . Shaded area is "inside" lines 1 and 2 in Figure 2.

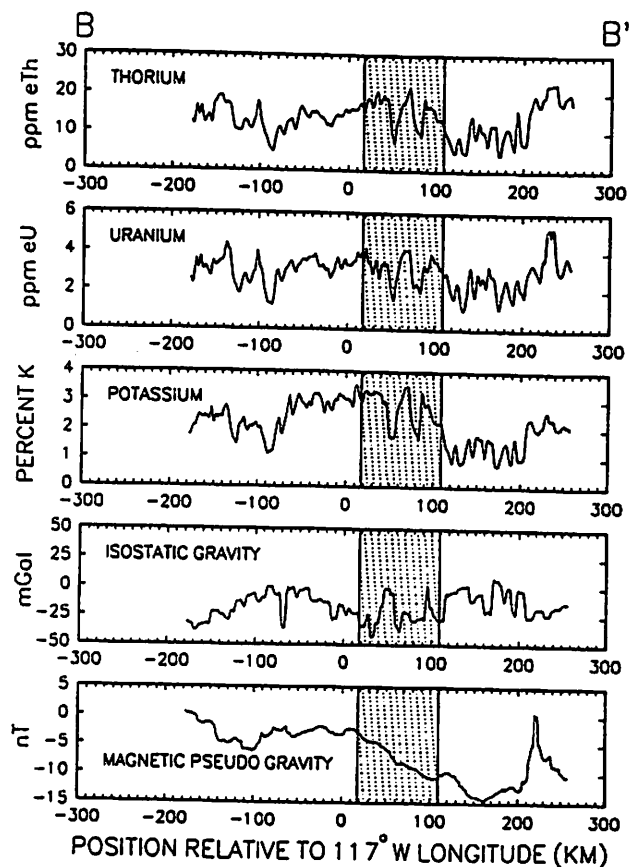


FIG. 5. Stacked profiles of the geophysical data along cross section B-B'. The x-axis is the position relative to 117°W . Shaded area is "inside" lines 1 and 2 in Figure 2.

REFERENCES

- Armstrong, R. L., Taubeneck, W. H., and Hales, P. O., 1977, Rb-Sr and K-Ar geochronometry of Mesozoic granitic rocks and their Sr isotopic composition, Oregon, Washington and Idaho: *Geol. Soc. Am. Bull.*, 88, 397-411.
- Babaie, H. A., 1987, Paleogeographic and tectonic implications of the Golconda allochthon, southern Toiyabe Range, Nevada: *Geol. Soc. Am. Bull.*, 99, 231-243.
- Baranov, V., 1957, A new method for interpretation of aeromagnetic maps: pseudo-gravimetric anomalies: *Geophysics*, 22, 359-383.
- Blakely, R. J., 1988, Curie temperature isotherm analysis and tectonic implications of aeromagnetic data from Nevada: *J. Geophys. Res.*, 93, no. B10, 11817-11832.
- Blakely, R. J., and Jachens, R. C., 1991, Regional study of mineral resources in Nevada: Insights from three-dimensional analysis of gravity and magnetic anomalies: *Geol. Soc. Am. Bull.*, 103, 795-103.
- Blank, H. R., 1988, Basement structure in the Las Vegas region from potential-field data (abs.): Abstracts with Programs, 84th Annual Meeting, Cordilleran Section, *Geol. Soc. Am.*, 20, 144.
- Catchings, R. D., and Mooney, W. D., 1991, Basin and range crustal and uppermost mantle structure, northwest to central Nevada: *J. Geophys. Res.*, 96, no. B4, 6247-6267.
- Cordell, Lindrith, 1978, Regional geophysical setting of the Rio Grande rift: *Geol. Soc. Am. Bull.*, 89, 1073-1090.
- Cordell, Lindrith, and McCafferty, A. E., 1989, A terracing operator for physical property mapping with potential field data: *Geophysics*, 54, 621-634.
- Duval, J. S., 1976, Statistical interpretation of airborne gamma-ray spectrometric data using factor analysis, in *Exploration for Uranium Ore Deposits*, Proceedings: Vienna, Internat. Atom. Energy Agen., 71-80.
- , 1977, High sensitivity gamma-ray spectrometry: State of the art and trial application of factor analysis: *Geophysics*, 42, 549-559.
- , 1983, Composite color images of aerial gamma-ray spectrometric data: *Geophysics*, 48, 722-735.
- , 1988, Aerial gamma-ray contour maps of regional surface concentrations of potassium, uranium and thorium in Nevada: U.S. Geol. Survey Map GP-982, scale 1:750,000.
- Duval, J. S., and Pitkin, J. A., 1988, Interpretation of aerial gamma-ray data for Nevada: U.S. Geol. Survey Open-File Report 88-288.
- Grant, F. S., Misener, D. J., and Johnson, I. M., 1978, The application of pattern recognition algorithm to the interpretation of airborne gamma-ray spectrometer data (abs.): *EOS, Trans., Am. Geophys. Union*, 59, 1031.
- Hastings D., 1988, New public domain GIS coming of age: *Photogrammetric Eng. Remote Sensing*, 54, no. 1, 88-89.
- Hauge, T. A., Allmendinger, R. W., Caruso, C., Hauser, E. C., Klemperer, S. L., Opdyke, S., Potter, C. J., Sanford, W., Brown, L., Kaufman, S., and Oliver, J., 1987, Crustal structure of western Nevada from COCORP deep seismic-reflection data: *Geol. Soc. Am. Bull.*, 98, 320-329.
- Hildenbrand, T. G., and Kucks, R. P., 1988, Filtered magnetic anomaly maps of Nevada: *Nev. Mines and Geol. Map 93B*, scale 1:1,000,000 (4 sheets) and 1:2,000,000 (1 sheet).
- Hilpert, L. S., and Roberts, R. J., 1964, Economic geology, in *Mineral and water resources of Utah*: U.S. Congress, 88th, 2nd Session, Comm. Print, 28-34.
- Lozar, R. C. (editor), 1989, Proceeding of the 1988 Geographical Resource Analysis Support System (GRASS) user group meeting: USACERL Technical Manuscript N-89/18.
- Lozar, R. C., and Goran, W. D., 1987, GRASS for military land use planning: *The Military Engineer*, 516, 468-469.
- Newton, A. R., and Slaney, V. R., 1978, Geological interpretation of an airborne gamma-ray spectrometer survey of the Hearne Lake area, Northwest Territories: *Geol. Surv. Canada Paper* 77-32.
- Pires, A. C. B., and Harthill, N., 1989, Statistical analysis of airborne gamma-ray data for geologic mapping purposes: Crixas-Itapaci area, Goias, Brazil: *Geophysics*, 54, 1326-1332.
- Pirkle, F. L., Howell, J. A., Wecksung, G. W., Duran, B. S., and Stablein, N. K., 1984, An example of cluster analysis applied to a large geological data set: aerial radiometric data from Copper Mountain, Wyoming: *Math. Geology*, 16, 479-498.
- Potter, C. J., Liu, C., Huang, J., Zheng, L., Hauge, T. A., Hauser, E. C., Allmendinger, R. W., Oliver, J. E., Kaufman, S., and Brown, L., 1987, Crustal structure of north-central Nevada: results from COCORP deep seismic profiling: *Geol. Soc. Am. Bull.*, 98, 330-337.
- Richards, J. A., 1986, Remote sensing digital image analysis: Springer-Verlag.
- Saltus, R. W., 1988, Regional, residual, and derivative gravity maps of Nevada: *Nev. Bur. Mines and Geol. Map 94B*, scale 1:750,000.
- Stewart, J. H., and Carlson, J. E., 1978, Geologic map of Nevada: U.S. Geol. Surv., scale 1:500,000.
- Stewart, J. H., Moore, W. J., and Zietz, Isidore, 1977, East-west patterns of Cenozoic igneous rocks, aeromagnetic anomalies, and mineral deposits, Nevada and Utah: *Geol. Soc. Am. Bull.*, 88, 67-77.
- Turner, R. M., and Bawiec, W. J., 1991, Digital geologic coverage of Nevada—a representation of the geologic map of Nevada, 1978: U.S. Geol. Survey Digital Data Series 2.
- Zoback, M. L., and Thompson, G. A., 1978, Basin and range rifting in northern Nevada: Clues from a mid-Miocene rift and its subsequent offsets: *Geology*, 6, 111-116.

The northern Nevada rift: Regional tectono-magmatic relations and middle Miocene stress direction

ARY LOU ZOBACK }
DWIN H. MCKEE } U.S. Geological Survey, 345 Middlefield Road, Menlo Park, California 94025
CHARD J. BLAKELY }
GEORGE A. THOMPSON } Department of Geophysics, Stanford University, Stanford, California 94305

ABSTRACT

As defined by the most recent aeromagnetic surveys, the north-northwest-trending northern Nevada rift zone extends for at least 500 km from southern Nevada to the Oregon-Nevada border. At several places along the rift, the magnetic anomaly is clearly related to north-northwest-trending dikes and flows that, based on new radiometric dating, erupted between 17 and 14 Ma and probably during an even shorter time interval. The tectonic significance of the rift is dramatized by its length, its coincidence in time and space (at its northern terminus) with the oldest silicic volcanic complex along the Yellowstone hot-spot trend, and its parallelism with the subduction zone along the North American coast prior to the establishment of the San Andreas fault.

The northern Nevada rift is also equivalent in age, trend, and composition to feeder dikes that fed the main eruptive pulse (~95% volumetrically) of the Columbia River flood basalts in northern Oregon ~15.5–16.5 Ma. Because of these similarities, both regions are considered to be part of an enormous lithospheric rift that propagated rapidly south-southeast and north-northwest, respectively, from a central mantle plume. The site of the initial breaching of the North America plate by this plume is probably the McDermitt volcanic center at the northern end of the rift near the Oregon-Nevada border. The present north-northwest trend of the rift and its internal elements, such as dikes and lava-filled grabens, record the orientation of the arc-normal extensional stress in this back-arc region at the time of emplacement. Aeromagnetic evidence presented by others has been interpreted to indicate block rotations at these sample localities is not consistent with either a rotation of dikes within the rift or with regional rotation of the entire rift. The

present north-northwest trend of the rift reflects the state of stress in the Basin and Range during middle Miocene time and is consistent with stress indicators of similar age throughout the Basin and Range and Rio Grande rift provinces.

INTRODUCTION

The northern Nevada rift, prominently expressed in aeromagnetic maps, is a middle Miocene alignment of basaltic (and some rhyolitic) dikes and associated graben-filling lava flows that we believe is a significant key to tectono-magmatic processes throughout a broad region (Zoback and Thompson, 1978) (Fig. 1). The rift originated at the same time the Yellowstone mantle plume broke through the North American lithosphere and fed the Columbia River flood basalts. As shown in Figure 1, feeder dikes of the Columbia River basalts have the same north-northwest trend as the rift, and both are interpreted as superb mid-Miocene stress indicators related to extension in a direction perpendicular to the then-active subduction zone along the western margin. This subduction zone was gradually replaced by the San Andreas fault as the Mendocino triple junction progressed northward (Atwater, 1970, 1989). As the San Andreas transform lengthened, a new Basin and Range opening direction ensued in the Great Basin, rotated about 50° clockwise from the previous opening direction (Zoback and Thompson, 1978; Zoback and others, 1981). This change probably occurred between 10 and 6 Ma based on crosscutting fault relationships and timing of inception of modern basins (Anderson and Ekren, 1977; Stewart, 1978; Zoback and others, 1981). The modern direction of least principal stress is between N60°–70°W (Zoback and Zoback, 1980; Zoback, 1989). As the timing of this change

coincides generally with growth of the San Andreas transform system, the clockwise change in stress tensor orientation has been attributed to the superposition of broad-scale right-lateral lithospheric shear along the western plate boundary. Beyond the influence of the San Andreas system, north of the Snake River plain in northeastern Nevada and Idaho, the earlier direction of extension (which is generally perpendicular to the modern regional topographic bulge) is still dominant (for example, Stickney and Bartholomew, 1987).

Our present objective is to marshal and interpret recent data from the northern Nevada rift, including (1) aeromagnetic data showing the full extent of the rift, (2) detailed geologic maps of the dikes in two ranges where they are extensively exposed, (3) improved radiometric dating, and (4) data on the deformational history of the rift after its formation. These data provide a foundation for reassessing tectonic events in light of recent research on mantle plumes. We also want to reaffirm our earlier interpretation of the northern Nevada rift as an indication of mid-Miocene stress direction (Zoback and Thompson, 1978), an interpretation that has recently been called into question. Li and others (1990) suggested, on the basis of paleomagnetic data, that blocks "comparable to or smaller than the width of the rift" have been tectonically rotated about 19° counterclockwise and that this rotation should be applied as a correction to the pre-rotation stress direction. Although small blocks within or adjacent to the normal-oblique fault zones may have been rotated, this interpretation is not viable on a larger scale because the dike swarms within the rift are precisely parallel to the 500-km-long rift trend as defined by aeromagnetic anomalies. Thus the individual dikes, the dike swarms, and the entire rift

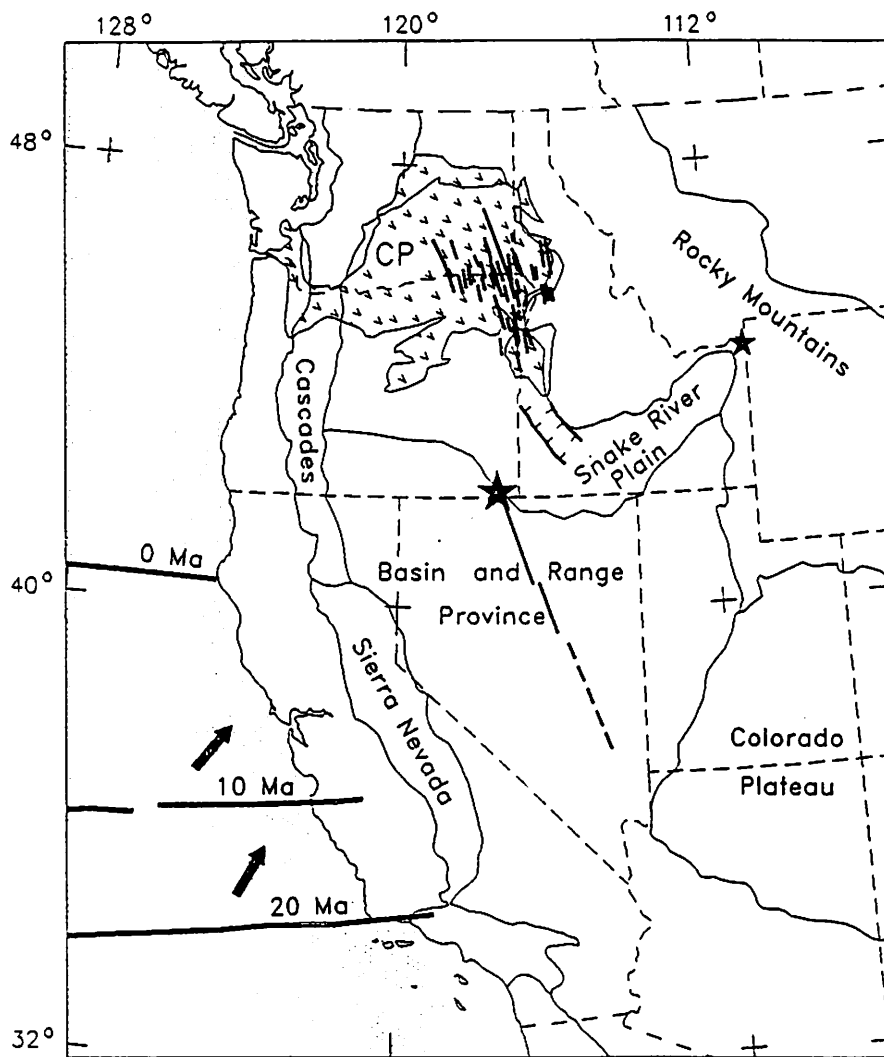


Figure 1. Middle Miocene igneous and tectonic features in the western United States. Main part of north-northwest-trending northern Nevada rift is shown by heavy dark lines; southern extension is interpreted from aeromagnetic data indicated by dashed line. The left-stepping offset of the central part of the rift is diagrammatic and representative of cumulative offset on several cross faults (Table 2). The left step and gap separating the southern segment from the main part of the rift is real and inferred directly from the aeromagnetic data shown in Figure 2B. The large star at north end of rift indicates McDermitt caldera, the middle Miocene location of the Yellowstone hot spot; current position of hot spot is indicated by small star. The Columbia River Basalt Group is shown by checked pattern; feeder dikes in eastern Oregon and Washington are indicated by heavy lines. Western graben of the Snake River Plain is shown by hachured lines. East-west lines along coast give approximate location of the Mendocino triple junction at the different ages indicated (Atwater, 1989); heavy arrows indicate convergence direction of Juan de Fuca plate relative to North America corresponding to the adjacent times (Stock and Molnar, 1988). CP = Colorado Plateau.

all yield the same mid-Miocene stress direction.

NORTHERN NEVADA RIFT

The northern Nevada rift (Fig. 1) can be traced magnetically for at least 500 km south-

ward from the Oregon border to southern Nevada (McKee and Noble, 1986; Blakely and Jachens, 1991). Basaltic rocks that define the rift are middle Miocene, about the same age as the silicic McDermitt volcanic center (Rytuba and McKee, 1984), which is located at the north end of the rift in the emergence area

of the Yellowstone hot spot (for example, Pierce and Morgan, 1992). From this focal area the hot spot tracked northeastward to its present position at Yellowstone, forming the eastern Snake River Plain in its wake (Morgan, 1972).

As originally described on the basis of aeromagnetic anomalies, the northern Nevada rift extends north-northwest from about Eureka, Nevada (point A, Fig. 2A), to approximately the Oregon-Nevada border (point B, Fig. 2A). Philbin and others (1963) first described this north-northwest-trending aeromagnetic anomaly, and Roberts (1966) noted its trend in the context of northwest alignments of mineral deposits, which he considered to be mineral belts. Mabey (1966) and Robinson (1970) described the anomaly and expanded on the interpretation that the aeromagnetic pattern is caused by basaltic rocks concentrated in a deep, narrow zone. Stewart and others (1975) considered the anomaly to be the southern segment of a lineament across Oregon and Nevada; they noted that many of the volcanic rocks that lie on or near the lineament are middle Miocene in age. They considered the Oregon segment of the lineament to be the Brothers fault zone, a series of linear features seen on air photos trending northwest across Oregon, whereas they considered the Nevada segment to have formed within a deep-seated extensional system. Zoback and Thompson (1978) named the then-known 250-km-long Nevada segment the *northern Nevada rift* and used it to determine the middle Miocene least principal stress direction. Rather than tying the rift into the Brothers fault zone, Zoback and Thompson linked its formation to a much more extensive zone of rifting of the lithosphere that included similarly oriented feeder dikes of the Columbia Plateau flood basalts and the middle Miocene location of the Yellowstone hot spot. The north-northwest trend of the rift and the feeder dikes for the contemporaneous major pulse of Columbia River flood-basalt volcanism is consistent with geologic evidence throughout the Basin and Range and Rio Grande rift that supports a Miocene least principal stress direction perpendicular to this north-northwest trend (Zoback and others, 1981; Rehrig and Heidrick, 1976; Lipman, 1981; Henry and Price, 1986).

From analysis of low-altitude (National Uranium Resource Evaluation [NURE]) aeromagnetic profiles, Blakely and Jachens (1991) suggested that the magnetic anomaly associated with the rift extends much farther to the south-southeast than previously recognized, to at least latitude 38°N and perhaps to

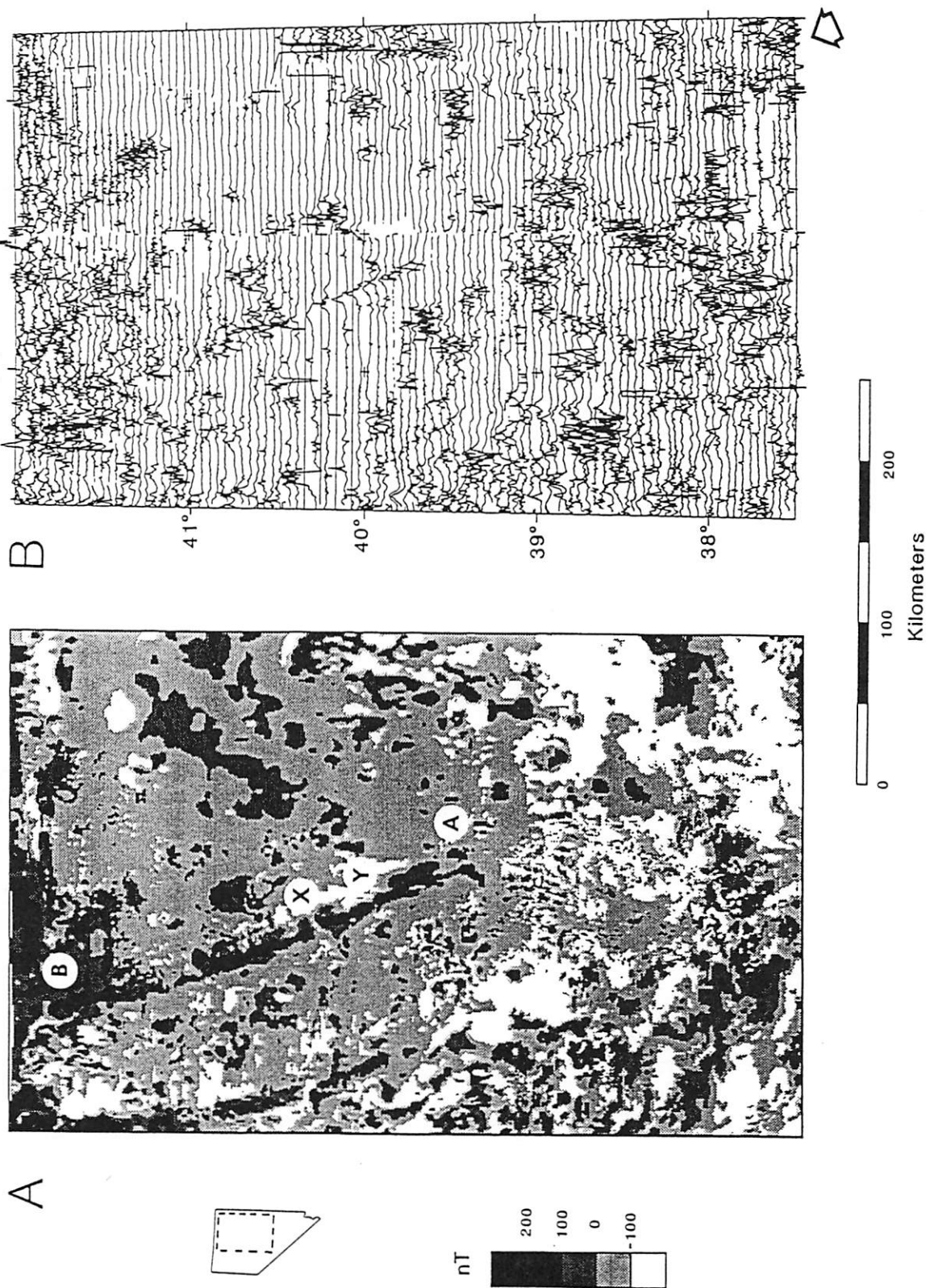


Figure 2. Magnetic anomalies over the northern Nevada rift. A. Aeromagnetic compilation modified from Hildenbrand and Kucks (1988). Points A and B indicate approximate ends of the anomaly caused by the northern Nevada rift; X and Y indicate regions of left-lateral offsets of the rift (better shown in B). B. Aeromagnetic profiles from the National Uranium Resource Evaluation (NURE). Arrows indicate the position of the northern Nevada rift as inferred from these magnetic data.

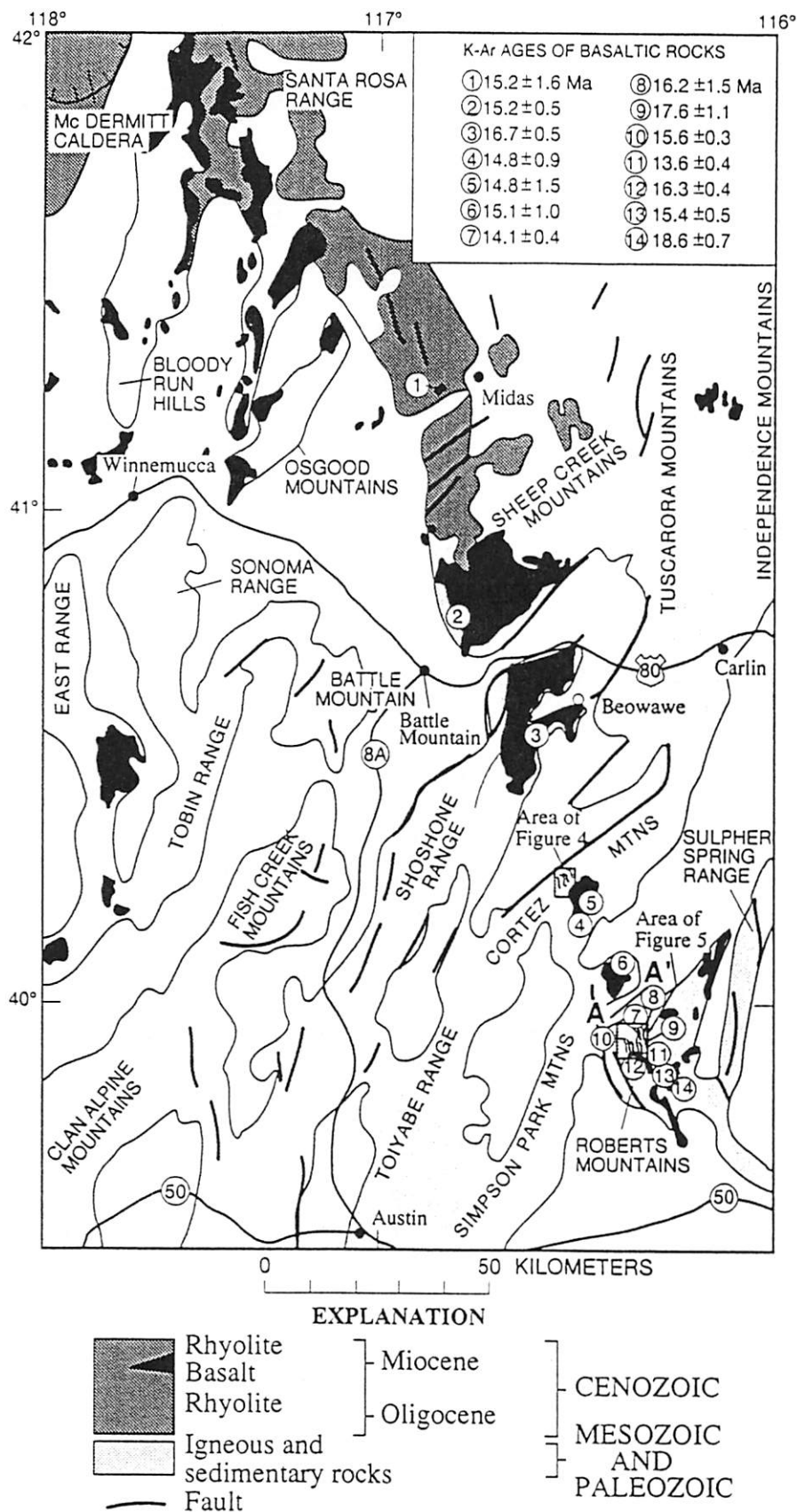


Figure 3. Generalized geologic map of north-central Nevada showing the distribution of middle Miocene igneous rocks associated with the aeromagnetic anomaly and the northern Nevada rift. Location of samples of basalt for isotopic age determinations noted by number. Section line A-A' gives location of gravity and magnetic profile shown in Figure 7.

latitude 37°N (Fig. 2B), resulting in a total length in Nevada of at least 500 km. Parallel magnetic anomalies west of the northern Nevada rift may have a similar source but lack the associated basaltic dikes in outcrop (McKee and Blakely, 1990).

Geologically, the northern Nevada rift may be divided into northern, central, and southern segments. Each segment displays characteristic features.

Northern Segment

The northern part of the rift, from the Oregon-Nevada border to Midas, Nevada (Fig. 3), crosses a broad tableland capped by rhyolites and basalt, tuffaceous sedimentary rocks, and gravel of late Miocene age. Along the southern part of the northern segment of the rift in more mountainous terrain, middle Miocene rhyolitic dikes, domes, and flows with some interfingering basaltic andesite and basalt flows seem to coincide with the aeromagnetic anomaly. Several large north-northwest-trending feeder dikes for the rhyolite exposed in the Midas region (Zoback and Thompson, 1978) lie along the aeromagnetic anomaly; basaltic flows underlie the rhyolite. The northern part of the northern segment, north of latitude 41°30'N, is defined solely on the basis of the aeromagnetic high.

Central Segment

The central part of the rift from Midas to the southern edge of the Roberts Mountains (Fig. 3) is characterized by middle Miocene trachybasalt flows, which generally lie on Paleozoic bedrock. Minor rhyolite flows and domes are locally associated with the trachybasalt. Locally the aggregate thickness of these mafic flows exceeds 1 km (Beowawe region, Fig. 3), but most exposures are generally <300 m thick. North-northwest-trending basalt and trachybasalt dike swarms are well exposed in two ranges in the southern part of the central segment of the rift, the Cortez Mountains (Figs. 3 and 4) and the Roberts Mountains (Figs. 3 and 5), where they structurally underlie remnants of the basalt flows. Individual dikes in the Cortez Mountains are as much as 5 km long and range in width from 3 m to as much as 250 m where they join, although the average is <10 m (Fig. 4) (Gilluly and Masursky, 1965; Gilluly and Gates, 1965). The overall width of the swarm exposed in the Cortez Range is about 6 km; however, the main zone of intrusion, as indicated by the region of the largest and most continuous dikes, is only about 3 km wide.

Southern Segment

The southern segment of the rift, south of latitude $39^{\circ}30'N$, has little surface volcanic or intrusive expression and is defined almost entirely on the basis of low-altitude aeromagnetic profiles (Blakely and Jachens, 1991), confirmed in a few places by ground magnetic traverses. Although basaltic dikes do not crop out along this segment of the rift, magnetic anomalies indicate that magnetic (presumably mafic intrusive) rocks extend from depth to very near the topographic surface. A few exposures of basaltic flows, presumably of middle Miocene age, are located beneath the linear magnetic anomaly south of latitude $39^{\circ}30'N$, notably in the White River Valley south of the town of Lund; these exposures may be related to the southern segment of the northern Nevada rift. In the southern segment, the anomaly decays in amplitude, loses continuity, and appears to be offset left-laterally at about latitude $39^{\circ}30'N$ (Fig. 2B).

Composition of Basaltic Rocks along the Rift

The rocks that cause the strong aeromagnetic anomaly defining the northern Nevada rift are basaltic in character. Most are trachybasalts to trachyandesites (Le Maitre, 1984) with SiO_2 content around 50 wt% but some as high as 59 wt% (Gilluly and Gates, 1965; Stewart and McKee, 1977). Others are olivine-bearing basalt with SiO_2 content of about 48 wt% and total alkalis of <5 wt% (McKee and Mark, 1971). In the Roberts Mountains, dikes and flows of both basaltic types occur together and yield overlapping K-Ar ages (see, for example, numbers 8 and 9, Table 1).

North of the northern Nevada rift in eastern Oregon, middle Miocene (~15 Ma) basaltic rocks from the eastern Oregon volcanic plateaus province show a wide variation in silica, aluminum, and potassium content (Carlson and Hart, 1987). The eastern Oregon basalts are generally less alkalic than basaltic rocks from the northern Nevada rift region, and the relative amounts of high-silica versus lower silica types are opposite in these two regions, but the overall range in variation is comparable.

The Columbia River Basalt Group exhibits subtle differences in composition as compared to most basaltic rocks to the south both in the eastern Oregon volcanic plateaus and the northern Nevada rift. Trachyandesite and trachybasalt are rare in the Columbia River Basalt Group (Swanson and others, 1979); most of the Columbia River basalts are less alkalic, more iron rich, and average several

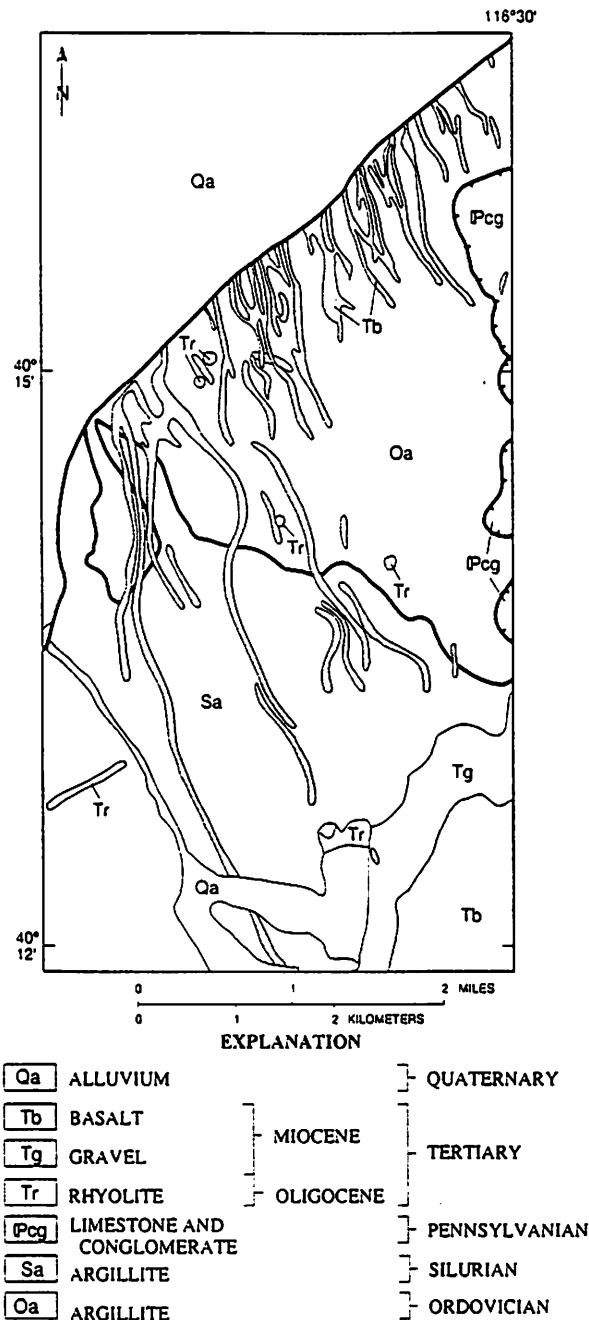


Figure 4. Mapped middle Miocene basaltic dike swarm in the Cortez Mountains. Note that the average trend of the dikes is about $N22^{\circ}W$, the same as dikes in the Roberts Mountains (Fig. 5) and as the northern Nevada rift as a whole. Map modified from Gilluly and Masursky (1965) and Muffler (1964).

The strike of the zone of dike intrusion is $N23^{\circ}W = 2^{\circ}$.

A spectacular north-northwest-trending basaltic dike swarm is exposed in the Roberts Mountains (McKee, 1986; Fig. 5; cover of this volume). Here the dikes intrude lower Paleozoic limestone and dolomite. Many of the dikes are fine grained and commonly exhibit an ophitic texture. As shown in Figure 5, the main zone of dikes is exposed for a length of nearly 10 km with a consistent $N22^{\circ}W$ trend despite the obvious structural complex-

ity in the range. This complexity is partly associated with west-to-east thrusting during the Devonian to Mississippian Antler orogeny along the Roberts Mountains thrust and later high-angle and low-angle faulting in Mesozoic time (Winterer, 1968). The overall width of the zone of dike exposures in the Roberts Mountains is about 6 km; however, the main zone of intrusion is only about 2 km wide. Average dike width is on the order of 10–25 m, although some individual dikes are >150 m wide.

TABLE 1. K-Ar AGES OF BASALTIC ROCKS (DIKES AND FLOWS) FROM NORTH TO SOUTH ALONG THE CENTRAL NEVADA MAGNETIC ANOMALY

No. of figures	General location	Occurrence (material dated, w.r. = whole rock)	K ₂ O (wt%)	⁴⁰ Ar* (mol/g)	% ⁴⁰ Ar*	Age in m.y. ±σ	Reference
1	N. side Midas Canyon	lava flow (w.r.)	0.884	1.9369 × 10 ⁻¹¹	17	15.2 ± 1.6	Wallace and others, 1990
2	Southern Sheep Creek Range	lava flow (w.r.)	0.733	1.6120 × 10 ⁻¹¹	36	15.2 ± 0.5	McKee and Silberman, 1970
3	N.E. Shoshone Range	lava flow (w.r.)	1.575	3.8087 × 10 ⁻¹¹	43	16.7 ± 0.5	McKee and Silberman, 1970
4	E. side Cortez Mountains	lava flow (plagioclase)	0.295	0.713 × 10 ⁻¹¹	19	16.7 ± 0.9	Wells and others, 1971
5	S.E. Cortez Mountains	lava flow (w.r.)	1.56	3.3465 × 10 ⁻¹¹	19	14.8 ± 1.5	Armstrong, 1970
6	N. Simpson Park Range	lava flow (w.r.)	1.44	3.1502 × 10 ⁻¹¹	16	15.1 ± 1.0	Armstrong, 1970
7	N. Roberts Mountains	dike (w.r.)	1.385	2.8281 × 10 ⁻¹¹	28	14.1 ± 0.4	
8	N. Roberts Mountains	dike (w.r.)	2.360	5.4569 × 10 ⁻¹¹	6.2	16.2 ± 1.5	
9	N. Roberts Mountains	dike (w.r.)	0.358	9.1091 × 10 ⁻¹²	13	17.6 ± 1.1	
10	N. Roberts Mountains	dike (w.r.)	1.161	2.6192 × 10 ⁻¹¹	51	15.6 ± 0.3	
11	Central Roberts Mountains	lava flow (w.r.)	1.661	3.2745 × 10 ⁻¹¹	42	13.6 ± 0.4	
12	Central Roberts Mountains	lava flow (w.r.)	1.948	4.6043 × 10 ⁻¹¹	50	16.3 ± 0.4	
13	S. Roberts Mountains	lava flow (w.r.)	1.760	3.9224 × 10 ⁻¹¹	24	15.4 ± 0.5	
14	S. Roberts Mountains	lava flow (w.r.)	1.725	4.6506 × 10 ⁻¹¹	34	18.6 ± 0.7	

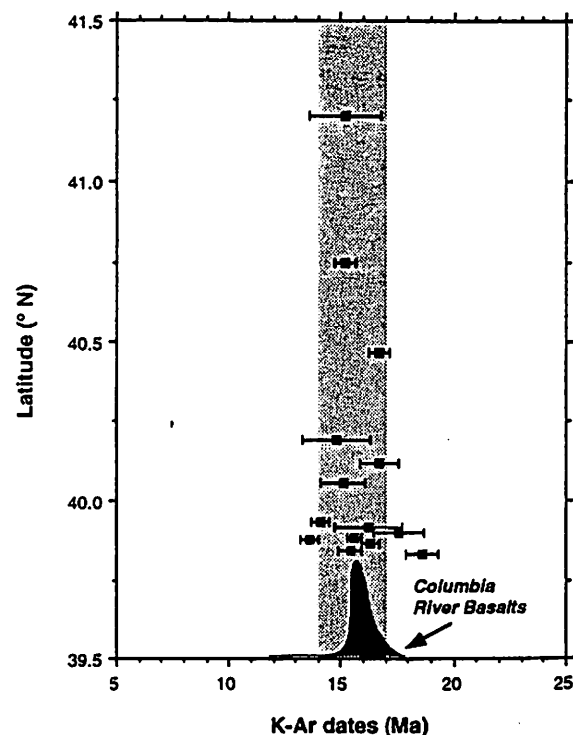
Constants used: $\lambda_e + \lambda_{\beta} = 0.581 \times 10^{-10} \text{ yr}^{-1}$; $\lambda_{\beta} = 4.962 \times 10^{-10} \text{ yr}^{-1}$; $^{40}\text{K}/\text{K}_{\text{tot}} = 1.167 \times 10^{-4} \text{ mol/mol}$.

percent more SiO₂ (Hooper, 1988) than does basalt from eastern Oregon and northern Nevada rift regions. The northern Nevada rift basaltic rocks are somewhat alkalic and of relatively small volume, the Oregon volcanic plateaus are characterized by more voluminous and less alkalic basalts, and the Columbia River basalts, by extremely voluminous high-alumina olivine tholeiitic basalt. These tholeiites exhibit trace-element characteristics, in particular high concentration of Ba and low Cs, Rb, and K, that suggest a mid-ocean-ridge basalt type of mantle source. The other basalts, with their wide variation in major- and trace-element composition, including the sensitive source indicator elements, suggest that varying amounts of crustal contamination and/or differentiation have taken place as the mantle-derived basalts ascended to the surface. It is clear that in middle Miocene time a very large volume of mafic magma was emplaced beneath the western United States from the Columbia Plateau region in the north to the northern Great Basin in the south. We believe that these magmas were produced from a single mantle plume and experienced differentiation and varying crustal contamination during ascent (see also Pierce and Morgan, 1992). Thompson and Gibbs (1991) have also associated Columbia River basaltic volcanism with emergence of a mantle plume near the Oregon-Nevada-Idaho border.

Age of Basaltic Rocks along the Rift

Fourteen samples of basaltic rocks from the central part of the rift between Midas and the Roberts Mountains, a distance of about 150 km, have been dated by K-Ar methods

Figure 6. Plot of the K-Ar ages of the basaltic rocks along the northern Nevada rift. Note the age range is middle Miocene, between 17 and 14 Ma, indicated by the shaded zone. This age range overlaps the 17.2 to 15.5 Ma time interval of the eruption of 90%–95% of the Columbia River Basalt Group, indicated by volume versus time curve at the bottom of the figure after McKee and others (1977) and Baksi (1988).



(Table 1; Figs. 3 and 6). Ten samples are from lava flows and four are from dikes. Dates range from 18.6 ± 0.7 to 13.6 ± 0.4 Ma with most values falling between about 14 to 17 Ma (Fig. 6). The uncertainties in these dates preclude determination of the time span of emplacement; it could be nearly instantaneous, or it could be as great as 5–6 m.y. Geologic relationships such as crosscutting contacts do not improve this resolution. The 14 dates clearly indicate that most of the basaltic volcanism along the rift took place in the middle Miocene in the interval from 17 to 14 Ma and perhaps as short as 16 to 15 Ma. This age interval is one of widespread igneous activity throughout the northern Great Basin, eastern Oregon volcanic plateaus, and the Columbia Plateau as shown in Figure 6, which emphasizes the synchronicity of the main pulse of basaltic activity on the Columbia Plateau (~95% of the voluminous flood basalts erupted in this time interval; Hooper, 1988; Baksi, 1988) and mafic activity to the south, including the basaltic rocks that define the northern Nevada rift.

Aeromagnetic Anomaly along the Rift

The amplitude and areal extent of the central segment of the aeromagnetic anomaly requires deep-seated magnetic sources in addition to surface volcanic rocks (Robinson, 1970). Although flows at the surface yield

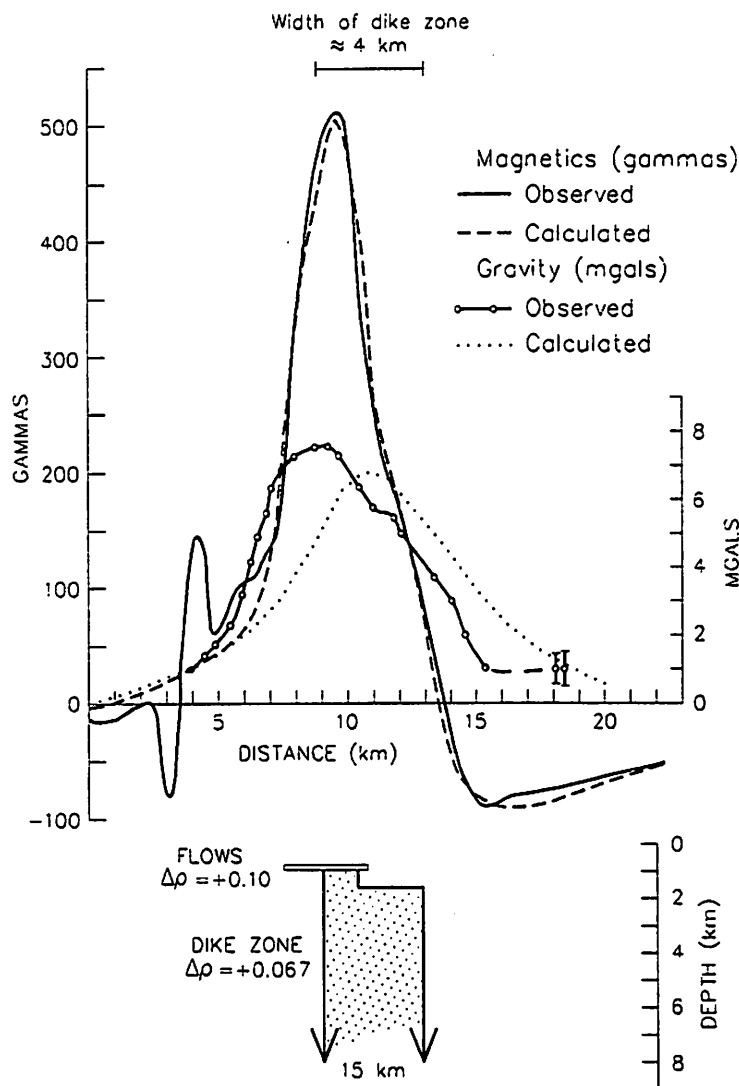


Figure 7. Ground gravity and magnetic data collected along a profile perpendicular to the rift in Horse Creek Valley (profile A-A', Fig. 3). The calculated two-dimensional magnetic model based on near-surface flows and an underlying dike zone (see text for details of model) fits the observed magnetic data quite well. Predicted gravity based on the same model (using measured densities and assuming the dike zone is composed of 33% dike rock, see text) generally matches the overall shape and amplitude of the observed gravity values but is shifted to the east, suggesting that at least part of the observed gravity anomaly is due to lateral variations in basement lithologies and densities.

normal, reversed, as well as transitional field directions (Zoback, 1978; Li and others, 1990), the marked throughgoing positive aeromagnetic anomaly indicates that the bulk of the magnetization must be induced. Modeling of both airborne and ground magnetic profiles across the well-defined central segment of the rift magnetic anomaly suggests that the primary source of the anomaly is a 3.0- to 5.5-km-wide zone of magnetic material that extends from the surface to depths of around 10–15 km (Zoback, 1978). The inferred "base" of the magnetic material gen-

erally coincides with the inferred depth to the Curie-temperature isotherm in this region (Blakely, 1988). On the basis of the exposed geologic relations, this deep magnetic zone is interpreted to be a zone of dike intrusion extending nearly vertically through the crust and feeding the basaltic andesite flows (Zoback, 1978).

Magnetic models of the southern part of the anomaly, south of latitude 39°30'N, also indicate narrow, deeply projecting, vertical magnetic sources suggestive of dike intrusion. Based on models of low-altitude mag-

netic profiles, the magnetic part of the rift in the southern section has a cross-sectional structure similar to, but somewhat smaller than, the northern parts of the anomaly. In particular, magnetic sources associated with the rift are located very near the present-day topographic surface, project to at least 6-km depth, and are generally <4 km wide (Blakely and others, 1989).

Other Geophysical Expression

A single, well-sampled ground gravity profile across the rift in Horse Creek Valley (A-A' on Fig. 3) indicates a gravity high spatially associated with the magnetic high (Fig. 7). In this region, the main dike zone is overlain by a thin series of basaltic andesite flows. Calculated gravity and magnetic anomalies are also shown in Figure 7 based on a model that fits both the ground magnetic and aeromagnetic data (measured remanent direction and magnetic intensity were used for the flows, and a susceptibility of $k = 0.0027$ emu [0.034 SI units] was used for the dike zone, which extends to about 15-km depth). Predicted gravity values derived from this magnetic model are based on the assumption that one-third of the main zone of intrusion is occupied by dikes, and hence the estimated density contrast is correspondingly divided by three. The densities used in the model were based on measurements of field samples: 2.65 g/cm³ for the Paleozoic sedimentary rocks, which are dominantly siliciclastic (from Mabey, 1965); 2.75 g/cm³ for the basaltic andesite (from the Cortez Range); and 2.85 g/cm³ for the dike rock (both values from Zoback, 1978). These densities resulted in a +0.1 g/cm³ density contrast between the flows and the Paleozoic rocks and a +0.067 g/cm³ (0.20/3) density contrast for the underlying dike zone. Between 6- and 12-km depth, this density contrast was decreased to +0.05 g/cm³, and below 12-km depth, because of the general increase in density with depth of crustal rocks (for example, Catchings, 1992), the density contrast was assumed to be zero.

The calculated gravity anomaly is centered over the magnetic body, as expected; however, the observed gravity anomaly is shifted to the west. This westward shift suggests that at least part of the observed gravity anomaly may be due to lateral variations in basement rocks and densities (possibly related to the previously mentioned Roberts Mountains thrust). Alternately, a body centered beneath the observed gravity high could be consistent with the magnetic anomaly if the overall magnetization vector was oriented about due

west. This magnetization direction predicts a slightly differently shaped magnetic anomaly, however, and was not observed in any of the paleomagnetic investigations of the dikes or flows along the rift (Zoback, 1978). Furthermore, a 4-km westward shift of the ~4-km-wide magnetic body would result in the source of the magnetic anomaly being significantly offset from the exposed dike swarms, rather than lying directly beneath them. For these reasons, we believe that the observed gravity anomaly is not entirely due to the dike zone. The observed gravity data do limit the maximum gravity signature associated with the magnetically inferred dike zone to be <5 mGal. Clearly, a dike zone consisting of 100% dike rock would create very large gravity anomalies, between 15 and 20 mGal, which are not observed here or anywhere else along the trend. Thus, probably no more than 25%–30% of the zone of intrusion is occupied by dikes.

Seismic reflection profiles across the rift at about latitude 40°N (Allmendinger and others, 1987; Potter and others, 1987) indicate a well-developed zone of subhorizontal layering in the middle and lower crust (between depths of about 18 to 35 km). Lower crustal layering was pervasive on the entire Basin and Range COCORP seismic reflection transect (Allmendinger and others, 1987); however, this layering apparently was best developed and thickest directly beneath the northern Nevada rift and in a zone extending 25 km to the west-southwest (Potter and others, 1987). Potter and others (1987) suggested that this strongly layered fabric might be produced by intrusions related to the rift. Holbrook and others (1991) attributed the subhorizontal reflections in this area to both sill-like mafic intrusions and ductile shearing.

We note that this zone of subhorizontal layering closely coincides with a regional gradient in residual gravity anomalies. This correlation is best seen in maps showing "basement gravity" (Jachens and Moring, 1990). Such maps are constructed by first eliminating the gravitational effects of long-wave-length topography (Simpson and others, 1986) and then eliminating the gravitational effects of low-density materials in the basins. When applied to the entire state of Nevada, this analysis shows a north-northwest-trending gravity gradient lying parallel to and centered about 10 km west of the northern Nevada rift between latitudes 41°N and 39°30'N (Blakely and Jachens, 1991), generally coinciding with the zone of well-developed subhorizontal layering in the middle and lower

crust interpreted by Potter and others (1987). We suggest that both the gravity gradient and the seismic layering may represent a broad zone of intrusion and extension in the middle and lower crust related to middle Miocene rifting, significantly broader than the magnetic and geologic expression of the rift. Therefore, the rift, as represented by magnetic anomalies and geologic mapping, may be simply the upper crustal part of a deeper and broader zone of crustal extension and magmatic intrusion.

Offsets and Extension

The consistent N20°–25°W trend of the magnetic anomaly, of the exposed basaltic feeder dike swarms, and of the structural troughs that were filled by basaltic flows indicate an extensional origin for the northern Nevada rift. The consistent trend of all these features suggests that the rift did not exploit a pre-existing feature but instead responded to the prevailing least principal stress at the time of formation, horizontal and oriented N65°–70°E (Zoback and Thompson, 1978; Christiansen and McKee, 1978). As described in the introduction, some time after formation of the rift (between ~10 and 6 Ma) there was a clockwise change in the least principal stress orientation throughout the northern Basin and Range, which has been attributed to the superposition of broad-scale right-lateral lithospheric shear along the western plate boundary (Zoback and Thompson, 1978). The modern direction of least principal stress is between N60°–70°W (Zoback and Zoback, 1980; Zoback, 1989).

In the vicinity of the northern Nevada rift the typical north-northeast-trending range and basin blocks of the northern Basin and Range province are largely replaced by complementary north-northwest and east-northeast trends. The modern direction of least principal stress is oriented approximately perpendicular to the typical north-northeast ranges and the bounding normal faults have nearly pure dip-slip displacements (Zoback and Zoback, 1980; Zoback, 1989). Of the typical north-northeast-trending basins judged on the basis of gravity to be deeper than 1 km, only two cut across the rift, whereas at least five others change trend near the rift (Blakely and Jachens, 1991). Zoback and Zoback (1980) suggested that the complementary north-northwest (parallel to the rift) and east-northeast trends in the modern topography represent reactivation of pre-existing faults that locally were able to accommodate strain by oblique-normal slip, whereas regionally,

favorably oriented (north-northeast) faults were breaking through the upper crust.

In detail, the aeromagnetic high associated with the central part of the northern Nevada rift is segmented, offset both laterally (in a left-stepping sense, see Fig. 2A, sites X and Y, and diagrammatically in Fig. 1) and vertically, by the Basin and Range normal faults that strike approximately orthogonal to it. These normal faults strike between about N40°–80°E, and striae measurements demonstrate that they have oblique left-lateral normal slip (Zoback, 1978, 1989). Detailed gravity and geologic investigations were used to constrain the minimum amount of vertical displacement across these major east-northeast-striking normal faults (it is impossible to estimate the amount of material eroded from the range tops, as most ranges are capped by the middle Miocene volcanic rocks). Detailed modeling of magnetic profiles straddling these fault zones limits the total lateral offsets. This modeling is described in detail in Zoback (1978), and the results are summarized in Table 2. Note that for the four main fault zones crossing the central part of the rift (fault zones bound the northwestern sides of the associated ranges; see Fig. 3), the estimates of lateral offsets are significant and in some cases exceed the vertical offsets on the faults. Note too that the mean best estimate of extension direction (representing total post-middle Miocene deformation) across the four fault zones is N72°W ± 9°, close to the modern extension direction, indicating that the rift has not rotated on a regional scale.

POST-RIFT TECTONIC ROTATION?

Recent paleomagnetic results have been interpreted as casting doubt on the suitability of the northern Nevada rift and its present orientation as an indicator of middle Miocene stress orientation. Li and others (1990) sampled three localities along the northern Nevada rift: 18 sites at the Midas trough, 22 sites at Argenta rim, and 19 sites at the Cortez Mountains. After eliminating several sites judged to reflect transitional field behavior, they found locality mean paleomagnetic directions to be statistically indistinguishable but rotated approximately 19° counterclockwise with respect to the expected middle Miocene direction. Moreover, when data from all three localities were combined, the overall mean showed the same discordant direction. Li and others (1990) concluded that all three localities have rotated ~19° counterclockwise about vertical axes since the formation

TABLE 2. ESTIMATES OF FAULT OFFSETS ALONG MAJOR EAST-NORTHEAST-TRENDING CROSS FAULTS ALONG THE NORTHERN NEVADA RIFT*

Fault zone (south to north)	Fault trend	Vertical offset (m) [†]	Horizontal separation (m) [‡]	Lateral offset (m) ^{**}	Extension direction ^{††}
Roberts Mountains	N 65° E	3,260 (2,900–3,350)	2,283 (1,670–3,350)	1,585 (850–1,740)	N 60° W (N 39° W–N 71° W)
Simpson Park Range (northeast end of range)	N 69° E	1,680 (1,250–2,120)	1,176 (720–2,120)	1,720 (1,130–2,290)	N 77° W (N 49° W–N 93° W)
Cortez Range	N 54° E	3,510 (3,170–3,660)	2,458 (1,830–3,660)	1,680 (1,520–1,830)	N 70° W (N 66° W–N 83° W)
Argenta Rim (northeast end Shoshone Range)	N 75° E	2,350 (2,290–2,440)	1,645 (1,320–2,440)	3,445 (3,140–3,750)	N 79° W (N 67° W–N 86° W)

*Faults bound northwest side of range. Uncertainty ranges in offsets given in parentheses.

†Minimum estimate determined from gravity modeling of basin fill, and combined topography of range and projection of dip slope.

‡Computed from vertical offset estimate assuming a 55° dipping fault; uncertainty range from uncertainties in vertical offset estimate and allowing for a possible fault dip between 45°–60°.

**Determined from offset of main magnetic source zone as determined from modeling of two-dimensional profiles that straddle these offsets.

††Net horizontal direction of opening along fault, ϵ (in northwest quadrant) = $(90^\circ - \text{fault trend}) + \tan^{-1}(\text{lateral offset/horizontal separation})$; uncertainty range broadest possible using end members uncertainty values for separation and offset.

of the northern Nevada rift about 15 Ma. Accordingly, the northern Nevada rift would have been oriented nearly north-south during its formation in the middle Miocene, and paleostress orientations inferred from the present-day orientation of the northern Nevada rift would thus be in error.

The aeromagnetic anomaly manifested by the northern Nevada rift has several characteristics that should be considered in this regard. First, the gradients that define the boundaries of the exposed rift are extraordinarily linear and continuous over distances of more than 200 km. This suggests that the rift is similarly continuous without significant lateral offsets except those related to the younger east-northeast-trending, rift-crossing, basin-bounding faults (Table 2). Only two models could accommodate 19° of vertical-axis rotation and leave the rift so homogeneous: (1) either the rotating block was sufficiently large to include the entire rift *in situ* or (2) the rotation was accommodated by numerous crustal blocks with lateral dimensions comparable to or smaller than the width of the rift. The first model is highly unlikely, as noted also by Li and others (1990), because the rift can now be seen to span nearly the entire state of Nevada (Fig. 1), and there is no evidence of such a large-scale rotation in surrounding Basin and Range deformation. In fact, paleomagnetic data for an Oligocene ash-flow tuff crossing the southern segment of the rift rules out any large-scale systematic rotation. Declinations in the Windous Butte Formation at two sites along the southernmost part of the aeromagnetic anomaly (Stone Cabin and Wells Station) are identical to the declination at the type locality and everywhere else sampled (except one anomalous site) (Gromme and others, 1972). More-

over, MacDonald and others (1992) measured a magnetic direction in Eocene rocks in the Roberts Mountains that is consistent with no post-Eocene rotation.

Li and others (1990) favored the second model, systematic counterclockwise rotation of numerous small crustal blocks within the rift. Such rotations would produce right-stepping offsets of geological elements such as dikes or, on a larger scale, of the entire rift. Actual offsets of the rift step left, however, as shown by the aeromagnetic data and by measurements of left-lateral oblique-normal slip vectors on the cross faults (Table 2). One dike (the Sawtooth dike) internal to the rift also shows a left step, which, on the basis of field evidence indicating the absence of fault offset, has been interpreted as originating at the time of intrusion (Zoback and Thompson, 1978).

The observation that the overall orientation of the rift (~N20°W) is equivalent to the orientation of mapped dike swarms now contained in fault blocks within the rift is also difficult to reconcile with a block-rotation model. For example, Figures 3 and 4 show numerous dikes longer than 2 km in outcrop with orientations of approximately N20°W. This parallelism of dikes and overall trend of the rift is inconsistent with a model of systematic block rotation throughout the rift but does not rule out rotation of small blocks within fault zones having a left-lateral component of slip. As shown on their map, all three of the paleomagnetic locations of Li and others (Cortez Range, Argenta Rim, Midas trough) are within or adjacent to the major cross-fault zones that offset the rift in a left-lateral sense. Therefore, counterclockwise rotations might be related to localized deformation directly adjacent to the fault zone and

unrelated to the overall orientation of the rift or to the dike swarms within it.

REGIONAL RELATIONS: FLOOD BASALTS AND EMERGENCE OF THE YELLOWSTONE HOT SPOT

The interval between 17 and 14 Ma was a dynamic period in parts of Nevada, Oregon, Idaho, and Washington. During this geologically short interval the intrusive and extrusive rocks of the northern Nevada rift were emplaced, the bulk of the flood basalts of the Columbia River Basalt Group was erupted through its feeder dikes, and the McDermitt caldera was formed at the northern terminus of the northern Nevada rift (Fig. 1). The McDermitt caldera was the first of a succession of calderas tracking northeastward at a rate of 35 to 45 mm/yr along the eastern arm of the Snake River Plain toward the youngest caldera at Yellowstone (Armstrong and others, 1975; Christiansen and McKee, 1978; Rodgers and others, 1990). This rate is the sum of southwestward movement of the North American plate across the mantle plume and concomitant extension of the Basin and Range crust.

Hot-spot plumes are thought to ascend through the mantle as mushroom-shaped heads that are fed from below by narrow cylindrical conduits (Duncan and Richards, 1991; Sleep, 1992). The voluminous plume head is the source of flood basalts associated worldwide with the initial eruption of plumes through the lithosphere. The plume head and the thermal lithospheric uplift that accompanies it are ~2,000 km in diameter (Sleep, 1992). Thus it should not be surprising that the combined extent of the feeder dikes of the Columbia Plateau flood basalts, the graben of the western Snake River Plain, and the northern Nevada rift is about 1,000 km (Fig. 1). The topographic swell of about 1 km at the hot spot would have facilitated outward flow to the dikes. Thermal subsidence followed as the hot spot swell progressed toward its present position at Yellowstone, and waning, mainly basaltic volcanism continued in its track along the eastern Snake River Plain.

There is direct evidence from other areas that dikes can propagate great distances from hot-spot sources. Maps of Precambrian diabase dikes of the Canadian shield (Fahrig and West, 1986) show dikes extending hundreds of kilometers. Dikes radiating from the Mackenzie hot spot (1220 Ma) in northwestern Canada curve into the regional stress field and extend southeastward for 1,500 km. Rubin and Pollard (1987) analyzed active blade-

like propagation of dikes extending for tens of kilometers in Iceland and Hawaii.

Thompson and Gibson (1991) have also interpreted the Columbia River basalts and the emergence of the Yellowstone hot spot as linked parts of a fundamental process associated with a hot mantle plume penetrating the continental lithosphere. They attribute the larger eruptive volume to the north as localized by previously rifted and thinned lithosphere evidenced by the underlying Eocene Pasco basin.

CONCLUSIONS

The northern Nevada rift, as defined by an alignment of basaltic dikes and associated middle Miocene lava flows prominently expressed in aeromagnetic maps, can be traced magnetically for at least 500 km southward from the Oregon border to southern Nevada (Zoback and Thompson, 1978; McKee and Noble, 1986; Blakely and Jachens, 1991). The consistent N20°–25°W trend of the magnetic anomaly, of the exposed basaltic feeder dike swarms, and of the structural troughs that were filled by basaltic flows indicates an extensional origin for the northern Nevada rift. The consistent trend of all these features indicates that the rift did not exploit a pre-existing feature but instead responded to the prevailing least principal stress at the time of formation, horizontal and oriented N 65°–70° E (Zoback and Thompson, 1978; Christiansen and McKee, 1978). New isotopic age determinations indicate that this rifting event occurred between ~17 and 14 Ma, and possibly over an even shorter interval. Both the rift and dikes within it have the same north-northwest trend as feeder dikes of the Columbia Plateau flood basalts, the bulk of which erupted ~16–15 Ma, the same general time interval as basalt eruptions of the northern Nevada rift. On the basis of similar age, trend, and chemistry, the voluminous Columbia Plateau flood basalts and the northern Nevada rift basalts are considered to be related and to represent two end members (both spatially and stylistically) of an enormous lithospheric “rift” that propagated north-northwest and south-southeast of the initial point of breaching of the North American lithosphere by the Yellowstone hot spot, at the 16 Ma silicic McDermitt volcanic center located at the north end of the northern Nevada rift. Differences in silica and alkali content as well as $^{87}\text{Sr}/^{86}\text{Sr}$ of basaltic rocks in the northern and southern parts of the rift may reflect different compositions of the lower crust through which the magma rose.

The higher $^{87}\text{Sr}/^{86}\text{Sr}$ andesitic to trachyandesitic basalts from northern Nevada may have been derived partly from an Early Proterozoic continental lithosphere; the lower-silica tholeiitic basalts from Washington and Oregon with lower $^{87}\text{Sr}/^{86}\text{Sr}$ may have come through a Late Proterozoic oceanic lithosphere. Both the overall trend of this rift as well as the parallelism of the individual dike zones within it indicate a regional middle Miocene least principal stress direction of east-northeast–west–southwest, which is consistent with the stress direction for that time inferred in other parts of the Basin and Range province and Rio Grande rift (for example, Zoback and others, 1981).

ACKNOWLEDGMENTS

We are indebted to John Bartley, Myron Best, John Geissman, Sherman Grommé, Bob Jachens, and Tony Lowry for careful reviews that greatly improved the paper.

NOTE ADDED IN PROOF:

Ongoing paleomagnetic investigations along the northern Nevada rift (Geissman and others, 1993), yield preliminary data that indicate that the Roberts Mountains have not sustained a significant post-Miocene counterclockwise vertical-axis rotation.

REFERENCES CITED

- Allmendinger, R. W., Hauge, T. A., Hauser, E. C., Potter, C. J., Klempner, S. L., Nelson, K. D., Knepper, P., and Oliver, J., 1987, Overview of the COCORP 40°N Transect, western United States: The fabric of an orogenic belt: *Geological Society of America Bulletin*, v. 98, p. 308–319.
- Anderson, R. E., and Ekren, E. B., 1977, Late Cenozoic fault patterns and stress fields in the Great Basin and westward displacement of the Sierra Nevada Block—Comment: *Geology*, v. 5, p. 388–389.
- Armstrong, R. L., 1970, Geochronology of Tertiary igneous rocks, eastern Basin and Range province, western Utah, eastern Nevada, and vicinity, U.S.A.: *Geochimica et Cosmochimica Acta*, v. 34, p. 203–232.
- Armstrong, R. L., Leeman, W. P., and Malde, H. E., 1975, K-Ar dating Quaternary and Neogene volcanic rocks of the Snake River Plain, Idaho: *American Journal of Science*, v. 275, p. 225–251.
- Atwater, T., 1970, Implications of plate tectonics for the Cenozoic tectonic evolution of western North America: *Geological Society of America Bulletin*, v. 81, p. 3513–3535.
- Atwater, T., 1989, Plate tectonic history of the northeast Pacific and western North America, in Winterer, E. L., Hussong, D. M., and Decker, R. W., eds., *The eastern Pacific Ocean and Hawaii: The geology of North America*, Volume N: Boulder, Colorado, Geological Society of America, p. 21–72.
- Baksi, A. K., 1988, Estimation of lava extrusion and magma production rates for two flood basalt provinces: *Journal of Geophysical Research*, v. 93, p. 11,809–11,815.
- Blakely, R. J., 1988, Curie temperature isotherm analysis and tectonic implications of aeromagnetic data from Nevada: *Journal of Geophysical Research*, v. 93, p. 11,817–11,832.
- Blakely, R. J., and Jachens, R. C., 1991, Regional study of mineral resources in Nevada: Insights from three-dimensional analysis of gravity and magnetic anomalies: *Geological Society of America Bulletin*, v. 103, p. 795–803.
- Blakely, R. J., Jachens, R. C., and McKee, E. H., 1989, The northern Nevada rift: A 500-km long zone that resisted subsequent deformation [abs.]: *Eos (American Geophysical Union Transactions)*, v. 70, p. 1336.
- Carlson, R. W., and Hart, W. K., 1987, Crustal genesis on the Oregon plateau: *Journal of Geophysical Research*, v. 92, p. 6191–6206.
- Catchings, R. D., 1992, A relation among geology, tectonics, and velocity structure, western to central Nevada Basin and Range: *Geological Society of America Bulletin*, v. 104, p. 1178–1192.
- Christiansen, R. L., and McKee, E. H., 1978, Late Cenozoic volcanic and tectonic evolution of the Great Basin and Columbia Intermontane regions, in Smith, R. B., and Eaton, G. P., eds., *Cenozoic tectonics and regional geophysics of the western Cordillera*: *Geological Society of America Memoir* 152, p. 283–311.
- Duncan, R. A., and Richards, M. A., 1991, Hotspots, mantle plumes, flood basalts, and true polar wander: *Reviews of Geophysics*, v. 29, p. 31–50.
- Fahrig, W. F., and West, T. D., 1986, Diabase dyke swarms of the Canadian Shield: *Geologic Survey of Canada Map* 1627A.
- Geissman, J. W., Acton, G. D., and Schneider, M., 1993, Revisional strain histories: an analysis of new paleomagnetic data from Miocene dikes in the Northern Nevada rift [abs.]: *Eos (American Geophysical Union Transactions)*, v. 74, in press.
- Gilluly, J., and Gates, O., 1965, Tectonic and igneous geology of the northern Shoshone Range, Nevada: U.S. Geological Survey Professional Paper 465, 153 p.
- Gilluly, J., and Masursky, H., 1965, Geology of the Cortez quadrangle, Nevada, with a section on gravity and aeromagnetic surveys by D. R. Mabey: U.S. Geological Survey Bulletin 1175, 117 p.
- Grommé, S. H., McKee, E. H., and Blake, M. C., Jr., 1972, Paleomagnetic correlations and potassium-argon dating of middle Tertiary ash-flow sheets in the eastern Great Basin, Nevada and Utah: *Geological Society of America Bulletin*, v. 83, p. 1619–1638.
- Henry, C. D., and Price, J. G., 1986, Early Basin and Range development in Trans-Pecos Texas and adjacent Chihuahuas: magmatism and orientation, timing and style of extension: *Journal of Geophysical Research*, v. 91, p. 6213–6224.
- Hildenbrand, T. G., and Kucks, R. P., 1988, Total-intensity magnetic anomaly map of Nevada: Nevada Bureau of Mines and Geology Map 93A, scale 1:750,000.
- Holbrook, W. S., Catchings, R. D., and Jarchow, C. M., 1991, Origin of deep crustal reflections: Implications of coincident seismic refraction and reflection data in Nevada: *Geology*, v. 19, p. 175–179.
- Hooper, P. R., 1988, The Columbia River Basalt, in MacDougall, J. D., ed., *Continental flood basalts: Dordrecht, The Netherlands, Kluwer Academic Press*, p. 1–33.
- Jachens, R. C., and Moring, B. C., 1990, Maps of thickness of Cenozoic deposits and the isostatic residual gravity over basement for Nevada: U.S. Geological Survey Open-File Report 90-404, 2 sheets, scale 1:1,000,000.
- John, D. A., Stewart, J. H., Kilbourn, J. E., Silberman, N. J., and Rowan, L. C., 1993, Geology and mineral resources of the Reno 1° x 2° quadrangle, Nevada and California: U.S. Geological Survey Bulletin 2019, 65 p.
- Le Maitre, R. W., 1984, A proposal by the IUGS Subcommittee on the systematics of igneous rocks for a chemical classification of volcanic rocks based on the total alkali silica (TAS) diagram: *Australian Journal of Earth Sciences*, v. 31, p. 243–255.
- Li, Y., Geissman, J. W., Nur, A., Ron, H., and Huang, Q., 1990, Paleomagnetic evidence for counterclockwise block rotation in the north Nevada rift: *Geology*, v. 18, p. 79–82.
- Lipman, P. W., 1981, Volcano-tectonic setting of Tertiary ore deposits, southern Rocky Mountains: *Arizona Geological Society Digest*, v. 14, p. 199–213.
- Mabey, D. R., 1965, Gravity and aeromagnetic surveys, in Gilluly, J., and Masursky, H., *Geology of the Cortez quadrangle, Nevada: U.S. Geological Survey Bulletin* 1175, p. 105–111.
- Mabey, D. R., 1966, Regional gravity and magnetic anomalies in part of Eureka County, Nevada, in Hansen, D. A., Heinrichs, W. E., Jr., Holmer, R. C., MacDougall, R. E., Rogers, G. R., Sumner, J. S., and Ward, S. H., eds., *Mining geophysics, Volume 1: Tulsa, Oklahoma, Society of Exploration Geophysicists*, p. 77–83.
- MacDonald, W. D., Palmer, H. C., and Hayatsu, A., 1992, Perspectives on interpretation of paleomagnetic results from block-faulted regions: Roberts Mountains, Nevada: *Eos (American Geophysical Union Transactions)*, v. 73, p. 146.
- McKee, E. H., 1986, Geologic map of the Roberts Wilderness Study Area, Eureka County, Nevada: U.S. Geological Survey Miscellaneous Field Studies Map MF-1844, scale 1:48,000.
- McKee, E. H., and Blakeley, R. J., 1990, Tectonic significance of linear, north-trending anomalies in north-central Nevada, in *Geology and ore deposits of the Great Basin, sponsored by Geological Society of Nevada and U.S. Geological Survey, Program with Abstracts*, p. 49.
- McKee, E. H., and Mark, R. K., 1971, Strontium isotopic composition of two basalts representative of the southern Snake River volcanic province, in *Geological Survey Research 1971: U.S. Geological Survey Professional Paper* 750-B, p. B92–B95.
- McKee, E. H., and Noble, D. C., 1986, Tectonic and magmatic development of the Great Basin of western United States during late Cenozoic time: *Modern Geology*, v. 10, p. 39–49.
- McKee, E. H., and Silberman, M. L., 1970, Geochronology of Tertiary igneous rocks in central Nevada: *Geological Society of America Bulletin*, v. 81, p. 2317–2328.
- McKee, E. H., Swanson, D. A., and Wright, T. L., 1977, Duration and volume of Columbia River Basalt volcanics, Washington, Oregon and Idaho: *Geological Society of America Abstracts with Programs*, no. 9, p. 463.
- Morgan, W. J., 1972, Plate motions and deep mantle convection: *Geological Society of America Memoir* 132, p. 7–22.

- Muffler, L.J.P., 1964, Geology of the Frenchie Creek Quadrangle north-central Nevada: U.S. Geological Survey Bulletin 1179, 99 p.
- Murphy, M. A., McKee, E. H., Winterer, E. L., Matti, J. C., and Dunham, J. B., 1978, Preliminary geologic map of the Roberts Creek Mountain quadrangle, Nevada: U.S. Geological Survey Open-File Map 78-376, scale 1:31,250.
- Philbin, F. W., Meuschke, J. L., and McCaslin, W. E., 1963, Aeromagnetic map of the Roberts Mountains, central Nevada: U.S. Geological Survey Open-File Map, March 7, 1963, scale 1:25,000.
- Pierce, K. L., and Morgan, L. A., 1992, The track of the Yellowstone hot spot: Volcanism, faulting, and uplift: Geological Society of America Memoir 179, p. 1-53.
- Potter, C. J., Liu, C.-S., Huang, J., Zheng, L., Hauge, T. A., Hauser, E. C., Allmendinger, R. W., Oliver, J. E., Kaufman, S., and Brown, L., 1987, Crustal structure of north-central Nevada: Results from COCORP deep seismic profiling: Geological Society of America Bulletin, v. 98, p. 330-337.
- Rehrig, W. A., and Heidrick, T. L., 1976, Regional tectonic stress during the Laramide and late Tertiary intrusive periods, Basin and Range province, Arizona: Arizona Geological Society Digest, v. 10, p. 205-228.
- Roberts, R. J., 1966, Metallogenic provinces and mineral belts in Nevada, in Papers presented at the AIME Pacific Southwest mineral industry conference, Sparks, Nevada, May 5-7, 1965, Part A, General session on exploration and mine development in Nevada: Nevada Bureau of Mines Report 13, p. 47-72.
- Robinson, E. S., 1970, Relation between geological structure and aeromagnetic anomalies in central Nevada: Geological Society of America Bulletin, v. 81, p. 2045-2060.
- Rodgers, D. W., Hackett, W. R., and Ore, H. T., 1990, Extension of the Yellowstone plateau, eastern Snake River Plain, and Owyhee plateau: Geology, v. 18, p. 1138-1141.
- Rubin, A. M., and Pollard, D. D., 1987, Origins of blade-like dikes in volcanic rift zones, in Decker, R. W., Wright, T. L., and Stauffer, P. H., eds., Volcanism in Hawaii: U.S. Geological Survey Professional Paper 1350, p. 1449-1470.
- Rytuba, J. J., and McKee, E. H., 1984, Peralakaline ash-flow tuffs and calderas of the McDermitt volcanic field, southeast Oregon and north central Nevada: Journal of Geophysical Research, v. 89, p. 8616-8628.
- Simpson, R. W., Jachens, R. C., Blakely, R. J., and Salus, R. W., 1986, A new isostatic residual gravity map of the conterminous United States with a discussion on the significance of isostatic residual anomalies: Journal of Geophysical Research, v. 91, p. 8348-8372.
- Sleep, N. H., 1992, Hotspot volcanism and mantle plumes: Annual Reviews of Earth and Planetary Science, v. 20, p. 19-43.
- Stewart, J. H., 1978, Basin-range structure in western North America: A review: Geological Society of America Memoir 152, p. 1-31.
- Stewart, J. H., and McKee, E. H., 1977, Geology and mineral deposits of Lander County, Nevada, with a section on mineral deposits by Harold K. Stager: Nevada Bureau of Mines and Geology Bulletin 88, 106 p.
- Stewart, J. H., Walker, G. W., and Kleinhampl, F. J., 1975, Oregon-Nevada lineament: Geology, v. 3, p. 265-268.
- Stickney, M. C., and Bartholomew, M. J., 1987, Seismicity and late Quaternary faulting of the northern Basin and Range province, Montana and Idaho: Bulletin of the Seismological Society of America, v. 77, p. 1602-1625.
- Stock, J., and Molnar, P., 1988, Uncertainties and implications of the Late Cretaceous and Tertiary position of North America relative to the Farallon, Kula and Pacific plates: Tectonics, v. 7, p. 1339-1384.
- Swanson, D. A., Wright, T. L., Hooper, P. R., and Bentley, R. D., 1979, Revisions in stratigraphic nomenclature of the Columbia River Basalt Group: U.S. Geological Survey Bulletin 1457-G, p. G1-G59.
- Thompson, R. N., and Gibson, S. A., 1991, Subcontinental mantle plumes, hotspots, and pre-existing thinspots: Geological Society of London Journal, v. 148, p. 973-977.
- Wallace, A. R., McKee, E. H., Zoback, M., and Zimmermar, R. A., 1990, New ages for volcanic rocks, western Elk County, Nevada: Isochron/West, no. 55, p. 3-6.
- Weils, J. D., Elliott, J. E., and Obradovich, J. D., 1971, Age of the igneous rocks associated with ore deposits, Cortez-Buckhorn area, Nevada: U.S. Geological Survey Professional Paper 750-C, p. C127-C135.
- Winterer, E. L., 1968, Tectonic erosion in the Roberts Mountains Nevada: Journal of Geology, v. 76, p. 347-357.
- Zoback, M. L., 1978, A detailed study of late Cenozoic deformation in the northern Basin and Range [Ph.D. thesis]: Stanford University, 247 p.
- Zoback, M. L., 1989, State of stress and modern deformation of the northern Basin and Range province: Journal of Geophysical Research, v. 94, p. 7105-7128.
- Zoback, M. L., and Thompson, G. A., 1978, Basin and Range rifting in northern Nevada: Clues from a mid-Miocene rift and its subsequent offsets: Geology, v. 6, p. 111-116.
- Zoback, M. L., and Zoback, M. D., 1980, Faulting patterns in north central Nevada and strength of the crust: Journal of Geophysical Research, v. 85, p. 275-284.
- Zoback, M. L., Anderson, R. E., and Thompson, G. A., 1981, Cenozoic evolution of the state of stress and style of tectonics in the western United States: Philosophical Transactions of the Royal Society of London, ser. A, v. 300, p. 407-434.

MANUSCRIPT RECEIVED BY THE SOCIETY FEBRUARY 8, 1993
 REVISED MANUSCRIPT RECEIVED JUNE 28, 1993
 MANUSCRIPT ACCEPTED JULY 8, 1993